University of Alberta

Autotaxin, Lysophosphatidate and Taxol Resistance

by

Nasser Samadi

A thesis submitted to the Faculty of Graduate Studies and Research

in partial fulfillment of the requirements for the degree of

Doctor of Philosophy

Medical Sciences -
Laboratory Medicine and Pathology

Fall 2009

Edmonton, Alberta

Examining Committee

Dr. David N Brindley, Biochemistry

Dr. Fiona J Bamforth, Laboratory Medicine and Pathology

Dr. George S Cembrowski, Laboratory Medicine and Pathology

Dr. Ing Swie Goping, Biochemistry

Dr. Raymond Lai, Laboratory Medicine and Pathology

Dr. Andrew J Morris, University of Kentucky

Dedication

Ahead of all I humbly thank GOD, the Most Compassionate the Most Merciful, who gave me health, thoughts, supportive family, great mentors and co-operative people to enable me achieve this goal.

My wonderful wife, Dr. Leila Molavi and my lovely son, Amin Samadi for their love, encouragement and patience throughout the peaks and valleys of this journey.

My kind mother who devoted her life to raising me to be the person I am today. You have done everything to help me reach here. Thank you for all the unconditional love, guidance, and support that you have always given me, helping me to succeed. Thank you for all your patience over all steps of my study.

My only brother, Dr. Mohammad Taghi Samadi, for all his support and understanding and patience, and to his beloved family.

The memory of my great father, who taught me to believe in myself... I hope I have made him proud.

Abstract

First-line treatment of breast and other cancers with Taxol is compromised by resistance in up to 40% of patients. To improve chemotherapy, it is vital to understand how Taxol resistance develops and to overcome this. Autotaxin (ATX) promotes cancer cell survival, growth, migration, invasion and metastasis. ATX converts extracellular lysophosphatidylcholine (LPC) into lysophosphatidate (LPA). As these lipids have been reported to affect cell signaling through their own G-protein-coupled receptors, ATX could modify the balance of this signaling. Also, ATX affects cell adhesion independently of its catalytic activity, We first investigated the interactions of ATX, LPC and LPA on the apoptotic effects of Taxol, which is commonly used in breast cancer treatment. LPC had no significant effect on Taxol-induced apoptosis in MCF-7 breast cancer cells, which do not secrete significant ATX. Addition of incubation medium from MDA-MB-435 melanoma cells, which secrete ATX, or recombinant ATX enabled LPC to inhibit Taxol-induced apoptosis of MCF-7 cells. Inhibiting ATX activity blocked this protection against apoptosis. We conclude that LPC has no significant effect in protecting MCF-7 cells against Taxol treatment unless it is converted to LPA by ATX. LPA strongly antagonized Taxol-induced apoptosis through stimulating phosphatidylinositol 3-kinase and inhibiting ceramide formation. LPA also partially reversed the Taxol-induced arrest in the G2/M phase of the cell cycle. Then, we described a novel action of LPA, which by activating phosphatidylinositol 3-kinase increases the expression of glycogen synthase kinase-3ß and survivin. Survivin is an anti-apoptotic protein, which also increases

the dynamicity of microtubules. Survivin decreased the effectiveness of Taxol in stabilizing microtubules and enabled MCF-7 breast cancer cells to escape from Taxol-induced arrest in G2/M and consequent cell death. Our work showed that inhibiting ATX activity and LPA-mediated signaling can reverse the resistance to Taxol-induced cell death. Our results support the hypothesis that therapeutic inhibition of ATX activity, which results in less LPA production, or inhibition of LPA signalling could improve the efficacy of Taxol as a chemotherapeutic agent for cancer treatment.

Acknowledgements

- The words fall short for my great mentor Dr. David N Brindley, to express my gratitude. He is a great supervisor that made this degree process, an experience I never forget.
- I am very indebted to my kind supervisor, Dr. Fiona J Bamforth. I started my journey at the University of Alberta with her and completion of this program would be impossible without her enormous support and guidance.
- I sincerely thank Dr. George S Cembrowski, for his strong support during the program and serving on my supervisor committee. He is an incredible mentor from whom I not only learned about scholarly conduct but earned life lessons that extend far beyond the academic area.
- My sincere thanks go to Dr. Ing Swie Goping, for her support and guidance in this project and serving on my supervisory committee. Collaborating with her lab was one of the most exciting parts of this thesis work.
- I am very grateful to Dr. Lewis Schang for his guidance in cell cycle studies.
- I would like to thank Dr. Michael Sawyer for his help for calculations of drug interactions and serving for my candidacy and final exam.
- I would like to thank Mr. Jay Dewald, a great technician in Dr. Brindley's lab. He trained me in the bench work at the beginning of my program and he was with me everywhere throughout this project.
- I thank Dr. Meltem Sariahmetoglu and Dr. Sabina Isgandarova for all their help and support during the program.
- I thank Raie Bekele and Bernard Kok, graduate students in Dr. Brindley's lab, for helping me through some experiments.
- I am very grateful to all my previous and recent labmates for providing a friendly and enjoyable environment in the group. Their ideas and suggestions for this project were always clever and useful.
- The words cannot express my gratitude to my family for their support and patience.
- Finally I am grateful to the Iranian Ministry of health and Medical Education, Canadian Institutes of Health Research and Bell McLeod Fund for supporting this project.

Table of Contents

CHAPTER 1 – 1 INTRODUCTION.....1

1.1 Introduction: overview.....2

1.2 Autotaxin expression and tumor progression.....3

1.2.1 Significance of Autotaxin in lysophosphatidate production**.....3**

1.2.2 Structure and function of autotaxin**.....5**

1.2.3 Regulation of autotaxin activity and lysophosphatidate production**…….9**

1.2.4 Role of autotaxin in tumor development**…….....10**

1.3 Extracellular lysophosphatidate and tumor progression.....15

1.3.1 The biologic role of extracellular lysophosphatidate**.....15**

1.3.2 Role of lipid phosphate phosphatases in lysophosphatidate degradation**……...…….……..17**

1.3.3 Lysophosphatidate and G protein coupled receptors**.....18**

1.3.4 Role of lysophosphatidate in tumor development**.....25**

1.4 Taxol, mechanisms of actions in chemotherapy……..……28

1.4.1 Pharmacology and functions**……...28**

1.4.2 Cellular response to Taxol**……..……31**

1.5 Markers predictive of Taxol resistance.....…...33

1.5.1 Chemoresistance in cancer treatment**……...……...…..33**

1.5.2 Mechanisms of Taxol resistance**……...36**

1.6 Survivin and Chemoresistance…….……..…..37

1.7 Thesis objectives…….39

CHAPTER 2 – MATERIALAS AND METHODS……..……41

2.1 Materials……42

2.2 Cell culture…….……44

2.3 Fetal bovine serum delipidation……..……..44

2.3.1 Preparation of charcoaled FBS**……44**

2.3.2 Measurement of ^{32}P-labeled lysophosphatidate in charcoal-treated FBS**……...….44**

2.4 Quantification of apoptotic nuclei using 4,6-diamidino-2-phenylindole (DAPI) stain.....44

2.5 Measurement of lysophosphatidate breakdown……...…..45

2.6 Mitochondrial membrane potential assay…….……..45

2.7 ATX expression assays……..…… 46

2.7.1 ATX mRNA expression detection**……...……46**

2.7.2 ATX protein detection**……..……47**

2.7.3 ATX activity assay**……...….47**

2.8 Isobalogram analysis……..48

2.9 Measurement of ceramide concentrations……...……49

2.9.1Ceramide mass assay**……..…49**

2.9.2 Phosphate assay**……...……..51**

2.10 Bromodeoxyuridine / propidium iodine double staining……..51

2.10.1 Labeling and fixation of cultured cells**……...…….....51**

2.10.2 Preparation of isolated nuclei**……...……...……52**

2.10.3 Staining of isolated nuclei**……...….53**

2.11 Immunocytochemistry……...…..54

2.12 Taxol uptake and distribution in MCF-7 cells…….…….55

2.12.1 Measurement of Taxol uptake and distribution**……..55**

2.12.2 Measurement of Taxol metabolites by thin layer chromatography**56**

2.13 Cellular distribution localization of Taxol…….,……56

2.13.1 Collection of cell ghost and the cytosolic compartment**…….56**

2.13.2 Measurement of lactate dehydrogenase (LDH) activity**…….57**

2.13.3 Measurement of intracellular distribution of Taxol**…...…….57**

2.13.4 GSK-3αß and survivin protein detection**…….……...……57**

2.14 Knockdown of survivin expression using siRNA……...……...58

2.15 Knockdown of GSK-3ß expression using siRNA……..……59

2.16 Statistical analysis……60

CHAPTER 3 – RESULTS……...……61

3.1 Introduction…….…….....….62

3.2 ATX is expressed in MDA-MB-231 and MDA-MB-435 cells but not in

MCF-7 cells …….……64

3.3 Lysophosphatidate protects MCF-7 cells from Taxol-induced apoptosis.65

3.3.1 The effect of activated charcoal in removal of autotaxin and LPA**..65**

3.3.2 Measurement of half-life of LPA**……..69**

3.3.3 The role of LPA in protection of cancer cells against Taxol-induced apoptosis**…….……...…70**

3.3.4 The role of LPA on Taxol-induced changes in mitochondrial potential**……...……..72**

3.4 LPA shows a strong antagonistic effect with Taxol……...…….74

3.5 ATX protects MCF-7 and MDA-MB-435 cells against Taxol-induced apoptosis only in the presence of LPC…….……76

3.5.1 Concentrated medium from MDA-MB-435 cells and protection against Taxol-induced apoptosis in MCF-7 cells**……..……76**

3.5.2 Recombinant ATX and protection against Taxol-induced apoptosis in MCF-7 cells**……..77**

3.5.3 Concentrated media from MCF-7 cells and protection against Taxol-induced apoptosis in MCF-7 cells**……78**

3.6 LPA_1 and LPA_3 receptors are not involved in LPA-induced protection against apoptosis in MCF-7 cells……82

3.7 The PI3K/Akt pathway is involved in LPA-mediated protection against Taxol-induced apoptosis……..…….85

3.8 LPA attenuates Taxol-induced ceramide production……..……..88

3.9 LPA attenuates Taxol-induced G2/M arrest……..…….88

3.10 How does LPA decrease Taxol-induced G2/M arrest?.....91

3.11 LPA does not change Taxol expulsion by MCF-7 cells……..……..97

3.12 LPA does not change Taxol metabolite formation in MCF-7 cells.....100

3.13 LPA releases cells from Taxol-induced G2/M arrest and cell death through activation of PI3K/ Akt/ GSK-3β and surviving protein…… 102

CHAPTER 4 ─ GENERAL DISCUSSION ANF FUTURE DIRECTIONS111

4.1 Discussion…….....…….…..112

4.2 Future directions……..……...….127

BIBLIOGRAPHY……..…130

PUBLICATIONS……..…….169

APPENDIX…….170

List of Tables

Table 1 **Effect of LPA on Taxol-induced changes in mitochondrial potential……...…….…….75**

List of Figures

Figure 1.1 Domain structure and isoforms of ATX/NPP2.....**5**

Figure 1.2 Catalytic and non-catalytic activities of autotaxin (NPP2).....**9**

Figure 1.3 Principal steps in metastasis.....**11**

Figure 1.4 Chemical structure of Lysophosphatidate.....**15**

Figure 1.5 Synthesis and degradation of LPA in serum.....**16**

Figure 1.6 LPA signaling pathways mediated by GPCRs and LPA receptors**19**

Figure 1.7 Activation of phosphoinositide 3-kinases pathway.....**23**

Figure 1.8 Chemical structure of Taxol.....**29**

Figure 1.9 Binding of Taxol to the tubulin heterodimers.....**32**

Figure 1.10 Apoptosis pathways.....**35**

Figure 1.11 Regulation of survivin at synthesis and degradation levels.....**38**

Figure 3.1 Differential expression of ATX in MDA-MB-435 and MCF-7 cells……**66**

Figure 3.2 Differential expression of ATX in MDA-MB-435 and MDA-MB-231 cells……..…..**67**

Figure 3.3 The effect of activated charcoal in removal of autotaxin…….…..**68**

Figure 3.4 The effect of active charcoal in removal of LPA……...…**68**

Figure 3.5 Breakdown of LPA……...…….**69**

Figure 3.6 Protective effect of LPA on Taxol-induced apoptosis in MCF-7 cells……...….**71**

Figure 3.7 Taxol killing curve for MDA-MB-435 cells…..…..……..**72**

Figure 3.8 Effect of LPA on Taxol-induced change in mitochondrial Potential…….....**73**

Figure 3.9 Concentrated media from MDA-MB-435 cells protects against Taxol-induced apoptosis in MCF-7 cells……..…….**79**

Figure 3.10 Recombinant ATX protects against Taxol-induced apoptosis in MCF-7 cells……...…….**80**

Figure 3.11 The effect of concentrated medium from MCF-7 cells on Taxol-Induced apoptosis…….……..**81**

Figure 3.12 LPA_1 receptors have no significant effect on LPA-induced protection against Taxol-induced apoptosis in MCF-7 cells…….**83**

Figure 3.13 $LPA_{1/3}$ receptors have no significant effect on LPA-induced protection against Taxol-induced apoptosis in MCF-7 cells…….**84**

Figure 3.14 Phosphatidylinositol 3-kinase is required for LPA-mediated protection against Taxol-induced apoptosis……...……**86**

Figure 3.15 The effects of lysophosphatidate LPA on the PI3K/AKT and mitogen-ERK pathways…….**87**

Figure 3.16 The role of Taxol and LPA in controlling ceramide concentrations……...…....**88**

Figure 3.17 Effects of LPA and Taxol on cell cycle progression of MCF-7 breast cancer cells……. **90**

Figure 3.18 Lysophosphatidate does not block the entry of Taxol treated MCF-7 cells into G2/M……...…….**93**

Figure 3.19 Lysophosphatidate releases MCF-7 cells from Taxol-induced G2/M…….…….**94**

Figure 3.20 Morphology of MCF-7 cells after triple staining with DAPI, anti-phospho-histone and with anti-tubulin…….…..**95**

Figure 3.21 Lysophosphatidate releases MCF-7 cells from Taxol-induced arrest in G2/M and cell death……..**98**

Figure 3.22 LPA does not affect Taxol expulsion when Taxol is removed…..**99**

Figure 3.23 LPA does not affect Taxol expulsion when Taxol is maintained**100**

Figure 3.24 LPA does not change metabolite formation in Taxol-treated cells.....**101**

Figure 3.25 Lysophosphatidate increases the expression of glycogen synthase kinase-3 and survivin.....**104**

Figure 3.26 Inhibition of phosphatidylinositol 3-kinase or glycogen synthase-3 attenuates the expressions of survivin and phospho-survivin.**….106**

Figure 3.27 Knockdown of glycogen synthase-3 attenuates the expressions of survivin and phospho-survivin**…….……108**

Figure 3.28 Knockdown of survivin expression sensitizes MCF-7 cells to Taxol-induced G2/M arrest and cell death and decreases lysophosphatidate-induced rescue**……110**

Figure 4.1 LPA signaling pathways, which promote survival or apoptosis in different cell types **……...……114**

Figure 4.2 Schematic representation of the mechanism of autotaxin action in protecting the cells against apoptosis**…….……..117**

Figure 4.2 Schematic representation of the mechanism of lysophosphatidate action**……..……..118**

Figure 4.3 Schematic representation of the mechanism of lysophosphatidate action in releasing of the cells from mitotic arrest**.....126**

List of Abbreviations

AIF	Apoptosis inducing factor
ATX	Autotaxin
BrdU	Bromodeoxyuridine
BSA	Bovine serum albumin
CI	Combination index
cPA	Cyclic phosphatidate
DAG	Diacylglycerol
DAPI	4,6-diamidino-2-phenylindole
DETAP	Diethylenetriaminepentaacetic acid
DIALBO	direct Inhibitor of Apoptosis proteins binding protein with low pI
DISC	Death inducing signaling complex
ECM	Extracellular matrix
ER	Estrogen receptor
ERK	Extracellular signal-regulated kinases
FADD	Fas-associated Death Domain
FAK	Focal adhesion kinase
FBS	Fetal bovine serum
FDA	Food and Drug Administration
GAPDH	Glyceraldehyde 3-phosphate dehydrogenase
GFP	Green fluorescent protein
GPCRs	G protein coupled receptors
GSK-3	Glycogen synthase kinase-3
HtrA2	High temperature requirement protein A2
IAP	Inhibitor of apoptosis
IP_3	1,4,5-inositol triphosphate
LCAT	Lecithin-cholesterol acyltransferase

LDH	Lactate dehydrogenase
LPA	Lysophosphatidate
LPC	Lysophosphatidylcholine
LPP	Lipid phosphate phosphatise
Lyso PLD	Lysophospholipase D
mAb	Monoclonal antibody
MAG	Monoacylglycerol
MAPK	Mitogen-activated protein kinase
MDR	Multidrug resistance
MORFO	Modulator of oligodendrocyte remodeling and focal adhesion organization
NADH	Nicotinamide adenine dinucleotide
NGFR	Nerve growth factor receptor
NPP	Nucleotide pyrophosphatase/phosphodiesterase
PA	Phosphatidate
PAI-I	Plasminogen activator inhibitor-1
PBS	Phosphate buffered saline
PC	Phosphatidylcholine
PDE	Phosphodiester
PDGF	Platelet derived growth factor
P-gp	P-glycoprotein
PH	Pleckstrin homology
PI3K	Phosphoinositide 3-kinase
PKB	Protein kinase B
PKCß	Protein kinase Cß
PLC	Phospholipase C
PLD	Phospholipase D
PtdIns	Phosphatidylinositol

PtdIns(4)P	Phosphatidylinositol 4-phosphate
PtdIns(4,5)P_2	Phosphatidylinositol 4,5-bisphosphate
PtdIns(3,4,5)P	Phosphatidylinositol 3,4,5-trisphosphate
rATX	Recombinant autotaxin
RT-PCR	Reverse transcription polymerase chain reaction
SDS-PAGE	Sodium dodecyl sulfate polyacrylamide gel electrophoresis
SH2	Src homology 2 domain
Smac	Second mitochondria-derived activator of caspase
SMB	Somatomedin B-like
S1P	Sphingosine 1-phosphate
SPC	Sphingosylphosphorylcholine
sPLA_2	Secretory phospholipase A_2
TLC	Thin layer chromatography
TMRE	Tetramethylrhodamine ethyl ester
TNF	Tumor necrosis factor
TRAIL	TNF-related apoptosis inducing ligand
VEGF	Vascular endothelial growth factor

CHAPTER 1

INTRODUCTION

1.1 Introduction: overview

Breast cancer is the most common malignancy among women in North America and approximately one-third of these women develop metastases and die [1]. Dysregulation of normal mechanisms of apoptosis plays an important role in the pathogenesis and progression of breast cancer. Importantly, the efficacy of chemotherapy can be compromised by the survival signals that tumor cells receive. One such factor appears to be autotaxin (ATX), since there is a strong association of the expression of this protein with tumor cell growth, migration, invasion and metastasis [2-5]. ATX is a lysophospholipase that generates lysophosphatidate (LPA), a bioactive lipid molecule, from circulating lysophosphatidylcholine (LPC). Extracellular LPA is also implicated in the etiology of human cancer since it stimulates cell proliferation, differentiation, motility and survival [5-7]. However, the role of ATX and LPA in resistance against chemotherapy is not known.

To introduce the research project, in this chapter, I will first provide an overview on the domain structure and functions of ATX and describe the mechanisms that control ATX activity and LPA concentrations in the circulation. Then, I will discuss the role of ATX and LPA in tumor progression. There is also a brief description of structure, pharmacokinetics and mechanisms of action for anti cancer chemotherapy drug, Taxol, and how chemoresistance against Taxol can be developed.

1.2 Autotaxin expression and Tumor progression

1.2.1 Significance of Autotaxin in lysophosphatidate production

ATX is a 125 kDa glycoprotein that was initially isolated from human melanoma cells. ATX was originally known as an ecto-nucleotide pyrophosphatase/phosphodiesterase (NPP) [8]. Although ATX/NPP2 is able to hydrolyze nucleotides *in vitro*, it functions mainly as a lysophospholipase D (lysoPLD) that produces LPA from circulating LPC [7].

The NPP family consists of seven structurally related extracellular enzymes. ATX/NPP2 is unique because it is the only lysoPLD within the family. Two other important family members are NPP1 and NPP3. NPP1 is involved in bone matrix mineralization by generating pyrophosphate, an inhibitor of calcification. NPP3 promotes differentiation and invasion of glial cells [9]. The functions of NPP4 and NPP5 are unknown. NPP6 and NPP7 are choline-specific phospholipases C. NPP6 converts LPC into monoacylglycerol (MAG) and phosphocholine, but it can also hydrolyze glycerophosphorylcholine and sphingosylphosphorylcholine (SPC). NPP7 is known as alkaline sphingomyelinase which hydrolyzes sphingomyelin to generate ceramide in the intestinal tract to protect the mucosa from inflammation and tumorigenesis [10,11].

The major physiological substrate for ATX is LPC. LPC is abundantly present in plasma and serum at more than 200 μM in a predominantly albumin-bound form [12]. Plasma LPC is synthesized mainly by lecithin-cholesterol

acyltransferase (LCAT), which catalyzes the transesterification of phosphatidylcholine (PC) and free cholesterol. LPC generated by LCAT is mainly saturated since LCAT preferentially transfers the fatty acid from position-2 of PC. The liver secretes mainly unsaturated LPC, which is presumably synthesized by a phospholipase A_1 [13]. LPC is also detected in conditioned media from tumor cells [2]. In addition to LPC, ATX can also hydrolyze SPC to produce sphingosine 1-phosphate (S1P) [7] However, the significance of the SPC to S1P conversion by ATX *in vivo* is debatable [11].

LysoPLD purified from human plasma can hydrolyze three classes of LPC: acyl>alkyl>alkenyl [14]. PC with two saturated medium-length acyl substitutes, but not *sn*-glycero-3-phosphocholine or PCs with two saturated short- or long-chain acyl groups, can be utilized by human plasma lysoPLD. Of the saturated acyl-LPCs, *sn*-1-14:0 LPC is the best substrate; among C18-LPCs, unsaturated species are better substrates than saturated ones [15]. Compared with *sn*-1-20:4 LPC, *sn*-2-20:4 LPC is a better substrate for lysoPLD. When Co^{2+} was added to the reaction, it shifted the optimal chain lengths of saturated acyl-LPC and -PC from 14 to 12 and from 10 to 8, respectively. Co^{2+} also promoted lysoPLD activity toward all acyl-LPCs except 18:2-LPC. This ineffectiveness of Co^{2+} on the lysoPLD activity for 18:2 LPC, together with the higher affinity of serum lysoPLD activity for 18:2 LPC, may indicate that the lysoPLD that acts on 18:2 LPC is a unique isoform [16].

1.2.2 Structure and function of autotaxin

ATX has a domain structure consisting of two N-terminal somatomedin B-like (SMB) domains, a central catalytic phosphodiester (PDE) domain and a C-terminal nuclease-like domain (Figure 1.1 A) [9,10].

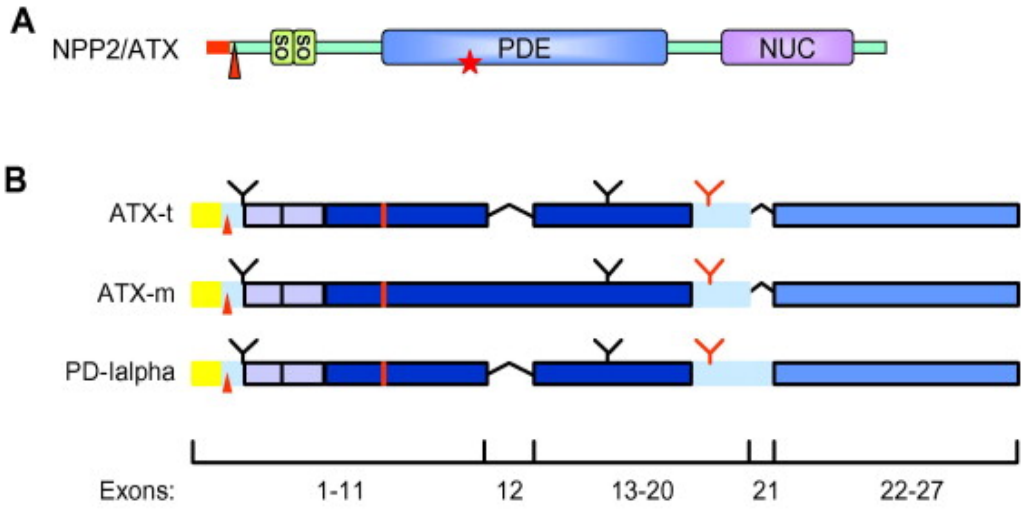

Figure 1.1 Domain structure and isoforms of ATX/NPP2. A) ATX consists of a N-terminal signal peptide (red) with a furin cleavage site (red arrow). Two SMB domains (SO) are followed by a large catalytic domain (PDE) containing a conserved Thr residue (T210). T210 residue is essential for catalyic activity of ATX (red star). NUC shows the C-terminal nuclease-like domain. **B)** Spliced isoforms of ATX. ATX-t is the teratocarcinoma isoform, which is identical to plasma lysoPLD and is widely expressed. ATX-m is the melanoma isoform, containing a 52-AA insertion in the catalytic domain. PDI-alpha is 'brain-specific' isoform which has a 25-AA insertion just before the NUC domain. Sites for N-glycosylation (Y) and furin cleavage (red arrow) are indicated. Red Y indicates the N542-linked glycan that is essential for catalytic activity. The figure adopted from Callewaert [17].

It has been suggested that sequences in all three domains together comprise a lysophospholipid-binding pocket. The SMB domains are rich in Cys residues that play a key role in forming intramolecular disulfide bridges rather

than ATX homodimers [10]. The SMB domain of vitronectin is an extracellular matrix protein that interacts with plasminogen activator inhibitor-1 (PAI-I) [18]. The second SMB domain of ATX contains an RGD motif that is known to bind integrins.

The central catalytic domain of ATX (approximately 400 amino acids) is structurally unrelated to that of the classic phospholipases. This domain has been predicted to fold similarly to the catalytic domain of alkaline phosphatases [10,19]. Sequence comparison with alkaline phosphatase suggested that the NPP catalytic mechanism is similar and occurs in two steps. In the first step the activated OH group of key residue (T210 in ATX) attacks the phosphate group of the substrate (LPC), resulting in the formation a phosphate ester linkage. Then, the intermediate is attacked and LPA released (together with free choline, in case of ATX) [10].

The C-terminal domain of ATX is structurally related to DNA and RNA non-specific endonucleases, but it lacks the key residues required for enzymatic activity. Mutagenesis experiments suggest that an intact nuclease-like domain is needed for proper folding, subcellular localization and secretion of ATX [10,20]. At the C-terminal end, the modulator of oligodendrocyte remodeling and focal adhesion organization (MORFO) domain entails the nuclease-like domain, which is probably catalitically inactive. The MORFO domain play a key role in non-catalytic activity of ATX through binding to a unknown cell surface receptor [21].

ATX also has an N-terminal hydrophobic domain, which functions as a signal peptide. Full-length ATX is processed as a pre-pro-enzyme by cleavage of the signal peptide followed by a second furin-mediated cleavage. It traffics along the classical export pathway and is secreted as an active glycoprotein [22-24]. ATX is N-glycosylated on three sites (N52, N410 and N524) (Figure 1.1 B). The glycosylation of N524, a conserved residue in the catalytic domain, is essential for the catalytic activity of ATX. The N542-linked glycan is hidden inside the folded protein to provide a structural function, probably by stabilizing the interaction between the catalytic and nuclease-like domain of ATX [17].

ATX has at least three different isoforms (Figure 1.1 B). The shortest form, having 863 amino acids, was initially cloned from a teratocarcinoma cell line and is the predominant isoform (ATXt) [25]. It is identical to plasma lysoPLD. The melanoma-derived isoform (ATXm; 915 amino acids) contains a highly basic insertion (52 residues) in the catalytic domain [26]. The brain-specific isoform (originally termed PD-1alpha) is low frequent isoform that expressed mainly in oligodendrocytes and contains a 24-residue insertion close to nuclease-like domain [27]. The catalytic activities, substrate preferences or extracellular localizations of different isoforms are still unknown.

ATX has also non-catalytic activity through the MORFO domain, a novel functionally active domain. The MORFO domain is located at the C-terminal end of the protein and functions independently of enzymatic activity of ATX. The MORFO domain antagonizes adhesion of oligodendrocytes to extracellular matrix

molecules such as fibronectin in an active and pertussis toxin-sensitive manner. This domain also facilitates morphological maturation of oligodendrocytes. Therefore, ATX functions as a matricellular protein that mediates an intermediate adhesive state and interfere in cellular remodeling [28]. The MORFO domain was found to promote dephosphorylation at the Tyr 925 residue of focal adhesion kinase and to stimulate redistribution of paxillin, a focal adhesion-associated adaptor protein, and α-actinin away from focal adhesion complexes. The effect on paxillin distribution can be mimicked by a peptide representing the EF hand loop region, suggesting that the EF hand-like motif is sufficient and necessary for this effect of MORFO domain [29,30]. Focal adhesions are multi-molecular signaling complexes that establish a link between the actin cytoskeleton and the extracellular matrix. For controlled cellular remodeling, focal adhesions have to undergo constantly high rate turnover, which leads to a reduction in the efficiency of the linkage between the extracellular matrix and cytoskeleton. ATX by its MORFO domain regulates focal adhesion dynamics, thereby enabling the establishment of a complex and expanded process network by oligodendrocytes (Figure 1.2) [31].

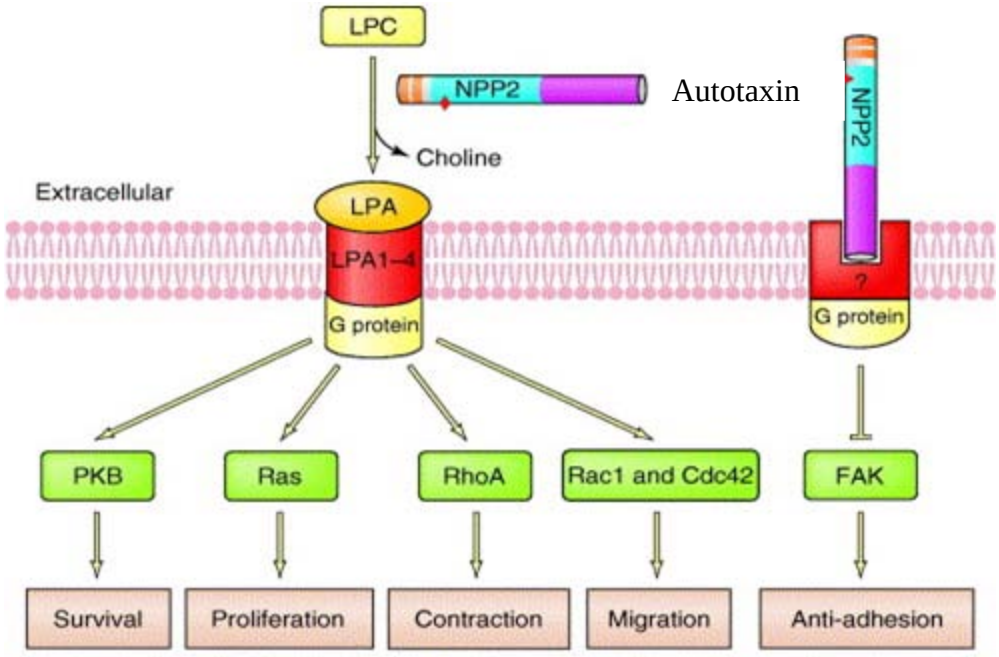

Figure 1.2 Catalytic and non-catalytic activites of autotaxin (NPP2). Autotaxin (ATX) generates LPA from LPC. LPA interacts with specific G-protein coupled receptors and activates multiple signaling pathways followed by stimulation of the survival, proliferation, contraction and migration of the cell. PKB (Akt) promotes survival by the phosphorylation and inactivation of the pro-apoptotic proteins. Ras stimulates cell proliferation by increasing signaling by MAP kinases. RhoA stimulates the reorganization of the actin cytoskeleton. Rac1 and Cdc42 promote cell migration through the formation of lamellipodia and filopodia, respectively. ATX also has non-catalytic activities: the nuclease-like domain of NPP2 interacts with unknown G-protein-coupled receptor, leading to the dephosphorylation of FAK and loss of components from the focal adhesions. Abbreviations: FAK, focal adhesion kinase; LPA, lysophosphatidate; LPA1–4, LPA receptors 1–4; LPC, lysophosphatidylcholine; PKB, protein kinase B. The figure adopted from Stefan [10].

1.2.3 Regulation of autotaxin activity and lysophosphatidate production

There is constitutively active ATX with abundant substrate, LPC, in plasma. However, the plasma level of LPA is relatively low. One mechanism that counteracts LPA accumulation is the degradation of newly produced LPA by cell-associated or soluble phosphates. Another mechanism is suggested by the finding

that ATX is inhibited by its products LPA and S1P [24]. LPA and S1P inhibit ATX function by reducing in V_{max} and an increase in K_m. This implies that inhibition of ATX results from a combination of a decreased turnover and decreased affinity of the active site for its substrates. The inhibition constant (K_i) for LPA and S1P is almost 1000-fold lower than the K_m for LPC, indicating that ATX binds LPA and S1P much more strongly than it binds its physiological substrate [11].

The inhibitory effect of LPA and S1P is specific for ATX. Maximal inhibition of ATX is induced by long-chain LPA (18:1, 16:0 and 14:0), whereas short-chain LPA (6:0) has no effect. The requirement of a long acyl chain suggests that LPA and S1P directly interact with a hydrophobic pocket on ATX [24]. The observed inhibition of ATX by S1P suggests that changes in extracellular S1P levels may affect LPA production and signaling. In circulation, the S1P concentration is significant (0.1 μM). Therefore, ATX activity in plasma can be permanently suppressed by S1P under basal conditions. Cyclic PA (1-acyl-*sn*-glycerol-2,3-cyclic phosphate; cPA) is a naturally occurring LPA analog which also inhibits ATX activity without activating LPA receptors [32].

1.2.4 Role of autotaxin in tumor development

Tumor progression and metastasis is the main cause of death among cancer patients. The process of tumor metastasis is very selective and includes a series of sequential steps. A tumor cell that initiates a metastatic process must detach from the primary mass, invade the local tissue stroma, penetrate local lymphatic and

blood vessels, survive within the circulation, become captured in capillaries of distant organs, penetrate the corresponding parenchyma, settle in to the new microenvironment and divide to form the new tumor (Figure 1.3) [33].

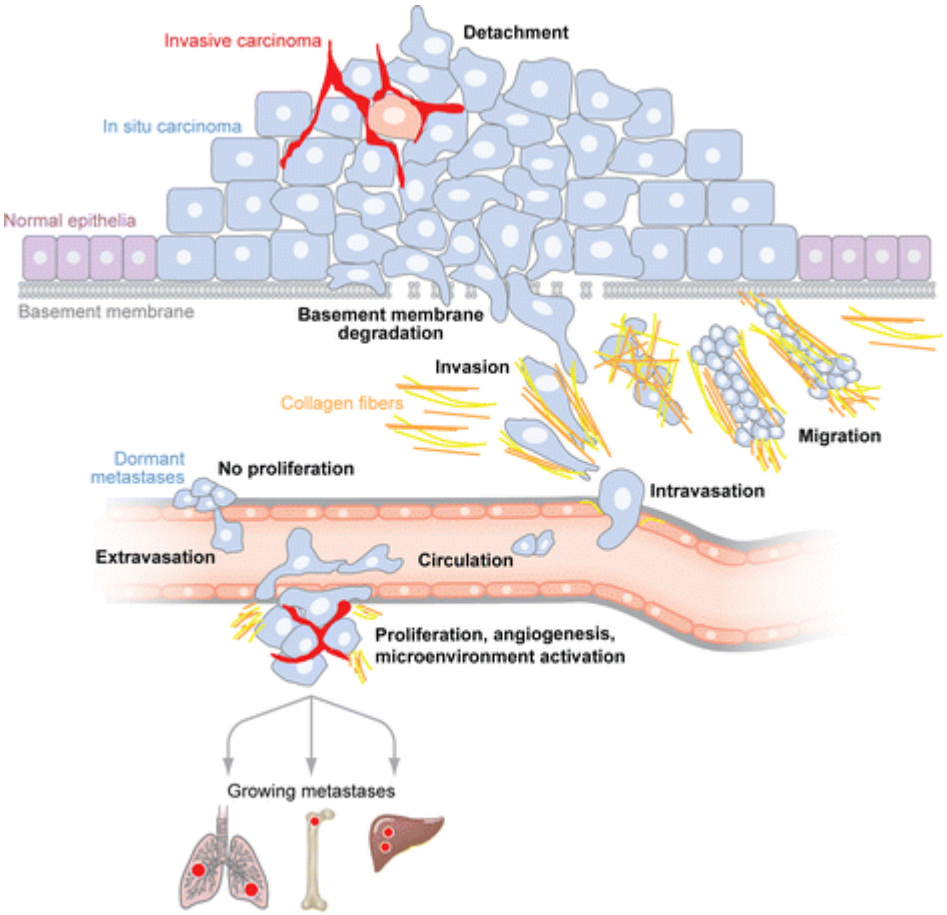

Figure 1.3 Principal steps in metastasis. Alteration of normal epithelial cells leads to carcinoma in situ, which, as a result of loss of adherens junctions, develops gradually to the invasive carcinoma stage. After degradation of basement membrane, tumor cells invade the surrounding stroma, migrate into blood or lymph vessels and circulate until they arrest in the capillaries of a distant organ. The figure adopted from Bacac [34].

To successfully complete the sequence of events for metastasis, tumor cells need to be able to interact with local microenvironment, migrate, invade, resist apoptosis, and induce angiogenesis. These functions are regulated by two distinct mechanisms: adhesion and proteolysis, which verify tumor cell interaction with other cells and with the extracellular matrix (ECM). These mechanisms also facilitate tumor cell migration, stimulate angiogenesis, and activate survival signals [34].

Malignant cells directly secrete a variety of proteins that include growth factors and extracellular proteinases or promote the host cells to produce bioactive molecules that are able to degrade the matrix and its component adhesion molecules. The matrix degradation takes place in tumor cell surface that the amount of the active degradative enzymes is higher than the natural proteinase inhibitors present in the matrix or that secreted by normal cells. Then, proteins secreted by tumor cell into the extracellular matrix are involved in cell adhesion, motility, intercellular communication and invasion [35].

The outcome of metastasis is determined by multiple interactions of metastatic cells with tumor microenvironment. At primary metastatic sites, malignant cells interact with host cells including endothelial cells, pericytes, epithelial cells, fibroblasts, myoepithelial cells and leukocytes. The microenvironment of cancer cells also provides the necessary signals that turn on variety of different transcription factors [36].

There is a strong association of ATX expression with tumor progression [6]. The role of ATX in tumor development depends on the non-catalytic effects of ATX on cell adhesion, or the catalytic activity of ATX, which converts LPC into LPA in tumor microenvironment (Figure 1.2). ATX was originally identified as a tumor cell motility factor. Secreted ATX also was mainly considered for the increased motility of human MDA-MB-435 tumor cells following α6β4 integrin overexpression [37]. ATX over expression in Ras-NIH3T3 cells promotes tumor aggressiveness, metastasis and angiogenesis in nude mice [3]. ATX also protects NIH3T3 fibroblasts against apoptosis upon serum deprivation [38]. ATX is overexpressed in several human cancers including glioblastoma, lung, breast cancer, renal cell carcinoma, neuroblastoma, thyroid carcinoma and Hodgkin lymphoma [6]. Highest ATX expression is detected in Glioblastoma Multiforme, a very malignant cancer with a high infiltration rate [39]. ATX stimulates glioblastoma cell motility, which is also dependent upon LPC concentrations and the presence of functional LPA receptors [40]. Furthermore, ATX expression is increased in the stromal cells from prostate carcinoma patients [41]. ATX expression is strongly upregulated by the v-Jun oncogene [42] and the α6β4 integrin, through the transcription factor NFAT1, which binds to the ATX promotor at two distinct sites [37]. ATX is down-regulated by CST6, a tumor suppressor gene for breast cancer [43]. Induction of ATX expression by the Epstein-Barr virus promotes the growth and survival of Hodgkin lymphoma cells and specific knockdown of ATX decreases LPA levels and attenuates cell growth and viability [44]. In lymphoma tissues, ATX expression is mainly restricted to

CD^{30+} anaplastic large-cell lymphomas and EBV-positive Hodgkin lymphoma [44]. Expression of ATX in mammary epithelium of transgenic mice is sufficient to induce a high frequency of late-onset, estrogen receptor-positive, invasive, and metastatic mammary cancer [45]. ATX also promotes the expression of matrix metalloproteinase-3 by activating of the mitogen-activated protein kinase (MAPK) cascade in human fibrosarcoma [46].

There are different explanations for the role of ATX in tumor cell survival, growth and migration. First, the expression of ATX is closely linked to the invasiveness of breast cancer cells [4]. Combination of ATX expression with Ras transformation produces NIH3T3 fibroblasts with greatly amplified tumorigenesis and metastatic potential compared to Ras-transformed controls [3]. Furthermore, ATX strongly stimulates motility in human coronary artery smooth muscle cells, proliferation in human endothelial cells and motility in human coronary artery smooth muscle cells suggesting that ATX contributes to the metastatic cascade through stimulating angiogenesis [47]. Furthermore, rATX, particularly in the presence of LPC, dramatically increases motility and proliferation of melanoma, breast cancer cells, ovary-derived fibroblast and hepatoma cells [2]. ATX also stimulates cell motility of MDA-MB-231 breast cancer , PC-3 prostate cancer and A-2058 melanoma cells [48]. ATX increases the proliferation and migration of thyroid carcinoma cells and also affects the angiogenic potential of thyroid carcinoma cells [49]. Inhibition of ATX production or activity blocks LPC-induced migration of MDA-MB-231 breast cancer and MDA-MB-435 melanoma cells [5]. In prostate cancer, high expression levels of ATX are associated with

both malignant potentials and poor outcomes [50]. Serum ATX is high in patients with hepatocellular carcinoma and this may be due to hepatic fibrosis from which hepatocellular carcinoma often arises [51]. Expression of ATX or LPA receptors in mammary epithelium of transgenic mice is sufficient to induce a high frequency of late-onset, estrogen receptor (ER)-positive, invasive, and metastatic mammary cancer [45].

1.3 Extracellular lysophosphatidate and tumor progression

1.3.1 The biologic role of extracellular lysophosphatidate

LPA is the simplest biologically active lipid phosphate. It is composed of a glycerol backbone, a phosphate group and a single acyl-chain in either the *sn-1* or *sn-2* positions (Figure 1.4).

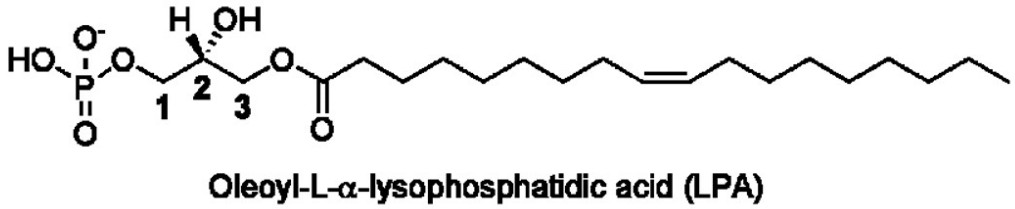

Figure 1.4 Chemical structure of Lysophosphatidate

Serum is a rich source of bioactive LPA with concentrations of up to 10 μM, as other body fluids such as plasma, saliva, follicular fluid and malignant effusions. In serum, LPA predominantly binds to albumin [12]. Extracellular LPA is produced by activated platelet, injured corneal tissue, neurones, adipocytes and tumor cells. There are at least two different metabolic pathways postulated for the production of LPA. The first pathway is predominant in serum and plasma, and

involves the conversion of circulating LPC to LPA by ATX as the predominant lysoPLD (Figure 1.5 A). In platelets and certain cancer cells, the second pathway occurs with the hydrolysis of phosphatidate (PA) by secretory phospholipase A_2 ($sPLA_2$) to produce saturated LPA in microvesicles. These microvesicles are discarded from cells during inflammation and platelet aggregation [52] (Figure 1.5 B). This combined regulation of ligand and receptor distribution, in addition to the diversity of second messenger activation, provides a wide range of biological roles for LPA signaling in different tissues and developmental stages.

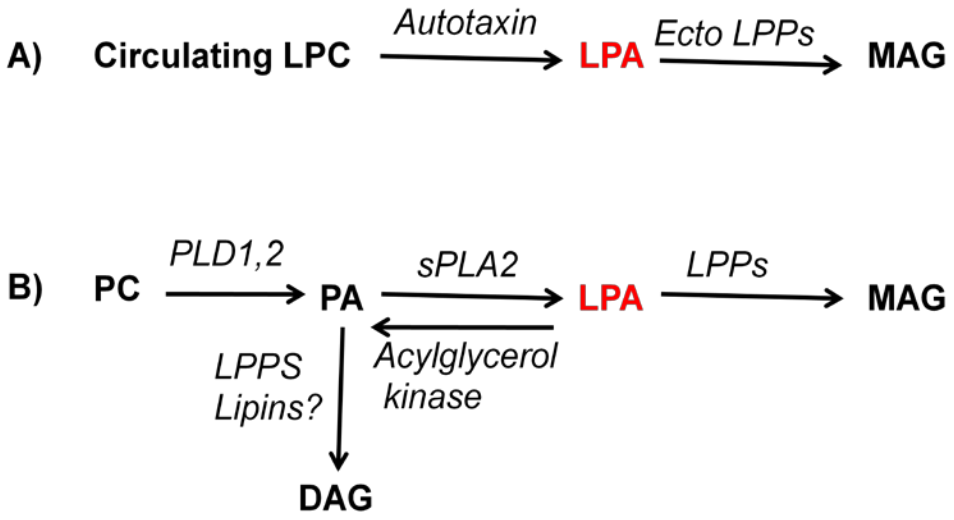

Figure 1.5 Synthesis and degradation of LPA in serum. **A**) In serum, lysophosphatidylcholine (LPC) is metabolized by autotaxin (ATX) to lysophosphatidate (LPA), which is converted to monoacylglycerol (MAG) by the ecto-activities of the lipid phosphate phosphatases (LPPs). **B**) In activated platelets, LPA is also generated by secretory phospholipase A_2 (PLA2) from phosphatidate (PA).

1.3.2 Role of lipid phosphate phosphatases in lysophosphatidate degradation

Extracellular LPA is degraded through dephosphorylation to MAG by lipid phosphate phosphatases (LPPs). Mammalian LPPs are known as Mg^{2+}-independent and *N*-ethylmaleimide-insensitive phosphatidate phosphatases (PAP2). There are three LPPs (LPP1, LPP2, and LPP3) and a splice variant (LPP1a), which hydrolyze lipid phosphates, including PA, LPA, sphingosine 1-phosphate, ceramide 1-phosphate, and diacylglycerol (DAG) [7]. The LPPs belong to a phosphatase/phosphotransferase family that includes S1P phosphatases, glucose 6-phosphatase, and the sphingomyelin synthases. LPPs have six transmembrane domains, three conserved active site domains, and a glycosylation site on the hydrophilic loop between the first and second active site domains. The active sites are located on the outer surface of plasma membranes or the lumenal surface of internal membranes. Mammalian LPPs form homo- and hetero-oligomers, which are catalytically active compared with the monomeric forms [52]. Lipid phosphates are potent mediators of cell signaling and control variety of different functions including cell migration and division, blood vessel formation, wound repair, and tumor progression [52]. LPPs regulate circulating concentrations of LPA or S1P. Increased expression of LPP1 in ovarian cancer cells increases LPA degradation, decreases cell proliferation and colony-formation, and increases cell death. Decreased LPP activities occur in tumors, and this has been proposed as a mechanism that results in increased LPA-induced growth in ovarian cancers [53]. It has been shown that LPP1 degrades

extracellular LPA in vivo [54]. Another function of ecto-LPP is that dephosphorylated products readily enter cells. The uptake of MAG following LPA dephosphorylation enhances intracellular LPA production by acylglycerol kinase (Figure 1.5B) [7]. LPP1 overexpression in fibroblasts attenuated LPA-induced activation of extracellular signal-regulated kinases (ERK), phospholipase D (PLD), Ca^{2+} transients, and cell division [55]. Increased ecto-LPP-1 activity also decreased LPA production by platelets and LPA-induced shape changes and aggregation [56]. Ecto-LPP activities regulate extracellular LPA accumulation and proliferation of preadipocytes [57]. These studies establish a role for the ecto-LPP activities in regulating cell signaling.

1.3.3 Lysophosphatidate and G protein coupled receptors

LPA interacts distinctively with specific G protein coupled receptors (GPCRs) that mediate a wide variety of biological effects including cell proliferation [58], cell survival [59], cell migration [5,60] and platelet aggregation [61,62]. GPCRs are the largest family of transmembrane receptors and represent targets of many therapeutics [63]. Diverse actions of LPA are mediated by at least eight G-protein coupled receptors present on the cell surface: LPA_1/EDG2, LPA_2/EDG4, LPA_3/EDG7, LPA_4/GPR23/p2y9, LPA_5/GRP92, LPA_6/GPR87, LPA_7/p2y5, and LPA_8/p2y10 [64-66]. It is also clear that termination of LPA signaling is regulated primarily at the receptor level through receptor desensitization and internalization [11]. Among the eight LPA receptors, LPA1, LPA2 and LPA3 are members of the endothelial differentiation gene (EDG) family [67]. The expression of these receptors is cell specific, enabling different cells to respond in a unique manner

through signaling pathways that are activated by G proteins including $G_{i/o}$, G_s, G_q and $G_{12/13}$ (Figure 1.6).

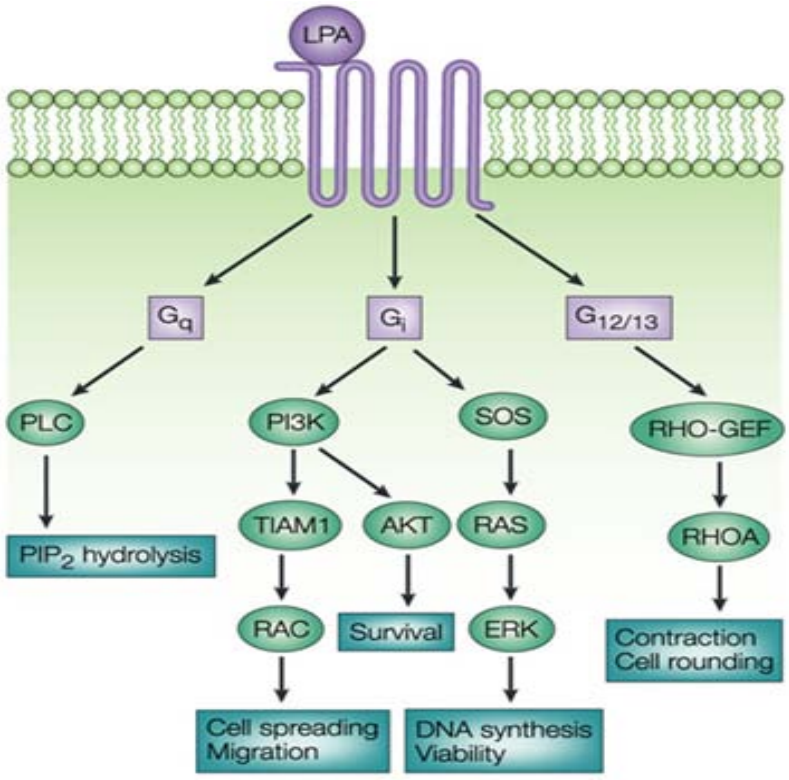

Figure 1.6 LPA signaling pathways mediated by GPCRs and LPA receptors. LPA receptors activate diverse second messenger pathways through the coupling of heterotrimeric G-protein. This figure shows examples of the signaling proteins and the pathways they mediate to produce an effect on cell function. The figure adopted from Mills [6].

G-protein coupled receptors (GPCRs) are integral membrane proteins, consisting of a single polypeptide chain with seven transmembrane domains. They control variety of physiological functions by mediating the signal of different stimuli such as peptide hormones, neurotransmitters, neuropeptides, autocrine factors and even photons. The ligand transmits its activity to an intracellular signal through activation of a heterotrimeric guanosine triphosphate-binding

protein (G-protein) by the receptor. The dissociation of α– from βγ– subunits results in a wide range of downstream intracellular signals leading to both short-term effects (e.g. changes in intracellular Ca^{2+} levels) and long-term effects (e.g. gene transcription). GPCRs are a very important class of therapeutic targets for the pharmaceutical industry and nearly half of the drugs currently in use act on these receptors for example ß-adrenoreceptor antagonists for treatment of hypertention. GPCRs also interact with a wide range of other proteins with potential roles specifically in receptor biosynthesis, distribution, signaling, desensitization, clustering, internalization, trafficking and degradation [68].

Activation of $G_{i/o}$ decreases cAMP concentrations and induces Ras-dependent signaling leading to the activation of ERK pathway. These signals are associated with cell proliferation. $G_{i/o}$ also activates phosphatidylinositol 3-kinase (PI3K), which is an effector for cell migration, and survival [69].

Three classes of PI3Ks have been defined on the basis of their molecular structure and substrate specificity. The class I enzymes use phosphatidylinositol (PtdIns), phosphatidylinositol 4-phosphate (PtdIns(4)P) and phosphatidylinositol 4,5-bisphosphate ($PtdIns(4,5)P_2$) as substrates to produce PtdIns(3)P, $PtdIns(3,4)P_2$ and phosphatidylinositol 3,4,5-trisphosphate ($PtdIns(3,4,5)P_3$), respectively. Class I PI3Ks are all heterodimers containing a 110-kDa catalytic subunit and a regulatory subunit (p85 or p101). Four isoforms of the catalytic subunits have been characterized (p110α, β, γ and δ) and divided into two subclasses (A and B) depending on the type of regulatory subunit. Class I_A

includes p110α, β and δ associated with a p85 regulatory subunit that contains Src homology 2 (SH2) domains. When the p85 SH2 domains are bound to the phosphorylated Tyr–X–X–Met motif interacted with receptor or adapter proteins, the p110/p85 heterodimers are activated downstream of tyrosine kinases. Class I_B is represented by the catalytic subunit p110γ associated with a p101 regulatory subunit that has no homology with any known protein but causes p110γ to be directly activated by G protein βγ subunits (Figure 1.7) [70,71].

Class II enzymes phosphorylate PtdIns and PtdIns(4)P and contain a C2 domain related to a Ca^{2+}-binding motif. The regulation and function of these PI3Ks are still poorly understood. Class III PI3Ks can only phosphorylate PtdIns. They contribute to membrane trafficking through an interaction between PtdIns(3)P and FYVE domain present on trafficking proteins [72]. The lipid products of PI3Ks are important in PI3K membrane targeting or modulation of PI3K activity by interacting with a number of signaling proteins. PtdIns(3,4,5)P_3 binds to a conserved protein motif called the pleckstrin homology (PH) domain, followed by inducing the activation of the serine/threonine kinase Akt/protein kinase B (PKB) and its upstream activators, the phosphoinositide-dependent kinases (PDK). These kinases phosphorylate a number of substrates involved in the control of cell proliferation and survival.

Other targets of PI3K lipid products are the non classical protein kinase C isoforms. The cloning of p110γ has defined a novel type of PI3K potentially involved in GPCR-induced responses. In kidney cells, LPA can activate the

production of PtdIns(3,4)P_2 and PtdIns(3,4,5)P_3 as strong as protein growth factors [73]. PI3K activation is an important part of LPA signaling in different cellular systems. For example, in NIH3T3 fibroblasts, LPA activates both PI3K and Akt (PKB), and inhibition of this pathway prevents LPA-induced DNA synthesis [74]. In Schwann cells, activation of a PI3K/Akt pathway by LPA promoted survival signals [59]. The $G_{i/o}$-dependent activation of PI3K/Akt pathway is involved in growth and survival of PC12 rat pheochromocytoma [75] and PC-3 prostate cancer cells [76]. In platelets, activation of Akt is dependent on Gi, but not Gq or G12/13 [77].

$G_{12/13}$ is associated with activation of Rho and Cdc2 and involves cytoskeletal responses, such as stress fiber formation, cell rounding, neurite retraction and wound healing. Rho stimulates cell proliferation [78]. $LPA_{1,2,3}$ are coupled to $G_{i/o}$ and $G_{12/13}$, and both $LPA_{1,2}$ is coupled to $G_{12/13}$, which can activate Rac and Rho, cytoskeletal responses that control cell shape changes required for cell migration. Rac activation leads to membrane ruffling and production of lamellipodial protrusions at leading edge of migrating cells. Rho activation induces cell rounding, dissolution of old cell adhesion and regulates the correction and retraction forces observed at trailing edges. This suggests that the activation of $G_{i/o}$ and $G_{12/13}$ by LPA_1, LPA_2 and/or LPA_3 receptors [79,80].

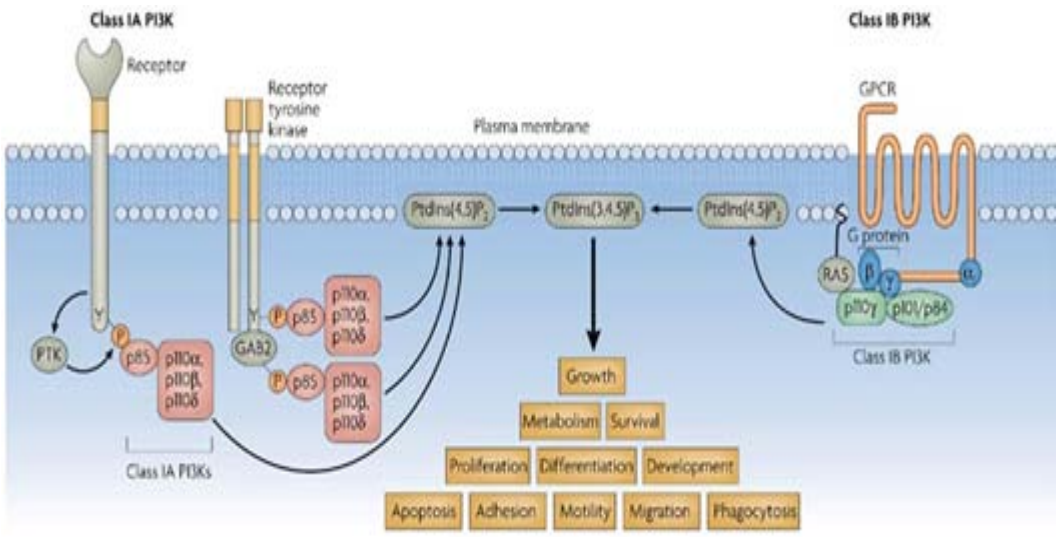

Figure 1.7 Activation of phosphoinositide 3-kinases pathway. After cell stimulation, class I PI3Ks are recruited to the inner face of the plasma membrane and generate phosphatidylinositol-3,4,5-trisphosphate (PtdIns(3,4,5)P_3) by direct phosphorylation of phosphatidylinositol-4,5-bisphosphate (PtdIns(4,5)P_2). Class IA phosphoinositide 3-kinases (PI3K) isoforms (p110α, p110ß and p110δ) bind directly or indirectly to receptors through the interaction of their regulatory subunits (p85) with tyrosine-phosphorylated motifs on the receptor cytoplasmic domains or soluble adaptor proteins such as GAB2. The only class IB PI3K isoform is recruited to G-protein-coupled receptors (GPCRs) by direct interaction with G-protein ßγ subunits, through both the catalytic p110 and the regulatory subunits. RAS, in its active GTP-bound state, also binds directly to the p110γ subunit of PI3Kγ further regulating its catalytic activity. Activation of all class I PI3Ks leads to the generation of the lipid second messenger PtdIns(3,4,5)P_3 at the cell membrane, which serves as surface for pleckstrin-homology-domain-containing proteins (such as AKT, also known as PKB) to bind. This leads to a cascade of phosphorylating events and protein–protein interactions of downstream targets to control multiple biological processes. PTK, protein tyrosine kinase. The figure adopted from Rommel [81].

G_q activation causes activation of the phospholipase C pathway and an increase in cytosolic Ca^{2+} and activation of protein kinase Cß (PKCß) via 1,4,5-inositol triphosphate (IP_3) synthesis. Then, the increased Ca^{2+} concentration down-regulates the G_s-mediated cAMP pathway [82]. Increase in the cytoplasmic free Ca^{2+} concentration provides a significant stimulus for vascular smooth

muscle cells contraction and growth [83]. Platelet derived growth factor (PDGF)-stimulated activation of PLCγ_1 results in IP_3 production and stimulation of intracellular Ca^{2+} release with the associated activation of calcium Ca^{2+}-dependent proliferative proteins such as cAMP-responsive element binding protein [84]. Both PLCγ_1 and PI3K have been shown to be necessary for PDGF-stimulated vascular smooth muscle cell migration and proliferation [85]. Ca^{2+} transients have been shown to be necessary for PDGF-induced vascular smooth muscle cell chemotaxis [86]. Ca^{2+} transients also play a significant role in vascular smooth muscle cell migration in response to serum and after injury [87]. It has been shown that constitutively active alpha subunits of G_q and $G_{12/13}$ families inhibit activation of the pro-survival Akt signaling cascade [88]. Activation of Gq/phospholipase C (PLC) pathway also stimulates cardiac hyperthrophy by increasing in cytosolic Ca^{2+} and activation of PKC [89].

Glycogen synthase kinase-3 (GSK-3) is another downstream target for PI3K/Akt signaling pathway that regulates variety of different cellular functions including glycogen metabolism, morphogenesis and cell proliferation [90]. GSK-3 also regulates microtubule assembly and stabilization by controlling the expression and phosphorylation of microtubule-binding proteins [91-93]. Mammalian GSK-3 exists as two isoforms encoded by two distinct genes, GSK-3α (51 kDa) and GSK-3β (47 kDa) [94] with two splice variants of GSK-3β [95,96]. The activity of GSK-3 is controlled by phosphorylation and interaction with inhibitory proteins. GSK-3 is constitutively active and is inactivated by extracellular signals through phosphorylation of an N-terminal serine residue, Ser-

9 in GSK-3β and Ser-21 in GSK-3α. Different kinases have been implicated in mediating serine phosphorylation and inactivation of GSK-3 including PI3K/Akt, protein kinase A and protein kinase C [97-99]. GSK-3 activity is increased by phosphorylation of a tyrosine residue, Tyr-216 in GSK-3β and Tyr-279 in GSK-3α through the Ca^{2+}-sensitive tyrosine kinase, Pyk2, as a direct consequence of PLC activation [100]. The GSK-3 pathway has a critical role in the expression and phosphorylation of microtubule regulatory proteins including survivin [93].

1.3.4 Role of lysophosphatidate in tumor development

Extracellular LPA is implicated in the etiology of human cancer since it stimulates cell growth, proliferation, differentiation, motility and survival [6,7]. LPA levels are high in ascites fluid and plasma of patients with ovarian tumors [6,58,101]. LPA promotes ovarian tumor development through increased cyclin D expression [102]. LPA also increases vascular endothelial growth factor production, which stimulates angiogenesis [103]. In a colon cancer cell line, LPA increases the synthesis of macrophage migration inhibitory factor, which promotes tumor growth [104]. LPA stimulates cell migration, invasion, colony formation, tumorigenesis and metastasis of mouse ovarian cancer in immunocompetent mice [105]. LPA production is believed to promote prostate cancer development and progression via a pro-inflammatory milieu [106]. LPA-induced breast cancer cell migration and invasion is Ral GTPases/beta-arrestin dependent [107]. LPA-stimulated cell growth is mediated by Gi- and Rho-dependent pathways in ovarian cancer cells [108]. LPA-mediated transcriptional changes in at least 39 genes in the human epithelial ovarian tumor

microenvironment, influence tumor progression through modulation of cell adhesion molecules like claudin-1. This LPA-mediated expression signature is associated with poor prognosis in ovarian cancer patients [109]. LPA also induces IL-8 expression by a nuclear factor-kappaB-dependent signal pathway through LPA_1/G_i receptor [110]. LPA promotes gastric cancer migration and invasion through neuroepithelial cell transforming gene-1 and RhoA activation [111]. LPA through activation of LPA receptors decreases the abundance of the p53 tumor suppressor, thereby promoting cell survival and cell cycle progression [112].

Diverse biological action of LPA is dependent on the specific activation of different LPA receptors. Expression of $LPA_{1,2,3}$ receptors in mammary epithelium of transgenic mice is sufficient to induce a high frequency of late-onset, estrogen receptor (ER)-positive, invasive, and metastatic mammary cancer [45]. $LPA_{1,2,3}$ play a key role in cellular motility of prostate cancer cells [113]. Applying antagonist against LPA_1 receptor in cancer cells blocks the production of tumor-derived cytokines that are potent activators of osteoclast-mediated bone destruction and reduces the progression of osteolytic bone metastases [114]. LPA_2 receptor and Gi/Src pathway mediate cell motility through cyclooxygenase 2 expression in ovarian cancer cells [115]. LPA_2 also mediates LPA-stimulated endometrial cell invasion and the subsequent activation of MMP-7 [116]. Expression of $LPA_{2,3}$ receptors during ovarian carcinogenesis contributes to ovarian cancer aggressiveness [117]. LPA stimulates the proliferation and motility of malignant pleural mesothelioma cells through $LPA_{1,2}$ receptors [118]. The

absence of LPA_2 receptor attenuates tumor formation in colitis-associated cancer by reducing number of tumors, epithelial cell proliferation, mucosal damage and infiltration by macrophages. Loss of function of LPA_2 receptor also attenuated beta-catenin, Krüppel-like factor 5, and cyclooxygenase-2 expression in colitis-associated cancer progression in vivo [119]. The unique CXXC motif of LPA_2 is responsible for the binding to TRIP6 and Siva-1, and disruption of these macromolecular complexes or knockdown of TRIP6 or NHERF2 expression attenuates LPA_2-mediated protection from chemotherapeutic agent-induced apoptosis [120]. Malignant ascites from pancreatic cancer patients has been reported to stimulate migration of pancreatic cancer cells through LPA and LPA_1 receptors but in these cells, LPA_2 receptors are coupled to the $G_{12/13}$/Rho-signaling pathway, leading to the inhibition of EGF-induced migration and invasion [121].

LPA has critical role in protecting the cells against apoptosis. LPA promotes fibroblast survival largely by G_i-mediated activation of ERK1/ERK2 [74]. LPA rescues intestinal epithelial cells from radiation- and chemotherapy-induced apoptosis through $LPA_{1,2}$ receptors [122]. LPA promotes survival of androgen-insensitive prostate cancer cells by activation of nuclear factor-kappaB [123]. LPA also protects epithelial ovarian cancer from immune cell attack and the induction of apoptosis by cytoskeleton disrupting reagents [124]. Colon cancer cells are protected from apoptosis by LPA through LPA_2 receptor and by involvment of Erk, Bad, and Bcl-2 [125]. LPA induces the expression of **v**ascular endothelial growth factor (VEGF) leading to protection against apoptosis in B-cell

derived malignancies [126]. LPA also protects chronic lymphocytic leukemia cells from apoptosis induced by histone deacetylase inhibitor through activation of histone deacetylases [127]. Although LPA mediates survival of ovarian cancer cells [128], Schwann cells [129], macrophages [130], fibroblasts [74], and neonatal cardiac myocytes [131], it can promote apoptosis in hippocampal neurons [132] and PC12 cells [133].

1.4 Taxol, mechanisms of actions in chemotherapy

1.4.1 Pharmacology and functions

Taxol (paclitaxel) is a commonly used chemotherapeutic agent in the treatment of metastatic and early stage breast cancer with significant benefits in terms of overall survival and disease-free survival of breast cancer [134]. Taxol was originally isolated from the bark of the Pacific yew tree, *Taxus brevifolia* [135]. It was initially approved by the United States (US) Food and Drug Administration (FDA) for use in advanced ovarian cancer in 1992 and subsequently certified for the treatment of metastatic breast cancer in 1994. Since Taxol was originally isolated from a natural source having a limited supply, it is now derived semi-synthetically from the inactive taxane precursor, 10-deacetylbaccatin III, found in the needles of the European yew tree, *Taxus baccata* [136]. The chemical structure is illustrated in Figure 1.8.

Since Taxol is a highly hydrophobic compound, it is administered in solution with alcohol and purified Cremophor ® EL (polyoxyethylated castor oil) to help delivery. This solvent can cause severe hypersensitivity reactions, thus

premedication with dexamethasone is recommended. Following intravenous infusion, Taxol demonstrates nonlinear pharmacokinetics. It is metabolized in the liver and is excreted predominantly in bile. The elimination $T_{1/2}$ is 15–50 h [137]. Recent development of ABI-007, an albumin bound Taxol particle, helps to avoid the hypersensitivity induced by Cremophor ® EL. The standard protocol for treatment of patients with Taxol is 175 mg/m^2 every three weeks for six cycles [138]. Common side-effects of Taxol include alopecia, myelosuppression, gastrointestinal symptoms and febrile neutropenia. Peripheral neuropathy is particularly associated with Taxol and increases with increasing dose [137]. Taxol is more effective in terms of response rates when it is administered in a dose-dense setting, as a weekly or two-weekly regime, when compared to conventional three-weekly scheduling [139]. Taxol is predominantly metabolized in the liver by cytochromes p450 2C8 and 3A4 and it is excreted in bile [140].

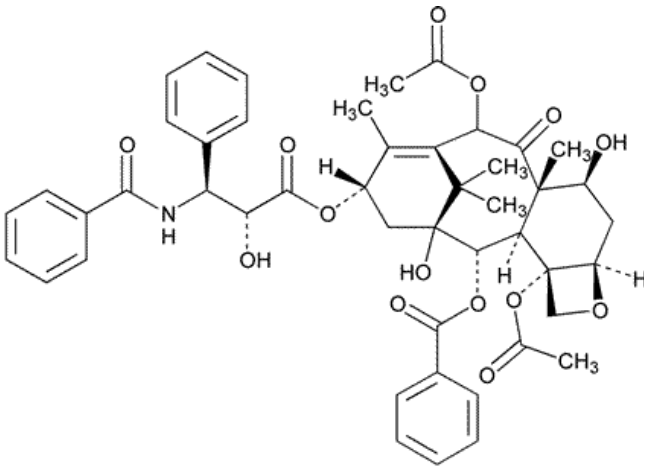

Figure 1.8 Chemical structure of Taxol. The figure adopted from Fitzpatrick [141].

Docetaxel, a second-generation taxane, is derived semi-synthetically by the esterification of a side chain to 10-deacetylbaccatin III (the inactive taxane precursor). It is administered in solution with polysorbate 80 and ethanol, a vehicle associated with significantly less hypersensitivity reactions than Cremophor ® EL [137]. Docetaxel can be given as part of a weekly or standard three-weekly regime [142]. Docetaxel differs from Taxol with its linear pharmacokinetics and elimination $T_{1/2}$ of 1 h but it has the same common side-effects. In addition, oedema and fluid accumulation, pleural effusions and ascites are also commonly seen with docetaxel and can be dose-dependent. [137].

The cytotoxic effects of Taxol are expressed using IC_{50} values (concentration that reduces an effect by 50%). The IC_{50} values relate to parameters such as dynamicity, shortening rate of microtubules and clonogenic survival [135]. In vitro, it has been demonstrated that the cytotoxic effects of Taxol are time and drug dependent [143]. The cytotoxicity (IC_{50}) of Taxol for HeLa, MCF-7 and A549 cells ranged between 2.5 and 7.5 nM. Increasing Taxol concentration above 50 nM induced no additional cytotoxicity after 24 h drug exposure [144].

Taxol is a member of the microtubule-stabilizing agent that functions. Other agents including docetaxel, epothilones A and B, discodermolide and eleutherobin function in the same way. These agents inhibit the metaphase-anaphase transition, blocking mitosis and inducing apoptosis by suppressing spindle microtubule dynamics [145].

The cellular target for Taxol is the taxane site on β-tubulin [146]. Docetaxel shares the same binding site as Taxol, though with greater affinity [147]. The taxane-binding site on microtubules is only present in assembled tubulin [148]. Taxol binds to the intermediate domain on β-tubulin [146]. This pocket for Taxol lies within a hydrophobic cleft near the surface of β-tubulin and allows for Taxol to interact with proteins by hydrogen bonding and hydrophobic contact (Figure 1.9) [149]. The binding of Taxol causes lateral polymerization and microtubule stability [148]. The sites of interaction between Taxol and β-tubulin involve amino acid residues 217–233 of β-tubulin. The molecular docking model of Taxol and β-tubulin demonstrates a T-shaped Taxol conformation within the β-tubulin site. Segments of α-helices H1, H6, H7 and the loop between H6 and H7 interact hydrophobically with Taxol. In addition, Taxol comes in contact with β-strands, B8 and B10. Other drugs that bind to the taxane site include epothilones, discodermolide and eleutherobin [149].

1.4.2 Cellular response to Taxol

Several outcomes are associated with Taxol treatments. Short-term drug treatment causes sustained or chronic mitotic arrest until the drug is cleared. This mechanism enables the cells to survive and continue dividing as diploid (2N) cells. Alternatively, mitotic slippage or adaptation can take place, when the cells exit mitosis without engaging in anaphase or cytokinesis, producing tetraploid (4N) multinucleated G_1 cells without chromosomal segregation. The determination of cell fate following mitotic slippage is complicated with a number of possible associated outcomes. Cells can survive and continue dividing as

tetraploid (4N) cells (Adaptation I). Alternatively, adapted cells can exit G_1 undergoing senescence or apoptosis as tetraploid (4N) cells (Adaptation II). Furthermore, cells can escape to G1 overriding mitotic checkpoint signalling leading to apoptosis in interphase (Adaptation III). Finally, cells can undergo cell death directly in mitotic arrest [150,151].

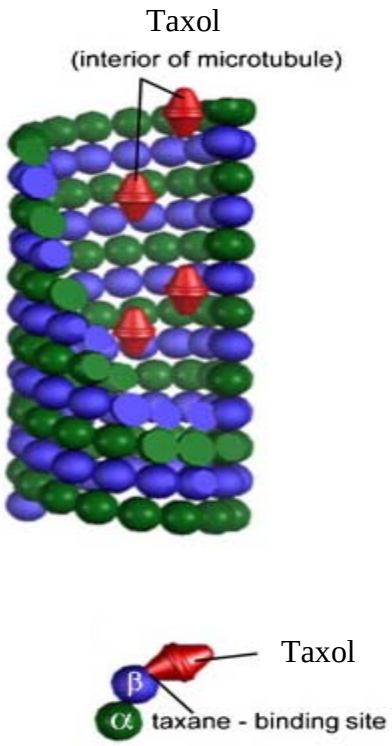

Figure 1.9 Binding of Taxol to the tubulin heterodimers. Taxol binds to the interior surface of the microtubule after binding to the taxane-binding site of ß-tubuline, suppressing microtubule dynamics. The figure adopted from Jordan [145].

The fate of tumor cells associated with the use of chemotherapeutic agent depends on factors such as the mechanism of drug action, drug dosage and the genetic characteristics of the tumor cells. These factors, in combination with

cellular resistance mechanisms will influence the response of tumor cells to chemotherapy, and eventually lead to tumor cell death or survival and chemoresistance [138].

1.5 Markers predictive of Taxol resistance

1.5.1 Chemoresistance in cancer treatment

Although chemotherapy comprises part of the successful treatment of breast cancer patients, around 50% of patients fail to respond to chemotherapeutic agents [134]. Cellular chemotherapeutic resistance is a major factor involved in poor response and reduced survival in patients with metastatic breast cancer. Taxol is a common chemotherapeutic agent in the treatment of breast cancer with a response rate of between 25% and 69% observed when used as first-line treatment [152].

The purpose of treatment for cancer primarily is to induce cell death in cancer cells. Resistance to apoptosis is likely to promote the tumor survival, which results in tumor progression and chemoresistance. Tumor cells depend on different mechanisms to evade apoptosis in order to survive under conditions of oncogenic or environmental stress signals. In addition, resistance to cell death may support the survival of tumor cells in response to chemotherapy or radiotherapy [153].

Most apoptosis signaling pathways finally result in the activation of caspases, a family of cysteine proteases that act as common death effector molecules in various forms of cell death [154]. There are two major apoptosis signaling pathways: the death receptor (extrinsic) pathway and the mitochondria

(intrinsic) pathway (Figure 1.10). Defective or inefficient signaling in both these models has been demonstrated as a mechanism for the evasion of death in tumor cells. Death receptors of the tumor necrosis factor (TNF) receptor super-family including CD95 (Fas, Apo1), nerve growth factor receptor (P75 NGFR), and TNF-related apoptosis inducing ligand (TRAIL) receptors (TRAIL-R1/DR4, TRAIL-R2/DR5) can be stimulated through their respective ligands or agonistic antibodies. Activation of these receptors results in receptor aggregation or oligomerization and enrolment of the adaptor molecule Fas-associated Death Domain (FADD) and caspase-8 to form the death inducing signaling complex (DISC) [155]. Then, caspase-8 becomes activated and initiates apoptosis by direct cleavage of downstream effector caspases. The intrinsic pathway is initiated by anticancer drugs, growth factor withdrawal, hypoxia, or by induction of oncogenes. These factors induce permeabilization of the outer mitochondrial membrane and activate the mitochondrial pathway. This pathway is engaged by the release of pro-apoptotic factors from the mitochondrial intermembrane space into the cytosol including cytochrome *c*, apoptosis inducing factor (AIF), second mitochondria-derived activator of caspase (Smac)/direct Inhibitor of Apoptosis proteins (IAP) binding protein with low pI (DIABLO), or Omi/high temperature requirement protein A2 (HtrA2) [156]. The release of cytochrome *c* into the cytosol triggers caspase-3 activation through formation of apoptosome complex, which consists of the cytochrome *c*/Apaf-1/caspase-9. Smac/DIABLO promotes caspase activation by neutralizing IAP proteins that inhibit caspase-3, -7 and -9,

whereas overexpression of the anti-apoptotic protein Bcl-2 blocks mitochondrial outer membrane permeabilization and inhibits death execution [157].

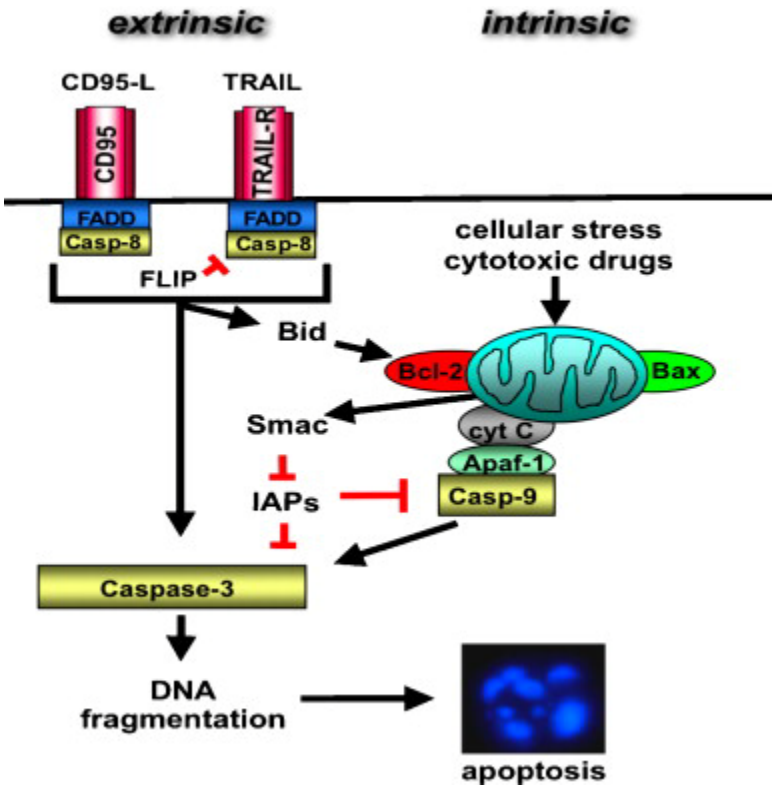

Figure 1.10 Apoptosis pathways. Apoptosis pathways can be initiated by binding with death receptors by their respective ligands followed by receptor trimerization, recruitment of adaptor molecules (FADD) and activation of caspase-8 (receptor pathway). The mitochondrial pathway is initiated by the release of pro-apoptotic factors such as cytochrome *c* or Smac from mitochondria in the cytosol. Apoptosis pathways are regulated by pro-apoptotic Bcl-2 family proteins such as Bax and Bak, anti-apoptotic Bcl-2 family proteins including Bcl-2 and Bcl-X_L, and Inhibitor of Apoptosis (IAPs) proteins. Smac promotes apoptosis by neutralizing IAP-mediated inhibition of caspase-3 and -9. The picture adopted from [158].

1.5.2 Mechanisms of Taxol resistance

Intrinsic and acquired drug resistance to Taxol is common. Multiple factors underlay Taxol resistance. First, mutations in β-tubulin affect sensitivity of the cells to Taxol by changing in microtubule dynamics and stability. These mutations can also alter the binding of Taxol to β-tubulin subunits leading to chemoresistance [159].

Different expressions of β-tubulin isotypes can be another reason for Taxol resistance. There are six isotypes of β-tubulin in humans including M40, II, III, IVA, IVB, and VI. The different β-tubulin isotypes have different distribution within tissues. Nevertheless, the isotype-specific sequence differences are also highly conserved, which suggests that there are important functional differences between the isotypes. The isotypes have specific functional roles and different cell types synthesize different isotypes. However, little is known about the functions of the isotypes. If β-tubulin isotypes have specific functional roles, they may be separated in different subcellular compartments of the same cell according to function [159].

The proteins that regulate microtubule dynamics have a critical role in Taxol resistance by modulating microtubule stability. These proteins include MAP1A, MAP1B, MAP2, MAP4, tau and survivin [138]. Tau is predominantly a neuronal microtubule-associated protein, although it can be expressed in epithelial and glial cells. Tau functions primarily by enabling tubulin assembly and

microtubule stabilization [160]. Survivin is a member of the IAP family and cytoplasmic/mitochondrial survivin is cytoprotective [161].

1.6 Survivin and chemoresistance

Survivin is predominantly expressed during mitosis and it associates physically with the mitotic apparatus to regulate microtubule dynamics during mitosis. Increased survivin expression in breast cancer cells leads to Taxol-resistance by enabling cells to exit faster from G2/M [162].

In breast cancer, the level of survivin expression is correlated with poor prognostic parameters including higher histological grade and high tumor cell proliferation [163]. Survivin expression in the majority of interphase tumor cells is higher than normal cells in cancer patients [164,165] and it is found in the cytoplasm and nuclei of tumor and normal proliferating cells [166].

Significantly, the other function of survivin is to control cell division and proper cytokinesis. Nuclear survivin interacts with microtubules and increases dynamicity, thus promoting an appropriate structure of the mitotic spindles and nuclear separation [138]. The cell cycle–dependent transcriptional control of survivin is regulated by various oncogenic pathways including PI3K/Akt and GSK-3ß in cancer cells [93,162,167]. Survivin can be phosphorylated by PI3K/Akt [168] or the main mitotic kinase, $p34^{cdc2}$-cyclin B1[169], which both increase viability, and by aurora-B kinase that is important for survivin localization and binding to centromeres [170]. PI3K/Akt pathway is also a major route for upregulation of survivin synthesis [171]. The half-life of survivin is

about 30 min and this is extended by phosphorylation, which protects survivin from ubiquitination and degradation (Figure 1.11) [172].

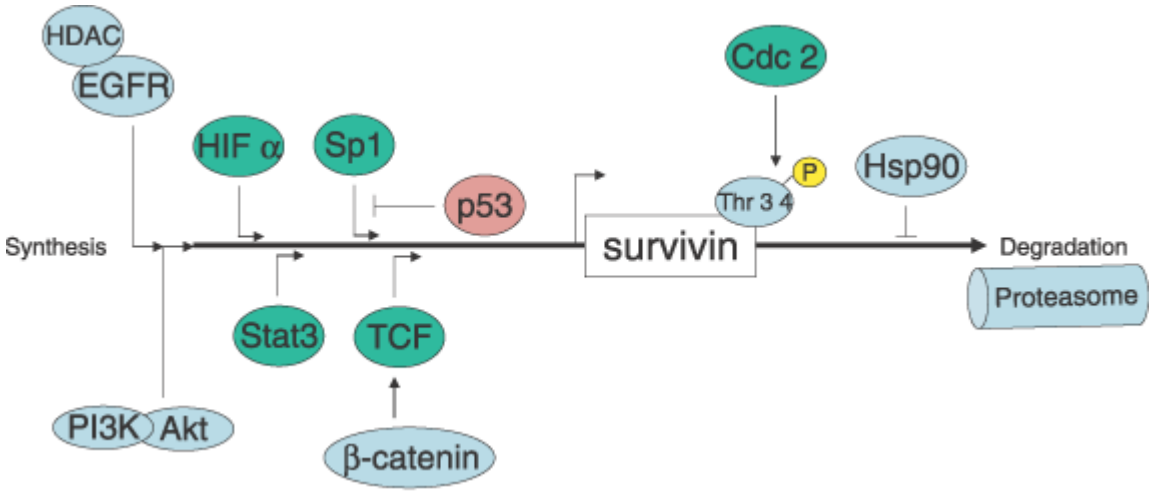

Figure 1.11 Regulation of survivin at synthesis and degradation levels. The Figure adopted from Yamamoto [171].

Multidrug resistance (MDR) is another common reason for Taxol resistance through which resistance to one drug can result in cross-resistance to other structurally unrelated drugs. One of the first members of these energy-dependent drug efflux pumps to be described was the P-glycoprotein (P-gp) encoded by the MDR-1 gene, localized to chromosome 7. P-gp protein functions by increasing the efflux of drugs out of the cell and decreasing intracellular levels of the drug leading to drug resistance [173]. When drugs bind to P-gp, one of the ATP-binding domains is activated and hydrolysis of ATP causes a conformational change in P-gp, resulting in the release of drugs into the extracellular space [138].

1.7 Thesis objectives

Breast cancer is the most common cancer among women and approximately one-third of these women develop metastases. Resistance to chemotherapeutic agent is a major obstacle for treatment of patients with breast cancer. Taxol is one of the first-line treatments for the patients with early-stage and metastatic breast cancer. However, resistance to Taxol develops in up to 40% of patients. To improve chemotherapy, it is vital to understand how Taxol resistance develops and to overcome this process. LPA is a small but biologically very active phospholipid molecule that through specific cell surface receptors stimulates tumor cell growth, proliferation, differentiation, motility and survival. The discovery that ATX is the main enzyme that generates extracellular LPA from circulating LPC led to studies that established the role of ATX in tumor progression including proliferation, migration and survival of tumor cells as well the importance of ATX as a predictive marker in the prognosis and monitoring of the treatment in cancer patients. However, when we started this project, the role of ATX and LPA in resistance against chemotherapy was not known. It was the objective of this thesis work to investigate if ATX antagonizes Taxol-induced apoptosis and Taxol-induced G2/M arrest and whether it depends on the catalytic or non-catalytic effects of ATX. We discovered that ATX through the conversion of LPC to LPA protects MCF-7 and MDA-MB-435 tumor cells against Taxol-induced apoptosis. We then determined the role of LPA receptors and downstream targets including PI3K/Akt and MAPK pathways and ceramide formation in induction of LPA-induced cell protection. We also studied the role of

LPA in Taxol-induced G2/M arrest and whether LPA released the cells from G2/M or delayed entry into G2/M. Immunocytochemistry studies were also performed to determine any detectable change in cell morphology related to abnormal spindle formation, apoptosis and mono- and multinucleation of the cells. Another aim of this study was to determine if LPA could affect Taxol expulsion from the cells and the metabolism of Taxol, or if LPA could affect microtubule dynamicity. We also studied the role of LPA in expression of survivin, an important protein in microtubule dynemicity. Investigation on the target signaling pathways whereby LPA promotes survivin expression was another dimension of this research project. We determined the role of PI3K/Akt and GSK-3 pathways in LPA-survivin axis by applying inhibitor against PI3K and GSK-3 proteins and knockdown of GSK-3ß and survivin. We believe that elucidating how ATX and LPA interfere with Taxol-induced apoptosis and G2/M arrest is essential for understanding chemoresistance against Taxol and for developing new strategies to improve the efficacy of chemotherapy.

CHAPTER 2

MATERIALS AND METHODS

2.1 Materials

RPMI1640 medium, penicillin and streptomycin were obtained from GIBCO (Carlsbad, CA, USA). Trypsin-ethylenediaminetetraacetic acid, TMRE, goat anti-mouse IgG, ATX primers, anti-rabbit and anti-mouse IgG, HRP-linked antibodies were obtained from Molecular Probes (Carlsbad, CA, USA). Superscript II reverse transcriptase was from Invitrogen (Carlsbad, CA, USA). DAG kinase, PD98059 and dithiothreitol were purchased from EMD Chemicals Inc. (Gibbstown, NJ, USA). Fatty acid-free bovine serum albumin, paclitaxel (Taxol), activated charcoal (Norit), Hoechst33258, ATP, diethylenetriaminepentaacetic acid (DETAPEC), pertussis toxin, oleoyl-L-α-lysophosphatidic acid, sodium salt (LPA), oleoyl-L-α-LPC, ceramide, monoclonal anti-glyceraldehyde 3-phosphate dehydrogenase (GAPDH), monoclonal anti α-tubulin, monoclonal anti total GSK-3 α/ß, polyclonal phospho-GSK-3 α/ß (pTyr 279/216), sodium pyruvate, Nicotinamide adenine dinucleotide (NADH), RNAse A, normal goat serum, normal donkey serum, sodium borate and propidium iodide were purchased from Sigma-Aldrich (Oakville, ON, Canada). VPC51299 and PC8a202 were provided by Drs KR Lynch and TL Macdonald (University of Virginia, Charlottesville, VA, USA). LY294002 was obtained from Biomol Int. (Plymouth Meeting, PA, USA). S32826 was provided by Dr JA Boutin (Institut de Recherches Servier). [^{32}P]LPA was synthesized as before [55]. Rabbit polyclonal antibody against ATX and rATX were gifts from Dr T Clair, through the Intramural Research Program of NIH, National Cancer Institute, Center for Cancer Research (Bethesda, MD, USA). Goat anti-rabbit IgG was obtained from

Rockland (Gilbertsville, PA, USA). Polyclonal anti-Akt, phospho-Akt (S473), polyclonal phospho-GSK-3 αß (Ser 21/9) and monoclonal phospho-p44/42 MAPK were obtained from Cell Signaling Technology (Danvers, MA, USA). Polyclonal anti-MAPK (sc-93) was from Santa Cruz Biotechnology (Santa Cruz, CA, USA). FS-3 compound for the ATX assay obtained from Echelon Company (San Jose, CA, USA). Fetal bovine serum (FBS) purchased from Medicorp Inc. (Montréal, PQ, Canada). RNAqueous kit, DNA-free kit and Syber Green buffer mix were obtained from Ambion (Austin, TX, USA). Bromodeoxyuridine (BrdU), mouse anti-BrdU and FITC goat anti–mouse IgG antibody were purchased from BD Pharmingen (Mississauga, ON, Canada). [*o*-benzamido-3H]Taxol was obtained from Moravek Biochemicals (Brea, California, USA). Anti-phospho-Histone H3 was purchased from Millipore (Billerica, Massachusetts, USA). Aqueous counting scintillation fluid was purchased from Amersham Biosciences (Piscataway, NJ, USA). Oregon Green 488 Taxol and monoclonal anti GSK-3 α/ß were from Invitrogen (Carlsbad, CA, USA). siRNA for survivin and siControl were from Qiagen (Missisauga, ON, Canada). SMART pool siRNA for GSK-3ß and siControl were purchased from Dharmacon, Inc. (Lafayette, CO). Polyclonal anti-survivin and anti phospho-survivin (T34) were obtained from Abcam (Cambridge, MA, USA). Other reagents and their sources are mentioned within the text.

2.2 Cell culture

The MCF-7 and MDA-MB-435 cells were obtained from the American Type Culture Collection. Cells were maintained in RPMI1640 medium (GIBCO) with 10% FBS and 1% penicillin/streptomycin in a humidified atmosphere with 5% CO_2 at 37 °C.

2.3 Fetal bovine serum delipidation

2.3.1 Preparation of charcoaled FBS

The activated charcoal (Norit) was washed twice with phosphate-buffered saline (PBS) and then added to FBS (2 g charcoal per 50 ml of FBS). The mixture was rotated overnight at 4 °C**.** The mixture was centrifuged in 2800 rpm for 20 min and the supernatant was filtered twice through 0.22 μm sterile filters (Millipore).

2.3.2 Measurement of ^{32}P-labeled lysophosphatidate in charcoal-treated FBS

To evaluate the efficiency of activated charcoal in removing LPA from FBS, 1 μC ^{32}P-labeled LPA was added to 50 ml of FBS. After delipidation of FBS by activated charcoal, the amount of ^{32}P-labeled LPA was measured using liquid scintillation counter**.**

2.4 Quantification of apoptotic nuclei using 4,6-diamidino-2-phenylindole (DAPI) stain

MCF-7 cells (2×10^4 cells/well) were grown in 96-well plates. Cells (about 70% confluent) were washed with PBS and treated in serum-free media

for 24 h. Cells were then fixed in 4% paraformaldehyde for 20 min and permeabilized in 0.1% Triton X-100 for 15 min. Fixed cells were stained with 1 µg/ml Hoechst 33258 for 15 min after evaporation of the fixing solution. Nuclear morphology of the cells was observed by fluorescence microscopy. Triplicate samples were prepared for each treatment and at least 300 cells were counted in random fields for each sample and apoptotic nuclei were identified.

2.5 Measurement of lysophosphatidate breakdown

Six-well plates were seeded with 2×10^5 cells and these were grown to 70% confluence. After washing the cells twice with PBS, the media was changed to 2 ml of serum-free media containing 1 µC of ^{32}P-labeled LPA with either 1 or 20 µM of non-radioactive LPA.

The half-life of LPA was determined by measuring $^{32}P_i$- and ^{32}P-labeled LPA in the medium that was collected at indicated time points up to 24 h. After washing with PBS, cell lysates were collected by scrapping twice with 0.5 ml of ice-cold methanol. Chloroform (1ml) was added to the combined methanol extracts followed by 0.9 ml of 2 M KCl and the mixture was vortexed and then centrifuged. The chloroform phase (100 µl) from the cell extracts was dried under N_2 and dissolved in 2 ml of aqueous counting scintillation fluid (Amersham Biosciences).

2.6 Mitochondrial membrane potential assay

Breakdown of the mitochondrial membrane potential ($\Delta\Psi m$) was determined using tetramethylrhodamine ethyl ester (TMRE) staining. MCF-7 cells (2×10^5) were grown to confluence in six-well plates over 48 h in RPMI 1640

medium with 10% FBS. The medium was changed to RPMI 1640 medium with 10% of charcoal-treated FBS. Cells were incubated for an additional 48 h with LPA-depleted FBS in the presence of Taxol or LPA. LPA concentrations were maintained by adding half of the original concentration of LPA every 10 h on the basis of the calculated half-life of LPA. Cells were then trypsinized, collected in 96 V-bottomed plate and exposed to TMRE (500 nM) for 30 min at 37 °C. Excess dye was removed with PBS containing 0.1% fatty acid-free bovine serum albumin (BSA) and cell-associated fluorescence was measured with Calibur Flow Cytometer (Becton Dickinson, San José, CA, USA) using Cell Quest software.

2.7 ATX expression assays

2.7.1 ATX mRNA expression detection

Total RNA was extracted using the RNAqueous kit, according the manufacture's instruction. DNA-free kit was also applied to remove contaminating DNA from RNA preparation. Total RNA was treated with superscript II reverse transcriptase. Real-time reverse transcription polymerase chain reaction (RT-PCR) was performed with 25 µl of master mix containing 2 x Syber Green buffer mix and forward and reverse primers (Invitrogen). The internal control was the constitutively expressed housekeeping human GAPDH. Primers for human ATX were as follows:

sense, 5'-ACAACGAGGAGAGCTGCAAT-3'

antisense, 5'-AGAAGTCCAGGCTGGTG AGA-3´

Primers for human GAPDH were as follows:

sense, 5'-ACAGTCAGCCGCATCTTCTT-3'

antisense, 5'-GACAAGCTTCCCGTTCTCAG-3'

Samples were assayed in triplicate on the 7500 Real Time PCR System (Applied Biosystems).

2.7.2 ATX protein detection

Serum-free medium from MD-MB-435 cells was concentrated up to 200 µl per 10^6 cells by centrifugation using a Centricon Millipore's Ultracel YM cellulose membrane (Millipore Corporation, Bedford, TX, USA) and analysed using 10% sodium dodecyl sulfate polyacrylamide gel electrophoresis (SDS–PAGE). Nitrocellulose membranes were treated with Odyssey blocking buffer overnight at 4°C and then incubated with 1:5000 dilutions of ATX antibody for 1 h followed by four washes with PBS+0.1% Tween-20. Blots were incubated in 1:10 000 dilutions of goat anti-rabbit IgG for 45 min. After washing four times, ATX was visualized at 800 nm with the Odyssey Infrared Scanner.

2.7.3 ATX activity assay

ATX activity was assayed using FS-3 compound (a synthetic, fluorescent LPC analog) as a lysoPLD/autotaxin substrate and ~20 times concentrated conditioned serum-free medium from MCF-7 and MDA MB-435 cells. Assays were performed in 96-well plates with concentrated medium comprising one-third of the total volume, 1 µM FS-3 and 30 µM fatty acid-free BSA concentrations of

assay buffer (140 mM NaCl, 5 mM KCl, 1 mM $CaCl_2$, 1 mM $MgCl_2$, 50 mM Tris/HCl at pH 8.0). Fluorescence was read at 15 min intervals by a Synergy2 system (BioTek, Winooski, VT) with excitation and emission wavelengths of 485 and 538 nm, respectively. Results were shown at 2 h, at which point all fluorescence changes as a function of time were linear.

2.8 Isobalogram analysis

The interaction between LPA and Taxol was evaluated by the isobologram technique (CalcuSyn software, Biosoft, Cambridge, UK), a dose-oriented geometric method of assessing drug interactions. Briefly, the concentration of one agent producing a 50% effect (apoptosis) was plotted on the horizontal axis, and the concentration of another agent producing the same degree of effect was plotted on the vertical axis; a straight line joining these two points represents zero interaction (addition) between two agents.

The experimental iso-effect points were the concentrations (expressed relative to the IC_{50} concentrations) of the two agents that when combined kill 50% of the cells. When the experimental iso-effect points felt below that line, the combination effect of the 2 drugs was considered to be synergistic. Within the designed assay range, a set of iso-effect points was generated because there were multiple Taxol and LPA concentrations that achieved the same iso-effect. A quantitative index of these interactions was provided by the isobologram equation CI = (a/A) + (b/B), where, for our study, (A) and (B) represent the respective concentrations of Taxol and LPA required to produce a fixed level of apoptosis (IC_{50}) when administered alone, (a) and (b) represent the concentrations required

for the same effect when the drugs were administered in combination, and combination index (CI) represents an index of drug combination. CI values of <1 indicate synergy, a value of 1 represents addition, and values of >1 indicate antagonism. For all estimations of CI, we used only isobols where intercept data for both axes were available.

2.9 Measurement of ceramide concentrations

2.9.1 Ceramide mass assay

Approximately 1 x 10^6 MCF-7 breast cancer cells were plated on 10 cm culture dishes and grown to confluence in RPMI1640 medium with 10% FBS at 37ºC in an atmosphere of 5% CO2. The medium was replaced with RPMI1640 medium containing 10% of charcoal-treated FBS, and the cells were incubated for 48 h with the indicated concentrations of Taxol, LPA and LY294002. After washing with PBS, cell lysates were collected by scrapping twice with 0.5 ml of ice-cold methanol. Chloroform (1 ml) was added to the combined methanol extracts followed by 0.9 ml of 1 M KCl containing 0.2M HCl, and the mixture was vortexed and then centrifuged. The top layer was removed and 1.9 ml of synthetic top phase obtained by mixing chloroform/methanol/1M KCl containing 0.2M HCl (1:1:0.9 by volume) was added to wash the organic bottom layer, and the mixtures were vortexed and then centrifuged. The top layer was removed and 0.9 ml of the bottom organic phase was collected to a new tube, where it was dried under N_2, and dissolved in 100 µl of chloroform/methanol (9:1). Twelve µl were immediately removed to measure total lipid-phosphate. Samples containing 30 nmol of total phospholipid were dried under N_2 to use in the ceramide mass assay.

Diacylglycerol kinase (DAG kinase) reaction mixture containing 50 mM imidazole, 1 mM diethylenetriaminepentaacetic acid, 50 mM NaCl, 12.5 mM $MgCl_2$, 1 mM EGTA, 10 mM DTT, 1mM ATP, 1.5% N-octyl-ß-D-glucopyranoside, 1mM cardiolipin and 2 µg of recombinant DAG kinase (equivalent to 4 mU from Biomol) was incubated for 20 min at 37ºC. This procedure phosphorylated contaminants in the reaction mixture before the addition of 1 µCi/assay of [γ-^{32}P]ATP at 10 Ci/mol (GE Healthcare Life Sciences). One hundred µl of this incubation mixture was then added to the dried down samples and standards of ceramide (range of 100-1000 pmol ceramide for standard curve, Avanti Polar Lipids).

Samples were vortexed before placing the tubes in a 37ºC water bath for 5 min. The tubes were then moved to a sonicating water bath (Brounsonic 1200) for 10 min. The tubes were moved back to the 37ºC water bath for 5 min and returned to the sonicating water bath for 5 min, and finally back at 37ºC for 20 min. One ml of methanol was added to stop the reaction followed by 1 ml chloroform, and 0.8 ml of 2M KCL and 0.2 M H_3PO_4. This mixture was vigorously vortexed and then centrifuged to separate the phases. The top phase was aspirated and the bottom phase was washed twice with synthetic top phase with vortexing and centrifugation between each wash. A sample of the bottom phase (0.8 ml) was dried under N_2 and dissolved in 100 µl of chloroform/methanol (9:1). Fifty µl was loaded on to glass-supported silica gel 60 thin layer chromatography (TLC) plates and the plate was developed with chloroform/methanol/ammonium hydroxide (65:35:7.5, by vol.). The plates were dried and then they were turned upside down,

and developed with chloroform/methanol/acetic acid/acetone/water (65:35:7.5, by vol). After drying, plates were subjected to audioradiography for at least 6 h to overnight using Kodak Biomax film. Ceramide-1- phosphate, produced from ceramide by DAG kinase, was identified by a ceramide-1-phosphate standard. Bands also were scrapped and ^{32}P-labeling was measured by liquid scintillation counting.

2.9.2 Phosphate assay

Ceramide concentration was expressed as a percentage of total phospholipid. Total phospholipid was determined from the 12 µl of the chloroform-extracted sample of cells described above. The samples and a standard curve of 1-100 nmol of glycerol-3-phosphate in water were evaporated. Fifty µl of perchloric acid was added and the samples were heated to 180ºC for 30 min. This step allows the acid to digest the organic phosphate to inorganic phosphate. After cooling the samples to room temperature, 278 µl of water followed by 55 µl of 2.5% ammonium molybdate and 55 µl of fresh 10% ascorbic acid was added. The samples were then placed in 90ºC water bath for 15 min. A portion (180 µl) of this mixture was added to duplicate wells of a 96 well plate and absorbance was measured at 700 nm using an Easy Reader EAR 340 AT (SLT-Labinstruments, Austria).

2.10 Bromodeoxyuridine / propidium iodine double staining

2.10.1 Labeling and fixation of cultured cells

Approximately 1 x 10^6 MCF-7 breast cancer cells were plated on 10 cm culture dishes and the cells were grown to confluence in RPMI1640 medium with 10% FBS at 37ºC in an atmosphere of 5% CO2. The medium was replaced with

RPMI1640 medium containing 10% of charcoal-treated FBS. After 70% confluency, the cells were incubated with a final concentration of 1 µM BrdU for indicated times at 37ºC. Then the medium was aspirated off and the cells were rinsed twice with serum-free medium at 37°C. Fresh charcoal-treated media was added and the cells were returned to the incubator quickly. At desired time intervals for fixing the cells, medium was aspirated off and the cells were rinsed with fresh serum-free medium at 37°C. Then 1.0 ml of trypsin (0.05% vol/vol) was added and incubated for 5 min at 37ºC. Nine ml medium with charcoal-treated FBS was added and the total number of cells was recorded by hemocytometer. After centrifugation, the cells were fixed in 60% ethanol (vol/vol) in PBS and left at 4ºC overnight before staining.

2.10.2 Preparation of isolated nuclei

The fixed cells were vortexed for 15 second and centrifuged and remove supernatant. Then the cells were incubated with 5.0 ml of 0.04% pepsin (vol/vol) in 0.1 N HCl for 20 min on a rocker at room temperature (incubation time was optimized for MCF-7 cells). The tubes containing pepsin and nuclei were then centrifuged and the supernatant was aspirated off and the pellet was vortex for 5-10 second. Then, 3.0 ml of 2 N HCl was added to each tube while vortexing at low speed. Then the tubes were incubated for 20 min at 37ºC. The tubes were shaken twice during incubation.

2.10.3 Staining of isolated nuclei

Six ml of sodium borate (0.1 M) was added to each tube while vortexing. Then the tubes were centrifuged and the supernatant was aspirate off. The pellet was vortexed and 6.0 ml of PBS containing 0.5% Tween-20 and 0.5% BSA (vol/vol) was added while vortexing. Then, the tubes were centrifuged. After aspirating the supernatant, 0.2 ml of 1:100 dilution of anti-BrdU monoclonal antibody (mAb) in PBS containing 0.5% Tween-20 (vol/vol) was added and the samples were incubated for 60 min at room temperature, in the dark. Then 3.0 ml of PBS + 0.5% Tween-20 + 0.5% BSA (vol/vol) was added while vortexing.

After centrifugation, the supernatant was aspirated off. Then, 0.2 ml of the second Ab (goat anti-mouse-FITC) in PBS containing 0.5% Tween-20 and 0.5% BSA (vol/vol) and 1.0% (vol/vol) normal goat serum was added at 1:100 dilution and incubated for 45 min in the dark at room temperature. Three ml PBS containing 0.5% Tween-20 and 0.5% BSA (vol/vol) was added and the tubes were centrifuged. The supernatant was aspirated off and propidium iodide (10 µg/ml in PBS containing 0.5% Tween-20 and 0.5% BSA) (vol/vol) was added. The suspension was incubated overnight in propidium iodide at 4ºC in the dark. One hour prior to running the sample on the flow cytometer, RNAse (20 µg/ml) was add to the tubes. The samples were measured with Calibur Flow Cytometer (Becton Dickinson, San José, CA, USA) using Cell Quest software.

2.11 Immunocytochemistry

First, 18 mm glass coverslips that were flame-sterilized by briefly holding them with forceps over an open flame (Bunsen burner) were placed in 12-well culture plates. Approximately 2×10^5 MCF-7 breast cancer cells were plated on the coverslips and grown to confluence. The medium was replaced with RPMI1640 medium containing 10% of charcoal-treated FBS in the presence and absence of Taxol (50 nM) and LPA (5 µM) for indicated times. Then the medium was aspirated off and the cells were rinsed twice with serum-free medium at 37°C and the cells were fixed in 4% paraformaldehyde for 15 min. Then the cells were permeablized with 0.1% Triton X-100 for 2 min. The cells were then rinsed four times with PBS over 5 min. Next, the cells were incubated with 4% normal donkey serum in PBS for 1 h to block non-specific immunostaining. After aspirating off donkey serum, the cells were incubated with 1:300 dilution of monoclonal anti α-tubulin and 1:100 dilution of polyclonal anti-Histone H3.1 (Phospho-Ser 10) in 4% of donkey serum in PBS for 1 h. After rinsing the cells four times with PBS over 5 min, the cells were incubated in 1:300 dilutions of goat anti-rabbit and anti-mouse IgG, HRP-linked antibodies as well as 1 µg/ml Hoechst33258 (DAPI) for 1 h. Then the cells were rinsed four times with PBS over 5 min and each coverslip was inverted onto a slide containing 10 µl of mounting media. Chromatin (DAPI), microtubule structures (anti-α-tubulin) and mitotic cells (phospho-histone H3) were visualized by fluorescence microscopy using blue, green, and red filters, respectively. Triplicate samples were prepared for each treatment and at least 300 cells were counted in random fields for each

sample. Then the percentage of the cells with abnormal spindles, mononucleated and multinucleated cells, dead and dying cells and the cells arrested in mitosis were reported for each treatment. The images were also captured by Zeiss LSM 510 confocal microscopy (Carl Zeiss Inc) at excitation wavelengths of 488 nm for tubulin, 534 nm for p-Histon H_3 and 488 nm for DAPI.

2.12 Taxol uptake and distribution in MCF-7 cells

2.12.1 Measurement of Taxol uptake and distribution

Approximately 2 x 10^5 MCF-7 breast cancer cells were plated in 3.5 cm cell culture dishes and grown to confluence in RPMI1640 medium with 10% FBS at 37ºC in an atmosphere of 5% CO_2. The medium was replaced with 1.5 ml RPMI1640 medium containing 10% of charcoal-treated FBS with 50 nM Taxol containing 0.5µCi [^{3}H]Taxol. After 26 h incubation, LPA (5µM) was added to some dishes. Also Taxol was removed from some dishes and 1.5 ml of medium or medium containing LPA (5 µM) was added to the dishes. At the indicated time points, medium was collected and after washing the cells three times with ice-cold RPMI1640 medium containing 0.1% BSA, cell lysates were collected by scrapping twice with 0.5 ml of ice-cold methanol. Chloroform (1ml) was added to the combined methanol extracts followed by 0.9 ml of 2 M KCl and the mixture was vortexed and then centrifuged. The chloroform phase (100 µl) from the cell extracts was dried under N_2 and dissolved in 2 ml of aqueous counting scintillation fluid (Amersham Biosciences). Radioactivity in the medium was measured by adding of 100 µl of the media directly to 2 ml of aqueous counting scintillation fluid (Amersham Biosciences).

2.12.2 Measurement of Taxol metabolites by thin layer chromatography

Aliquots of 0.2 ml of the chloroform phase were dried down under N_2 and dissolved in 100 µl of chloroform/methanol (9:1). Each sample was loaded on to plastic-supported silica gel 60 thin layer chromatography (TLC) plates and the plates were developed with toluene/acetone/formic acid (60:39:1, by vol.) for 12 cm [174]. The plates were dried and the radioactive metabolites were identified by comparison of the R_f values. The R*f* for [^{3}H]Taxol was determined by BioScan 200 Imaging Scanner Bioscan. The migration of non-radiolabeled Taxol was also visualized by using 5% vanillin-sulfuric acid**.** Bands also were cut and [**^{3}**H]-labeling was measured by liquid scintillation counting.

2.13 Cellular distribution localization of Taxol

2.13.1 Collection of cell ghost and the cytosolic compartment

Approximately 2 x 10^6 MCF-7 breast cancer cells were plated in 10 cm cell culture dishes and grown to confluence in RPMI1640 medium with 10% FBS at 37ºC in an atmosphere of 5% CO_2. The medium was replaced to 5 ml RPMI1640 medium containing 10% of charcoal-treated FBS containing 0.5µCi [^{3}H]Taxol in 50 nM non-radioactive Taxol. After 26 h incubation, LPA (5µM) was added to some dishes. Also Taxol was removed from some dishes and 5 ml of medium or medium containing 5 µM LPA was added. At the indicated time points, medium was collected and after washing of the cells twice with ice-cold PBS, 4 ml of digitonin lysis buffer containing 10 mM HEPES, 0.5 mM DDT. 0.081 mM digitonin, pH 7.4, protease inhibitors, 100 nM phosphatase inhibitor (Microcystin-LR), and 100 nM protease inhibitor was added to each plate when the dishes were

placed onto an ice-cold glass plate. The digitonin lysis period was 4-5 minutes (digitonin lysis period was optimized by lactate dehydrogenase, LDH, assay). At the end of the lysis period, 3.5 ml of digitonin lysis solution (cytosolic compartment) was collected. After washing twice with ice-cold PBS, the cell lysate (membrane bound compartment) was collected by scrapping twice with 0.5 ml of ice-cold cell ghost buffer (10 mM HEPES, 0.5 mM DTT, 250 mM sucrose, pH 7.4, 100 nM phosphatase inhibitor and 100 nM protease inhibitor).

2.13.2 Measurement of lactate dehydrogenase (LDH) activity

Each sample of the cytosolic extract (25 µl per well) was plated in duplicate in a 96-well plate. Two hundred µl of freshly prepared LDH cocktail (5.65 ml of 1 M Tris pH 7.4, 26.5ml double distilled water, 5 mg sodium pyruvate and 7.77 mg nicotinamide adenine dinucleotide) was added to each well. Then the decrease in absorbance at 340 nm was calculated/min with a SPECTRAmax 250 microplate spectrophotometer using Softmax Pro Alias program to determine LDH activity.

2.13.3 Measurement of intracellular distribution of Taxol

Lipid extraction (1ml methanol, 1ml chloroform and 0.9 ml 2M KCl) was done in cytosolic and membrane bound fractions. Radioactivity was measured by adding 100 µl of extracted bottom phase to a scintillation vial, drying the solvent and then adding to 4 ml of scintillation solution.

2.13.4 GSK-3αß and survivin protein detection

Cytosolic and membrane bound compartments applied for acetone precipitation to precipitate proteins. First, we added four times the sample volume of ice-cold aceton to

the samples and after vortexing, incubated in -20ºC for 2 h. Then we centrifuged the tubes for 1 h in 3500 *x g*. After decanting the supernatant, the pellets were re-suspended in 100 µl of RIPA buffer (NaCl 150mM, NP-40 1%, deoxycholic acid 0.5%, SDS 0.1%, Tris pH 8.0 50mM, phosphatase inhibitor 100 nM and protease inhibitor 100 nM) and analysed using 12% SDA-PAGE. Nitrocellulose membranes were treated with Odyssey blocking buffer overnight at 4°C and then incubated with 1:1000 dilutions of anti total GSK-3 α/ß, phospho-GSK-3 α/ß (pTyr 279/216 and pSer 21/9), survivin and phospho-survivin (T34). We applied 1/2000 dilutions of anti calnexin, as the loading control for membrane bound compartment, and 1/5000 dilutions of anti GAPDH, as the loading control for cytosolic compartment. After 1 h incubation with the antiboies, blots were washed four times with PBS+0.1% Tween-20. Blots were then incubated in 1:5000 dilutions of goat anti-rabbit IgG for 45 min. After washing four times, ATX was visualized at 700 and 800 nm with the Odyssey Infrared Scanner.

2.14 Knockdown of survivin expression using siRNA

Knockdown of survivin was achieved by seeding about 2 x 10^5 cells on 3.5 cm dishes with 2 mL of antibiotic-free RPMI 1640 containing 10% FBS. Cells were grown up to almost 50% confluency. Ten microliters of stock siRNA with the targeting sequence of 5'-GCAUUCGUCCGGUUGCGCU-3' and siControl (20 µM) (Qiagen, Missisauga, ON, Canada) was diluted in 4 mL opti-Mem Reduced Serum Medium (Invitrogen Life Technologies) and incubated for 5 min at room temperature. Then, 3 µL of HiPerFect transfection reagent (Qiagen, Mississauga, Ontario) was added to each tube and incubated for 15 min at room temperature.

Each dish of cells received 500 µL of the siRNA and the HiPerFect solutions. The final concentration of siRNA was 20 nM. Cells were then incubated for 24 h at 37°C and the cell lysate was collected by scrapping twice with 0.2 ml of RIPA buffer (150mM NaCl 1% NP-40 0.5% deoxycholic acid 0.1% SDS 50mM Tris pH 8.0, 100 nM phosphatase inhibitor and 100 nM protease inhibitor).

2.15 Knockdown of GSK-3ß expression using siRNA

Cells (2 x10^5) were plated on 3.5 cm dishes with 2 mL of antibiotic-free RPMI 1640 containing 10% FBS. Cells were grown until 50% confluency. Knockdown of GSK-3ß was obtained by using 50 nM siGenome set of four siRNA from Dharmacon, Inc. (Lafayette, CO). The target sequences include:

5´-GAAGAAAGAUGAGGUCUAU-3´

5´- GGACCCAAAUGUCAAACUA-3´

5´- GAUGAGGUCUAUCUUAAUC-3´

5´- GAAGUCAGCUAUACAGACA-3´

Ten microliters of stock siRNA (50 µM) was diluted in 1.5 mL of Opti-MEM Reduced Serum Medium. In a separate tube, 30 µL of Lipofectamine 2000 (Invitrogen Life Technologies) was mixed with 1.5 mL Opti-MEM and incubated at room temperature for 15 min. The diluted siRNAs and the Lipofectamine solutions were then combined and incubated for another 15 min at room temperature. Each dish of cells received 2 mL of the siRNA-Lipofectamine 2000 complex that was added drop-wise while swirling the dish. The final

concentration of siRNAs was 50 nM. Cells were then incubated for 24 h at 37°C and the cell lysate was collected as described above.

2.16 Statistical analysis

The results were expressed as the mean ± SD from at least three independent experiments. The significance of differences were analyzed by one-way analysis of variance (ANOVA) or two-way ANOVA followed by a Newman-Keuls post-hoc test. Paired T-tests were also performed between two samples. A P value of < 0.05 was set for the significant difference among study groups. Statistical analysis and graphing were performed using GraphPad 4 software (Prism).

CHAPTER 3

RESULTS

A version of first part of this chapter has been published. Samadi N, Gaetano C, Goping IS, Brindley DN. 2009. Oncogene. 28: 1028–1039.

Results from the last part of this chapter are in preparation for publication.

3.1 Introduction

In the present study, we investigated the role of ATX, LPA and LPC in chemoresistance against Taxol in MCF-7 breast cancer cells and MDA-MB-435 melanoma cells. First we determined the concentration-dependent killing activity of Taxol in both cell lines. Then we showed the protective effect of LPA on Taxol-induced nuclei fragmentation as well as loss of mitochondrial membrane potential in these cells. Isobologram analysis was also applied to evaluate the interactions between Taxol and LPA at the IC_{50} (inhibitory concentration 50%) to determine the antagonistic effect between LPA and Taxol.

To detect the role of ATX in protection against Taxol-induced apoptosis in cancer cells, we first determined ATX expression by measuring its mRNA, protein concentration and activity levels in both MCF-7 and MDA-MB-435 cells. Then, concentrated conditioned media from MDA-MB-435 cells, which secrete ATX, or recombinant ATX (rATX) was applied in the presence or absence of LPC, to show whether ATX protects MCF-7 cells against Taxol-induced mitochondrial membrane potential loss and nuclei fragmentation. Applying two different ATX inhibitors (VPC8a202 and S32826) confirmed the protective role of ATX in the presence of LPC against Taxol-induced apoptosis.

We also determined the mechanism through which LPA protects cancer cells against Taxol-induced apoptosis. We examined the role of PI3K/Akt and MAPK/ERK pathways in LPA-induced protection by applying LY294002 and PD98059, respectively. Western blot analyses for phospho- and total Akt, phospho- and total ERK (p42 and p44 MAPK) was also performed to show the

role of Taxol and LPA on induction of total and phosphorylated protein levels of Akt and MAPK.

To determine the protective mechanism of LPA against Taxol-induced apoptosis, we also measured ceramide mass in the cells treated with an optimum concentration of Taxol in the presence and absence of LPA and a PI3K inhibitor (LY294002). The mass of ceramide (pmol) was normalized to the concentration of phospholipid phosphate (nmol) in each individual lipid extract.

We also investigated the interactions of LPA versus Taxol on the cancer cell cycle. We already know that Taxol causes G2/M arrest in breast cancer cells. We determined if LPA changed the induction of G2/M arrest by Taxol. First cells were incubated with optimum concentrations of Taxol and LPA in the presence and absence of the PI3K inhibitor. Then the DNA content was measured using propidium iodide (PI) staining. Acquisition and analysis were performed on a Becton–Dickinson FACScan with CellQuest software. Then, we tested two possibilities to explain the role of LPA in changing in the number of cells arrested in G2/M by Taxol: LPA inhibits MCF-7 cells entering G2/M or LPA releases cells from Taxol-induced G2/M arrest. To test these hypotheses, we labeled the cells with BrdU before and after inducing G2/M arrest. BrdU is a synthetic thymidine analog that is incorporated into the DNA when the cell is dividing (S phase). Then, we chased the labeled cells through cell cycle. We also investigated the role of LPA in changing the percentage of the cells that are in mitosis, mitotic cells with abnormal spindle, dead cells, mononucleated and multinucleated cells by immunocytochemistry. Our studies showed a significant release of the cells

from G2/M by LPA. To investigate the mechanisms through which LPA can release the cells from Taxol-induced G2/M arrest, we designed two hypotheses: possibility of expulsion of Taxol from the cells in the presence of LPA or changing in microtubule dynamicity by LPA. To test the first hypothesis, we applied [^{3}H]Taxol and detected the radioactivity in the media and cell lysate. To test the second hypothesis, we investigated the role of survivin and possible signaling pathways including PI3K/Akt and GSK-3 pathways in survivin regulation by applying inhibitors against both pathways as well as applying experiments with survivin and GSK-3ß knockdown.

3.2 ATX is expressed in MDA-MB-231 and MDA-MB-435 cells but not in MCF-7 cells

The expression of ATX in the MCF-7, MDA-MB-231 and MDA-MB-435 cells was determined and compared at three different levels: mRNA (real-time RT-PCR), protein (Western blot analysis) and activity (by applying fluorescent substrate for ATX and measuring the ATX activity by a Synergy2 system).

Real-time RT-PCR analysis showed that MDA-MB-435 cells expressed relatively high levels of ATX mRNA compared to MCF-7 and MDA-MB-231 cells (Figures 3.1 A and 3.2 A). MDA-MB-435 cells secreted ATX protein into the serum-free medium, whereas ATX was not detectable in the equivalent medium concentrated from MCF-7 or MDA-MB-231 cells (Figures 3.1 B and 3.2 B). The ATX activity secreted by MDA-MB-435 cells was about 24 times higher ($p<0.001$) than that from MCF-7 cells (Figure 3.1 C) and about 20 times higher ($p<0.001$) than that from MDA-MB-231 cells (Figure 3.2 C) when the

background of the medium was subtracted. These results establish a significant difference between MCF-7 and MDA-MB-435 cells in terms of ATX expression. Essentially, the MCF-7 cells provide a well characterized model system for studying apoptosis in the absence of ATX production. Therefore, the effects of introducing ATX activity using concentrated conditioned media from MDA-MB-435 cells or rATX can be examined. MDA-MB-231 cells, which produce very little ATX, were also applied for studying the role of LPA and LPC in migration of cancer cells [5].

3.3 Lysophosphatidate protects MCF-7 cells from Taxol-induced apoptosis

3.3.1 The effect of activated charcoal in removal of autotaxin and LPA

There was no significant ATX activity in charcoal-treated FBS (2 g charcoal /50 ml of FBS after overnight rotating in 4 ºC) compared to FBS (Figure 3.3). Addition of activated charcoal (2 g charcoal/50 ml) to the media containing 1 µCi of ^{32}P-labeled LPA showed a 98% decrease in radioactivity after overnight rotating at 4 ºC (Figure 3.4). These results show that charcoal treatment is effective in removing endogenous LPA from serum used for the incubations; therefore, the action of different concentrations of added LPA could be determined accurately.

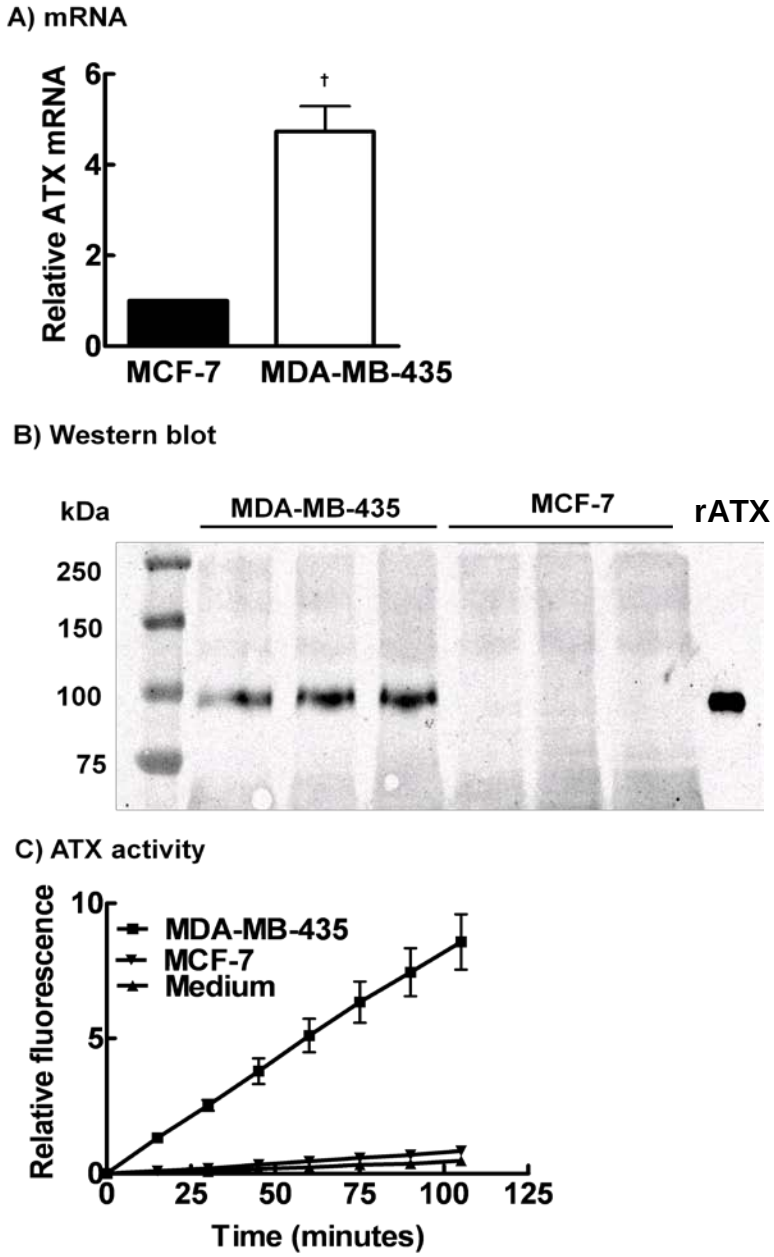

Figure 3.1 Differential expression of ATX in MDA-MB-435 and MCF-7 cells. In (**A**), mRNA for ATX was determined by real-time RT-PCR and expressed relative to that of glyceraldehyde 3-phosphate dehydrogenase (GAPDH). (**B**) A representative western blot obtained by loading 40 g of total protein from three independent samples of concentrated serum-free medium obtained from either MDA-MB-435 or MCF-7 cells is shown. A standard of rATX is shown on the right. In (**C**), 20 times concentrated serum-free medium from MCF-7 and MDA MB-435 cells was assayed for ATX activity using the FS-3 compound. Fluorescence was measured at excitation and emission wavelengths of 485 and 538 nm, respectively. The results are shown as the average of relative fluorescence activity ± s.e.m. from three independent experiments. † $P<0.001$.

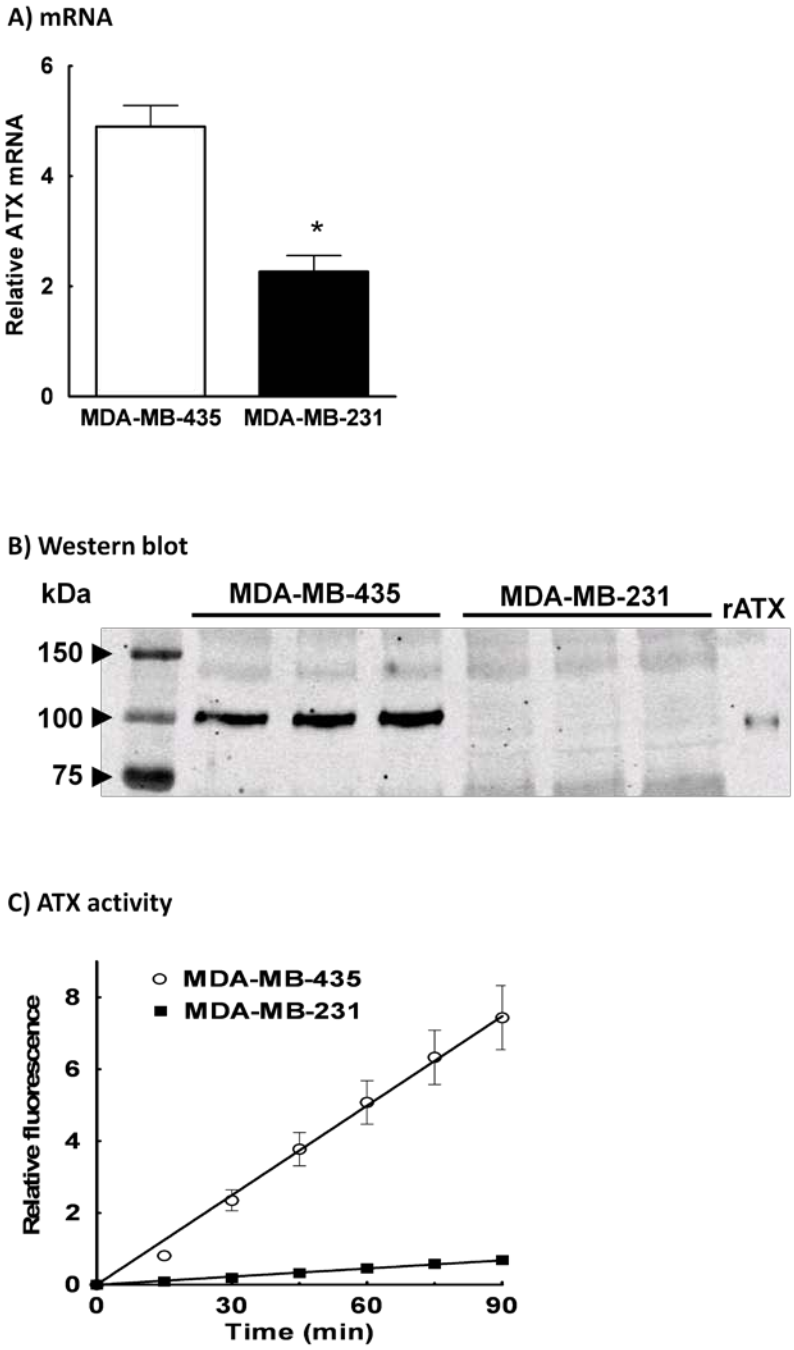

Figure 3.2 Differential expression of ATX in MDA-MB-435 and MDA-MB-231 cells. In (**A**), mRNA for ATX was determined by real-time RT-PCR and expressed relative to that of glyceraldehyde 3-phosphate dehydrogenase (GAPDH). (**B**) A western blot obtained as mentioned in Figure 3.1. A standard of rATX is shown on the right. In (**C**), 20 times concentrated serum-free medium from MDA MB-435 and MDA-MB-231 cells was assayed for ATX activity as mentioned in Figure 3.1. The results are shown as the average of relative fluorescence activity ± s.e.m. from three independent experiments. $^{*}P<0.05$.

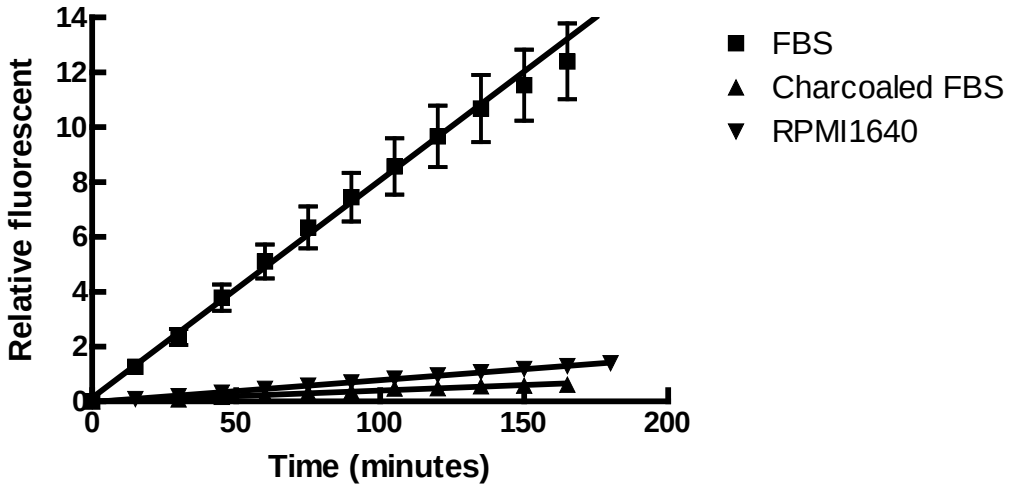

Figure 3.3 The effect of activated charcoal in removal of autotaxin. Charcoal-treated FBS was prepared by adding 2 g active charcoal to 50 ml of FBS. After overnight rotating at 4ºC, charcoal-treated FBS was centrifuged and filtered twice with syringe driven filter (0.22 µm). Then, both charcoal-treated and non-treated FBS were assayed for ATX activity using the FS-3 compound. Fluorescence was measured at excitation and emission wavelengths of 485 and 538 nm, respectively. The results are shown as the average of relative fluorescence activity ± s.e.m. from three independent experiments.

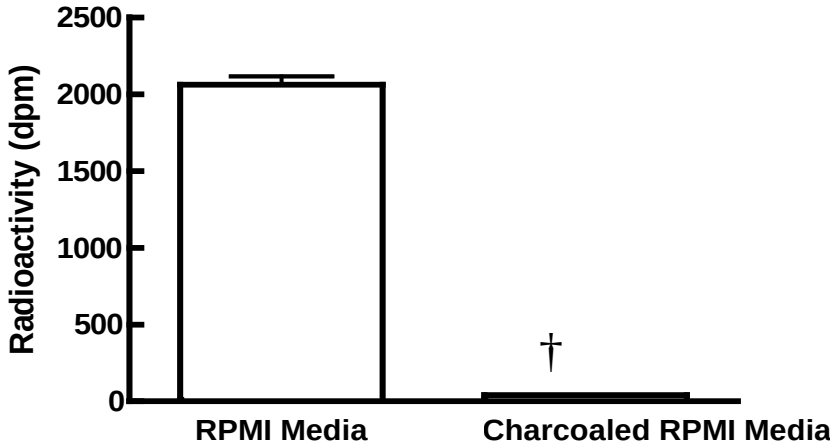

Figure 3.4 The effect of active charcoal in removal of LPA. ^{32}P-labeled LPA (1 µC) was added to 50 ml of RPMI 1640 and then activated charcoal (2 g) was added and shacked overnight at 4 ºC. After centrifugation and syringe driven filtration (0.22 µm), the radioactivity was measured in 50 µl of each sample using scintillation solution. The results are shown as the average of relative fluorescence activity ± s.e.m. from two independent experiments. † $P<0.001$

3.3.2 Measurement of half-life of LPA

The half-life of LPA was calculated with the same number of the cells that were used for TMRE staining (2 x 10^5 cells were grown to 70% confluence) by measuring the conversion of ^{32}P-labeled LPA to $^{32}P_i$ in the medium that was collected at indicated time points up to 24 h. Our measurement showed a half-life of about 8 h for LPA at 1 or 20 μM (Figure 3.5). This was relatively independent of the LPA concentration used.

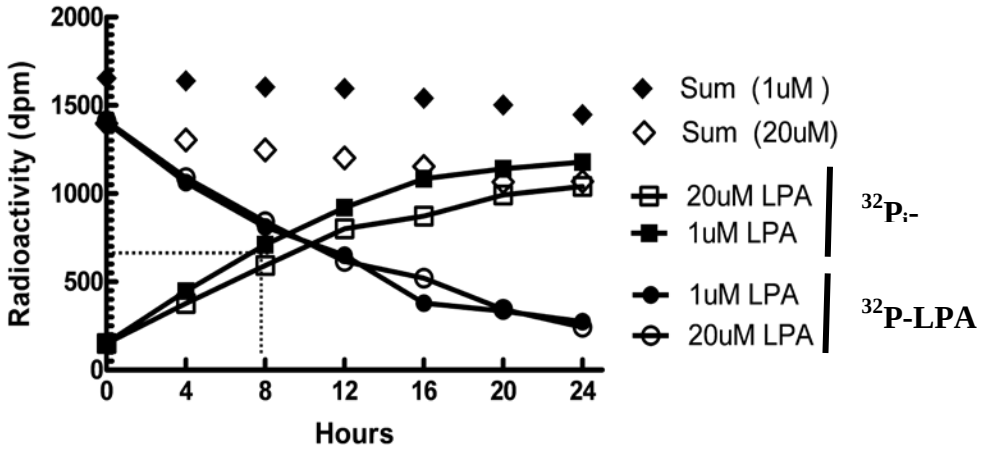

Figure 3.5 Breakdown of LPA. Six-well plates were seeded with 2 x 10^5 cells and these were grown to 70% confluence. After washing the cells twice with PBS, the media was changed to 2 ml of serum-free media containing ^{32}P-labeled LPA (1 μCi) with either 1 or 20 μM of non-radioactive LPA. The half-life of LPA was determined by measuring $^{32}P_i$- and ^{32}P-labeled LPA after lipid extraction in the medium that was collected at indicated time points up to 24 h.

3.3.3 The role of LPA in protection of cancer cells against Taxol-induced apoptosis

We next established conditions for studying Taxol-induced apoptosis and how LPC and LPA modify this process. Apoptosis was detected both by morphological examination using DAPI staining and by measuring mitochondrial TMRE uptake. We used medium supplemented with 10% FBS that had been treated with activated charcoal-treated to remove ATX and lipid mediators including LPC and LPA.

Treating MCF-7 cells with 50 nM Taxol produced an optimum increase in the percentage of recovered apoptotic nuclei from 0.8% to about 12% after 24 h and 26% after 48 h incubation (Figure 3.6A). MDA-MB-435 cells treated with 50 nM Taxol also showed a significant increase in the percentage of apoptotic nuclei from 0.7% to about 9% after 24 h and about 18% after 48 h incubation (Figure 3.7). This provides part of the picture, since treatment with 50 nM Taxol for 24 and 48 h decreased the number of cells attached to the dishes by about 60 and 70%, respectively (Figure 3.6B). We could not recover most of these cells from the medium presumably because of complete fragmentation. These results are compatible with those of *[175]*, who concluded that Taxol induces both apoptotic and non-apoptotic death in MCF-7 cells.

The next experiments determined whether LPA can protect against apoptosis induced by 50 nM Taxol over 24 h. LPA (0.5 µM) alone had no significant effect on the percentage of apoptotic nuclei, but it produced a maximum decrease in the percentage of apoptotic cells remaining on the plates in the presence of Taxol. Less effect was observed at 5 and 10 µM LPA (Figure 3.6

C). However, 0.5–10 µM LPA increased the recovery of viable cells from 49 ± 4.3% to 68 ± 6.1% (Figure 3.6 D).

Figure. 3.6 Protective effect of LPA on Taxol-induced apoptosis in MCF-7 cells. (**A**) The percentage of apoptotic nuclei from MCF-7 cells that were incubated with 0–200 nM Taxol for 24 h (□) or 48 h (▲) is shown. (**B**) The percentage of viable cells recovered from the wells expressed relative to untreated cells is shown. (**C** and **D**). The percentage of apoptotic nuclei and viable cells, respectively, that were recovered after adding different concentration of LPA with 50 nM Taxol and incubating for 24 h is shown. Results are expressed as means ± s.e.m. from three independent experiments.

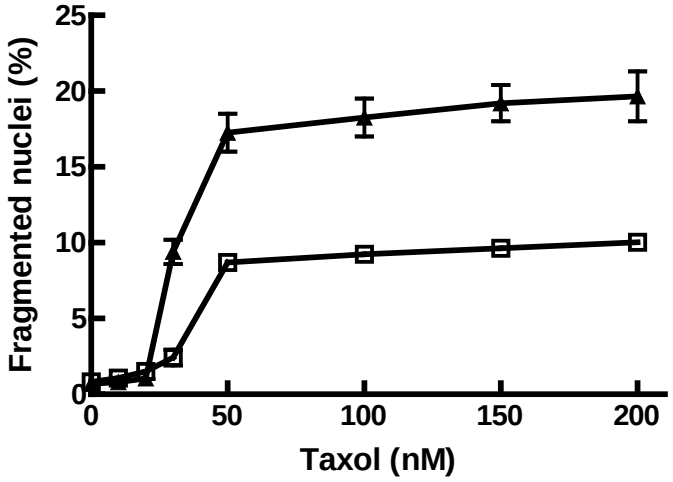

Figure 3.7 Taxol killing curve for MDA-MB-435 cells. The percentage of apoptotic nuclei from MDA-MB-435 cells that were incubated with 0–200 nM Taxol for 24 h (□) or 48 h (▲) is shown.

3.3.4 The role of LPA on Taxol-induced changes in mitochondrial potential

To confirm the protective effect of LPA against Taxol-induced apoptosis, we applied TMRE Flow cytometric assay. Our results show that Taxol increased the percentage of apoptotic (TMRE negative) cells and this effect was optimum at 20 nM Taxol. Although Taxol produced a maximum of 35% apoptotic cells after 24 h, we chose to use 48 h incubations, which consistently increased the population of apoptotic cells to about 55% (Figure 3.8 A). We then studied the effects of maintaining 0-20 μM LPA through this 48 h incubation on the effects of different concentrations of Taxol (0-50 nM). LPA had a significant protective effect against Taxol-induced apoptosis with a concentration range of 5-20 μM. Maximum protection was obtained with 5 μM LPA against 20 nM Taxol in which the

percentage of apoptotic cells decreased from 54 ± 2% to 33 ± 3% ($p<0.05$) (Figure 3.8 B).

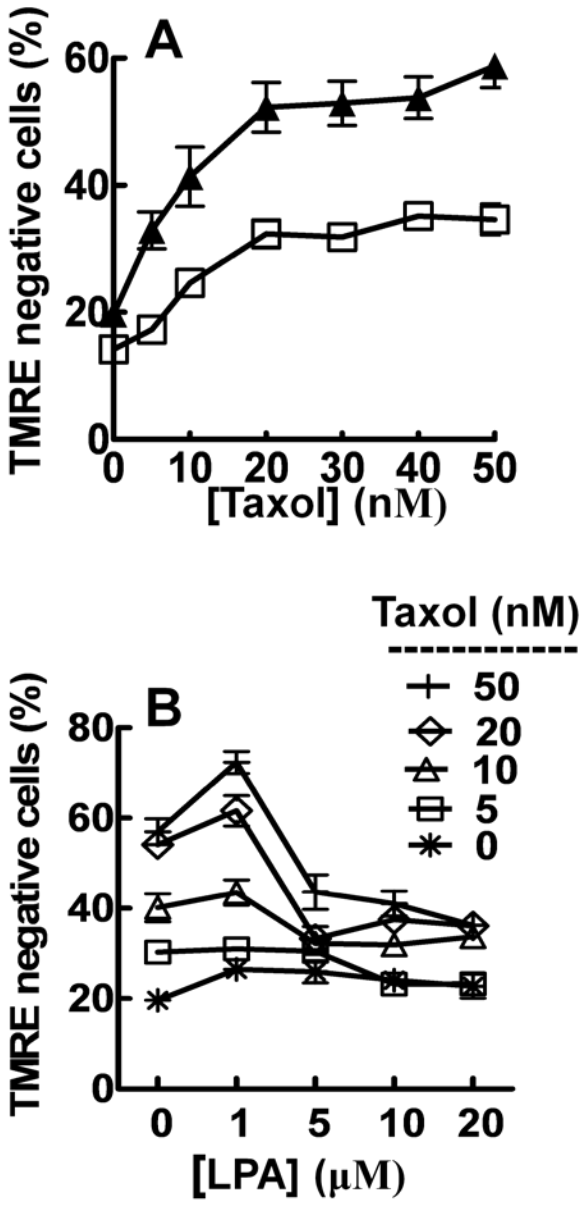

Figure 3.8 Effect of LPA on Taxol-induced change in mitochondrial potential. (**A**) The percentage of tetramethylrhodamine ethyl ester (TMRE) negative MCF-7 cells that were obtained after incubated with 0–50 nM Taxol for 24 h (□) or 48 h (▲) is shown. (**B**) The percentage of TMRE-negative cells obtained after adding different concentrations of Taxol (0–50 nM) with 0–20 μM LPA is shown. The results are shown as means ± s.e.m. of three experiments.

3.4 LPA shows a strong antagonistic effect with Taxol

The dose response interactions between different concentrations of Taxol and LPA at the IC_{50} (inhibitory concentration 50%) point were evaluated by the isobologram method. The effects of 48 h co-exposure to different doses of LPA on the response of MCF-7 breast cancer cells to Taxol were shown in Table 1. IC_{50} values were chosen to analyze the combination effect of LPA and Taxol in terms of cytotoxicity. All LPA concentrations used produced an antagonistic effect on Taxol-induced apoptosis with CI values of very much higher than 1 (Table 1). This antagonism was particularly apparent at 10 and 20 μM LPA ($p<0.01$). For example, a dose of 50 nM Taxol was required when 20 μM LPA was present to produce an equivalent level of apoptosis to that obtained with 7.2 nM Taxol in the absence of LPA. Thus, the presence of 20 μM LPA produced a 6.9-fold decrease at IC_{50} in Taxol sensitivity.

Table 1. Effect of LPA on Taxol-induced changes in mitochondrial potential. The dose response interactions between Taxol (5-50 nM) and LPA (1-20 μM) was calculated by the isobologram technique (CalcuSyn software, Biosoft, Cambridge, UK.). Fractional apoptosis indicates the percentage of apoptosis induced at different combinations of Taxol and LPA. The dose response index shows the efficacy of Taxol in induction of apoptosis in the presence of LPA. Combination Index values of >1 indicates antagonism between Taxol and LPA. For all estimations of CI, we used only isobols where intercept data for both axes were available.

Combination Dose			***Taxol Dose***	***Dose Response***	***Combination***
Taxol (nM)	***LPA (μM)***	***Fractional apoptosis***	***(nM) (alone)***	***Index***	***Index***
5	***1***	***0.31***	***4.6***	***0.9***	***22.2***
10	***5***	***0.32***	***5.0***	***0.5***	***231***
20	***10***	***0.38***	***8.0***	***0.4***	***1630***
50	***20***	***0.36***	***7.2***	***0.2***	***1490***

3.5 ATX protects MCF-7 and MDA-MB-435 cells against Taxol-induced Apoptosis only in the presence of LPC

3.5.1 Concentrated medium from MDA-MB-435 cells and protection against Taxol-induced apoptosis in MCF-7 cells

We studied whether ATX protects MCF-7 cells against Taxol-induced apoptosis by changing the balance of cell activation by LPC versus LPA. MCF-7 cells were incubated with 10% charcoal-treated FBS and concentrated media from MDA-MB-435 cells or MCF-7 cells (up to 200 µl per 10^6 cells by centrifugation using a Centricon Millipore's Ultracel YM) in the presence or absence of LPC or LPA. Concentrated medium from MDA-MB-435 cells showed an average of 24 times more ATX activity compared with equivalent medium from MCF-7 cells (Figure 3.1 C).

Concentrated medium from MDA-MB-435 cells supplemented with 200 µM LPC decreased percentage apoptosis measured by DAPI staining from 7.4 ± 1.3% to 4.4 ± 0.6% (88% of the effect of 0.5 µM LPA) (Figure 3.9 A). The percentage of viable cells recovered also increased (49 ± 3% to 77 ± 7%; $P<0.05$) (Figure 3.9B). Concentrated medium from MDA-MB-435 cells appeared to decrease apoptosis (6.1 ± 0.8%) in the absence of added LPC or LPA, but this was not statistically significant. LPC in the absence of conditioned medium had no protective effect (Figure 3.9 A).

We also applied an ATX inhibitor, VPC8a202 [176], to determine whether the effect of concentrated medium depended upon ATX activity. VPC8a202 (1µM) decreased ATX activity by 87% as expected and it abolished the protective

effect of LPC plus concentrated media from MDA-MB-435 cells (Figure 3.9 A). There was no increase in the percentage of viable cells after applying the ATX inhibitor alone (Figure 3.9 B).

The TMRE assay also showed a significant decrease in apoptosis ($P<0.01$) in cells treated with concentrated medium from MDA-MB-435 cells when 200 µM LPC was added (Figure 3.9 C). Concentrated medium alone, or LPC alone, had no significant protective effect (Figure 3.9 C). VPC8a202 (1 µM) abolished the protective effects of concentrated media with LPC. As a control, the effects of VPC8a202 were shown to be specific for LPC, since it did not alter the protective effect of LPA on Taxol-induced apoptosis (Figures 3.9 B, C).

3.5.2 Recombinant ATX and protection against Taxol-induced apoptosis in MCF-7 cells

To confirm that the effects of concentrated medium on cells depended on ATX activity, we used rATX (50 ng/ml), which protected against Taxol-induced apoptosis and increased the number of viable cells recovered when LPC was present (Figures 3.10 A, B). Blocking ATX activity with 1 µM of ATX inhibitors VPC8a202, or S32826 [177], or heating at 70 °C abolished the protective effect of rATX.

3.5.3 Concentrated media from MCF-7 cells and protection against Taxol-induced apoptosis in MCF-7 cells

Concentrated medium from MCF-7 cells that contained no significant ATX activity failed to provide any significant protection with LPC against Taxol-induced apoptosis in DAPI staining (Figure 3.11 A). There was no significant effect of concentrated medium from MCF-7 cells in the presence of LPC on the Taxol-induced decrease in the number of viable cells (Figure 3.11 B). The TMRE assay also showed no effect on percentage of apoptosis in cells treated with concentrated medium from MCF-7 cells when 200 µM LPC was added (Figure 3.11 C).

These combined experiments established that ATX activity protects MCF-7 cells against Taxol-induced apoptosis by converting LPC to LPA. LPC, itself, has no protective effect against Taxol-induced apoptosis in these cells.

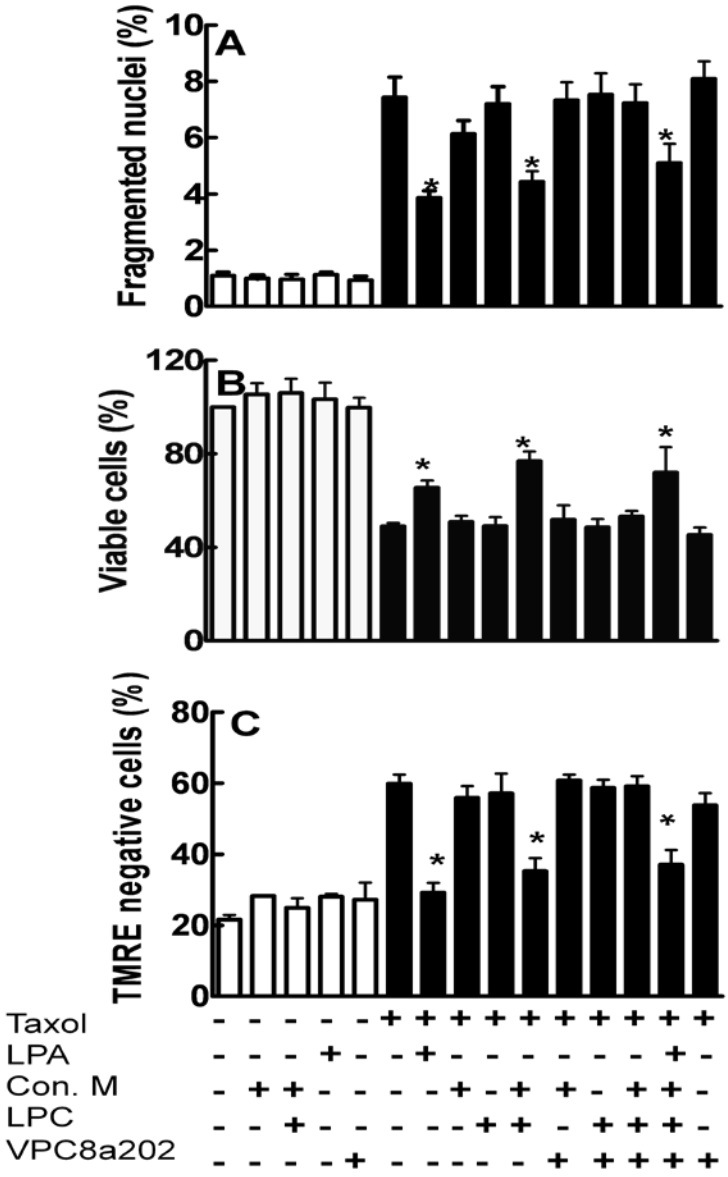

Figure 3.9 Concentrated media from MDA-MB-435 cells protects against Taxol-induced apoptosis in MCF-7 cells. Combinations of concentrated medium from MDA-MB-435 cells (medium/435) with 0.5 μM LPA for 4,6-diamidino-2-phenylindole (DAPI) staining and 5 μM LPA for the tetramethlyrhodamine ethyl ester (TMRE) assay), 200 μM LPC and the ATX inhibitors, VPC8a202 (1 μM) and S32826 (1 μM), were added with 50 nM (**A,B**) or 30 nM Taxol (**C**). Panels **A** and **B** show the percentage of fragmented nuclei and the relative number of viable cells on the dishes as determined by DAPI staining after a 24 h incubation. Panel **C** shows the percentage of TMRE-negative cells after a 48 h incubation. The results are shown as means ± s.e.m. of three experiments. $^{*}P<0.05$.

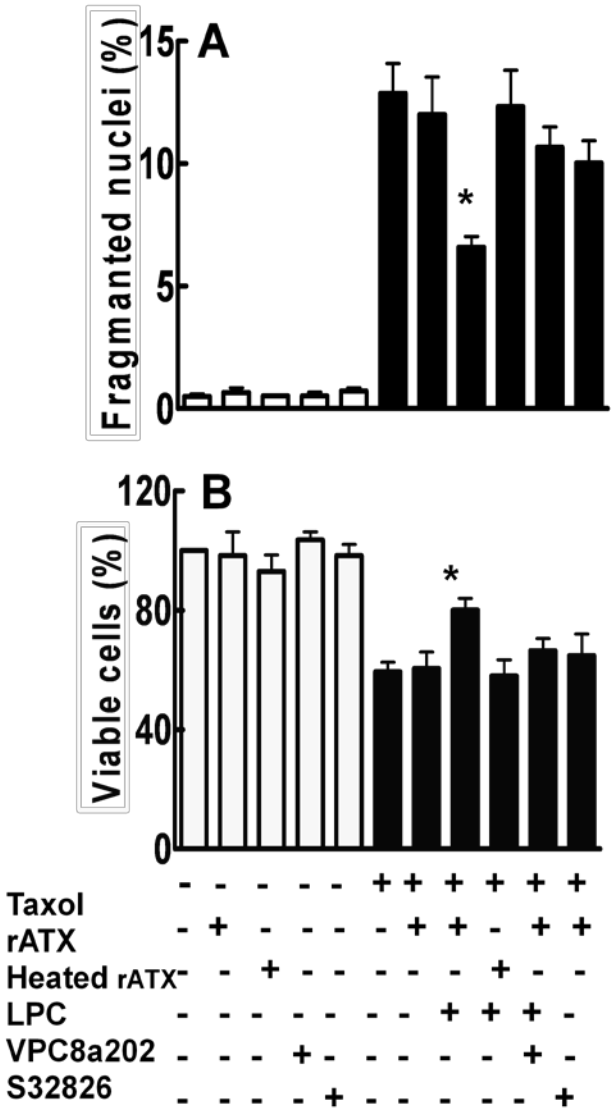

Figure 3.10 Recombinant ATX protects against Taxol-induced apoptosis in MCF-7 cells. Combinations of recombinant ATX (rATX) (50 ng/ml) with 0.5 µM LPA, 200 µM LPC and the ATX inhibitors, VPC8a202 (1 µM) and S32826 (1 µM), were added with 50 nM Taxol. Panel **A** shows the percentage of fragmented nuclei on the dishes as determined by DAPI staining after a 24 h incubation with 50 ng/ml rATX, rATX heated for 10 min at 70 °C to inhibit ATX activity >96% and/or the ATX inhibitors. Panel **B** shows the percentage of viable cells on the dishes determined by DAPI staining after a 24 h incubation with the same concentrations of rATX, Taxol, LPA, LPC and ATX inhibitors. The results are shown as means ± s.e.m. of three experiments. $^{*}P<0.05$.

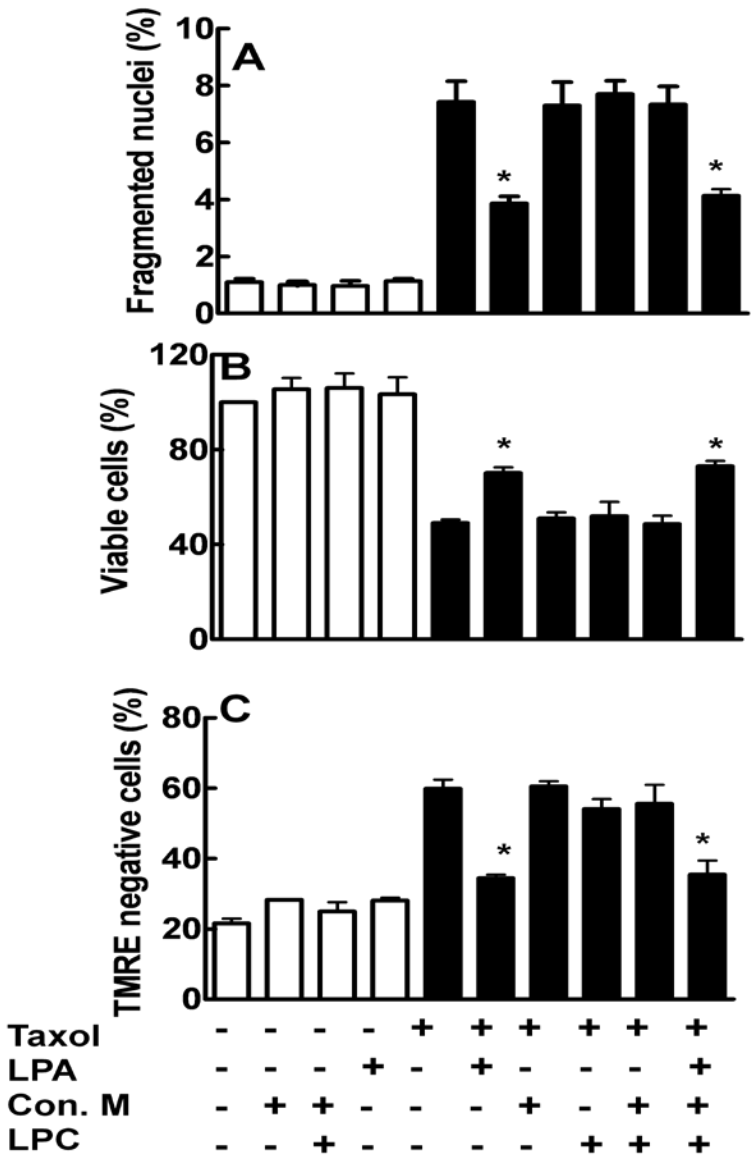

Figure 3.11 The effect of concentrated medium from MCF-7 cells on Taxol-induced apoptosis. Combinations of concentrated medium from MCF-7 cells (Medium/MCF-7), together with 0.5 μM LPA, or 200 μM LPC were added with 50 nM Taxol (A,B) or 30 nM Taxol (C). Panels **A** and **B** show the percentage of apoptotic cells and the relative number of viable cells on the dishes as determined by DAP1 staining after 24 h incubation. Panel **C** shows the percentage of TMRE negative cells after 48 h incubation. The results are shown as means ± SEM of three experiments. * $p<0.05$

3.6 LPA_1 and LPA_3 receptors are not involved in LPA-induced protection against apoptosis in MCF-7 cells

We applied pertussis toxin which inactivates $G\alpha_{i/o}$ and the functional coupling to LPA_1 receptors to show the role of LPA_1 receptors in LPA protective effect against Taxol-induced apoptosis. There was no significant change in the number of fragmented nuclei induced by LPA in Taxol-treated cells (Figure 3.12 A). Also pertussis toxin produced no change in the percentage of viable cells after applying with LPA and Taxol (Figure 3.12 B).

To confirm the results with pertussis toxin, we also applied VPC 32179, an antagonist against $LPA_{1/3}$ receptors. DAPI staining showed no significant change in the percentage of apoptotic nuclei (Figure 3.13A) or viable cells (Figure 3.13 B) when 1μM VPC 51299 was applied with Taxol and LPA. Our results excluded the role of LPA_1 and LPA_3 receptors in LPA-induced protection in MCF-7 cells.

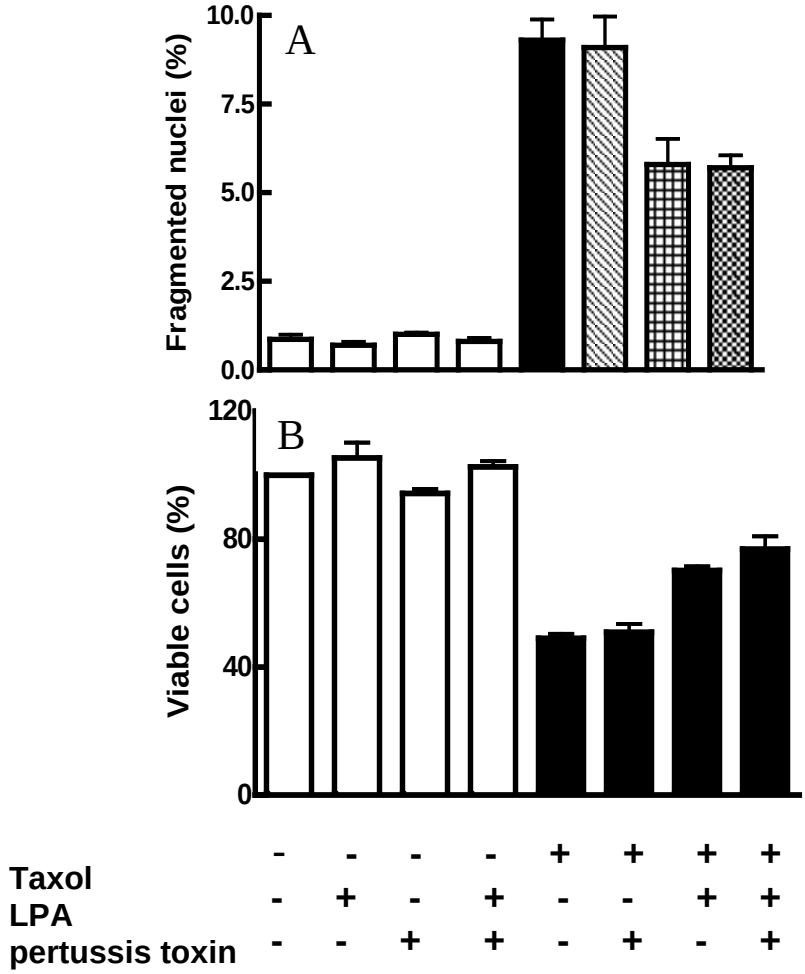

Figure 3.12 LPA_1 receptors have no significant effect on LPA-induced protection against Taxol-induced apoptosis in MCF-7 cells. Combinations of 50 nM Taxol with 0.5 μM LPA and pertussis toxin (100 ng/ml) were incubated with MCF-7 cells for 24 h and then 4,6-diamidino-2-phenylindole (DAPI) staining was applied to calculate the number of fragmented nuclei and viable cells. **(A)** The percentage of apoptotic nuclei is shown. (**B**) The percentage of viable cells recovered from the wells expressed relative to untreated cells is shown. Results are expressed as means ± s.e.m. from three independent experiments. $^{*}P<0.05$.

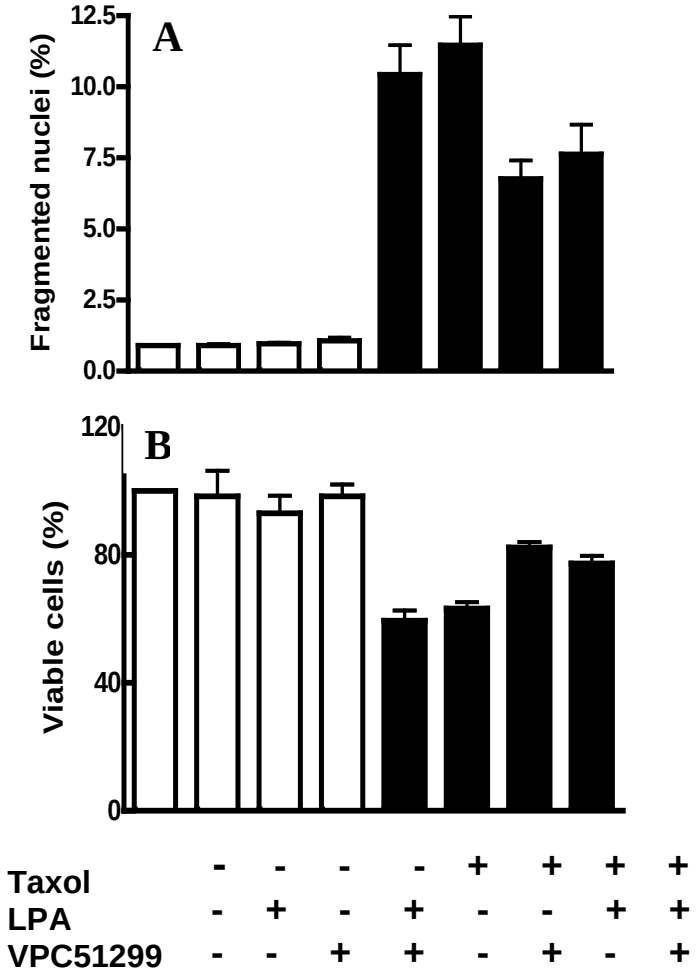

Figure 3.13 $LPA_{1/3}$ receptors have no significant effect on LPA-induced protection against Taxol-induced apoptosis in MCF-7 cells. Combinations of 50 nM Taxol with 0.5 µM LPA and the $LPA_{1/3}$ receptor antagonist, VPC51299 (1µM) were incubated with MCF-7 cells for 24 h and then 4,6-diamidino-2-phenylindole (DAPI) staining was applied to calculate the number of fragmented nuclei and viable cells. **(A)** The percentage of apoptotic nuclei is shown. (**B**) The percentage of viable cells recovered from the wells expressed relative to untreated cells is shown. Results are expressed as means ± s.e.m. from three independent experiments. $^{*}P<0.05$.

3.7 The PI3K/Akt pathway is involved in LPA-mediated protection against Taxol-induced apoptosis

These experiments determined the signaling pathways used by LPA to protect against Taxol-induced apoptosis. To examine the possible roles of the PI3K-Akt and MEK-ERK pathways, we determined the effects of LY294002 (PI3K inhibitor) and PD98059 (MEK inhibitor). LY294002 (50 μM) almost completely abrogated the effects of LPA in protecting against apoptosis using both DAPI staining and TMRE flow cytometery (Figures 3.14 A,B). PD98059 (40 μM) showed no significant effect on the LPA-mediated protection against Taxol-induced apoptosis, although it did block the activation of p42/44 MAPK (Figures 3.15 A-C). Also, phospho-42/44p MAPK and total 42/44p MAPK showed a significant increase over 12 h in response to LPA (Figures 3.15 A-C). There was no significant effect of Taxol on the expression of phospho-42/44p MAPK and total 42/44p MAPK ($p>0.05$).

LPA (5 μM) increased ($p<0.05$) the expression of both phospho-Akt and total Akt by about two fold over 12 h (Figure 15 A). Taxol (30 nM) alone had no significant effect. When Taxol was added with LPA (5 μM), there was still a 50% increase in phospho-Akt and total Akt compared to non-treated cells (Figure 15 A) and an increase in the phospho-Akt/total Akt ratio (Figure 3.15 D). Applying 50 μM LY294002 abolished the effect of LPA on the elevation of both activated and total Akt ($p<0.05$).

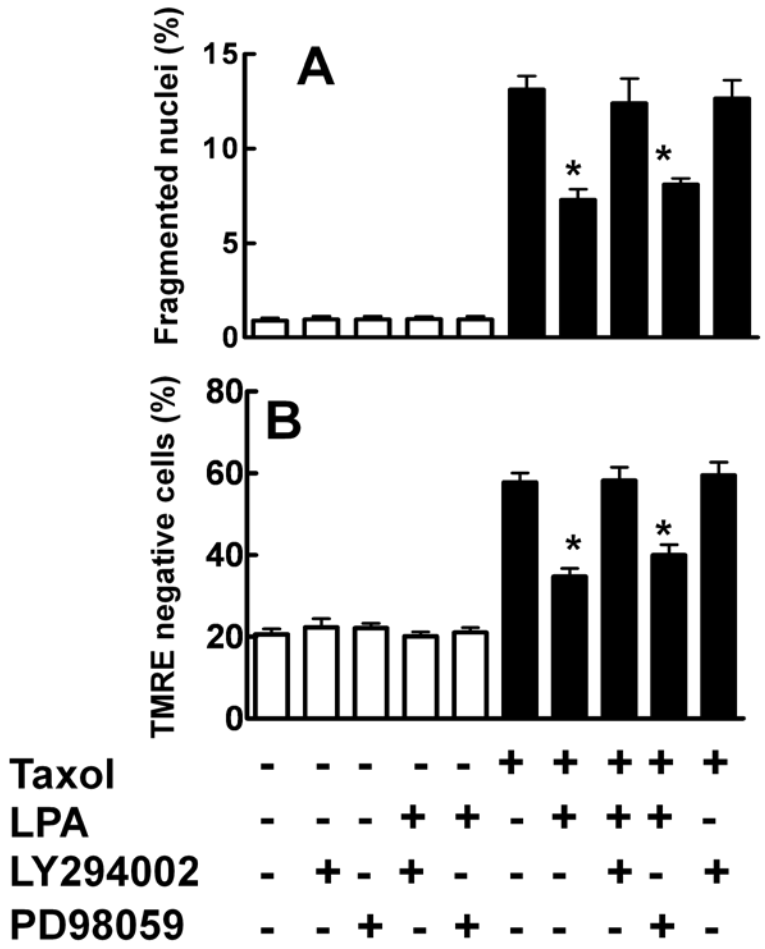

3.14 Phosphatidylinositol 3-kinase is required for LPA-mediated protection against Taxol-induced apoptosis. (**A**) The effects of 50 μM LY294002 and 40 μM PD9805 on the percentage of apoptotic nuclei in MCF-7 cells treated for 24 h in the presence or absence of 50 nM Taxol and 0.5 μM LPA are shown. (**B**) The effects of 50 μM LY294002 and 40 μM PD9805 on percentage of tetramethlyrhodamine ethyl ester-negative cells after treatment in the presence or absence of 30 nM of Taxol with 5 μM LPA are shown. Results are shown as means±s.e.m. of three experiments. $^{*}P<0.05$.

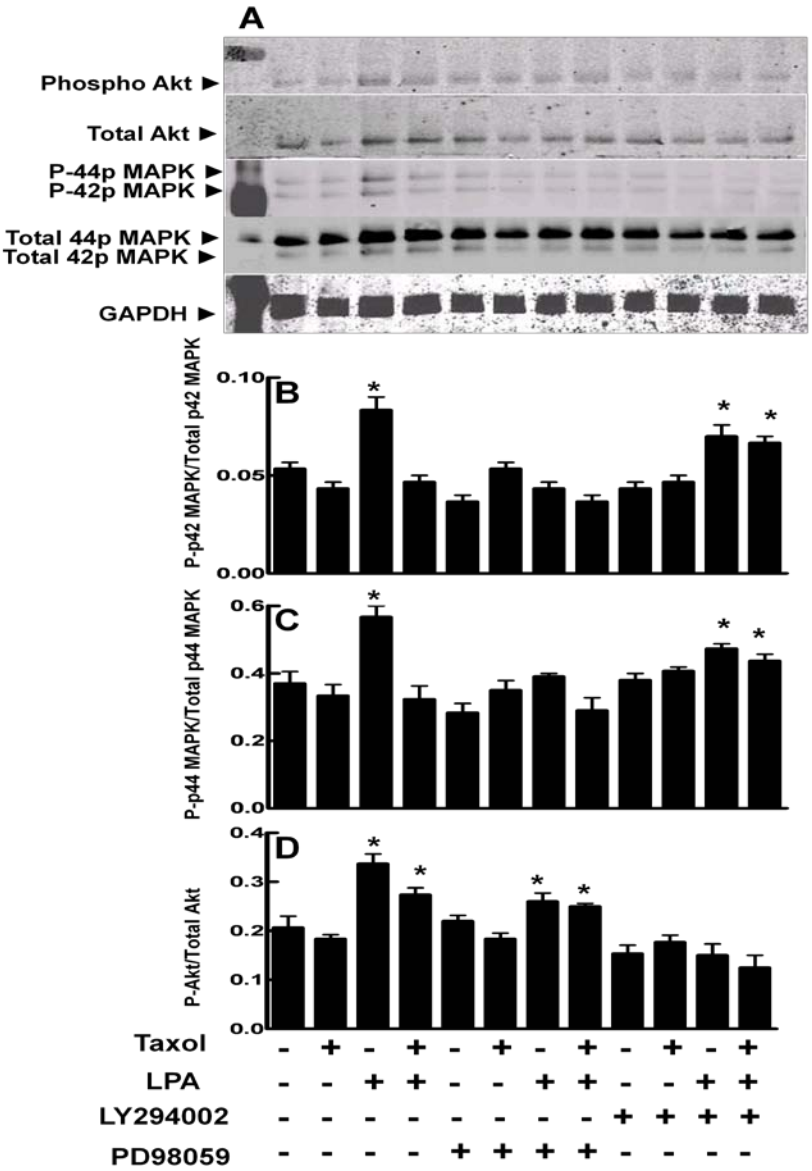

3.15 The effects of lysophosphatidate LPA on the PI3K/AKT and mitogen-ERK pathways. MCF-7 cells were incubated for 12 h with 30 nM Taxol and 5 μM LPA in the presence of 50 μM LY294002 (PI3K inhibitor) and 40 μM PD98059 (MAPK inhibitor). Results in (**A**) show the Western blot analyses for phospho- and total Akt, phospho- and total ERK (p42 and p44 MAPK) and glyceraldehyde phosphate dehydrogenase (GAPDH), which was used as a loading control. The results are representative of three independent experiments and they were quantified by densitometric analysis using a Licor Imaging System. (**B**) The densitometric ratio of phospho-p42MAPK/total p42MAPK is shown; (**C**) phospho-p44MAPK/total p44MAPK ratio is shown and in (**D**), phospho-Akt/total Akt is shown. The results are shown as means ± s.e.m. of three independent experiments. *Indicates the difference (P<0.05) from the non-treated cells.

3.8 LPA attenuates Taxol-induced ceramide production

To determine the protective mechanism of LPA against Taxol-induced apoptosis, we measured ceramide mass. There was a 2.9-fold increase in ceramide production in Taxol-treated cells ($p<0.05$) after 24 h of incubation. LPA (0.5 μM) decreased ($p<0.05$) Taxol-induced increase in ceramides to 1.9-fold. LY294002 (50 μM) blocked the effect of LPA in decreasing of ceramide production by about 80% (Figure 3.16).

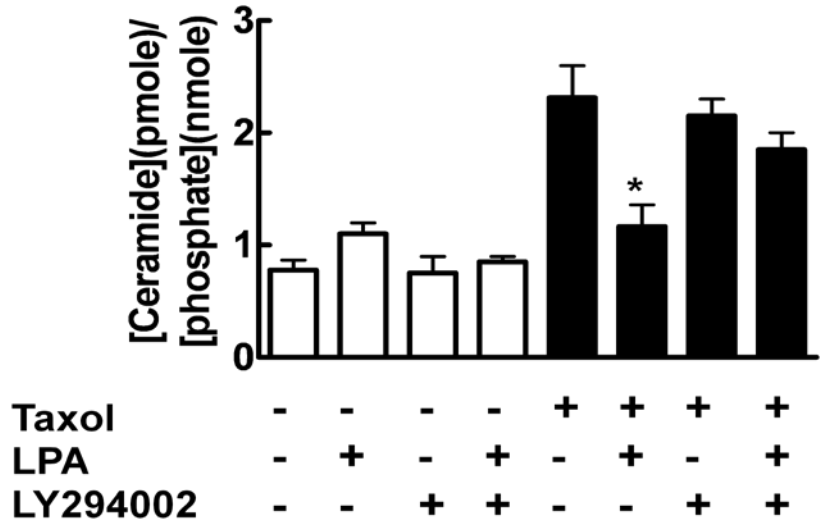

3.16 The role of Taxol and LPA in controlling ceramide concentrations. Ceramide mass was determined in MCF-7 cells after treating with 50 nM Taxol in the presence or absence of 0.5 μM of LPA or 50 μM LY294002 for 24 h. The mass of ceramide (pmol) was normalized to the concentration of phospholipid phosphate (nmol) in each individual lipid extract. The results are expressed as means ± s.e.m. of eight individual dishes for each treatment. $^{*}P<0.05$.

3.9 LPA attenuates Taxol-induced G2/M arrest

Taxol-induced apoptosis is accompanied by an increase in the accumulation of cells in the G2/M phase of the cell cycle [138]. Under our

conditions this represented an increase from about 16 to 43% ($p<0.05$) (Figures 3.17 A and C), which is compatible with previous studies [178,179].

Adding 5 μM LPA decreased the cells in G2/M to 28% and this represented reversal of the Taxol-induced effect of about by 44% ($p<0.05$) (Figures 17 C and D). Adding LY294002 blocked most of the LPA effect in reducing ($p<0.05$) the cells trapped in G2/M in the presence of Taxol (Figures 17 D and H). As controls, we showed that 50 μM LY294002 or 5 μM LPA alone, or in combination had no significant effect on the cells in G2//M phase (Figures 3.17 B, E and F). These results demonstrated the dominant role of the PI3K pathway in LPA-protection against Taxol-induced cell cycle arrest.

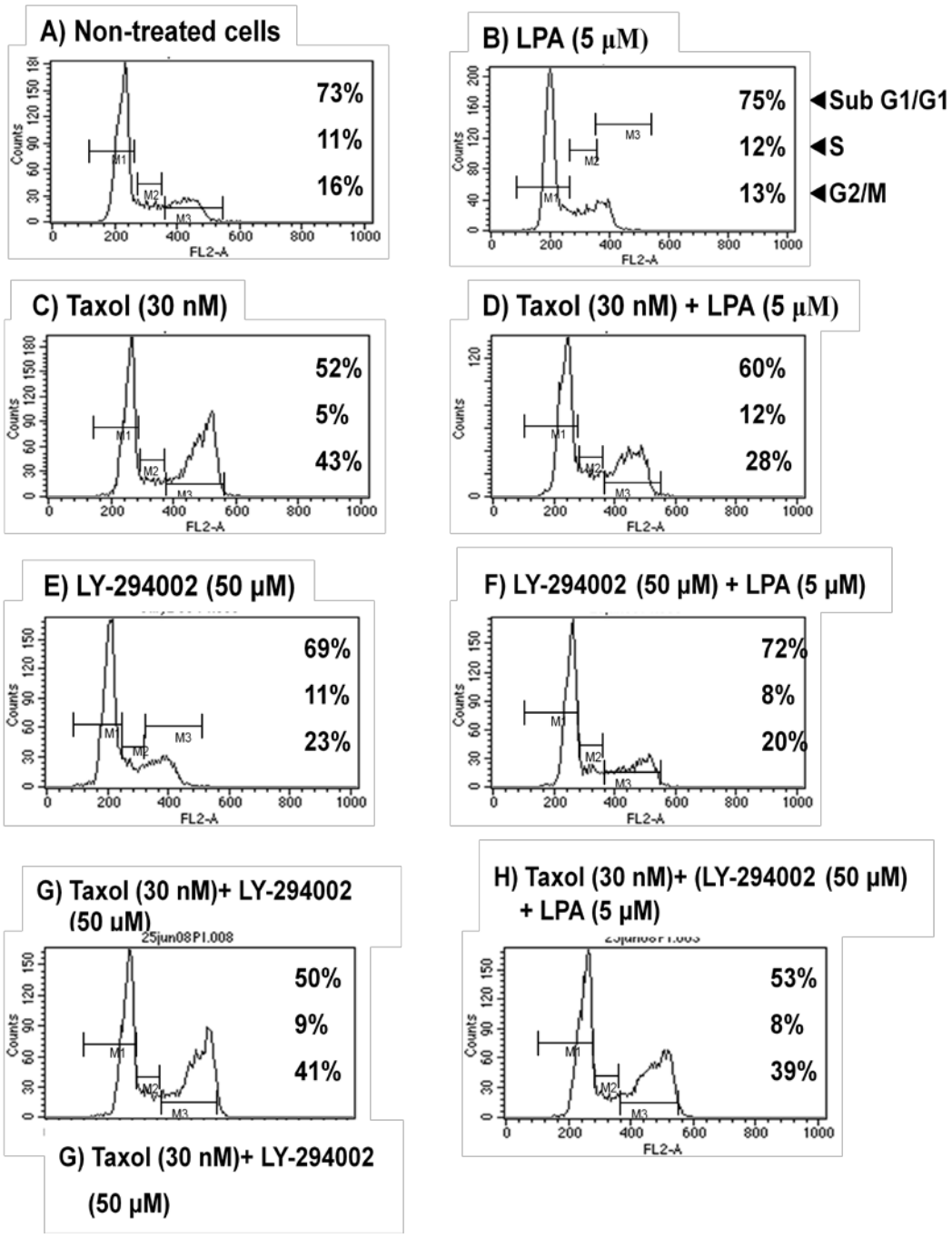

3.17 Effects of LPA and Taxol on cell cycle progression of MCF-7 breast cancer cells. MCF-7 cells were incubated for 48 h with 30 nM Taxol and 5 µM LPA. Then the cells were collected and stained with propidium iodide before analysis by fluorescence-activated cell sorting. DNA histograms were measured using CellQuest software and the percentage of G0/G1, S and G2/M cells were calculated. Results are representative of two independent experiments. The action of LPA in partially reversing the Taxol-induced G2/M arrest was also confirmed in a single experiment with a 24 h incubation.

3.10 How does LPA decrease Taxol-induced G2/M arrest?

To understand how LPA antagonizes the Taxol-induced arrest in G2/M (Figure 3.17), we investigated how LPA affects cell cycle progression in the presence or absence of Taxol. MCF-7 cells were first treated with BrdU. BrdU is a synthetic nucleoside that is an analogue of thymidine and it is commonly used in the detection of proliferating cells. BrdU can be incorporated into the newly synthesized DNA of replicating cells during the S phase of the cell cycle, substituting for thymidine during DNA replication. Antibodies specific for BrdU can then be used to detect the incorporated BrdU, thus indicating cells that were actively replicating their DNA.

We applied different protocols of labeling with BrdU and treatment with Taxol and LPA. In the first protocol (Protocol A; Figure 3.18), we labeled the cells with BrdU for 1 h. We then followed their progression through the cell cycle by FACS analysis for 12 h after treatment with 50 nM Taxol in the presence or absence of 5 μM LPA. These concentrations were established to give optimum cell killing and efficient rescue, respectively (Figure 3.8). The Taxol concentration is similar to that expected during chemotherapy and LPA concentrations are in the physiological range.

There was no significant change in the entry of labeled cells into G2/M and continuation to G1 when we applied LPA alone (Protocol A; Figures 3.18 A,B). Without Taxol, cells passed through S phase rapidly (within 2h). Adding Taxol significantly delayed the transit of cells through S phase ($p<0.05$) as

expected from previous work [180]. For example, after 2 h incubation, only 2.6± 1.2% of non-treated cells were in S phase but in Taxol-treated cells, 41.9± 7.8% of the cells were still in S phase.

LPA did not affect this delay (Figures 3.18 C,D). However, the presence of LPA allowed more Taxol-treated cells to enter G1 (55 ± 8% compared to 34 ± 6% after 12 h incubation) with a corresponding decrease in the number of cells in G2/M. These results indicate that LPA facilitates the release of some Taxol-treated cells from G2/M arrest.

To investigate this conclusion further, we treated MCF-7 cells with Taxol for 24 h to cause the accumulation of 33 ± 4% of the cells in G2/M (Protocol B; Figure 3.19 A,B). We then determined if LPA caused a release from this arrest by labeling cells that were passing through S-phase with BrdU for 2 h. The cells were then incubated with Taxol in the presence or absence of LPA. Maintaining Taxol for additional 12 h increased the percentage of BrdU-labeled cells in G2/M to 63 ± 6%. Applying LPA with the Taxol decreased the percentage of the cells arrested in G2/M after 8 and 12 h of incubation (36 ± 5% at 12 h). LPA also increased the percentage of cells in G1 after 12 h from 50 ± 6% to 62 ± 7%. Therefore, LPA releases cells from Taxol-induced G2/M arrest and these cells enter G1 to start a new cell cycle.

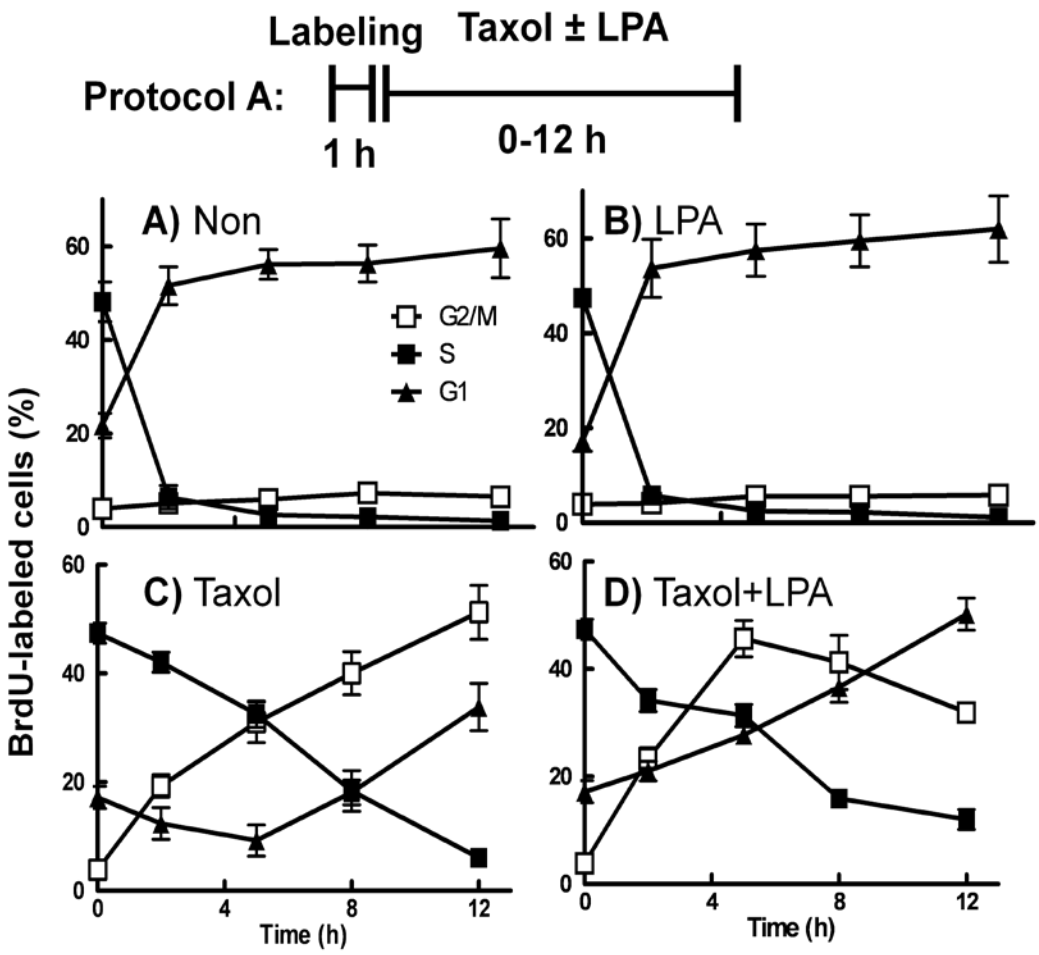

Figure 3.18 Lysophosphatidate does not block the entry of Taxol treated MCF-7 cells into G2/M. Panels **A-D**, cells were treated with BrdU for 1 h to label cells in S-phase. The cells were then incubated for 12 h in the presence or absence of 50 nM Taxol or 5 μM LPA (**Protocol A**) and the progression of cells through S, G2/M and G1 phases was quantified by FACS analysis. Results are means ± S.D. for three independent experiments.

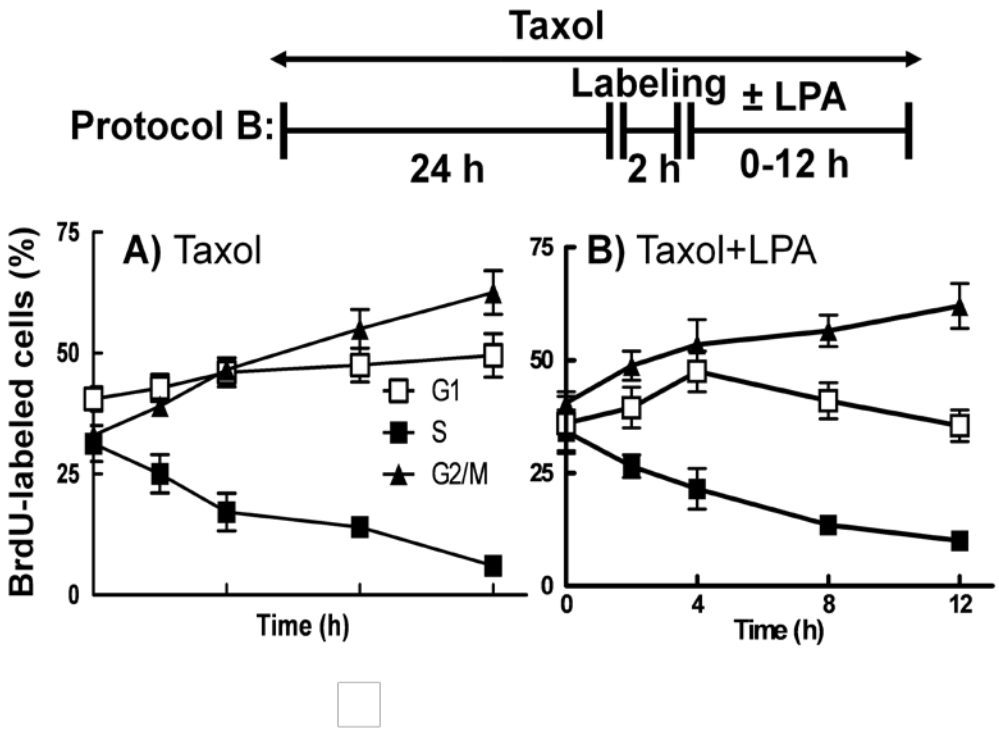

Figure 3.19 Lysophosphatidate releases MCF-7 cells from Taxol-induced G2/M. Panels **A** and **B,** cells were pre-incubated with 50 nM Taxol for 24 h and the cells entering S-phase were labeled for 2 h with BrdU (**Protocol B**). The progression of these cells through S, G2/M and G1 phases was then quantified. Results are means ± S.D. for three independent experiments.

To provide more information to support this conclusion, we incubated MCF-7 cells for 26 h with 50 nM Taxol and then studied their fates in the presence or absence of LPA during the next 12 h (Protocol C; Figure 3.20). We also removed Taxol from the incubations for the last 12 h to compare the extent to which the cells recovered from the Taxol treatment without the addition of LPA. The morphology of the cells was determined by triple staining with anti-tubulin, anti-phospho-histone H3 antibodies and DAPI. This enabled us to identify cells that were in mitosis, those with abnormal spindles, mononucleated cells, multinucleated cells and those that were dead or dying (Figure 3.20 A,B).

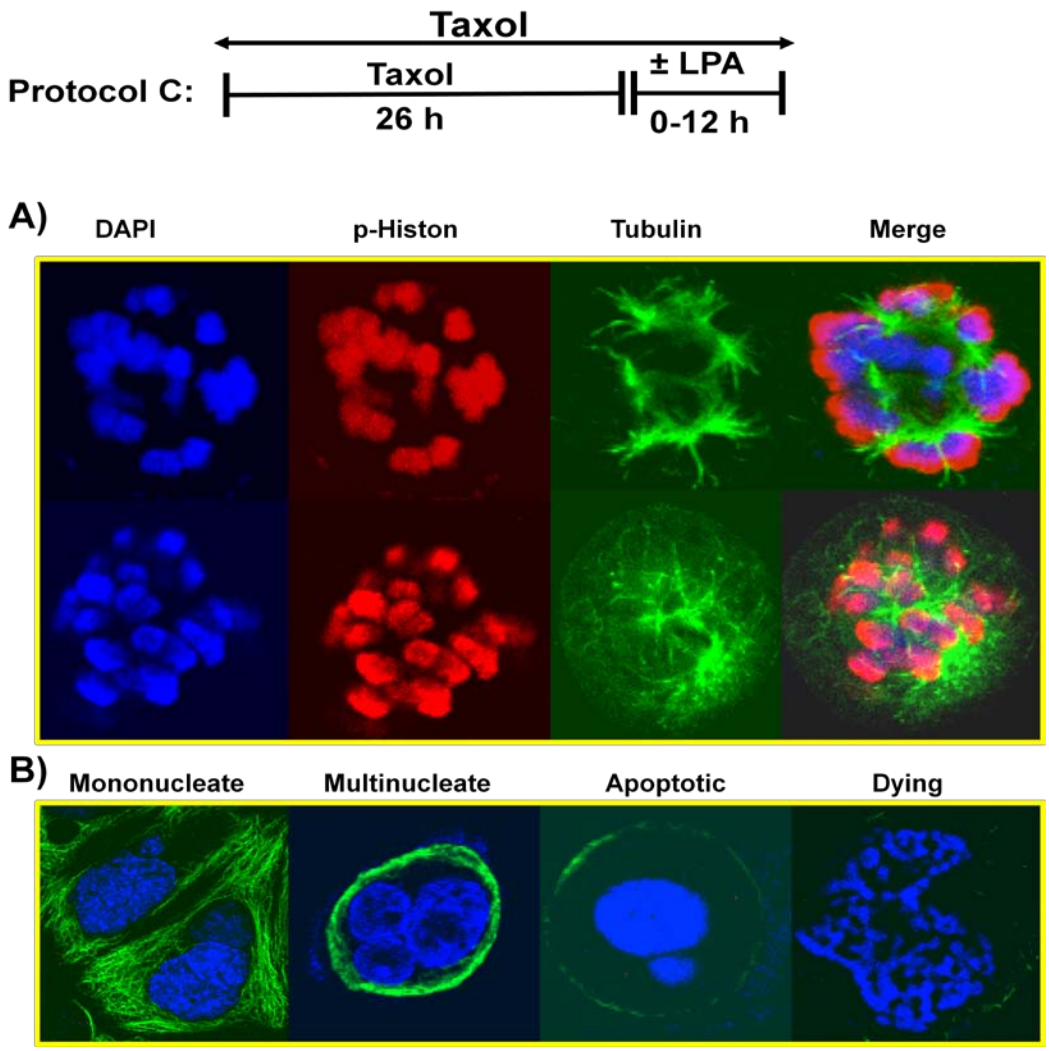

Figure 3.20 Morphology of MCF-7 cells after triple staining with DAPI, anti-phospho-histone and with anti-tubulin. MCF-7 cells were pre-incubated with 50 nM Taxol for 26 h and then Taxol was maintained or removed Taxol in the presence or absence of 5 µM LPA for the next 12 h (**Protocol C**). Cells were then stained with DAPI, anti-phospho-histone and with anti-tubulin at the times indicated and studied by confocal microscopy. The appearance of the cell in mitosis (P-histone positive) is shown in Panel **A**. The upper Panel shows cells with relatively normal morphology and the lower row show the cell in mitosis with abnormal spindle. Panel **B** shows mononucleated, multinucleated, apoptotic and dying cells, respectively, that did not stain for P-histone.

After incubating with Taxol for 26 h, 13±3% of the remaining cells were dead or dying (Figure 3.21 A). Incubating the cells for a further 12 h in Taxol increased this number to 22±4% and this value was similar when Taxol was

removed. LPA decreased the percentage of cell that were dead or dying when Taxol was maintained or removed during the final 12 h of incubation (Figure 3.21 A). After incubating with Taxol for 26 h, 45% of the cells were in mitosis as determined by DAPI and P-histone staining (Figure 3.21 B). Incubating the cells for a further 12 h in Taxol increased the percentage of cells in mitosis slightly (51±8%), whereas removal of Taxol decreased this proportion of cells slightly (40±5%). Incubating the cells with LPA in the presence or absence of Taxol for additional 12 h decreased the percentage of the cells that were in mitosis to about 15% (Figure 3.21 B). LPA also decreased the proportion of phospho-histone positive (mitotic) cells with abnormal spindles from 51± 7% in cells where Taxol was maintained to 31± 5% ($p<0.05$) (Figure 3.21 C). Removal of Taxol resulted in a small decrease in the percentage of cells with abnormal spindles and the presence of LPA further decreased this percentage.

LPA also markedly increased the percentage of mononuclated and multinucleated cells in incubations where Taxol was maintained or where it was removed (Figures 3.21 D,E). The appearance of multinucleated cells reflects the well-known “mitotic slippage” where cells escape Taxol-induced mitotic arrest in the absence of chromosome segregation or cytokinesis and enter a pseudo-G1 stage as tetraploid (4N) cells. It is after this mitotic slippage when Taxol-treated MCF-7 cells undergo apoptosis [181-184]. The enhanced accumulation of multinucleated cells by LPA indicates that they are resistant to death or they may exhibit delayed cell death. The other effect of LPA is a stimulation of cell cycle progression which produces normal G1 (2N) mononucleated cells in the presence

of Taxol. The observation that LPA facilitates normal spindle morphology and cell division in the presence of Taxol shows that LPA inhibits the action of Taxol. A possible explanation is that LPA induces Taxol efflux from the cell through an exporter e.g., P-glycoprotein.

3.11 LPA does not change Taxol expulsion by MCF-7 cells

To investigate the role of LPA in Taxol efflux from the cells, cells were treated with [^{3}H]Taxol for 26 h. Then the effect of LPA on Taxol expulsion from the cells was investigated for 12 h in the presence and absence of LPA (Protocol C, Figure 3.21). Figure 3.22 show the results from removing [^{3}H]Taxol after 26 h incubation, and adding RPMI1640 medium or medium containing LPA (5 µM). Removal of Taxol and incubating of the cells for additional 12 h decreased the amount of radioactivity in the cells from about 67± 15% (47.6± 10.7 x 10^5 dpm) to 48± 12% (34.1± 8.5 x 10^5 dpm) with a parallel increase in the amount of radioactivity in medium up to 12.6± 3.4% (9.1± 1.8 x 10^5 dpm). Slight expulsion of the [^{3}H]Taxol from the cells may be because of capable of pumping drug against a concentration gradient [185]. The presence of LPA did not significantly affect these Taxol distributions (35.8± 12.4 x 10^5 dpm).

Maintaining Taxol for additional 12 h increased intracellular Taxol from 67± 15% to 79± 19% (Figure 3.23). This increase was parallel with decrease in the percentage of radioactivity in medium showing a continuous uptake of [^{3}H]Taxol by the cells. The presence of LPA did not significantly affect Taxol

distributions (57.6± 15.4 x 10^5 dpm in LPA-treated cells compared to 60.9 x 10^5 dpm in the cells without treating with LPA).

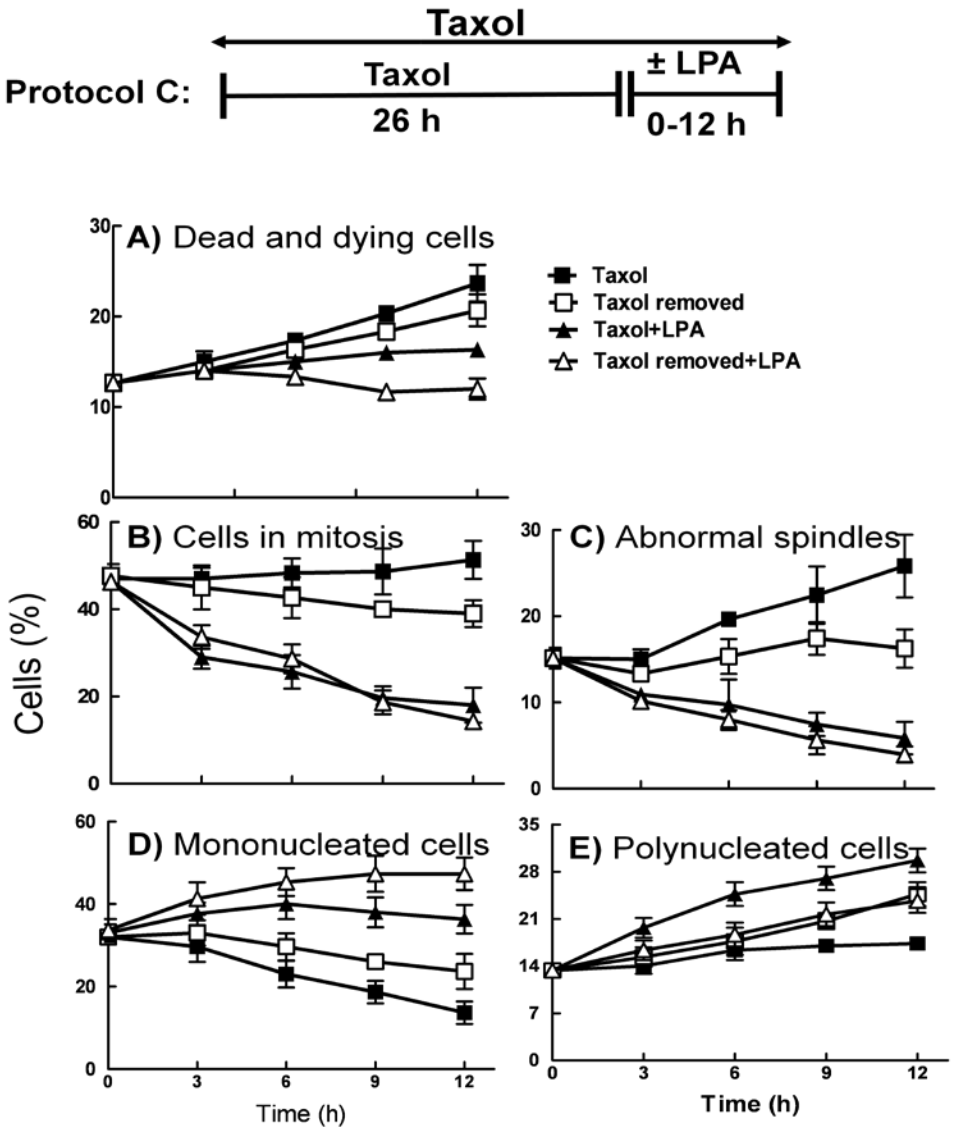

Figure 3.21 Lysophosphatidate releases MCF-7 cells from Taxol-induced arrest in G2/M and cell death. MCF-7 cells were preincubated with 50 nM Taxol for 26 h and then Taxol was maintained or removed Taxol in the presence or absence of 5 µM LPA for the next 12 h (**Protocol C**). Cells were then stained with DAPI, anti-phospho-histone and with anti-tubulin at the times indicated. The percentage of dead and dying cells was shown in Panel **A**, total cells in mitosis in Panel **B**, cells in mitosis with abnormal spindles in Panel **C**, mononucleated cells in Panel **D** and multinucleated cells in Panel **E**. Results are means ± S.D. (where large enough to be shown) for three independent experiments.

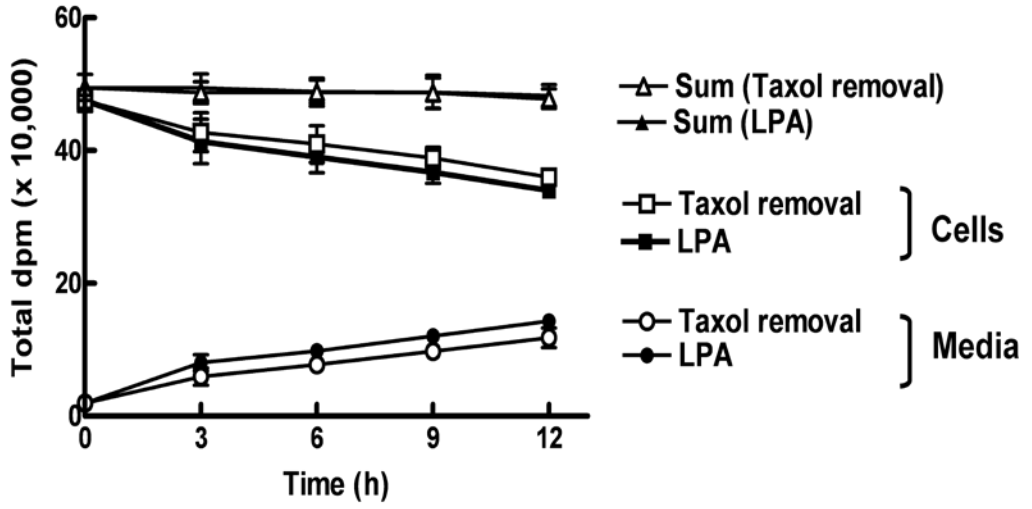

Figure 3.22 LPA does not affect Taxol expulsion when Taxol is removed. Approximately 2 x 10^5 MCF-7 breast cancer cells were grown to confluence in 3.5 cm cell culture dishes. The medium was replaced with 1.5 ml RPMI1640 medium containing 10% of charcoal-treated FBS with 50 nM Taxol containing 0.5 µCi [^{3}H]Taxol. After 26 h incubation Taxol was removed and 1.5 ml of medium or medium containing LPA (5 µM) was added. At the indicated time points, medium was collected and after washing the cells three times with ice-cold RPMI1640 medium containing 0.1% BSA, cells were collected by scrapping twice with 0.5 ml of ice-cold methanol. Chloroform (1 ml) was added to the combined methanol extracts followed by 0.9 ml of 2 M KCl and the mixture was vortexed and then centrifuged. The chloroform phase (100 µl) from the cell extracts was dried under N_2 and dissolved in 2 ml of aqueous counting scintillation fluid (Amersham Biosciences). Radioactivity in the medium was measured by adding 100 µl of the media directly to 2 ml of aqueous counting scintillation fluid (Amersham Biosciences). Results are means ± S.D. (where large enough to be shown) for three independent experiments.

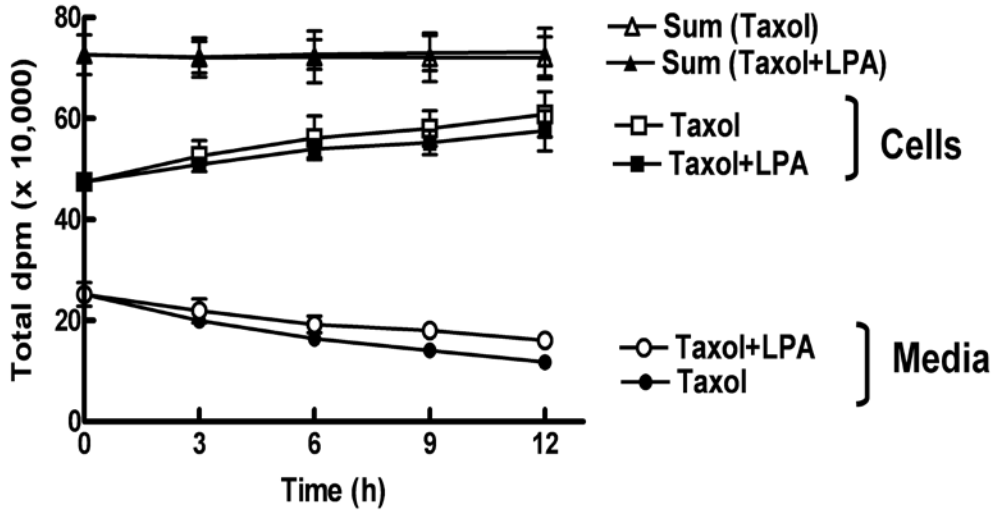

Figure 3.23 LPA does not affect Taxol expulsion when Taxol is maintained. Approximately 2 x 10^5 MCF-7 breast cancer cells were grown to confluence in plated in 3.5 cm cell culture dishes. The medium was replaced with 1.5 ml RPMI1640 medium containing 10% of charcoal-treated FBS with 50 nM Taxol containing 0.5µCi [^{3}H]Taxol. After 26 h incubation Taxol was maintained and LPA (5 µM) was added to the dishes. The samples were collected and analyzed as described in Figure 3.23. Results are means ± S.D. (where large enough to be shown) for three independent experiments.

3.12 LPA does not change Taxol metabolite formation in MCF-7 cells

We also analyzed the [^{3}H]Taxol remaining in the cells under all experimental conditions by TLC to detect metabolites such as 3-hydroxytaxol and 6α-hydroxytaxol [174]. The *Rf value* of Taxol was 0.31 (Figure 3.24 A,B Portion C). We considered the *Rf* values 0.20-0.25 values for Taxol metabolites as described [174] (Figure 3.24 A,B Portion B). There was not significant differences in production of these metabolites in the MCF-7 after 12 h incubation with LPA (5 µM) (1.53 ± 0.10%) or additional 12 h incubation with Taxol (50 nM) (2.00±0.32%) (Figure 3.25 A, B). There was also an additional peak that was moving faster than Taxol in TLC plate (Figure 3.24 A,B Portion D). This peak

was not related to LPA and appeared when the cells incubated with medium containing FBS. The LPA-induced release of MCF-7 cells from Taxol-induced G2/M arrest, therefore, does not depend on LPA-induced export of Taxol, or increased Taxol metabolism.

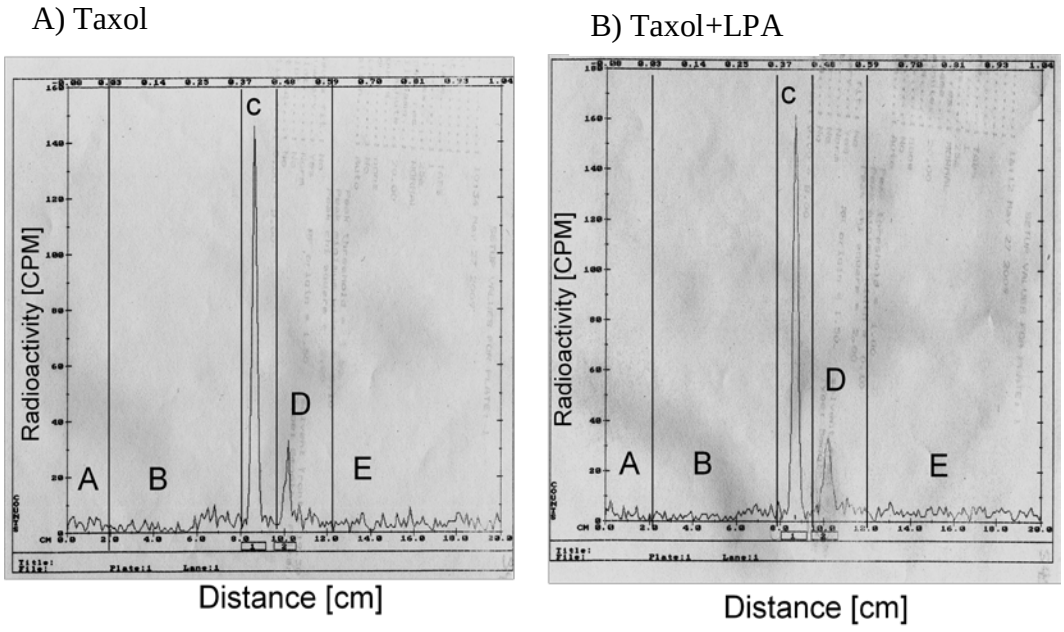

Figure 3.24 LPA does not change metabolite formation in Taxol-treated cells. RPMI1640 medium (1.5 ml) containing 10% of charcoal-treated FBS with 50 nM Taxol containing 0.5µCi [^{3}H]Taxol was added to the confluent number of cells. After 26 h incubation Taxol was maintained in some dishes (**A**) and the cells were incubated with LPA (5 µM) for 12 h in other dishes (**B**). After washing the cells three times with ice-cold RPMI1640 medium containing 0.1% BSA, cell lysates were collected by scrapping twice with 0.5 ml of ice-cold methanol. Aliquots of 0.2 ml of the chloroform phase was dried down under N_2 and dissolved in 100 µl of chloroform/methanol (9:1). Each sample was loaded on to plastic-supported silica gel 60 thin layer chromatography plates and the plates were developed with toluene/acetone/formic acid (60:39:1, by vol.) for 12 cm [174]. The plates were dried and the radioactive metabolites were identified by comparison of the R*f* values. The R*f* for [^{3}H]Taxol was determined by BioScan 200 Imaging Scanner Bioscan. The migration of non-radiolabeled Taxol was also visualized by using 5% vanillin-sulfuric acid**.** Bands also were cut in four different distances including A (0-2 cm): the origin spot of the samples, B (2-8 cm): the R*f* for metabolites, C (8-10 cm): the R*f* for [^{3}H]Taxol, D and E (10-20 cm): the R*fs* for FBS-dependent peak with R*f* greater than R*f* for [^{3}H]Taxol. Then, [^{3}H]-labeling was measured by liquid scintillation counting. Experiments were repeated four times with assistance of Raie Beleke, a graduate student in Brindley's lab.

3.13 LPA releases cells from Taxol-induced G2/M arrest and cell death through activation of PI3K, Akt, GSK-3 and survivin

An alternative explanation for how LPA could facilitate normal mitotic spindle formation, chromosomal segregation and cytokinesis in the presence of Taxol could be through interfering with Taxol-induced stabilization of microtubules. We already showed that the protective effects of LPA were dependent on the PI3K pathway (Figures 3.15, 3.16 and 3.17), therefore, we considered downstream targets that regulate microtubule dynamics.

A major molecule that is activated by PI3K is Akt and whereas Akt regulates numerous signaling pathways, we focused on the downstream target GSK-3, because of its role in regulating microtubule-associated proteins. Akt promotes the serine phosphorylation and thus inhibition of GSK-3α and GSK-3β activity. LPA can also activate pyk, a kinase, which causes the tyrosine phosphorylation of GSK-3 and its activation [100]. We also knew that GSK-3 can modify the functions of microtubule-associated proteins, such as survivin, that promote normal spindle formation and prevent apoptosis [93,186].

For these experiments we initially used a digitonin lysis technique that separates cytosolic enzymes from a "cell ghost" consisting of cell organelles [187] to determine if LPA causes a redistribution of proteins between these compartments. GAPDH and calnexin were used as loading markers for the cytosol and membrane fractions, respectively (Figure 3.26 A). In most experiments, we used Protocol C (Figure 3.21) so that we could relate the changes directly to the release of cells from Taxol-induced G2/M arrest.

Incubation of Taxol-treated cells with LPA for 12 h increased phosphorylations on both Ser residues, which inhibit GSK-3 activity and Tyr residues, which stimulate activity. These changes appear to reflect the increased expressions of total GSK-3α and GSK-3β in the cells that were exposed continuously to Taxol, or when Taxol was removed for the last 12 h (Figure 3.25 A). LPA also increased the expression of survivin and phospho-survivin, which were recovered mainly in the membrane-associated compartment rather than cytosol in the presence or absence of Taxol. These values for membrane-associated GSK-3β, survivin and phospho-survivin were quantified in Figure 3.25B. Phospho-survivin concentrations in cells treated with Taxol were increased by about 2 fold by the presence of LPA for 12 h.

Incubation of MCF-7 cells with Taxol alone for 26 h also increased the expression of GSK-3β, survivin and phospho-survivin by about 2-fold (Figure 3.25 C). Incubating with LPA alone had a greater effect of increasing the expression of GSK-3β, survivin and phospho-survivin by about 4.5-fold.

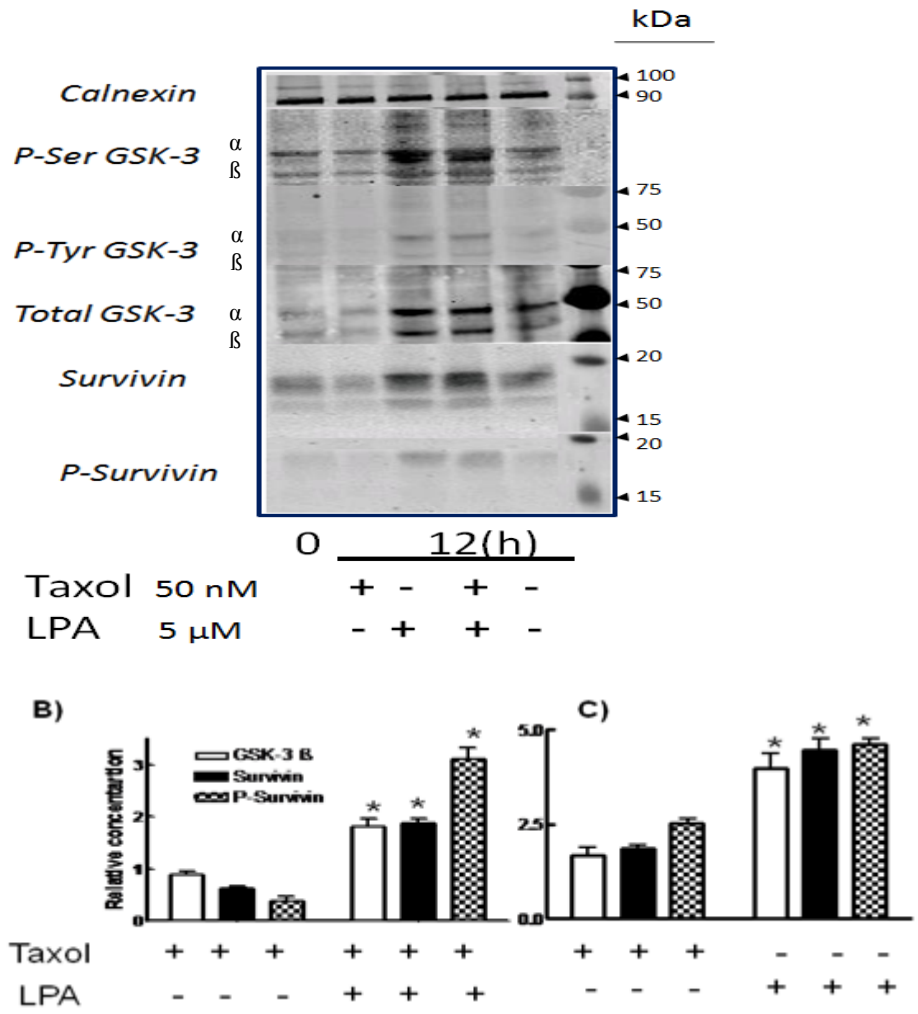

Figure 3.25 Lysophosphatidate increases the expression of glycogen synthase kinase-3 and survivin. MCF-7 cells were incubated with Taxol and LPA based upon Protocol C, Figure 3.21. The cells were then permeabilized with digitonin to release cytosolic enzymes from the cell ghosts (membrane fraction). **Panel A** shows a representative Western blot from the membrane fractions for GSK-3 visualized for P-serine, P-tyrosine or total GSK-3. Survivin and phospho-survivin are shown in the lower blots. Calnexin were used as loading controls for the membrane fractions. **Panel B** shows the relative expression of GSK-3β, survivin and P-survivin in the membrane fraction described in Panel A calculated relative to calnexin. Results are expressed relative to the values at the end of the 26 h pre-incubation with Taxol (O time). They are expressed as means ± S.D. of three independent experiments. Significant differences from the 26 h pre-incubation with Taxol values are indicated by *. **Panel C** shows the relative Western blot analyses for GSK-3β, survivin and P-survivin for cells that were incubated with 50 nM Taxol or 5 µM LPA for 26 h. Results are given as means ± S.D. of three independent relative to that for cells which were not incubated with Taxol or LPA. Significant changes are indicated by *.

To study the effect of the activities of PI3K and GSK-3 on the long-term expression of survivin, we determined the effects of the LY294002 (a PI3K inhibitor) and three GSK-3 inhibitors including AR-A014418, SB216763 and LiCl [188]. The cells were treated for 26 h with Taxol as described in Figure 3.21 and then incubated 12 h with the inhibitors. All of these inhibitors except SB216763 decreased the expression of survivin and phospho-survivin ($p<0.05$) (Figure 3.26 A,B). The inhibitors also decreased the LPA-induced increase in survivin and phospho-survivin that occurred in the presence of Taxol ($p<0.05$). The LY294002 decreased total GSK-3ß and GSK-3α expression. However, the impact of the LY294002 on GSK-3ß ($p<0.01$) was significantly higher than GSK-3α ($p<0.05$). The LY294002 also decreased phosphorylation level of GSK-3αß. GSk-3 inhibitors, except SB216763, decreased Tyr phosphorylation levels of GSK-3 αß. However, the higher decrease was in P-Tyr GSK-3ß ($p<0.01$) (Figure 3.26 A). There was also a significant increase in total GSK-3ß when we inhibited GSK-3 activity by applying different inhibitors. The results are consistent with previous study showing that GSK-3ß inhibitors increases GSK-3 expression through reducing protein degradation by its phosphorylation at Ser-9 [189].

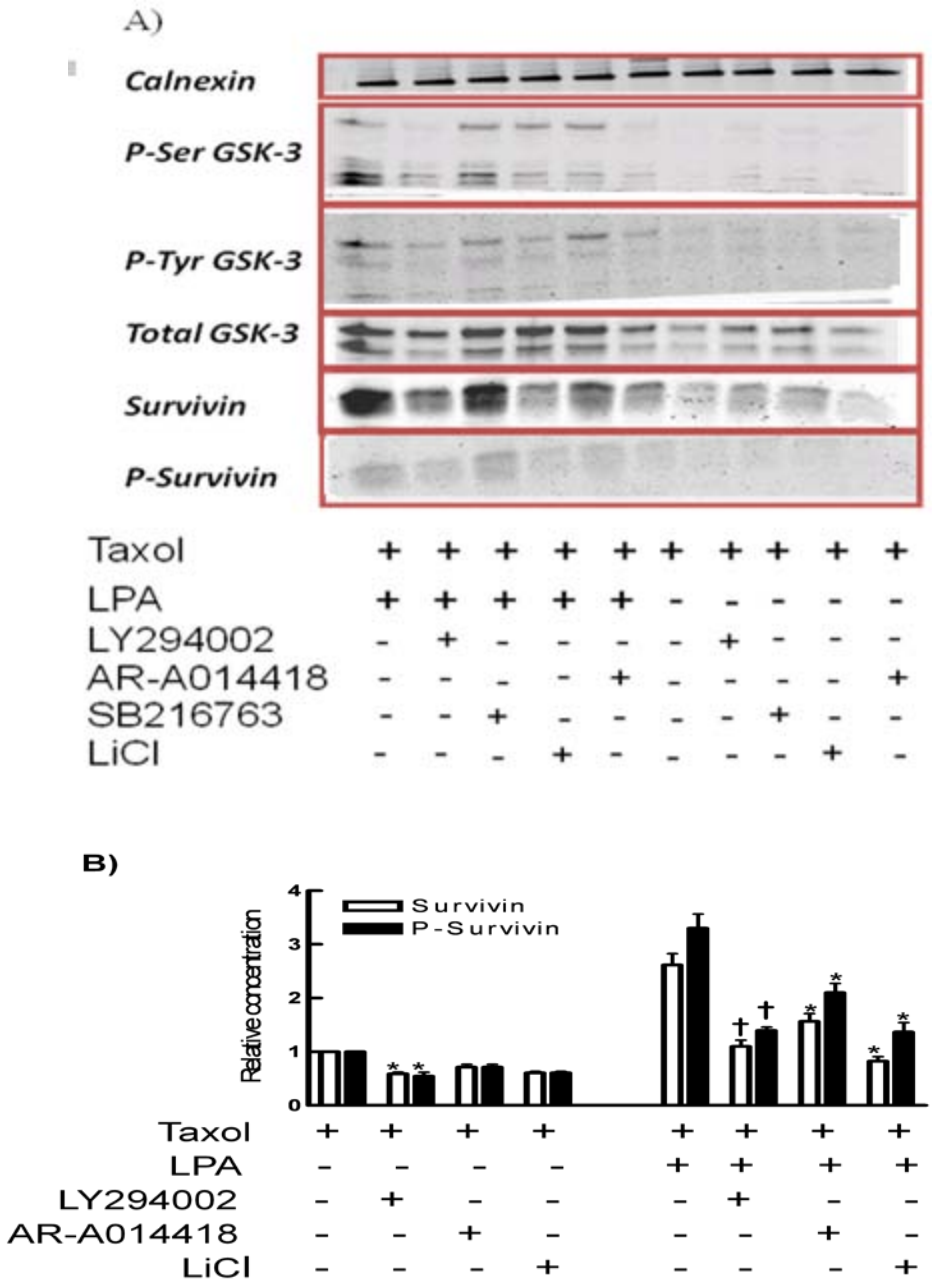

Figure 3.26 Inhibition of phosphatidylinositol 3-kinase or glycogen synthase-3 attenuates the expressions of survivin and phospho-survivin. MCF-7 cells were pre-incubated with 50 nM Taxol for 26 h and then Taxol was maintained in the presence or absence of 5 µM LPA, 20 µM LY294002, 1 µM AR-A014418 or 20 mM LiCl for the next 12 h (Protocol C, Figure 3.21). Panel A shows a representative Western blot for P-serine, P-tyrosine and total GSK-3, survivin and phospho-survivin when MCF-7 cells were incubated with PI3k and GSK-3 inhibitors. Results are means ± S.D. of three independent experiments, which are expressed relative to cells treated with Taxol (Panel B, left) or Taxol+LPA (Panel B right). Significant changes are indicated by * ($p<0.05$) and †($p<0.01$).

The specific role of GSK-3β on survivin expression was determined since the expression of this isoform is linked to survivin expression. Knockdown of GSK-3β was achieved by using a set of four siRNAs, which decreased GSK-3β expression by about 90% compared to scrambled siRNA without affecting the expression of GSK-3α (Figure 3.27 A). This knockdown decreased survivin and phospho-survivin expression in cells treated with Taxol alone and it blocked the LPA-induced expression of these proteins (Figure 3.27 B). Knockdown GSK-3ß was also achieved with applying a set of four independent siRNAs. The sequences for these siRNAs include:

5´-GAAGAAAGAUGAGGUCUAU-3´

5´- GGACCCAAAUGUCAAACUA-3´

5´- GAUGAGGUCUAUCUUAAUC-3´

5´- GAAGUCAGCUAUACAGACA-3´

Applying each individual siRNA decreased GSK-3β expression by 78%, 70%, 82% and 65% respectively, compared to scrambled siRNA without affecting the expression of GSK-3α. Knockdown of GSK-3ß by four independent siRNAs confirmed our results from applying a combination of four GSK-3ß siRNAs.

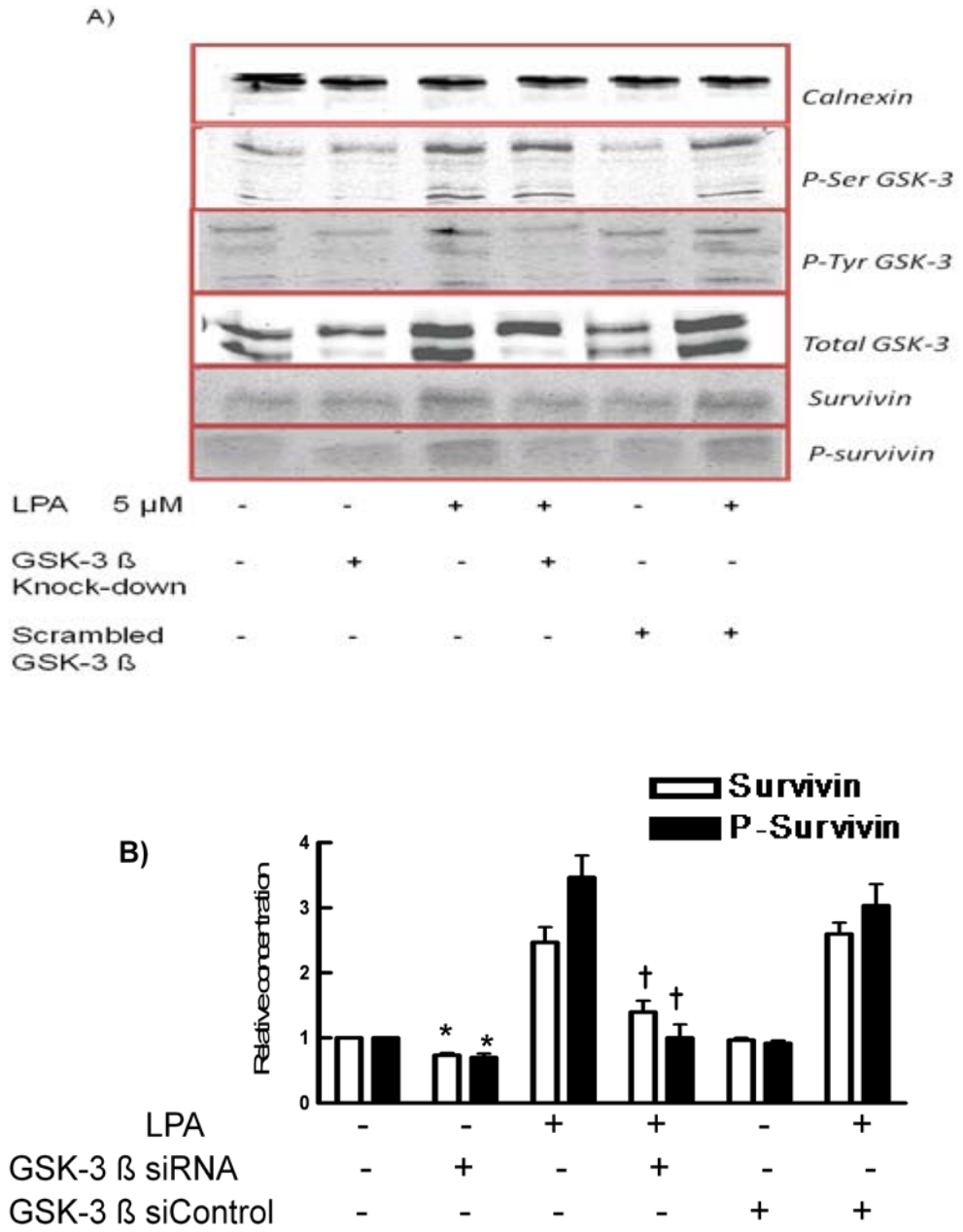

Figure 3.27 Knockdown of glycogen synthase-3 attenuates the expressions of survivin and phospho-survivin. MCF-7 cells were preincubated with 50 nM Taxol for 26 h and then Taxol was maintained in the presence or absence of 5 µM for the next 12 h (Protocol C, Figure 3.21). Panel A shows a representative Western blot for P-serine, P-tyrosine and total GSK-3, survivin and P-survivin when MCF-7 cells were incubated with a set of four different siRNA for GSK-3β or with control siRNA. Panel B shows the effect of knockdown GSK-3β on the expression of survivin and P-survivin in the total cell lysate. Results are means ± S.D. of three independent experiments, which are expressed relative to cells that were not incubated with siRNA. Significant changes are indicated by * ($p<0.05$) and †($p<0.01$).

Treatment of MCF-7 cells with siRNA for survivin decreased survivin expression by about 90% relative to the control siRNA (Figure 3.28 A). Then we followed Protocol C (Figure 3.21) to investigate the role of survivin in LPA-induced change in morphology of the cells. After 26 h incubation with Taxol (50 nM), 46 ± 13% of the cells were in mitosis. There was a significant decrease in the percentage of mitotic cells when the cells incubated with Taxol and LPA for additional 12 h (21 ± 8%). Survivin knockdown produced a small increase in the percentage of Taxol-treated cells after 12 h incubation (64 ± 18%) and it significantly decreased the effect of LPA in reversing this process (37 ± 11%) (Figure 3.28 B). Knockdown of survivin increased the number of cells with abnormal mitotic spindles in the cells treated Taxol and LPA (17 ± 3% in survivin knockdown cells compared to 6 ± 2% in wild type cells) (Figure 3.28 C). It also increased number of dead cells after 12 h incubation with Taxol and LPA (17 ± 5.2 in survivin knockdown cells compared to 22 ± 8% in wild type cells) (Figure 3.28 D). Survivin knockdown decreased the passage of cells into G1 as illustrated for the mononucleated and multinucleated cells (Figure 3.29 E,F).

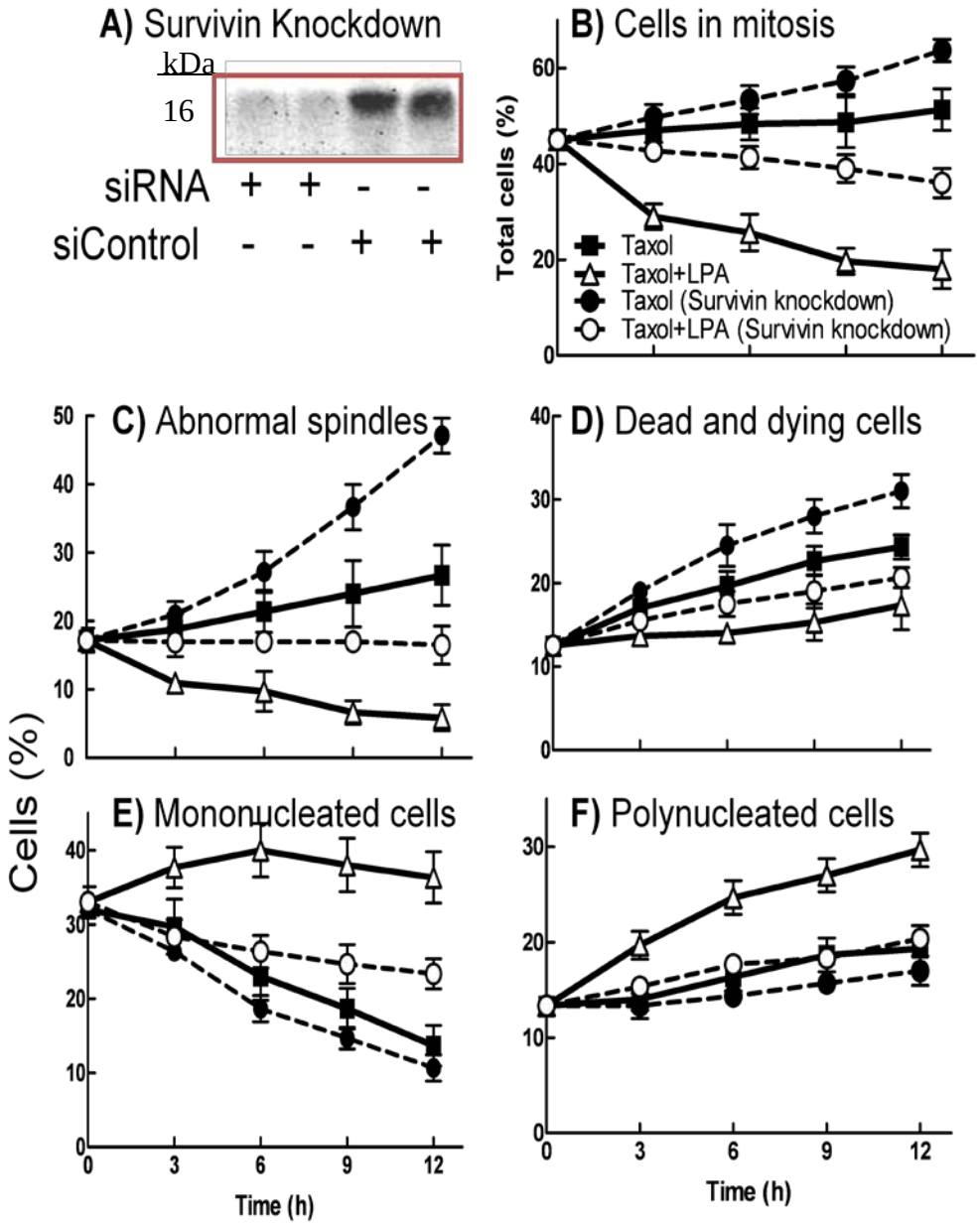

3.28 Knockdown of survivin expression sensitizes MCF-7 cells to Taxol-induced G2/M arrest and cell death and decreases lysophosphatidate-induced rescue. MCF-7 cells were incubated for 24h with siRNA for survivin or control siRNA and the expression of survivin is shown in Panel A. These treatments were then combined with incubation with Taxol for 26 h followed by incubation for an additional 12 h with Taxol in the presence or absence of LPA as described in Protocol C, Figure 3.21. Cells were identified by staining with DAPI, anti-phospho-histone and anti-tubulin. The other Panels show the percentage of cells in B) mitosis, C) mitotic cells with abnormal spindles D) dead and dying cells, e) mononucleated cella and E) multinucleated cells as indicated. Results are means ± S.D. (where large enough to be shown) of three independent experiments.

Chapter 4

GENERAL DISCUSSION AND FUTURE STUDIES

4.1 Discussion

Effective chemotherapy depends on successful induction of apoptosis and defects in apoptotic signaling are a major cause of drug resistance. Chemotherapeutic resistance results in poor responses and reduced overall survival in patients with metastatic breast cancer [138]. Investigating the dysregulation of apoptosis in cancer has been a demanding research area over the past decades. Defective apoptosis often occurs because of changes in the extrinsic and intrinsic pathways of apoptosis, or through alternative pathways of cell death, such as autophagy, mitotic catastrophe, or necrosis. Novel knowledge of the mechanisms by which cancer cells evade apoptosis, and the links to drug resistance, can improve the efficacy of chemotherapeutic agents and development of molecular targeted pro-apoptotic therapies for cancer treatment [190].

LPA is a small lipid signaling molecule that has been studied intensively in tumor cell proliferation, migration and invasiveness. In the circulation, LPA is mainly produced by ATX through conversion of LPC. ATX is an extracellular nucleotide pyrophosphatase/phosphodiesterase that plays a key role in tumor progression through both catalytic and non-catalytic activities [11]. However, the role of LPA and ATX in resistance to chemotherapy is unclear.

In this thesis work, we first applied doses of Taxol up to 50 nM to induce apoptosis in cancer cells. These Taxol concentrations are compatible with the doses are applied for the treatment of breast cancer patients [191]. LPA and LPC were used up to 20 and 200 μM, respectively, which is compatible with those in circulation and tumor microenvironment [192,193]. Taxol-induced apoptosis was

demonstrated by morphologic criteria after DAPI staining and by measuring mitochondrial membrane potential loss by TMRE flow cytometry.

Treating MCF-7 cells with 50 nM Taxol showed a significant increase in the percentage of recovered apoptotic nuclei up to 12% after 24 h and 26% after 48 h incubation. MDA-MB-435 cells treated with 50 nM Taxol also showed a considerable increase in the percentage of apoptotic nuclei to about 9% after 24 h and about 18% after 48 h incubation. Taxol is an important chemotherapeutic agent that induces apoptosis in variety of different cancer cells including ovarian [194], endometrial [195], lung [196], prostate [197], colorectal [198], thyroid [199], acute myeloid leukemia [200], melanoma [201], and breast [201] cancer cells. We demonstrated that Taxol-induced cell death is strongly antagonized by LPA when we measured nuclear fragmentation, loss of mitochondrial potential and the recovery of viable cells. LPA (0.5 μM) partially blocked the Taxol-induced increase in the percentage of apoptotic nuclei, but we needed 5 μM LPA to antagonize the effect of Taxol in increasing the proportion TMRE-negative cells.

The discrepancies suggest that cells that were protected at low LPA concentrations, where no differences in TMRE staining were observed, probably died by a mitochondria-independent and non-apoptotic (necrotic) mechanism. However, another major factor is that the DAPI and TMRE measurements determine only what happened to the cells remaining on the dishes. We, therefore, do not have information concerning the mechanisms of cell death of more than 50% of cells that were not recovered. Consequently, it is significant that 0.5–10 μM

LPA increased the number of cells that were recovered after Taxol treatment and that were then reflected in the percentage of apoptotic cells recorded in the DAPI and TMRE staining assays.

Accumulating evidence shows that LPA promotes survival of ovarian cancer cells [128,202], renal proximal tubular cells [203], lymphoblastoma T cells [204], macrophages [130], neonatal Schwann cells [59], fibroblast [74], mesangial cells [205], colon cancer cells [125], Burkitt's lymphoma cells [127], mesenchymal stem cells [206] and primary chronic lymphocytic leukemia cells [207] by preventing apoptosis (Figure 4.1)

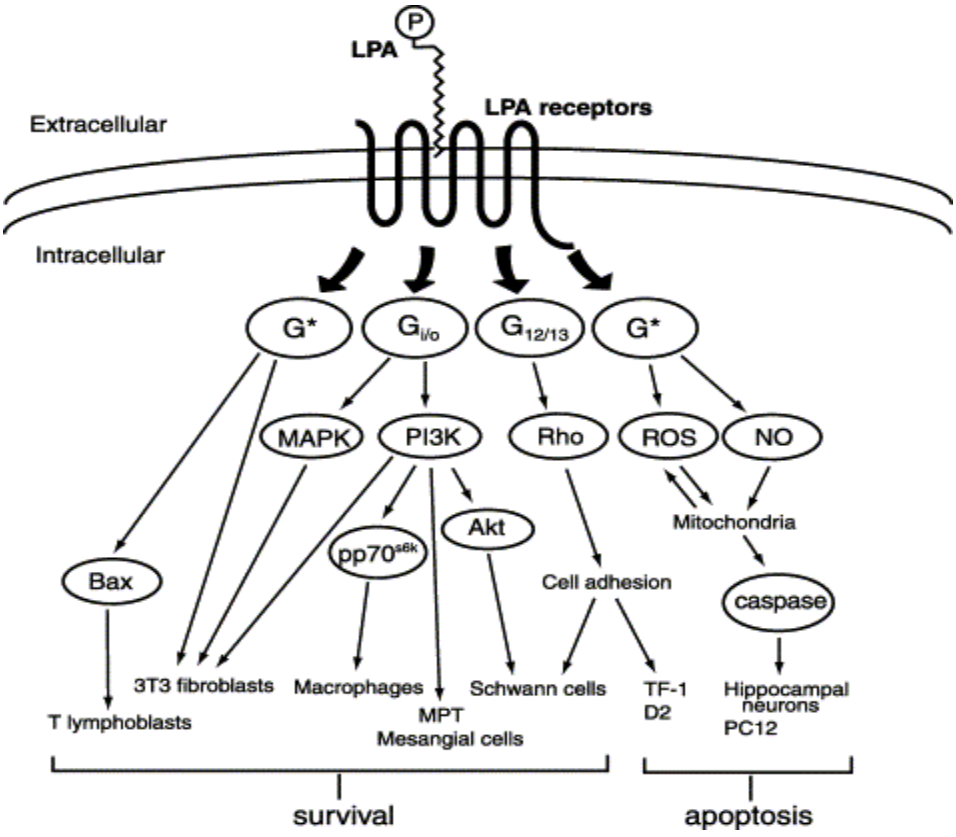

Figure 4.1 LPA signaling pathways, which promote survival or apoptosis in different cell types. The figure adopted from Ye [208]

Different cell types express different LPA receptors, which have specific roles, and therefore the effects of LPA signaling vary from cell to cell. In contrast to the survival role of LPA_1 in Schwann cells [59,209], overexpression of LPA_1 in ovarian cancer cells induced apoptosis and anoikis [210], whereas LPA_2 appeared to mediate LPA-stimulated survival of ovarian cancer cells [202]. In T lymphoblasts, both LPA_1 and LPA_2 promoted LPA-induced survival [204]. LPA also prevents apoptosis in colon cancer cells through LPA_2 receptor [125]. Inhibition of LPA_2 receptor expression increases pro-apoptotic Siva-1 protein levels and enhances adriamycin-induced caspase-3 cleavage and apoptosis [211]. LPA_2 receptor is also required for protection against radiation-induced intestinal injury [212]. LPA_2 is the predominant LPA receptor in MCF-7 cells [213]. This is compatible with our finding that 100 ng/ml pertussis toxin or 1 μM VPC51299 (an $LPA_{1/3}$ receptor antagonist) failed to block the LPA protection against Taxol-induced apoptosis in MCF-7 cells. Unfortunately, no effective specific antagonist for LPA_2 receptors has been developed.

Next, we investigated the mechanisms whereby LPA protects MCF-7 cancer cells against Taxol-induced apoptosis. We demonstrated that inhibition of PI3K blocked the protective effect of LPA on Taxol-induced apoptosis, whereas blocking ERK activation with PD98059 was without effect. PI3K is an important signaling pathway for survival of tumor cells. Activation of the PI3K-Akt pathway protects primary lymphocytic leukemia cells, ovarian cancer cells and intestinal epithelial cells from apoptosis, whereas G_i-mediated activation of ERK is necessary for the survival of fibroblasts and Schwann cells [74,207,214-217].

We demonstrated that ATX protects MCF-7 and MDA-MB-435 cancer cells against apoptosis by conversion of LPC to LPA. It has been shown that ATX protects fibroblasts[38] and Hodgkin lymphoma cells [44] through its catalytic activity. LPC is present in plasma and serum at >100 μM in a predominantly albumin-bound form [12] and it is also detected in media from tumor cells [2]. LPC stimulates prostate cancer cell migration [218]. Plasma levels of LPC are significantly decreased in colorectal cancer patients [219]. LPC inhibits the apoptotic effect cyclooxygenase-2 expression by a Raf-1 dependent mechanism in human cholangiocytes [220]. However, in our work, LPC alone did not antagonize Taxol-induced apoptosis unless concentrated medium from MDA-MB-435 cells or rATX was added The MDA-MB-435 medium, compared with that produced by MCF-7 cells, contained abundant ATX. The protective effect of ATX was blocked by VPC8a202 and S32826, two ATX inhibitors [176,177], or by heat inactivation of ATX activity. We also showed that LPC only stimulates the migration of MDA-MB-231 breast cancer cells in the presence of active ATX [5]. This effect of LPC was blocked by an antagonist of LPA_{1-3}. These results are compatible with the view that the putative LPC receptors, G2A and GPR4, are proton-sensing receptors whose activity is negatively regulated by LPC [221]. Many reported biological effects of LPC are probably mediated through ATX and LPA production.

We also showed that LPA attenuated the Taxol-induced increase in ceramides and subsequent apoptosis in a PI3K/Akt-dependent manner. Ceramide levels regulate sustained mitotic arrest, apoptosis and mitotic slippage [222], and

elevated ceramide concentrations are a known component of Taxol-mediated cell death [223-225]. Sustained ceramide elevation in the endoplasmic reticulum coordinately activates the stress responses and inactivates anti-apoptotic Akt, thus leading to apoptosis [225].

Figure 4.2 illustrates our conclusion about the mechanisms whereby ATX protects cancer cells from Taxol-induced apoptosis. To validate our proposed model, first we demonstrated that the protective function of ATX depends on its catalytic activity through converting LPC to LPA. LPA promotes variety of different biological effects including cell survival through activating LPA receptors. In MCF-7 cells, applying pertussis toxin and $LPA_{1/3}$ antagonist showed that LPA action is independent of $LPA_{1/3}$ receptors. This observation is consistent with the previous study showing that LPA_2 receptor is the major LPA receptor in MCF-7 cells [213]. Then, we validated mechanistic part of our model by showing that applying PI3K inhibitor abrogates the protective effects of LPA against Taxol-induced apoptosis. We also demonstrated a significant increase in ceramide formation induced by Taxol which is consistent with the previous studies [223,225]. Applying LPA attenuated ceramide formation and subsequent apoptosis through PI3K pathway. It has been well documented that ceramide promotes apoptosis through activating cathepsin D via a specific domain and mediating translocation of cathepsin D into the cytoplasm [226]. In cytoplasm, cathepsin D triggers cell death by activating pro-apoptotic Bcl-2 family members including Bid, Bax and Bak and attenuating Bcl-2 and Bcl-xl anti-apoptotic proteins [227,228]. Therefore, in MCF-7 cells, LPA attenuated ceramide

formation induced by Taxol in a PI3K/Akt dependent manner. Inhibition of ceramide formation by LPA leads to inhibition of pro-apoptotic and activation of anti apoptotic signals and eventually cell survival.

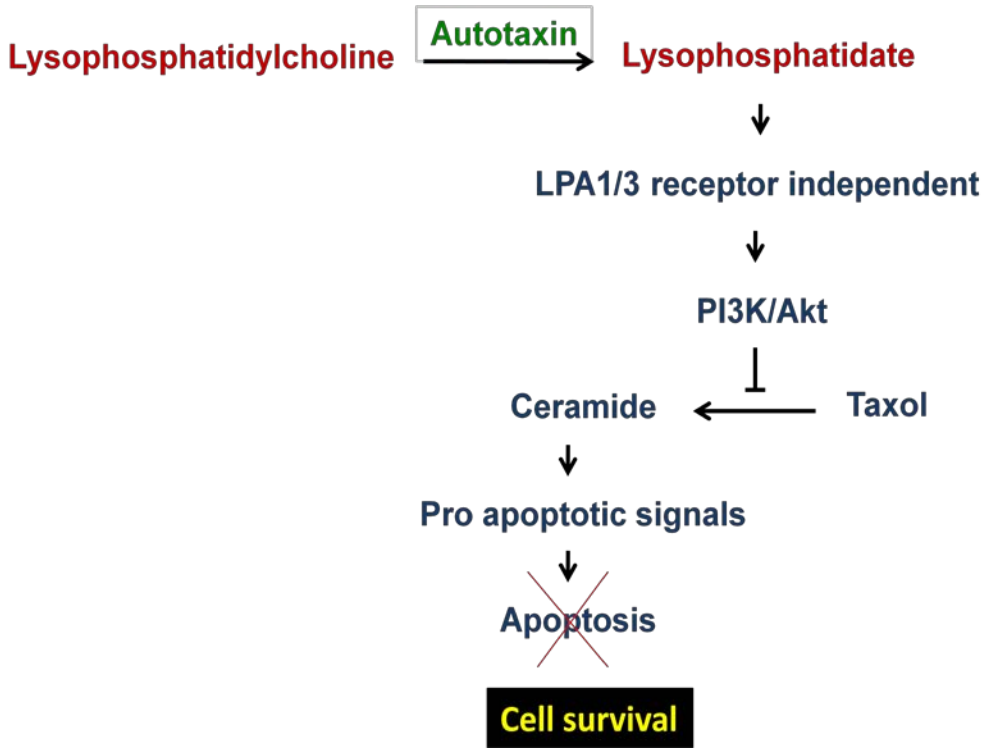

Figure 4.2 Schematic representation of the mechanism of autotaxin action in protecting the cells against apoptosis.

Taxol functions in suppressing spindle microtubule dynamics, thus inhibiting the metaphase anaphase transition, blocking mitosis (G2/M arrest) and inducing apoptosis [138]. In addition to drug concentration and time, cytotoxic

effect of Taxol depends on dynamicity and shortening rate of microtubules [135]. We showed that LPA attenuated the number of cells arrested in G2/M in a PI3K/Akt dependent manner. Then, we demonstrated that decrease in the number of cells arrested in G2/M does not result from an LPA-induced delay of entry into mitosis. Rather, LPA releases cells that are arrested in G2/M by Taxol and allows them to proceed into G1 and avoid cell death.

The impact of Taxol in arresting of the cells in G2/M is concentration dependent and low concentrations of Taxol block only a small portion of cells in the G2/M phase [229]. Our study showed that LPA action does not depend on Taxol removal from the cells, or an increased metabolism of Taxol. Therefore, we can conclude that LPA does not change intracellular concentration of Taxol by either expulsion of drug or increase in Taxol degradation.

Taxol-induced G2/M arrest results from stabilization of microtubule structure. Taxol binds to the intermediate domain on β-tubulin near the surface of β-tubulin and causes Taxol to interact with proteins through hydrogen bonding and hydrophobic contact. The binding of Taxol causes lateral polymerization and microtubule stability [148]. We established a novel effect of LPA signaling, which interacts with Taxol-induced G2/M arrest and microtubule stabilization through PI3K/Akt/GSK-3ß pathway and survivin.

Figure 4.3 depicts the proposed mechanism whereby LPA releases MCF-7 cells from Taxol-induced G2/M arrest by activating PI3K/Akt pathway followed by increase in the expression of GSK-3ß and survivin. We validated this Scheme;

first, by showing that inhibition of PI3K activity with LY294002 blocks the effect of LPA in releasing the cells from G2/M phase (Figure 3.17). Then we showed that LPA results in the long-term (after 12 h) increase in total and phosphorylated GSK-3β (Figure 3.25). LPA-induced GSK-3ß protein expression can be because of enhancing GSK-3ß gene expression and/or protein stability, which needs further elucidation. GSK-3 activity is increased by phosphorylation of a tyrosine residue, Tyr-216 in GSK-3β and Tyr-279 in GSK-3α through the Ca^{2+}-sensitive tyrosine kinase, Pyk2, as a direct consequence of PLC activation [100]. The GSK-3 pathway has a critical role in the expression and phosphorylation of microtubule regulatory proteins including survivin [93]. We also showed that inhibition of GSK-3ß increases the expression of total GSK-3ß. These results are compatible with the previous results showing that GSK-3ß inhibitors reduce GSK-3ß degradation through phosphorylation of Ser-9 [189].

In our model, GSK-3ß pathway promotes survivin expression. The proposed mechanism is consistent with the studies showing that survivin expression depends on that of GSK-3β pathway [93,186] and these proteins interact physically [93,230]. In normal cells, maximum expression of survivin is at the G_2/M transition of the cell cycle [167]. The cell cycle–dependent control of survivin expression is regulated by various oncogenic pathways including PI3K/Akt and GSK-3ß in cancer cells [93,162,167]. Survivin can be phosphorylated by PI3K/Akt [168] or the main mitotic kinase, $p34^{cdc2}$-cyclin B1[169]. This kinase, increases cell viability and by aurora-B kinase, which is important for survivin localization and binding to centromeres [170]. The half-

life of survivin is about 30 min and this is extended by phosphorylation, which protects survivin from ubiquitination and degradation [172]. Significantly, LPA caused about a 12-fold increase in phospho-survivin expression in the presence of Taxol and this could also contribute to the increase in survivin concentrations. Increased survivin expression mediates faster mitotic exit as explained by a previous study [162]. It is possible that high levels of survivin expression in LPA treated-cells increases the threshold of spindle checkpoint and even over-rides the mitotic checkpoint, allowing the cells to further progress to G_1 phase after a transient delay in M and S phase exit caused by Taxol treatment.

Increased expression of survivin and phospho-survivin was also attenuated by inhibiting GSK-3 activity, or specific knockdown of GSK-3β (Figures 3.26 and 3.27). Knockdown of survivin decreased the number of multinucleated cells and increased the number of dead cells, cells in mitosis, and cells with abnormal spindle when we treated the MCF-7 cells with 50 nM of Taxol (Figure 3.28). These results are consistent with the results from previous studies [162,231]. However, Yue et al. showed a significant decrease in mitotic index in DT40 cells with survivin knockdown when the cells are treated with lower concentrations of Taxol (<50 nM). DT40 cells are chicken cells expressing B-myb in a doxycyclin-dependent manner. The B-myb gene is required for recovery from the DNA damage downstream of p53. Nuclear survivin interacts with microtubules where it increases dynamicity, thus promoting an appropriate structure of the mitotic spindles and nuclear separation [138]. Increased microtubule rearrangement could facilitate the dissociation of Taxol from

β–tubulin and promote normalization of the spindle structure, as we observed. This would facilitate the release from Taxol-induced mitotic arrest allowing cells to undergo cytokinesis and proceed to G1 and escape apoptosis (Figure 4.3).

We applied simple delipidation technique by active charcoal to remove LPA from serum for all the TMRE and cell cycle studies. This technique provided us the possibility to keep the important elements for cell transition through cell cycle and proliferation including protein growth factors in serum.

Survivin plays a key role in resistance to chemotherapy in tumor cells [232,233]. Expression of survivin also correlates with by Taxol resistance in ovarian and prostate cancers [234,235]. In breast cancer, survivin expression is correlated with poor prognostic parameters including higher histological grade and high tumor cell proliferation [163]. Survivin is typically found at low levels in normal cells, but is elevated in many tumor cells [164,165]. Survivin is also localized in different areas of the cell; mitochondrial and cytosolic survivin suppress apoptosis through blocking the caspase activity [236], whereas nuclear survivin is induced at G_2/M of the cell cycle to ensure proper mitosis and cytokinesis [230].

Survivin's role as an anti-apoptotic protein was initially proposed based on the presence of a BIR domain, which is a caspase-inhibition domain of the inhibitor of apoptosis family proteins [237]. However, the structure of survivin's BIR domain is not consistent with a role as a direct inhibitor of apoptosis and it is more similar to orthologs in lower organisms that ensure accurate cell division [238]. Survivin also lacks structural motifs that are required by other inhibitors of

apoptosis to mediate caspase binding and inhibition [239]. While some groups state that survivin directly inhibits caspase activity [240], others dispute this [239]. Nevertheless, an inhibition of caspase action is unlikely to contribute significantly to the increased viability of the MCF-7 cells used for the present experiments since these cells do not express caspase-3 [241,242]. However, the LPA-induced increase in survivin could possibly protect other tumor cells from Taxol-induced apoptosis through blocking caspase-3 mediated apoptosis. Further to the controversy surrounding the anti-apoptotic effects of survivin, Dohi et al. [243] suggested that this anti-apoptotic activity was dependent on a mitochondrial pool that was discharged after death stimulation, whereas Wheatley et al. [244] question the validity of those results. Nevertheless, many publications show that increased survivin levels protect cells from multiple apoptosis-inducing agents, including Taxol [244,245]. This might reflect that the anti-apoptotic function of survivin is only apparent at elevated physiological concentrations, such as in tumour cells and even more so, in response to LPA.

While survivin has a controversial role as an inhibitor of apoptosis it has an undisputed role as a mitotic regulator [244,246,247]. Survivin facilitates mitosis due to its role as a member of the Chromosomal Passenger Complex family. In early phases of mitosis, this complex localizes to chromosome arms and accumulates at centromeres until metaphase where it facilitates mitotic checkpoint, chromosome biorientation and assembly of the mitotic spindle. In anaphase, the Chromosomal Passenger Complex relocates to the spindle midzone and then to the midbody during telophase and is required for cytokinesis [248].

Survivin has also been reported to localize to centrosomes and microtubules of the mitotic spindle [237,249], although this result has been disputed and is attributed to a cross-reacting antigen [250].

Taxol resistance is commonly associated with increased survivin expression [162,234,251], but the novelty of the present work is that we demonstrate that this can result from increased LPA signaling. This LPA effect was demonstrated with LPA alone and in the presence of Taxol. *In vivo,* increased exposure of tumors to LPA would be caused by increased ATX expression, which is associated with increased tumor aggressiveness, angiogenesis and metastasis [2-4,47]. The MCF-7 cells used in the present studies express mainly LPA_2 receptors [213], which are especially associated with increased development of breast and other cancers [45,119]. LPA_1, LPA_2 and LPA_3 receptors are all able to activate PI3K, which we showed to initiate the long-term expression of GSK-3β and survivin. We propose that this LPA-induced increase in survivin expression could contribute to the increased frequency of invasive and metastatic breast cancers in mice that express increased autotaxin, or LPA_1, LPA_2 or LPA_3 receptor activities [45].

Taxol treatment itself increases survivin expression [252] and we observed a similar effect in our experiments with MCF-7 cells. This probably occurs because of the Taxol-induced G2/M arrest and cells express more survivin during this phase of the cell cycle.

The roles of ATX and LPA in producing resistance to chemotherapy have received relatively little attention and so far no treatment of human cancer

depends on the inhibition of ATX or LPA signaling. The present work describes a novel pathway of LPA signaling, which though PI3K consistently increases the expression of GSK-3β, survivin and phospho-survivin. This pathway could contribute to increased tumorigenesis and aggressiveness, which is seen when ATX expression or signaling through LPA receptors increased [11,45]. The LPA-induced expression of survivin, which we demonstrate, also protects against Taxol-induced cell cycle arrest and cell death because of its action on microtubule dynamics. Survivin is also an anti-apoptotic protein whose expression should also protect against the action of other chemotherapeutic agents because of its proposed action in inhibiting caspase-3. The present studies provide mechanistic support to justify the importance of developing therapeutic agents that decrease ATX activity and signaling through LPA receptors. These could provide valuable adjuvants to chemotherapy and surgery and increase the survival of cancer patients.

In conclusion, our work demonstrates that the abundant extracellular lipid, LPC, protects MCF-7 breast cancer cells and MDA-MD-435 melanoma cells against Taxol-induced apoptosis, but only after its conversion to LPA by ATX. LPA itself showed strong antagonism against the apoptotic effects of Taxol in a PI3K/Akt dependent manner. We also demonstrated that LPA releases cells from Taxol-induced G2/M arrest through promoting PI3K/Akt/GSK-3ß pathway, which increases survivin expression. This work identifies that inhibition of ATX activity or LPA receptors could improve the treatment of cancers by Taxol and possibly other chemotherapeutic agents in patients who express high ATX

activity.

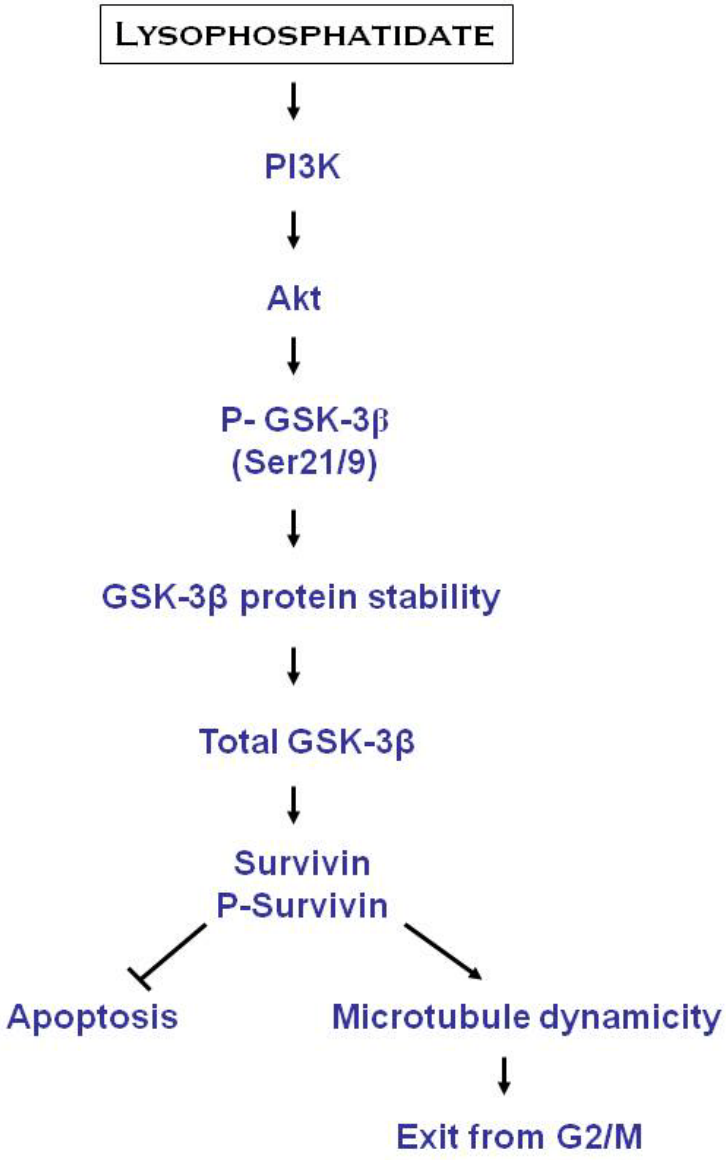

Figure 4.3 Schematic representation of the mechanism of lysophosphatidate action in releasing of the cells from mitotic arrest.

4.2 Future directions

Our work demonstrates that the abundant extracellular lipid, LPC, protects MCF-7 breast cancer cells and MDA-MD-435 melanoma cells against Taxol-induced apoptosis, but only after its conversion to LPA by ATX. LPA itself showed strong antagonism against the apoptotic effects of Taxol. This work identifies that inhibition of ATX activity could improve the treatment of cancers by Taxol and possibly other chemotherapeutic agents in patients who express high ATX activity. The recent study on the tumorigenic role of ATX in transgenic mouse by *Liu et al.* uncovered a new dimension of the *in vivo* role of ATX in tumor progression [45]. We need to extend our work by introducing green fluorescent protein (GFP)-labeled 4T1 breast cancer cells [253] into the mammary fat pad of ATX transgenic mice and comparing the extent of tumor development, metastasis and survival with those not overexpressing ATX. These experiments would also incorporate Taxol treatment to see if the ATX transgenic mice are Taxol resistant as we predict.

Further studies are also needed to detect ATX expression in circulation and cancerous tissues of patients with early stage and metastatic tumor. Development of cost-effective and applicable methods for ATX detection in blood, body fluids and tissues from cancer patients would also be very helpful to identify patients who express high ATX activity. Further inhibiting ATX activity with long-acting ATX inhibitors could provide an important adjuvant for improving the efficacy of chemothrapy in cancer treatment.

We also demonstrated that the effects of LPA in protecting against Taxol-induced G2/M arrest in result from LPA-induced release of the cells from Taxol-induced G2/M arrest, which allows them to proceed into G1 and avoid cell death. LPA-induced release from Taxol-induced mitotic arrest needs to be observed by monitoring this action of LPA by applying a spinning disk laser confocal microscope system. We will also apply fluorescent Taxol (Taxol-Oregon Green 488) and GFP-labeled tubulin to visualize the effects of LPA on its binding to microtubule structure. Live cell images of the cells escaping from G2/M arrest through the actions of LPA will be captured over the next 6 h.

We also investigate our proposed role of LPA signaling in chemoresistance through increasing GSK-3β and survivin expression. If survivin is the target protein for LPA signaling pathway in our model, we should demonstrate that overexpressing of survivin in MCF-7 cells, using Enhanced Green Fluorescent Protein (EGFP) fused to human survivin mimics the LPA effects even after knockdown of GSK-3ß, or applying a PI3K inhibitor. Furthermore, we need to uncover the mechanisms of LPA-induced GSK-3ß and survivin overexpression. There is a possibility that LPA stimulates GSK-3ß and/or survivin gene transcription. However, LPA may also stabilize these proteins by lowering their degradation.

LPA increased P-Ser and P-Tyr GSK-3ß and P-survivin in 12 h. We also need to determine the short-term regulation of Tyr phosphorylation and Ser

phosphorylation of GSK-3ß to test the proposed mechanism of how LPA induces alterations in GSK-3ß activity.

Our model for LPA action has been investigated in MCF-7 breast cancer cells. To validate the proposed model for cancer cells, it is necessary to show if the proposed mechanism is applicable for other cancer cells including MDA-MB-231 and MDA-MB-435 cells.

Completion of our model validation will reveal in details about the challenges associated with LPA-induced chemoresistance of Taxol, a widely used chemotherapeutic agent in the clinic.

BIBLIOGRAPHY

1. Jemal A, Siegel R, Ward E, Murray T, Xu J, Smigal C, Thun MJ: Cancer statistics, 2006. CA Cancer J Clin 2006;56:106-130.
2. Umezu-Goto M, Kishi Y, Taira A, Hama K, Dohmae N, Takio K, Yamori T, Mills GB, Inoue K, Aoki J, Arai H: Autotaxin has lysophospholipase d activity leading to tumor cell growth and motility by lysophosphatidic acid production. J Cell Biol 2002;158:227-233.
3. Nam SW, Clair T, Campo CK, Lee HY, Liotta LA, Stracke ML: Autotaxin (atx), a potent tumor motogen, augments invasive and metastatic potential of ras-transformed cells. Oncogene 2000;19:241-247.
4. Yang SY, Lee J, Park CG, Kim S, Hong S, Chung HC, Min SK, Han JW, Lee HW, Lee HY: Expression of autotaxin (npp-2) is closely linked to invasiveness of breast cancer cells. Clin Exp Metastasis 2002;19:603-608.
5. Gaetano CG, Samadi N, Tomsig JL, Macdonald TL, Lynch KR, Brindley DN: Inhibition of autotaxin production or activity blocks lysophosphatidylcholine-induced migration of human breast cancer and melanoma cells. Mol Carcinog 2009.
6. Mills GB, Moolenaar WH: The emerging role of lysophosphatidic acid in cancer. Nat Rev Cancer 2003;3:582-591.
7. Brindley DN: Lipid phosphate phosphatases and related proteins: Signaling functions in development, cell division, and cancer. J Cell Biochem 2004;92:900-912.

8. Stracke ML, Krutzsch HC, Unsworth EJ, Arestad A, Cioce V, Schiffmann E, Liotta LA: Identification, purification, and partial sequence analysis of autotaxin, a novel motility-stimulating protein. J Biol Chem 1992;267:2524-2529.

9. Goding JW, Grobben B, Slegers H: Physiological and pathophysiological functions of the ecto-nucleotide pyrophosphatase/phosphodiesterase family. Biochim Biophys Acta 2003;1638:1-19.

10. Stefan C, Jansen S, Bollen M: Npp-type ectophosphodiesterases: Unity in diversity. Trends Biochem Sci 2005;30:542-550.

11. van Meeteren LA, Moolenaar WH: Regulation and biological activities of the autotaxin-lpa axis. Prog Lipid Res 2007;46:145-160.

12. Croset M, Brossard N, Polette A, Lagarde M: Characterization of plasma unsaturated lysophosphatidylcholines in human and rat. Biochem J 2000;345 Pt 1:61-67.

13. Brindley DN, English D, Pilquil C, Buri K, Ling ZC: Lipid phosphate phosphatases regulate signal transduction through glycerolipids and sphingolipids. Biochim Biophys Acta 2002;1582:33-44.

14. Tokumura A, Majima E, Kariya Y, Tominaga K, Kogure K, Yasuda K, Fukuzawa K: Identification of human plasma lysophospholipase d, a lysophosphatidic acid-producing enzyme, as autotaxin, a multifunctional phosphodiesterase. J Biol Chem 2002;277:39436-39442.

15. Tokumura A: Physiological and pathophysiological roles of lysophosphatidic acids produced by secretory lysophospholipase d in body fluids. Biochim Biophys Acta 2002;1582:18-25.

16. Xie Y, Meier KE: Lysophospholipase d and its role in lpa production. Cell Signal 2004;16:975-981.

17. Jansen S, Callewaert N, Dewerte I, Andries M, Ceulemans H, Bollen M: An essential oligomannosidic glycan chain in the catalytic domain of autotaxin, a secreted lysophospholipase-d. J Biol Chem 2007;282:11084-11091.

18. Deng G, Royle G, Wang S, Crain K, Loskutoff DJ: Structural and functional analysis of the plasminogen activator inhibitor-1 binding motif in the somatomedin b domain of vitronectin. J Biol Chem 1996;271:12716-12723.

19. Gijsbers R, Ceulemans H, Stalmans W, Bollen M: Structural and catalytic similarities between nucleotide pyrophosphatases/phosphodiesterases and alkaline phosphatases. J Biol Chem 2001;276:1361-1368.

20. Cimpean A, Stefan C, Gijsbers R, Stalmans W, Bollen M: Substrate-specifying determinants of the nucleotide pyrophosphatases/phosphodiesterases npp1 and npp2. Biochem J 2004;381:71-77.

21. Yuelling LM, Fuss B: Autotaxin (atx): A multi-functional and multi-modular protein possessing enzymatic lysopld activity and matricellular properties. Biochim Biophys Acta 2008;1781:525-530.

22. Jansen S, Stefan C, Creemers JW, Waelkens E, Van Eynde A, Stalmans W, Bollen M: Proteolytic maturation and activation of autotaxin (npp2), a secreted metastasis-enhancing lysophospholipase d. J Cell Sci 2005;118:3081-3089.

23. Koike S, Keino-Masu K, Ohto T, Masu M: The n-terminal hydrophobic sequence of autotaxin (enpp2) functions as a signal peptide. Genes Cells 2006;11:133-142.

24. van Meeteren LA, Ruurs P, Christodoulou E, Goding JW, Takakusa H, Kikuchi K, Perrakis A, Nagano T, Moolenaar WH: Inhibition of autotaxin by lysophosphatidic acid and sphingosine 1-phosphate. J Biol Chem 2005;280:21155-21161.

25. Lee HY, Murata J, Clair T, Polymeropoulos MH, Torres R, Manrow RE, Liotta LA, Stracke ML: Cloning, chromosomal localization, and tissue expression of autotaxin from human teratocarcinoma cells. Biochem Biophys Res Commun 1996;218:714-719.

26. Murata J, Lee HY, Clair T, Krutzsch HC, Arestad AA, Sobel ME, Liotta LA, Stracke ML: Cdna cloning of the human tumor motility-stimulating protein, autotaxin, reveals a homology with phosphodiesterases. J Biol Chem 1994;269:30479-30484.

27. Fuss B, Baba H, Phan T, Tuohy VK, Macklin WB: Phosphodiesterase i, a novel adhesion molecule and/or cytokine involved in oligodendrocyte function. J Neurosci 1997;17:9095-9103.

28. Fox MA, Colello RJ, Macklin WB, Fuss B: Phosphodiesterase-ialpha/autotaxin: A counteradhesive protein expressed by oligodendrocytes during onset of myelination. Mol Cell Neurosci 2003;23:507-519.

29. Dennis J, White MA, Forrest AD, Yuelling LM, Nogaroli L, Afshari FS, Fox MA, Fuss B: Phosphodiesterase-ialpha/autotaxin's morfo domain regulates oligodendroglial process network formation and focal adhesion organization. Mol Cell Neurosci 2008;37:412-424.

30. Lee J, Jung ID, Nam SW, Clair T, Jeong EM, Hong SY, Han JW, Lee HW, Stracke ML, Lee HY: Enzymatic activation of autotaxin by divalent cations without ef-hand loop region involvement. Biochem Pharmacol 2001;62:219-224.

31. Webb DJ, Parsons JT, Horwitz AF: Adhesion assembly, disassembly and turnover in migrating cells -- over and over and over again. Nat Cell Biol 2002;4:E97-100.

32. Baker DL, Fujiwara Y, Pigg KR, Tsukahara R, Kobayashi S, Murofushi H, Uchiyama A, Murakami-Murofushi K, Koh E, Bandle RW, Byun HS, Bittman R, Fan D, Murph M, Mills GB, Tigyi G: Carba analogs of cyclic phosphatidic acid are selective inhibitors of autotaxin and cancer cell invasion and metastasis. J Biol Chem 2006;281:22786-22793.

33. Geho DH, Bandle RW, Clair T, Liotta LA: Physiological mechanisms of tumor-cell invasion and migration. Physiology (Bethesda) 2005;20:194-200.

34. Bacac M, Stamenkovic I: Metastatic cancer cell. Annu Rev Pathol 2008;3:221-247.

35. Handsley MM, Edwards DR: Metalloproteinases and their inhibitors in tumor angiogenesis. Int J Cancer 2005;115:849-860.

36. Weinberg RA: Mechanisms of malignant progression. Carcinogenesis 2008;29:1092-1095.

37. Chen M, O'Connor KL: Integrin alpha6beta4 promotes expression of autotaxin/enpp2 autocrine motility factor in breast carcinoma cells. Oncogene 2005;24:5125-5130.

38. Song J, Clair T, Noh JH, Eun JW, Ryu SY, Lee SN, Ahn YM, Kim SY, Lee SH, Park WS, Yoo NJ, Lee JY, Nam SW: Autotaxin (lysopld/npp2) protects fibroblasts from apoptosis through its enzymatic product, lysophosphatidic acid, utilizing albumin-bound substrate. Biochem Biophys Res Commun 2005;337:967-975.

39. Hoelzinger DB, Mariani L, Weis J, Woyke T, Berens TJ, McDonough WS, Sloan A, Coons SW, Berens ME: Gene expression profile of glioblastoma multiforme invasive phenotype points to new therapeutic targets. Neoplasia 2005;7:7-16.

40. Kishi Y, Okudaira S, Tanaka M, Hama K, Shida D, Kitayama J, Yamori T, Aoki J, Fujimaki T, Arai H: Autotaxin is overexpressed in glioblastoma multiforme and contributes to cell motility of glioblastoma by converting lysophosphatidylcholine to lysophosphatidic acid. J Biol Chem 2006;281:17492-17500.

41. Zhao H, Ramos CF, Brooks JD, Peehl DM: Distinctive gene expression of prostatic stromal cells cultured from diseased versus normal tissues. J Cell Physiol 2007;210:111-121.

42. Black EJ, Clair T, Delrow J, Neiman P, Gillespie DA: Microarray analysis identifies autotaxin, a tumour cell motility and angiogenic factor with lysophospholipase d activity, as a specific target of cell transformation by v-jun. Oncogene 2004;23:2357-2366.

43. Song J, Jie C, Polk P, Shridhar R, Clair T, Zhang J, Yin L, Keppler D: The candidate tumor suppressor cst6 alters the gene expression profile of human breast carcinoma cells: Down-regulation of the potent mitogenic, motogenic, and angiogenic factor autotaxin. Biochem Biophys Res Commun 2006;340:175-182.

44. Baumforth KR, Flavell JR, Reynolds GM, Davies G, Pettit TR, Wei W, Morgan S, Stankovic T, Kishi Y, Arai H, Nowakova M, Pratt G, Aoki J, Wakelam MJ, Young LS, Murray PG: Induction of autotaxin by the epstein-barr virus promotes the growth and survival of hodgkin lymphoma cells. Blood 2005;106:2138-2146.

45. Liu S, Umezu-Goto M, Murph M, Lu Y, Liu W, Zhang F, Yu S, Stephens LC, Cui X, Murrow G, Coombes K, Muller W, Hung MC, Perou CM, Lee AV, Fang X, Mills GB: Expression of autotaxin and lysophosphatidic acid receptors increases mammary tumorigenesis, invasion, and metastases. Cancer Cell 2009;15:539-550.

46. Haga A, Nagai H, Deyashiki Y: Autotaxin promotes the expression of matrix metalloproteinase-3 via activation of the mapk cascade in human fibrosarcoma ht-1080 cells. Cancer Invest 2009;27:384-390.

47. Nam SW, Clair T, Kim YS, McMarlin A, Schiffmann E, Liotta LA, Stracke ML: Autotaxin (npp-2), a metastasis-enhancing motogen, is an angiogenic factor. Cancer Res 2001;61:6938-6944.

48. Hama K, Aoki J, Fukaya M, Kishi Y, Sakai T, Suzuki R, Ohta H, Yamori T, Watanabe M, Chun J, Arai H: Lysophosphatidic acid and autotaxin stimulate cell motility of neoplastic and non-neoplastic cells through lpa1. J Biol Chem 2004;279:17634-17639.

49. Kehlen A, Englert N, Seifert A, Klonisch T, Dralle H, Langner J, Hoang-Vu C: Expression, regulation and function of autotaxin in thyroid carcinomas. Int J Cancer 2004;109:833-838.

50. Nouh MA, Wu XX, Okazoe H, Tsunemori H, Haba R, Abou-Zeid AM, Saleem MD, Inui M, Sugimoto M, Aoki J, Kakehi Y: Expression of autotaxin and acylglycerol kinase in prostate cancer: Association with cancer development and progression. Cancer Sci 2009.

51. Ikeda H, Watanabe N, Nakamura K, Kume Y, Nakai Y, Fujishiro M, Omata M, Igarashi K, Yokota H, Yatomi Y: [significance of serum autotaxin activity in gastrointestinal disease]. Rinsho Byori 2009;57:445-449.

52. Brindley DN, Pilquil C: Lipid phosphate phosphatases and signaling. J Lipid Res 2009;50 Suppl:S225-230.

53. Tanyi JL, Hasegawa Y, Lapushin R, Morris AJ, Wolf JK, Berchuck A, Lu K, Smith DI, Kalli K, Hartmann LC, McCune K, Fishman D, Broaddus R, Cheng KW, Atkinson EN, Yamal JM, Bast RC, Felix EA, Newman RA, Mills GB: Role of decreased levels of lipid phosphate phosphatase-1 in accumulation of lysophosphatidic acid in ovarian cancer. Clin Cancer Res 2003;9:3534-3545.

54. Tomsig JL, Snyder AH, Berdyshev EV, Skobeleva A, Mataya C, Natarajan V, Brindley DN, Lynch KR: Lipid phosphate phosphohydrolase type 1 (lpp1) degrades extracellular lysophosphatidic acid in vivo. Biochem J 2009;419:611-618.

55. Jasinska R, Zhang QX, Pilquil C, Singh I, Xu J, Dewald J, Dillon DA, Berthiaume LG, Carman GM, Waggoner DW, Brindley DN: Lipid phosphate phosphohydrolase-1 degrades exogenous glycerolipid and sphingolipid phosphate esters. Biochem J 1999;340 (Pt 3):677-686.

56. Smyth SS, Sciorra VA, Sigal YJ, Pamuklar Z, Wang Z, Xu Y, Prestwich GD, Morris AJ: Lipid phosphate phosphatases regulate lysophosphatidic acid production and signaling in platelets: Studies using chemical inhibitors of lipid phosphate phosphatase activity. J Biol Chem 2003;278:43214-43223.

57. Simon MF, Rey A, Castan-Laurel I, Gres S, Sibrac D, Valet P, Saulnier-Blache JS: Expression of ectolipid phosphate phosphohydrolases in 3t3f442a preadipocytes and adipocytes. Involvement in the control of lysophosphatidic acid production. J Biol Chem 2002;277:23131-23136.

58. Fang X, Schummer M, Mao M, Yu S, Tabassam FH, Swaby R, Hasegawa Y, Tanyi JL, LaPushin R, Eder A, Jaffe R, Erickson J, Mills GB: Lysophosphatidic acid is a bioactive mediator in ovarian cancer. Biochim Biophys Acta 2002;1582:257-264.

59. Weiner JA, Chun J: Schwann cell survival mediated by the signaling phospholipid lysophosphatidic acid. Proc Natl Acad Sci U S A 1999;96:5233-5238.

60. Panetti TS, Magnusson MK, Peyruchaud O, Zhang Q, Cooke ME, Sakai T, Mosher DF: Modulation of cell interactions with extracellular matrix by lysophosphatidic acid and sphingosine 1-phosphate. Prostaglandins 2001;64:93-106.

61. Simon MF, Chap H, Douste-Blazy L: Human platelet aggregation induced by 1-alkyl-lysophosphatidic acid and its analogs: A new group of phospholipid mediators? Biochem Biophys Res Commun 1982;108:1743-1750.

62. Rother E, Brandl R, Baker DL, Goyal P, Gebhard H, Tigyi G, Siess W: Subtype-selective antagonists of lysophosphatidic acid receptors inhibit platelet activation triggered by the lipid core of atherosclerotic plaques. Circulation 2003;108:741-747.

63. Kobilka BK: G protein coupled receptor structure and activation. Biochim Biophys Acta 2007;1768:794-807.

64. Lee CW, Rivera R, Gardell S, Dubin AE, Chun J: Gpr92 as a new g12/13- and gq-coupled lysophosphatidic acid receptor that increases camp, lpa5. J Biol Chem 2006;281:23589-23597.

65. Pasternack SM, von Kugelgen I, Aboud KA, Lee YA, Ruschendorf F, Voss K, Hillmer AM, Molderings GJ, Franz T, Ramirez A, Nurnberg P, Nothen MM, Betz RC: G protein-coupled receptor p2y5 and its ligand lpa are involved in maintenance of human hair growth. Nat Genet 2008;40:329-334.

66. Murakami M, Shiraishi A, Tabata K, Fujita N: Identification of the orphan gpcr, p2y(10) receptor as the sphingosine-1-phosphate and lysophosphatidic acid receptor. Biochem Biophys Res Commun 2008;371:707-712.

67. Parrill AL: Structural characteristics of lysophosphatidic acid biological targets. Biochem Soc Trans 2005;33:1366-1369.

68. Brady AE, Limbird LE: G protein-coupled receptor interacting proteins: Emerging roles in localization and signal transduction. Cell Signal 2002;14:297-309.

69. Yart A, Chap H, Raynal P: Phosphoinositide 3-kinases in lysophosphatidic acid signaling: Regulation and cross-talk with the ras/mitogen-activated protein kinase pathway. Biochim Biophys Acta 2002;1582:107-111.

70. Vanhaesebroeck B, Leevers SJ, Panayotou G, Waterfield MD: Phosphoinositide 3-kinases: A conserved family of signal transducers. Trends Biochem Sci 1997;22:267-272.

71. Stephens LR, Eguinoa A, Erdjument-Bromage H, Lui M, Cooke F, Coadwell J, Smrcka AS, Thelen M, Cadwallader K, Tempst P, Hawkins PT: The g beta gamma sensitivity of a pi3k is dependent upon a tightly associated adaptor, p101. Cell 1997;89:105-114.

72. Fruman DA, Rameh LE, Cantley LC: Phosphoinositide binding domains: Embracing 3-phosphate. Cell 1999;97:817-820.

73. Simonsen A, Wurmser AE, Emr SD, Stenmark H: The role of phosphoinositides in membrane transport. Curr Opin Cell Biol 2001;13:485-492.

74. Fang X, Yu S, LaPushin R, Lu Y, Furui T, Penn LZ, Stokoe D, Erickson JR, Bast RC, Jr., Mills GB: Lysophosphatidic acid prevents apoptosis in fibroblasts via g(i)-protein-mediated activation of mitogen-activated protein kinase. Biochem J 2000;352 Pt 1:135-143.

75. Wu EH, Wong YH: Pertussis toxin-sensitive gi/o proteins are involved in nerve growth factor-induced pro-survival akt signaling cascade in pc12 cells. Cell Signal 2005;17:881-890.

76. Kue PF, Daaka Y: Essential role for g proteins in prostate cancer cell growth and signaling. J Urol 2000;164:2162-2167.

77. Kim S, Jin J, Kunapuli SP: Akt activation in platelets depends on gi signaling pathways. J Biol Chem 2004;279:4186-4195.

78. He H, Pannequin J, Tantiongco JP, Shulkes A, Baldwin GS: Glycine-extended gastrin stimulates cell proliferation and migration through a rho-

and rock-dependent pathway, not a rac/cdc42-dependent pathway. Am J Physiol Gastrointest Liver Physiol 2005;289:G478-488.

79. Bian D, Mahanivong C, Yu J, Frisch SM, Pan ZK, Ye RD, Huang S: The g12/13-rhoa signaling pathway contributes to efficient lysophosphatidic acid-stimulated cell migration. Oncogene 2006;25:2234-2244.

80. Fukushima N, Weiner JA, Kaushal D, Contos JJ, Rehen SK, Kingsbury MA, Kim KY, Chun J: Lysophosphatidic acid influences the morphology and motility of young, postmitotic cortical neurons. Mol Cell Neurosci 2002;20:271-282.

81. Rommel C, Camps M, Ji H: Pi3k delta and pi3k gamma: Partners in crime in inflammation in rheumatoid arthritis and beyond? Nat Rev Immunol 2007;7:191-201.

82. Miura N, Atsumi S, Tabunoki H, Sato R: Expression and localization of three g protein alpha subunits, go, gq, and gs, in adult antennae of the silkmoth (bombyx mori). J Comp Neurol 2005;485:143-152.

83. Berridge MJ: Calcium signalling and cell proliferation. Bioessays 1995;17:491-500.

84. Cartin L, Lounsbury KM, Nelson MT: Coupling of ca(2+) to creb activation and gene expression in intact cerebral arteries from mouse : Roles of ryanodine receptors and voltage-dependent ca(2+) channels. Circ Res 2000;86:760-767.

85. Liu B, Itoh H, Louie O, Kubota K, Kent KC: The role of phospholipase c and phosphatidylinositol 3-kinase in vascular smooth muscle cell migration and proliferation. J Surg Res 2004;120:256-265.

86. Hollenbeck ST, Nelson PR, Yamamura S, Faries PL, Liu B, Kent KC: Intracellular calcium transients are necessary for platelet-derived growth factor but not extracellular matrix protein-induced vascular smooth muscle cell migration. J Vasc Surg 2004;40:351-358.

87. Moses S, Dreja K, Lindqvist A, Lovdahl C, Hellstrand P, Hultgardh-Nilsson A: Smooth muscle cell response to mechanical injury involves intracellular calcium release and erk1/erk2 phosphorylation. Exp Cell Res 2001;269:88-96.

88. Wu EH, Tam BH, Wong YH: Constitutively active alpha subunits of g(q/11) and g(12/13) families inhibit activation of the pro-survival akt signaling cascade. Febs J 2006;273:2388-2398.

89. Dorn GW, 2nd, Force T: Protein kinase cascades in the regulation of cardiac hypertrophy. J Clin Invest 2005;115:527-537.

90. Doble BW, Woodgett JR: Gsk-3: Tricks of the trade for a multi-tasking kinase. J Cell Sci 2003;116:1175-1186.

91. Sanchez C, Perez M, Avila J: Gsk3beta-mediated phosphorylation of the microtubule-associated protein 2c (map2c) prevents microtubule bundling. Eur J Cell Biol 2000;79:252-260.

92. Lovestone S, Hartley CL, Pearce J, Anderton BH: Phosphorylation of tau by glycogen synthase kinase-3 beta in intact mammalian cells: The effects

on the organization and stability of microtubules. Neuroscience 1996;73:1145-1157.

93. Panka DJ, Cho DC, Atkins MB, Mier JW: Gsk-3beta inhibition enhances sorafenib-induced apoptosis in melanoma cell lines. J Biol Chem 2008;283:726-732.

94. Woodgett JR: Molecular cloning and expression of glycogen synthase kinase-3/factor a. Embo J 1990;9:2431-2438.

95. Mukai F, Ishiguro K, Sano Y, Fujita SC: Alternative splicing isoform of tau protein kinase i/glycogen synthase kinase 3beta. J Neurochem 2002;81:1073-1083.

96. Schaffer B, Wiedau-Pazos M, Geschwind DH: Gene structure and alternative splicing of glycogen synthase kinase 3 beta (gsk-3beta) in neural and non-neural tissues. Gene 2003;302:73-81.

97. Cross DA, Alessi DR, Cohen P, Andjelkovich M, Hemmings BA: Inhibition of glycogen synthase kinase-3 by insulin mediated by protein kinase b. Nature 1995;378:785-789.

98. Fang X, Yu S, Tanyi JL, Lu Y, Woodgett JR, Mills GB: Convergence of multiple signaling cascades at glycogen synthase kinase 3: Edg receptor-mediated phosphorylation and inactivation by lysophosphatidic acid through a protein kinase c-dependent intracellular pathway. Mol Cell Biol 2002;22:2099-2110.

99. Fang X, Yu SX, Lu Y, Bast RC, Jr., Woodgett JR, Mills GB: Phosphorylation and inactivation of glycogen synthase kinase 3 by protein kinase a. Proc Natl Acad Sci U S A 2000;97:11960-11965.

100. Sayas CL, Ariaens A, Ponsioen B, Moolenaar WH: Gsk-3 is activated by the tyrosine kinase pyk2 during lpa1-mediated neurite retraction. Mol Biol Cell 2006;17:1834-1844.

101. Xu Y, Shen Z, Wiper DW, Wu M, Morton RE, Elson P, Kennedy AW, Belinson J, Markman M, Casey G: Lysophosphatidic acid as a potential biomarker for ovarian and other gynecologic cancers. Jama 1998;280:719-723.

102. Chappell J, Leitner JW, Solomon S, Golovchenko I, Goalstone ML, Draznin B: Effect of insulin on cell cycle progression in mcf-7 breast cancer cells. Direct and potentiating influence. J Biol Chem 2001;276:38023-38028.

103. So J, Wang FQ, Navari J, Schreher J, Fishman DA: Lpa-induced epithelial ovarian cancer (eoc) in vitro invasion and migration are mediated by vegf receptor-2 (vegf-r2). Gynecol Oncol 2005;97:870-878.

104. Sun B, Nishihira J, Suzuki M, Fukushima N, Ishibashi T, Kondo M, Sato Y, Todo S: Induction of macrophage migration inhibitory factor by lysophosphatidic acid: Relevance to tumor growth and angiogenesis. Int J Mol Med 2003;12:633-641.

105. Li H, Wang D, Zhang H, Kirmani K, Zhao Z, Steinmetz R, Xu Y: Lysophosphatidic acid stimulates cell migration, invasion, and colony

formation as well as tumorigenesis/metastasis of mouse ovarian cancer in immunocompetent mice. Mol Cancer Ther 2009;8:1692-1701.

106. Kulkarni P, Getzenberg RH: High-fat diet, obesity and prostate disease: The atx-lpa axis? Nat Clin Pract Urol 2009;6:128-131.

107. Li TT, Alemayehu M, Aziziyeh AI, Pape C, Pampillo M, Postovit LM, Mills GB, Babwah AV, Bhattacharya M: Beta-arrestin/ral signaling regulates lysophosphatidic acid-mediated migration and invasion of human breast tumor cells. Mol Cancer Res 2009;7:1064-1077.

108. Hurst JH, Hooks SB: Lysophosphatidic acid stimulates cell growth by different mechanisms in skov-3 and caov-3 ovarian cancer cells: Distinct roles for gi- and rho-dependent pathways. Pharmacology 2009;83:333-347.

109. Murph MM, Liu W, Yu S, Lu Y, Hall H, Hennessy BT, Lahad J, Schaner M, Helland A, Kristensen G, Borresen-Dale AL, Mills GB: Lysophosphatidic acid-induced transcriptional profile represents serous epithelial ovarian carcinoma and worsened prognosis. PLoS One 2009;4:e5583.

110. Chen SU, Lee H, Chang DY, Chou CH, Chang CY, Chao KH, Lin CW, Yang YS: Lysophosphatidic acid mediates interleukin-8 expression in human endometrial stromal cells through its receptor and nuclear factor-kappab-dependent pathway: A possible role in angiogenesis of endometrium and placenta. Endocrinology 2008;149:5888-5896.

111. Murray D, Horgan G, Macmathuna P, Doran P: Net1-mediated rhoa activation facilitates lysophosphatidic acid-induced cell migration and invasion in gastric cancer. Br J Cancer 2008;99:1322-1329.

112. Murph MM, Hurst-Kennedy J, Newton V, Brindley DN, Radhakrishna H: Lysophosphatidic acid decreases the nuclear localization and cellular abundance of the p53 tumor suppressor in a549 lung carcinoma cells. Mol Cancer Res 2007;5:1201-1211.

113. Hasegawa Y, Murph M, Yu S, Tigyi G, Mills GB: Lysophosphatidic acid (lpa)-induced vasodilator-stimulated phosphoprotein mediates lamellipodia formation to initiate motility in pc-3 prostate cancer cells. Mol Oncol 2008;2:54-69.

114. Boucharaba A, Serre CM, Guglielmi J, Bordet JC, Clezardin P, Peyruchaud O: The type 1 lysophosphatidic acid receptor is a target for therapy in bone metastases. Proc Natl Acad Sci U S A 2006;103:9643-9648.

115. Jeong KJ, Park SY, Seo JH, Lee KB, Choi WS, Han JW, Kang JK, Park CG, Kim YK, Lee HY: Lysophosphatidic acid receptor 2 and gi/src pathway mediate cell motility through cyclooxygenase 2 expression in caov-3 ovarian cancer cells. Exp Mol Med 2008;40:607-616.

116. Hope JM, Wang FQ, Whyte JS, Ariztia EV, Abdalla W, Long K, Fishman DA: Lpa receptor 2 mediates lpa-induced endometrial cancer invasion. Gynecol Oncol 2009;112:215-223.

117. Yu S, Murph MM, Lu Y, Liu S, Hall HS, Liu J, Stephens C, Fang X, Mills GB: Lysophosphatidic acid receptors determine tumorigenicity and aggressiveness of ovarian cancer cells. J Natl Cancer Inst 2008;100:1630-1642.

118. Yamada T, Yano S, Ogino H, Ikuta K, Kakiuchi S, Hanibuchi M, Kanematsu T, Taniguchi T, Sekido Y, Sone S: Lysophosphatidic acid stimulates the proliferation and motility of malignant pleural mesothelioma cells through lysophosphatidic acid receptors, lpa1 and lpa2. Cancer Sci 2008;99:1603-1610.

119. Lin S, Wang D, Iyer S, Ghaleb AM, Shim H, Yang VW, Chun J, Yun CC: The absence of lpa2 attenuates tumor formation in an experimental model of colitis-associated cancer. Gastroenterology 2009;136:1711-1720.

120. E S, Lai YJ, Tsukahara R, Chen CS, Fujiwara Y, Yue J, Yu JH, Guo H, Kihara A, Tigyi G, Lin FT: Lysophosphatidic acid 2 receptor-mediated supramolecular complex formation regulates its antiapoptotic effect. J Biol Chem 2009;284:14558-14571.

121. Komachi M, Tomura H, Malchinkhuu E, Tobo M, Mogi C, Yamada T, Kimura T, Kuwabara A, Ohta H, Im DS, Kurose H, Takeyoshi I, Sato K, Okajima F: Lpa1 receptors mediate stimulation, whereas lpa2 receptors mediate inhibition, of migration of pancreatic cancer cells in response to lysophosphatidic acid and malignant ascites. Carcinogenesis 2009;30:457-465.

122. Deng W, Balazs L, Wang DA, Van Middlesworth L, Tigyi G, Johnson LR: Lysophosphatidic acid protects and rescues intestinal epithelial cells from radiation- and chemotherapy-induced apoptosis. Gastroenterology 2002;123:206-216.

123. Raj GV, Sekula JA, Guo R, Madden JF, Daaka Y: Lysophosphatidic acid promotes survival of androgen-insensitive prostate cancer pc3 cells via activation of nf-kappab. Prostate 2004;61:105-113.

124. Meng Y, Kang S, Fishman DA: Lysophosphatidic acid inhibits anti-fas-mediated apoptosis enhanced by actin depolymerization in epithelial ovarian cancer. FEBS Lett 2005;579:1311-1319.

125. Rusovici R, Ghaleb A, Shim H, Yang VW, Yun CC: Lysophosphatidic acid prevents apoptosis of caco-2 colon cancer cells via activation of mitogen-activated protein kinase and phosphorylation of bad. Biochim Biophys Acta 2007;1770:1194-1203.

126. Hu X, Mendoza FJ, Sun J, Banerji V, Johnston JB, Gibson SB: Lysophosphatidic acid (lpa) induces the expression of vegf leading to protection against apoptosis in b-cell derived malignancies. Cell Signal 2008;20:1198-1208.

127. Ishdorj G, Graham BA, Hu X, Chen J, Johnston JB, Fang X, Gibson SB: Lysophosphatidic acid protects cancer cells from histone deacetylase (hdac) inhibitor-induced apoptosis through activation of hdac. J Biol Chem 2008;283:16818-16829.

128. Frankel A, Mills GB: Peptide and lipid growth factors decrease cis-diamminedichloroplatinum-induced cell death in human ovarian cancer cells. Clin Cancer Res 1996;2:1307-1313.

129. Weiner JA, Fukushima N, Contos JJ, Scherer SS, Chun J: Regulation of schwann cell morphology and adhesion by receptor-mediated lysophosphatidic acid signaling. J Neurosci 2001;21:7069-7078.

130. Koh JS, Lieberthal W, Heydrick S, Levine JS: Lysophosphatidic acid is a major serum noncytokine survival factor for murine macrophages which acts via the phosphatidylinositol 3-kinase signaling pathway. J Clin Invest 1998;102:716-727.

131. Karliner JS, Honbo N, Summers K, Gray MO, Goetzl EJ: The lysophospholipids sphingosine-1-phosphate and lysophosphatidic acid enhance survival during hypoxia in neonatal rat cardiac myocytes. J Mol Cell Cardiol 2001;33:1713-1717.

132. Holtsberg FW, Steiner MR, Keller JN, Mark RJ, Mattson MP, Steiner SM: Lysophosphatidic acid induces necrosis and apoptosis in hippocampal neurons. J Neurochem 1998;70:66-76.

133. Holtsberg FW, Steiner MR, Bruce-Keller AJ, Keller JN, Mattson MP, Moyers JC, Steiner SM: Lysophosphatidic acid and apoptosis of nerve growth factor-differentiated pc12 cells. J Neurosci Res 1998;53:685-696.

134. O'Driscoll L, Clynes M: Biomarkers and multiple drug resistance in breast cancer. Curr Cancer Drug Targets 2006;6:365-384.

135. Jordan MA: Mechanism of action of antitumor drugs that interact with microtubules and tubulin. Curr Med Chem Anticancer Agents 2002;2:1-17.

136. Gueritte F: General and recent aspects of the chemistry and structure-activity relationships of taxoids. Curr Pharm Des 2001;7:1229-1249.

137. Gligorov J, Lotz JP: Preclinical pharmacology of the taxanes: Implications of the differences. Oncologist 2004;9 Suppl 2:3-8.

138. McGrogan BT, Gilmartin B, Carney DN, McCann A: Taxanes, microtubules and chemoresistant breast cancer. Biochim Biophys Acta 2008;1785:96-132.

139. Green MC, Buzdar AU, Smith T, Ibrahim NK, Valero V, Rosales MF, Cristofanilli M, Booser DJ, Pusztai L, Rivera E, Theriault RL, Carter C, Frye D, Hunt KK, Symmans WF, Strom EA, Sahin AA, Sikov W, Hortobagyi GN: Weekly paclitaxel improves pathologic complete remission in operable breast cancer when compared with paclitaxel once every 3 weeks. J Clin Oncol 2005;23:5983-5992.

140. Steed H, Sawyer MB: Pharmacology, pharmacokinetics and pharmacogenomics of paclitaxel. Pharmacogenomics 2007;8:803-815.

141. Fitzpatrick FA, Wheeler R: The immunopharmacology of paclitaxel (taxol), docetaxel (taxotere), and related agents. Int Immunopharmacol 2003;3:1699-1714.

142. Mackey JR, Tonkin KS, Koski SL, Scarfe AG, Smylie MG, Joy AA, Au HJ, Bodnar DM, Soulieres D, Smith SW: Final results of a phase ii clinical trial of weekly docetaxel in combination with capecitabine in

anthracycline-pretreated metastatic breast cancer. Clin Breast Cancer 2004;5:287-292.

143. Torres K, Horwitz SB: Mechanisms of taxol-induced cell death are concentration dependent. Cancer Res 1998;58:3620-3626.

144. Liebmann JE, Cook JA, Lipschultz C, Teague D, Fisher J, Mitchell JB: Cytotoxic studies of paclitaxel (taxol) in human tumour cell lines. Br J Cancer 1993;68:1104-1109.

145. Jordan MA, Wilson L: Microtubules as a target for anticancer drugs. Nat Rev Cancer 2004;4:253-265.

146. Downing KH, Nogales E: Crystallographic structure of tubulin: Implications for dynamics and drug binding. Cell Struct Funct 1999;24:269-275.

147. Diaz JF, Valpuesta JM, Chacon P, Diakun G, Andreu JM: Changes in microtubule protofilament number induced by taxol binding to an easily accessible site. Internal microtubule dynamics. J Biol Chem 1998;273:33803-33810.

148. Abal M, Andreu JM, Barasoain I: Taxanes: Microtubule and centrosome targets, and cell cycle dependent mechanisms of action. Curr Cancer Drug Targets 2003;3:193-203.

149. Snyder JP, Nettles JH, Cornett B, Downing KH, Nogales E: The binding conformation of taxol in beta-tubulin: A model based on electron crystallographic density. Proc Natl Acad Sci U S A 2001;98:5312-5316.

150. Blagosklonny MV: Mitotic arrest and cell fate: Why and how mitotic inhibition of transcription drives mutually exclusive events. Cell Cycle 2007;6:70-74.

151. Weaver BA, Cleveland DW: Decoding the links between mitosis, cancer, and chemotherapy: The mitotic checkpoint, adaptation, and cell death. Cancer Cell 2005;8:7-12.

152. Paridaens R, Biganzoli L, Bruning P, Klijn JG, Gamucci T, Houston S, Coleman R, Schachter J, Van Vreckem A, Sylvester R, Awada A, Wildiers J, Piccart M: Paclitaxel versus doxorubicin as first-line single-agent chemotherapy for metastatic breast cancer: A european organization for research and treatment of cancer randomized study with cross-over. J Clin Oncol 2000;18:724-733.

153. Lowe SW, Cepero E, Evan G: Intrinsic tumour suppression. Nature 2004;432:307-315.

154. Boatright KM, Salvesen GS: Mechanisms of caspase activation. Curr Opin Cell Biol 2003;15:725-731.

155. Ashkenazi A, Herbst RS: To kill a tumor cell: The potential of proapoptotic receptor agonists. J Clin Invest 2008;118:1979-1990.

156. Kroemer G, Galluzzi L, Brenner C: Mitochondrial membrane permeabilization in cell death. Physiol Rev 2007;87:99-163.

157. Hunter AM, LaCasse EC, Korneluk RG: The inhibitors of apoptosis (iaps) as cancer targets. Apoptosis 2007;12:1543-1568.

158. Fulda S, Pervaiz S: Apoptosis signaling in cancer stem cells. Int J Biochem Cell Biol 2009.

159. Berrieman HK, Lind MJ, Cawkwell L: Do beta-tubulin mutations have a role in resistance to chemotherapy? Lancet Oncol 2004;5:158-164.

160. Wagner P, Wang B, Clark E, Lee H, Rouzier R, Pusztai L: Microtubule associated protein (map)-tau: A novel mediator of paclitaxel sensitivity in vitro and in vivo. Cell Cycle 2005;4:1149-1152.

161. Stauber RH, Mann W, Knauer SK: Nuclear and cytoplasmic survivin: Molecular mechanism, prognostic, and therapeutic potential. Cancer Res 2007;67:5999-6002.

162. Lu J, Tan M, Huang WC, Li P, Guo H, Tseng LM, Su XH, Yang WT, Treekitkarnmongkol W, Andreeff M, Symmans F, Yu D: Mitotic deregulation by survivin in erbb2-overexpressing breast cancer cells contributes to taxol resistance. Clin Cancer Res 2009;15:1326-1334.

163. Nassar A, Lawson D, Cotsonis G, Cohen C: Survivin and caspase-3 expression in breast cancer: Correlation with prognostic parameters, proliferation, angiogenesis, and outcome. Appl Immunohistochem Mol Morphol 2008;16:113-120.

164. Li F, Yang J, Ramnath N, Javle MM, Tan D: Nuclear or cytoplasmic expression of survivin: What is the significance? Int J Cancer 2005;114:509-512.

165. Engels K, Knauer SK, Metzler D, Simf C, Struschka O, Bier C, Mann W, Kovacs AF, Stauber RH: Dynamic intracellular survivin in oral squamous

cell carcinoma: Underlying molecular mechanism and potential as an early prognostic marker. J Pathol 2007;211:532-540.

166. Fukuda S, Pelus LM: Survivin, a cancer target with an emerging role in normal adult tissues. Mol Cancer Ther 2006;5:1087-1098.

167. Altieri DC: Targeted therapy by disabling crossroad signaling networks: The survivin paradigm. Mol Cancer Ther 2006;5:478-482.

168. Zhang Y, Park TS, Gidday JM: Hypoxic preconditioning protects human brain endothelium from ischemic apoptosis by akt-dependent survivin activation. Am J Physiol Heart Circ Physiol 2007;292:H2573-2581.

169. Altieri DC: Survivin in apoptosis control and cell cycle regulation in cancer. Prog Cell Cycle Res 2003;5:447-452.

170. Wheatley SP, Henzing AJ, Dodson H, Khaled W, Earnshaw WC: Aurora-b phosphorylation in vitro identifies a residue of survivin that is essential for its localization and binding to inner centromere protein (incenp) in vivo. J Biol Chem 2004;279:5655-5660.

171. Yamamoto H, Ngan CY, Monden M: Cancer cells survive with survivin. Cancer Sci 2008;99:1709-1714.

172. Zhao J, Tenev T, Martins LM, Downward J, Lemoine NR: The ubiquitin-proteasome pathway regulates survivin degradation in a cell cycle-dependent manner. J Cell Sci 2000;113 Pt 23:4363-4371.

173. Yusuf RZ, Duan Z, Lamendola DE, Penson RT, Seiden MV: Paclitaxel resistance: Molecular mechanisms and pharmacologic manipulation. Curr Cancer Drug Targets 2003;3:1-19.

174. Fujino H, Yamada I, Shimada S, Yoneda M: Simultaneous determination of taxol and its metabolites in microsomal samples by a simple thin-layer chromatography radioactivity assay--inhibitory effect of nk-104, a new inhibitor of hmg-coa reductase. J Chromatogr B Biomed Sci Appl 2001;757:143-150.

175. Saunders DE, Lawrence WD, Christensen C, Wappler NL, Ruan H, Deppe G: Paclitaxel-induced apoptosis in mcf-7 breast-cancer cells. Int J Cancer 1997;70:214-220.

176. Cui P, Tomsig JL, McCalmont WF, Lee S, Becker CJ, Lynch KR, Macdonald TL: Synthesis and biological evaluation of phosphonate derivatives as autotaxin (atx) inhibitors. Bioorg Med Chem Lett 2007;17:1634-1640.

177. Ferry G, Moulharat N, Pradere JP, Desos P, Try A, Genton A, Giganti A, Bleucher-Gaudin M, Lonchampt M, Bertrand M, Saulnier-Blache JS, Tucker GC, Cordi A, Boutin JA: S32826 : A nanomolar inhibitor of autotaxin. Discovery, synthesis and applications as a pharmacological tool. J Pharmacol Exp Ther 2008.

178. Demidenko ZN, Kalurupalle S, Hanko C, Lim CU, Broude E, Blagosklonny MV: Mechanism of g1-like arrest by low concentrations of paclitaxel: Next cell cycle p53-dependent arrest with sub g1 DNA content mediated by prolonged mitosis. Oncogene 2008.

179. Spankuch B, Kurunci-Csacsko E, Kaufmann M, Strebhardt K: Rational combinations of sirnas targeting plk1 with breast cancer drugs. Oncogene 2007;26:5793-5807.

180. Cheng H, Wu Y, An S, Dong S, Chen H, Zhang X, Guo A: In vitro sequence-dependent interaction between paclitaxel and gefitinib in human lung cancer cell lines. Print this page

J Clin Oncol 2009;27:suppl; abstr e22025.

181. Minn AJ, Boise LH, Thompson CB: Expression of bcl-xl and loss of p53 can cooperate to overcome a cell cycle checkpoint induced by mitotic spindle damage. Genes Dev 1996;10:2621-2631.

182. Lanni JS, Jacks T: Characterization of the p53-dependent postmitotic checkpoint following spindle disruption. Mol Cell Biol 1998;18:1055-1064.

183. Blajeski AL, Kottke TJ, Kaufmann SH: A multistep model for paclitaxel-induced apoptosis in human breast cancer cell lines. Exp Cell Res 2001;270:277-288.

184. Tao W, South VJ, Zhang Y, Davide JP, Farrell L, Kohl NE, Sepp-Lorenzino L, Lobell RB: Induction of apoptosis by an inhibitor of the mitotic kinesin ksp requires both activation of the spindle assembly checkpoint and mitotic slippage. Cancer Cell 2005;8:49-59.

185. Krishan A, Arya P: Monitoring of cellular resistance to cancer chemotherapy. Hematol Oncol Clin North Am 2002;16:357-372, vi.

186. Kaga S, Zhan L, Altaf E, Maulik N: Glycogen synthase kinase-3beta/beta-catenin promotes angiogenic and anti-apoptotic signaling through the induction of vegf, bcl-2 and survivin expression in rat ischemic preconditioned myocardium. J Mol Cell Cardiol 2006;40:138-147.

187. Gomez-Munoz A, Hamza EH, Brindley DN: Effects of sphingosine, albumin and unsaturated fatty acids on the activation and translocation of phosphatidate phosphohydrolases in rat hepatocytes. Biochim Biophys Acta 1992;1127:49-56.

188. Simon D, Benitez MJ, Gimenez-Cassina A, Garrido JJ, Bhat RV, Diaz-Nido J, Wandosell F: Pharmacological inhibition of gsk-3 is not strictly correlated with a decrease in tyrosine phosphorylation of residues 216/279. J Neurosci Res 2008;86:668-674.

189. Evenson AR, Fareed MU, Menconi MJ, Mitchell JC, Hasselgren PO: Gsk-3beta inhibitors reduce protein degradation in muscles from septic rats and in dexamethasone-treated myotubes. Int J Biochem Cell Biol 2005;37:2226-2238.

190. Melet A, Song K, Bucur O, Jagani Z, Grassian AR, Khosravi-Far R: Apoptotic pathways in tumor progression and therapy. Adv Exp Med Biol 2008;615:47-79.

191. Marchetti P, Urien S, Cappellini GA, Ronzino G, Ficorella C: Weekly administration of paclitaxel: Theoretical and clinical basis. Crit Rev Oncol Hematol 2002;44 Suppl:S3-13.

192. Moolenaar WH, van Meeteren LA, Giepmans BN: The ins and outs of lysophosphatidic acid signaling. Bioessays 2004;26:870-881.

193. Yue J, Yokoyama K, Balazs L, Baker DL, Smalley D, Pilquil C, Brindley DN, Tigyi G: Mice with transgenic overexpression of lipid phosphate phosphatase-1 display multiple organotypic deficits without alteration in circulating lysophosphatidate level. Cell Signal 2004;16:385-399.

194. Wang AC, Su QB, Wu FX, Zhang XL, Liu PS: Role of tlr4 for paclitaxel chemotherapy in human epithelial ovarian cancer cells. Eur J Clin Invest 2009;39:157-164.

195. Jiang SJ, Zhang S, Mu XY, Li W, Wang Y: [effects of trichostatin a and paclitaxel on apoptosis and microtubule stabilization in endometrial carcinoma cells: An in vitro research]. Zhonghua Yi Xue Za Zhi 2008;88:2427-2431.

196. Jin H, Yang R, Ross J, Fong S, Carano R, Totpal K, Lawrence D, Zheng Z, Koeppen H, Stern H, Schwall R, Ashkenazi A: Cooperation of the agonistic dr5 antibody apomab with chemotherapy to inhibit orthotopic lung tumor growth and improve survival. Clin Cancer Res 2008;14:7733-7740.

197. Narita S, So A, Ettinger S, Hayashi N, Muramaki M, Fazli L, Kim Y, Gleave ME: Gli2 knockdown using an antisense oligonucleotide induces apoptosis and chemosensitizes cells to paclitaxel in androgen-independent prostate cancer. Clin Cancer Res 2008;14:5769-5777.

198. Mhaidat NM, Alali FQ, Matalqah SM, Matalka, II, Jaradat SA, Al-Sawalha NA, Thorne RF: Inhibition of mek sensitizes paclitaxel-induced apoptosis of human colorectal cancer cells by downregulation of grp78. Anticancer Drugs 2009;20:601-606.

199. Pushkarev VM, Starenki DV, Saenko VA, Yamashita S, Kovzun OI, Popadiuk ID, Pushkarev VV, Tronko MD: Effects of low and high concentrations of antitumour drug taxol in anaplastic thyroid cancer cells. Exp Oncol 2009;31:16-21.

200. Hauswald S, Duque-Afonso J, Wagner MM, Schertl FM, Lubbert M, Peschel C, Keller U, Licht T: Histone deacetylase inhibitors induce a very broad, pleiotropic anticancer drug resistance phenotype in acute myeloid leukemia cells by modulation of multiple abc transporter genes. Clin Cancer Res 2009;15:3705-3715.

201. Qu Y, Wang J, Sim MS, Liu B, Giuliano A, Barsoum J, Cui X: Elesclomol, counteracted by akt survival signaling, enhances the apoptotic effect of chemotherapy drugs in breast cancer cells. Breast Cancer Res Treat 2009.

202. Goetzl EJ, Dolezalova H, Kong Y, Hu YL, Jaffe RB, Kalli KR, Conover CA: Distinctive expression and functions of the type 4 endothelial differentiation gene-encoded g protein-coupled receptor for lysophosphatidic acid in ovarian cancer. Cancer Res 1999;59:5370-5375.

203. Levine JS, Koh JS, Triaca V, Lieberthal W: Lysophosphatidic acid: A novel growth and survival factor for renal proximal tubular cells. Am J Physiol 1997;273:F575-585.

204. Goetzl EJ, Kong Y, Mei B: Lysophosphatidic acid and sphingosine 1-phosphate protection of t cells from apoptosis in association with suppression of bax. J Immunol 1999;162:2049-2056.

205. Inoue CN, Nagano I, Ichinohasama R, Asato N, Kondo Y, Iinuma K: Bimodal effects of platelet-derived growth factor on rat mesangial cell proliferation and death, and the role of lysophosphatidic acid in cell survival. Clin Sci (Lond) 2001;101:11-19.

206. Chen J, Baydoun AR, Xu R, Deng L, Liu X, Zhu W, Shi L, Cong X, Hu S, Chen X: Lysophosphatidic acid protects mesenchymal stem cells against hypoxia and serum deprivation-induced apoptosis. Stem Cells 2008;26:135-145.

207. Hu X, Haney N, Kropp D, Kabore AF, Johnston JB, Gibson SB: Lysophosphatidic acid (lpa) protects primary chronic lymphocytic leukemia cells from apoptosis through lpa receptor activation of the anti-apoptotic protein akt/pkb. J Biol Chem 2005;280:9498-9508.

208. Ye X, Ishii I, Kingsbury MA, Chun J: Lysophosphatidic acid as a novel cell survival/apoptotic factor. Biochim Biophys Acta 2002;1585:108-113.

209. Contos JJ, Fukushima N, Weiner JA, Kaushal D, Chun J: Requirement for the lpa1 lysophosphatidic acid receptor gene in normal suckling behavior. Proc Natl Acad Sci U S A 2000;97:13384-13389.

210. Furui T, LaPushin R, Mao M, Khan H, Watt SR, Watt MA, Lu Y, Fang X, Tsutsui S, Siddik ZH, Bast RC, Mills GB: Overexpression of edg-2/vzg-1

induces apoptosis and anoikis in ovarian cancer cells in a lysophosphatidic acid-independent manner. Clin Cancer Res 1999;5:4308-4318.

211. Lin FT, Lai YJ, Makarova N, Tigyi G, Lin WC: The lysophosphatidic acid 2 receptor mediates down-regulation of siva-1 to promote cell survival. J Biol Chem 2007;282:37759-37769.

212. Deng W, Shuyu E, Tsukahara R, Valentine WJ, Durgam G, Gududuru V, Balazs L, Manickam V, Arsura M, VanMiddlesworth L, Johnson LR, Parrill AL, Miller DD, Tigyi G: The lysophosphatidic acid type 2 receptor is required for protection against radiation-induced intestinal injury. Gastroenterology 2007;132:1834-1851.

213. Chen M, Towers LN, O'Connor KL: Lpa2 (edg4) mediates rho-dependent chemotaxis with lower efficacy than lpa1 (edg2) in breast carcinoma cells. Am J Physiol Cell Physiol 2007;292:C1927-1933.

214. Gauthier R, Harnois C, Drolet JF, Reed JC, Vezina A, Vachon PH: Human intestinal epithelial cell survival: Differentiation state-specific control mechanisms. Am J Physiol Cell Physiol 2001;280:C1540-1554.

215. Baudhuin LM, Cristina KL, Lu J, Xu Y: Akt activation induced by lysophosphatidic acid and sphingosine-1-phosphate requires both mitogen-activated protein kinase kinase and p38 mitogen-activated protein kinase and is cell-line specific. Mol Pharmacol 2002;62:660-671.

216. Dufour G, Demers MJ, Gagne D, Dydensborg AB, Teller IC, Bouchard V, Degongre I, Beaulieu JF, Cheng JQ, Fujita N, Tsuruo T, Vallee K, Vachon PH: Human intestinal epithelial cell survival and anoikis. Differentiation

state-distinct regulation and roles of protein kinase b/akt isoforms. J Biol Chem 2004;279:44113-44122.

217. Harnois C, Demers MJ, Bouchard V, Vallee K, Gagne D, Fujita N, Tsuruo T, Vezina A, Beaulieu JF, Cote A, Vachon PH: Human intestinal epithelial crypt cell survival and death: Complex modulations of bcl-2 homologs by fak, pi3-k/akt-1, mek/erk, and p38 signaling pathways. J Cell Physiol 2004;198:209-222.

218. Monet M, Gkika D, Lehen'kyi V, Pourtier A, Vanden Abeele F, Bidaux G, Juvin V, Rassendren F, Humez S, Prevarsakaya N: Lysophospholipids stimulate prostate cancer cell migration via trpv2 channel activation. Biochim Biophys Acta 2009;1793:528-539.

219. Zhao Z, Xiao Y, Elson P, Tan H, Plummer SJ, Berk M, Aung PP, Lavery IC, Achkar JP, Li L, Casey G, Xu Y: Plasma lysophosphatidylcholine levels: Potential biomarkers for colorectal cancer. J Clin Oncol 2007;25:2696-2701.

220. Gwak GY, Yoon JH, Lee SH, Lee SM, Lee HS, Gores GJ: Lysophosphatidylcholine suppresses apoptotic cell death by inducing cyclooxygenase-2 expression via a raf-1 dependent mechanism in human cholangiocytes. J Cancer Res Clin Oncol 2006;132:771-779.

221. Tomura H, Mogi C, Sato K, Okajima F: Proton-sensing and lysolipid-sensitive g-protein-coupled receptors: A novel type of multi-functional receptors. Cell Signal 2005;17:1466-1476.

222. Asakuma J, Sumitomo M, Asano T, Asano T, Hayakawa M: Selective akt inactivation and tumor necrosis actor-related apoptosis-inducing ligand sensitization of renal cancer cells by low concentrations of paclitaxel. Cancer Res 2003;63:1365-1370.

223. Charles AG, Han TY, Liu YY, Hansen N, Giuliano AE, Cabot MC: Taxol-induced ceramide generation and apoptosis in human breast cancer cells. Cancer Chemother Pharmacol 2001;47:444-450.

224. Sietsma H, Dijkhuis AJ, Kamps W, Kok JW: Sphingolipids in neuroblastoma: Their role in drug resistance mechanisms. Neurochem Res 2002;27:665-674.

225. Swanton C, Marani M, Pardo O, Warne PH, Kelly G, Sahai E, Elustondo F, Chang J, Temple J, Ahmed AA, Brenton JD, Downward J, Nicke B: Regulators of mitotic arrest and ceramide metabolism are determinants of sensitivity to paclitaxel and other chemotherapeutic drugs. Cancer Cell 2007;11:498-512.

226. Carpinteiro A, Dumitru C, Schenck M, Gulbins E: Ceramide-induced cell death in malignant cells. Cancer Lett 2008;264:1-10.

227. Heinrich M, Wickel M, Schneider-Brachert W, Sandberg C, Gahr J, Schwandner R, Weber T, Saftig P, Peters C, Brunner J, Kronke M, Schutze S: Cathepsin d targeted by acid sphingomyelinase-derived ceramide. Embo J 1999;18:5252-5263.

228. Zhang XF, Li BX, Ren R: [effect of ceramide on apoptosis of human colon cancer ht-29 cells]. Wei Sheng Yan Jiu 2006;35:537-540.

229. Yeung TK, Germond C, Chen X, Wang Z: The mode of action of taxol: Apoptosis at low concentration and necrosis at high concentration. Biochem Biophys Res Commun 1999;263:398-404.

230. Vong QP, Cao K, Li HY, Iglesias PA, Zheng Y: Chromosome alignment and segregation regulated by ubiquitination of survivin. Science 2005;310:1499-1504.

231. Lens SM, Wolthuis RM, Klompmaker R, Kauw J, Agami R, Brummelkamp T, Kops G, Medema RH: Survivin is required for a sustained spindle checkpoint arrest in response to lack of tension. Embo J 2003;22:2934-2947.

232. Li J, Liu P, Mao H, Wanga A, Zhang X: Emodin sensitizes paclitaxel-resistant human ovarian cancer cells to paclitaxel-induced apoptosis in vitro. Oncol Rep 2009;21:1605-1610.

233. Virrey JJ, Guan S, Li W, Schonthal AH, Chen TC, Hofman FM: Increased survivin expression confers chemoresistance to tumor-associated endothelial cells. Am J Pathol 2008;173:575-585.

234. Zaffaroni N, Pennati M, Colella G, Perego P, Supino R, Gatti L, Pilotti S, Zunino F, Daidone MG: Expression of the anti-apoptotic gene survivin correlates with taxol resistance in human ovarian cancer. Cell Mol Life Sci 2002;59:1406-1412.

235. Pratt MA, Niu MY, Renart LI: Regulation of survivin by retinoic acid and its role in paclitaxel-mediated cytotoxicity in mcf-7 breast cancer cells. Apoptosis 2006;11:589-605.

236. Shin S, Sung BJ, Cho YS, Kim HJ, Ha NC, Hwang JI, Chung CW, Jung YK, Oh BH: An anti-apoptotic protein human survivin is a direct inhibitor of caspase-3 and -7. Biochemistry 2001;40:1117-1123.

237. Li F, Ambrosini G, Chu EY, Plescia J, Tognin S, Marchisio PC, Altieri DC: Control of apoptosis and mitotic spindle checkpoint by survivin. Nature 1998;396:580-584.

238. Chantalat L, Skoufias DA, Kleman JP, Jung B, Dideberg O, Margolis RL: Crystal structure of human survivin reveals a bow tie-shaped dimer with two unusual alpha-helical extensions. Mol Cell 2000;6:183-189.

239. Verdecia MA, Huang H, Dutil E, Kaiser DA, Hunter T, Noel JP: Structure of the human anti-apoptotic protein survivin reveals a dimeric arrangement. Nat Struct Biol 2000;7:602-608.

240. Li F, Ackermann EJ, Bennett CF, Rothermel AL, Plescia J, Tognin S, Villa A, Marchisio PC, Altieri DC: Pleiotropic cell-division defects and apoptosis induced by interference with survivin function. Nat Cell Biol 1999;1:461-466.

241. Liang Y, Yan C, Schor NF: Apoptosis in the absence of caspase 3. Oncogene 2001;20:6570-6578.

242. Janicke RU, Sprengart ML, Wati MR, Porter AG: Caspase-3 is required for DNA fragmentation and morphological changes associated with apoptosis. J Biol Chem 1998;273:9357-9360.

243. Dohi T, Beltrami E, Wall NR, Plescia J, Altieri DC: Mitochondrial survivin inhibits apoptosis and promotes tumorigenesis. J Clin Invest 2004;114:1117-1127.

244. Wheatley SP, McNeish IA: Survivin: A protein with dual roles in mitosis and apoptosis. Int Rev Cytol 2005;247:35-88.

245. Altieri DC: Validating survivin as a cancer therapeutic target. Nat Rev Cancer 2003;3:46-54.

246. Altieri DC: The case for survivin as a regulator of microtubule dynamics and cell-death decisions. Curr Opin Cell Biol 2006.

247. Lens SM, Vader G, Medema RH: The case for survivin as mitotic regulator. Curr Opin Cell Biol 2006;18:616-622.

248. Lens SM, Medema RH: The survivin/aurora b complex: Its role in coordinating tension and attachment. Cell Cycle 2003;2:507-510.

249. Fortugno P, Wall NR, Giodini A, O'Connor DS, Plescia J, Padgett KM, Tognin S, Marchisio PC, Altieri DC: Survivin exists in immunochemically distinct subcellular pools and is involved in spindle microtubule function. J Cell Sci 2002;115:575-585.

250. Carvalho A, Carmena M, Sambade C, Earnshaw WC, Wheatley SP: Survivin is required for stable checkpoint activation in taxol-treated hela cells. J Cell Sci 2003;116:2987-2998.

251. Xiong H, Yu S, Zhuang L, Xiong H: Changes of survivin mrna and protein expression during paclitaxel treatment in breast cancer cells. J Huazhong Univ Sci Technolog Med Sci 2007;27:65-67.

252. Ling X, Bernacki RJ, Brattain MG, Li F: Induction of survivin expression by taxol (paclitaxel) is an early event, which is independent of taxol-mediated g2/m arrest. J Biol Chem 2004;279:15196-15203.

253. Muehlberg FL, Song YH, Krohn A, Pinilla SP, Droll LH, Leng X, Seidensticker M, Ricke J, Altman AM, Devarajan E, Liu W, Arlinghaus RB, Alt EU: Tissue-resident stem cells promote breast cancer growth and metastasis. Carcinogenesis 2009;30:589-597.

PUBLICATIONS

Samadi N, Gaetano C, Goping IS, Brindley DN. Autotaxin protects MCF-7breast cancer and MDA-MB-435 melanoma cells against Taxol-induced apoptosis. Oncogene. 2009 Feb 19;28(7): 1028-39.

Gaetano CG, **Samadi N**, Tomsig JL, Macdonald TL, Lynch KR, Brindley DN. Inhibition of autotaxin production or activity blocks lysophosphatidylcholine-induced migration of human breast cancer and melanoma cells. Mol Carcinog. 2009 Feb 9. [Epub ahead of print].

Samadi N, Cembrowski GS, Chan J. Effect of waist circumference on reference intervals of liver-related enzyme tests in apparently healthy adult Mexican Americans, black and white Americans. Clin Biochem. 2007 Feb;40(3-4):206-12.

APPENDIX

Oncogene (2009) 28, 1028–1039

www.nature.com/onc

ORIGINAL ARTICLE

Autotaxin protects MCF-7 breast cancer and MDA-MB-435 melanoma cells against Taxol-induced apoptosis

N Samadi[1], C Gaetano[2], IS Goping[2] and DN Brindley[2]

[1]*Department of Laboratory Medicine and Pathology, University of Alberta, Edmonton, Alberta, Canada and* [2]*Department of Biochemistry (Signal Transduction Research Group), University of Alberta, Edmonton, Alberta, Canada*

Autotaxin (ATX) promotes cancer cell survival, growth, migration, invasion and metastasis. ATX converts extracellular lysophosphatidylcholine (LPC) into lysophosphatidate (LPA). As these lipids have been reported to affect cell signaling through their own G-protein-coupled receptors, ATX could modify the balance of this signaling. Also, ATX affects cell adhesion independently of its catalytic activity. We investigated the interactions of ATX, LPC and LPA on the apoptotic effects of Taxol, which is commonly used in breast cancer treatment. LPC had no significant effect on Taxol-induced apoptosis in MCF-7 breast cancer cells, which do not secrete significant ATX. Addition of incubation medium from MDA-MB-435 melanoma cells, which secrete ATX, or recombinat ATX enabled LPC to inhibit Taxol-induced apoptosis of MCF-7 cells. Inhibiting ATX activity blocked this protection against apoptosis. We conclude that LPC has no significant effect in protecting MCF-7 cells against Taxol treatment unless it is converted to LPA by ATX. LPA strongly antagonized Taxol-induced apoptosis through stimulating phosphatidylinositol 3-kinase and inhibiting ceramide formation. LPA also partially reversed the Taxol-induced arrest in the G2/M phase of the cell cycle. Our results support the hypothesis that therapeutic inhibition of ATX activity could improve the efficacy of Taxol as a chemotherapeutic agent for cancer treatment. *Oncogene* (2009) **28,** 1028–1039; doi:10.1038/onc.2008.442; published online 15 December 2008

Keywords: ceramides; chemotherapy; chemoresistance; lysophosphatidate; lysophosphatidylcholine; phosphatidylinositol 3-kinase

Introduction

Breast cancer is the most common malignancy among women in North America and approximately one-third of these women develop metastases and die (Jemal *et al*., 2006). Dysregulation of normal mechanisms of apoptosis play an important role in the pathogenesis and progression of breast cancer. Importantly, the efficacy of chemotherapy can be compromised by the survival signals that tumor cells receive (Krajewski *et al*., 1999).

There is a strong association of autotaxin (ATX) expression with breast cancer cell survival, growth, migration, invasion and metastasis (Nam *et al*., 2000, 2001; Umezu-Goto *et al*., 2002; Yang *et al*., 2002; Hama *et al*., 2004). ATX was originally isolated from human melanoma A2058 cells (Stracke *et al*., 1992) and it generates lysophosphatidate (LPA) from circulating lysophosphatidylcholine (LPC). Although the involvement of LPA and ATX in the invasiveness of breast cancer has been studied (Yang *et al*., 2002), relatively little is known about how ATX might confer chemoresistance. First, the substrate of ATX, LPC, has been postulated to be an extracellular signaling lipid by acting on G2A and GPR4 (Kabarowski *et al*., 2001; Zhu *et al*., 2001; Rikitake *et al*., 2002; Lin and Ye, 2003; Radu *et al*., 2004; Kim *et al*., 2005). Unsaturated LPC is secreted by the liver (Brindley, 1993) and saturated LPC is produced by circulating lecithin:cholesterol acyltransferase in high-density lipoproteins (Aoki *et al*., 2002). LPC is present in blood at up to 200 μM (Moolenaar *et al*., 2004). ATX could, therefore, regulate cell activation through changing signaling by LPC versus LPA. Secondly, ATX decreases the adhesion of oligodendrocytes to the extracelllular matrix through a non-catalytic mechanism involving its C-terminus, and this facilitates morphological remodeling (Dennis *et al*., 2005). This suggests that ATX is a matrix-cellular protein that signals through integrin-dependent focal adhesion assembly and consequently cell interactions with the extracellular matrix (Fox *et al*., 2004). This and other non-catalytic effects of ATX could contribute to its association with the aggressiveness of cancer cells.

Autotaxin provides a major route for generating extracellular LPA, which is present at up to 20 μM in blood and extracellular fluid (Moolenaar *et al*., 2004; Yue *et al*., 2004). LPA is produced by activated platelets to facilitate wound healing and is secreted by cancer cells (Fang *et al*., 2000; Radeff-Huang *et al*., 2004). Extracellular LPA has been implicated in the etiology of human cancer, as it stimulates cell growth, proliferation, differentiation, motility and survival (Mills and Moolenaar, 2003; Brindley, 2004). Diverse actions of LPA are mediated by at least six G-protein coupled

Correspondence: Professor DN Brindley, Department of Biochemistry (Signal Transduction Research Group), University of Alberta, Edmonton, Alberta, Canada T6G 2S2.
E-mail: david.brindley@ualberta.ca
Received 24 July 2008; revised 8 October 2008; accepted 1 November 2008; published online 15 December 2008

receptors present on the cell surface: LPA_1/EDG2, LPA_2/EDG4, LPA_3/EDG7, LPA_4/GPR23/p2y9, LPA_5/GRP92 and LPA_6/p2y5 (Lee *et al*., 2006; Pasternack *et al*., 2008). The expression of these receptors is cell specific, enabling different cells to respond in a unique manner through signaling pathways that are activated by G_i, G_s, G_q and $G_{12/13}$. These signaling cascades include phosphatidylinositol 3-kinase (PI3K) and Akt, the extracellular signal-regulated kinase (ERK) pathway, and the small G-protein, RhoA, that mediates cell survival (Ye *et al*., 2002; Tigyi and Parrill, 2003; Radeff-Huang *et al*., 2004). Activation of LPA receptors also decreases the abundance of the p53 tumor suppressor, thereby promoting cell survival and cell cycle progression (Murph *et al*., 2007).

Lysophosphatidate levels are high in ascites fluid and plasma of patients with ovarian tumors (Xu *et al*., 1998; Fang *et al*., 2002; Mills and Moolenaar, 2003). LPA promotes ovarian tumor development through increased cyclin D expression (Chappell *et al*., 2001). LPA also increases vascular endothelial growth factor production, which stimulates angiogenesis (So *et al*., 2005). In a colon cancer cell line, LPA increases the synthesis of macrophage migration inhibitory factor, which promotes tumor growth (Sun *et al*., 2003). However, the effect of LPA on cell survival and apoptosis varies among cell types. LPA mediates survival of ovarian cancer cells, macrophages, fibroblasts and neonatal cardiac myocytes, while promoting apoptosis in hippocampal neurons and PC12 cells (Fang *et al*., 2002; Ye *et al*., 2002).

Taxol is a microtubule-stabilizing agent that interferes with spindle microtubule dynamics causing cell cycle arrest and apoptosis through interaction with β-tubulin (Bergstralh and Ting, 2006). This causes lateral polymerization and microtubule stability (Snyder *et al*., 2001). Taxol is widely used for treating metastatic and early-stage breast cancer, with benefits in overall and disease-free survival. However, resistance to Taxol is common and there is a need to identify patients who will respond to treatment (McGrogan *et al*., 2008).

In this study, we established that ATX protects MCF-7 breast cancer cells and MDA-MB-435 melanoma cells against Taxol-induced apoptosis through its production of LPA from the LPC that bathes most cells. LPA is strongly antagonistic to Taxol-induced apoptosis, whereas LPC has no significant effect. From our results, we predict that identifying patients who express high ATX activity and then inhibiting this activity could provide an important adjuvant for improving the efficacy of Taxol in cancer treatment.

Results

Expression of ATX in MCF-7 and MDA-MB-435 cancer cells

ATX expression in the MCF-7 and MDA-MB-435 cells used in our experiments was compared. Real-time reverse transcriptase–PCR (RT–PCR) analysis showed that MDA-MB-435 cells expressed relatively high levels of ATX mRNA compared with MCF-7 cells (Figure 1a). MDA-MB-435 cells secreted ATX protein into the serum-free medium, whereas ATX was not detectable in the equivalent medium concentrated from MCF-7 cells (Figure 1b). ATX activity secreted by MDA-MB-435 cells was about 24 times higher ($P<0.001$) than that from MCF-7 cells (Figure 1c). Therefore, MCF-7 cells provide a system for studying apoptosis in the absence of ATX and for examining the effects of introducing ATX.

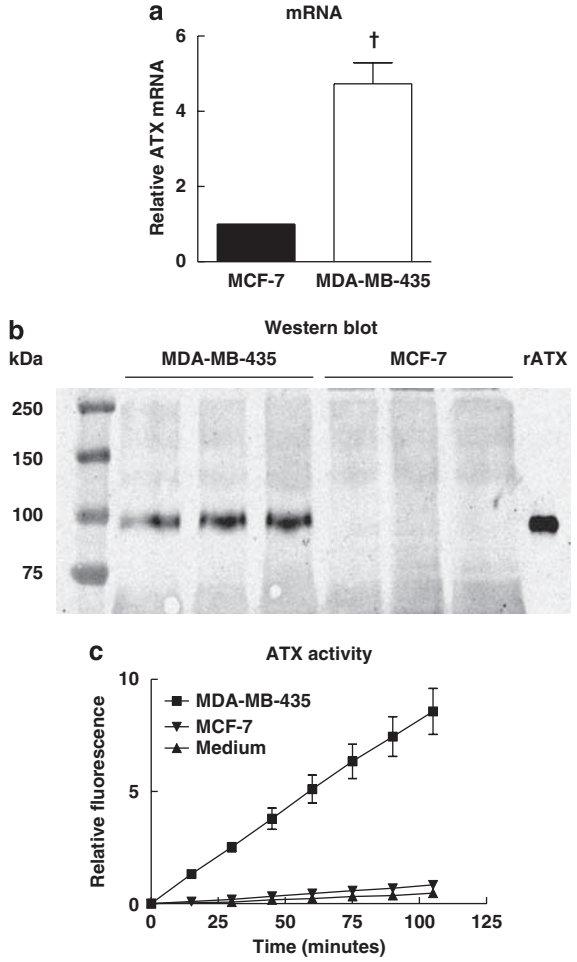

Figure 1 Differential expression of autotoxin (ATX) in MDA-MB-435 and MCF-7 cells. In (**a**), mRNA for ATX was determined by real-time RT-PCR and expressed relative to that of glyceraldehyde 3-phosphate dehydrogenase (GAPDH). (**b**) A western blot obtained by loading 40 μg of total protein from three independent samples of concentrated serum-free medium obtained from either MDA-MB-435 or MCF-7 cells is shown. A standard of recombinant rATX is shown on the right. In (**c**), 20 × concentrated serum-free medium from MCF-7 and MDA MB-435 cells was assayed for ATX activity using the FS-3 compound. Fluorescence was measured at excitation and emission wavelengths of 485 and 538 nm, respectively. The results are shown as the average of relative fluorescence activity ± s.e.m. from three independent experiments. †$P<0.001$.

LPA protects MCF-7 cells from Taxol-induced apoptosis

We next established conditions for studying Taxol-induced apoptosis and how LPC and LPA modify this

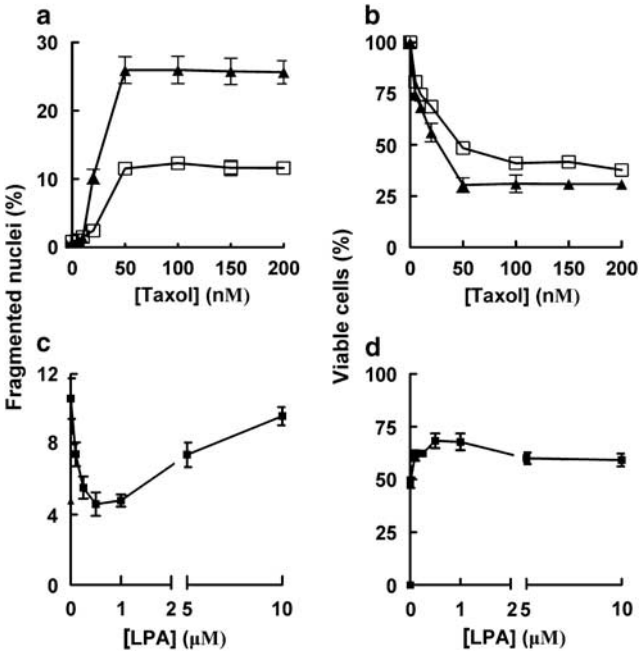

Figure 2 Protective effect of lysophosphatidate (LPA) on Taxol-induced apoptosis in MCF-7 cells. (**a**) The percentage of apoptotic nuclei from MCF-7 cells that were incubated with 0–200 nM Taxol for 24 h (□) or 48 h (▲) is shown. (**b**) The percentage of viable cells recovered from the wells expressed relative to untreated cells is shown. (**c** and **d**) The percentage of apoptotic nuclei and viable cells, respectively, that were recovered after adding different concentration of LPA with 50 nM Taxol and incubating for 24 h incubation is shown. Results are expressed as means ± s.e.m. from three independent experiments.

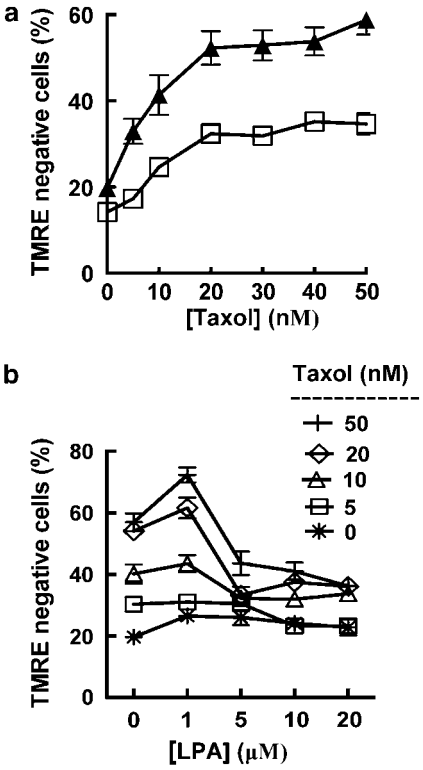

Figure 3 Effect of lysophosphatidate (LPA) on Taxol-induced change in mitochondrial potential. (**a**) The percentage of tetramethlyrhodamine ethyl ester (TMRE)-negative MCF-7 cells that were obtained after incubated with 0–50 nM Taxol for 24 h (□) or 48 h (▲) is shown. (**b**) The percentage of TMRE-negative cells obtained after adding different concentrations of Taxol (0–50 nM) with 0–20 μM LPA is shown. The results are shown as means ± s.e.m. of three experiments.

process. Apoptosis was detected both by morphological examination using 4,6-diamidino-2-phenylindole (DAPI) staining and by measuring mitochondrial tetramethlyrhodamine ethyl ester (TMRE) uptake. We used medium supplemented with 10% charcoal-treated fetal bovine serum (FBS) to remove lipid mediators including LPC and LPA. This treatment also removed ATX, as we could not detect significant ATX activity in media containing 10% charcoal-treated FBS (results not shown).

Treating MCF-7 cells with 50 nM Taxol produced an optimum increase in the percentage of recovered apoptotic nuclei from 0.8% to about 12% after 24 h and 26% after 48 h (Figure 2a), and a similar effect was observed with MDA-MB-435 cells (results not shown). This provides part of the picture, as treatment with 50 nM Taxol for 24 and 48 h decreased the number of cells attached to the dishes by about 60 and 70%, respectively (Figure 2b). We could not recover most of these cells from the medium presumably because of complete fragmentation. These results are compatible with those of Sunders *et al.* (1997), who concluded that Taxol induces both apoptotic and nonapoptotic death in MCF-7 cells.

The next experiments determined whether LPA can protect against apoptosis induced by 50 nM Taxol over 24 h. LPA (0.5 μM) alone had no significant effect on the percentage of apoptotic nuclei, but it produced a maximum decrease in the percentage of apoptotic cells remaining on the plates in the presence of Taxol. Less effect was observed at 5 and 10 μM LPA (Figure 2c). However, 0.5–10 μM LPA increased the recovery of viable cells from 49 ± 4.3 to 68 ± 6.1% (Figure 2d).

The second method used flow cytometry to detect apoptotic cells by TMRE-negative staining. Optimum apoptosis in the recovered cells was detected at 20 nM Taxol and this increased from 24 to 48 h (Figure 3a). We chose to use 48 h incubations, which increased the population of apoptotic cells to about 55%. LPA (5–20 μM) had a significant protective effect against different concentrations of Taxol. Maximum protection was obtained with 5 μM LPA against 20 nM Taxol in which the percentage of apoptotic cells decreased ($P<0.05$) from 54 ± 2 to 33 ± 3% (Figure 3b).

Isobologram analysis was used to evaluate the interactions between Taxol and LPA at the IC_{50} (inhibitory concentration 50%). All LPA concentrations used produced an antagonistic effect on Taxol-induced apoptosis with combination index values of >1 (Table 1). This antagonism was particularly apparent at 10 and 20 μM LPA ($P<0.01$). For example, 50 nM Taxol was required when 20 μM LPA was present to produce equivalent apoptosis to that obtained with

Table 1 Effect of LPA on Taxol-induced change in mitochondrial potential

Combination dose			*Taxol dose (nM) (alone)*	*Dose–response index*	*Combination index*
Taxol (nM)	*LPA (μM)*	*Fractional apoptosis*			
5	1	0.31	4.6	0.9	22.2
10	5	0.32	5.0	0.5	231
20	10	0.38	8.0	0.4	1630
50	20	0.36	7.2	0.2	1490

The dose–response interactions between different concentrations of Taxol and LPA in Figure 3b were assessed by isobologram analysis.

7.2 nM Taxol in the absence of LPA. Thus, 20 μM LPA produced a 6.9-fold decrease at IC_{50} in Taxol sensitivity.

ATX protects MCF-7 and MDA-MB-435 cells against Taxol-induced apoptosis by producing LPA

We next studied whether ATX protects MCF-7 cells against Taxol-induced apoptosis by changing the balance of cell activation by LPC versus LPA. MCF-7 cells were incubated with 10% charcoal-treated FBS and concentrated medium obtained from 10^6 MDA-MB-435 cells, or MCF-7 cells in the presence or absence of LPC or LPA. Concentrated medium from MDA-MB-435 cells showed an average of 32 times more ATX activity compared with equivalent medium from MCF-7 cells.

Concentrated medium from MDA-MB-435 cells supplemented with 10 μM LPC decreased percentage apoptosis measured by DAPI staining from $7.4 \pm 1.3\%$ to $4.4 \pm 0.6\%$ (88% of the effect of 0.5 μM LPA) (Figure 4a). The percentage of viable cells recovered also increased ($49 \pm 3\%$ to $77 \pm 7\%$; $P < 0.05$) (Figure 4b). Concentrated medium from MDA-MB-435 cells appeared to decrease apoptosis ($6.1 \pm 0.8\%$) in the absence of added LPC or LPA, but this was not statistically significant. LPC in the absence of conditioned medium had no protective effect (Figure 4a).

We also used an ATX inhibitor, VPC8a202 (Cui *et al*., 2007), to determine whether the effect of concentrated medium depended upon ATX activity. VPC8a202 (1 μM) decreased ATX activity by 87% as expected (results not shown) and it abolished the protective effect of LPC plus concentrated media from MDA-MB-435 cells (Figure 4a). There was no increase in the percentage of viable cells after applying the ATX inhibitor alone (Figure 4b).

The TMRE assay also showed a significant decrease in apoptosis ($P < 0.01$) in cells treated with concentrated medium from MDA-MB-435 cells when 200 μM LPC was added (Figure 4c). Concentrated medium alone or LPC alone had no significant protective effect (Figure 4c). VPC8a202 (1 μM) abolished the protective effect of concentrated media with LPC. As a control, the effect of VPC8a202 was shown to be specific, as it did not alter the protective effect of LPA on Taxol-induced apoptosis (Figures 4b and c).

To confirm that the effects of concentrated medium cells depended on ATX activity, we used recombinant ATX, which protected against Taxol-induced apoptosis and increased the number of viable cells recovered when LPC was present (Figures 4d and e). Blocking ATX activity with 1 μM of the inhibitors VPC8a202, or S32826 (Ferry *et al*., 2008), or heating at 70 °C abolished the protective effect of recombinant ATX. Furthermore, concentrated medium from MCF-7 cells that contained no significant ATX activity failed to provide any significant protection with LPC against Taxol-induced apoptosis (Figures 5a–c).

We also showed that the endogenous ATX produced by MDA-MB-435 cells protects these cells against Taxol-induced apoptosis when LPC is present, as this effect is blocked by the ATX inhibitors, VPC8a202 or S32826 (Figure 6). The inhibitors had no effect of the protection afforded by LPA.

LPA protects against Taxol-induced apoptosis by increasing PI3K/Akt and decreasing ceramide production

We examined the roles of the PI3K-Akt and MAPK/ERK kinase-ERK pathways on apoptosis by using LY294002 and PD98059, respectively. LY294002 (50 μM) almost completely abrogated the effects of LPA in protecting against apoptosis (Figures 7a and b). PD98059 (40 μM) showed no significant effect on the LPA protection against Taxol-induced apoptosis, although it blocked the activation of p42/44 mitogen-activated protein kinase (MAPK) (Figures 8a–c). Also, phospho-42/44p MAPK and total 42/44p MAPK showed a significant increase over 12 h in response to LPA. There was no significant effect of Taxol alone on the expression of phospho-42/44p MAPK and total 42/44p MAPK.

Lysophosphatidate (5 μM) increased ($P < 0.05$) the expression of both phospho-Akt and total Akt by about twofold over 12 h (Figure 8a) and the ratio of phospho-Akt/total Akt (Figure 8d). Taxol (30 nM) alone had no significant effect. When Taxol was added with LPA (5 μM), there was still a 50% increase in phospho-Akt and total Akt compared with nontreated cells (Figure 8a) and an increase in the phospho-Akt/total Akt ratio (Figure 8d). Applying 50 μM LY294002 abolished the effect of LPA on the elevation of activated and total Akt.

To determine the protective mechanism of LPA against Taxol-induced apoptosis, we measured ceramide mass. There was a 2.9-fold increase in ceramide accumulation in Taxol-treated cells ($P < 0.05$) after 24 h of incubation. LPA (0.5 μM) decreased ($P < 0.05$) the Taxol-induced increase in ceramides to 1.9-fold. LY294002 (50 μM) blocked the effect of LPA in decreasing ceramide accumulation by about 80% (Figure 9).

Interactions of LPA versus Taxol on the cell cycle

Taxol-induced apoptosis is accompanied by increased accumulation of cells in the G2/M phase of the cell cycle (McGrogan *et al*., 2008). Under our conditions, this represented an increase from about 16 to 43% ($P < 0.05$) (Figures 10a and c), which is compatible with previous studies (Spankuch *et al*., 2007; Demidenko *et al*., 2008).

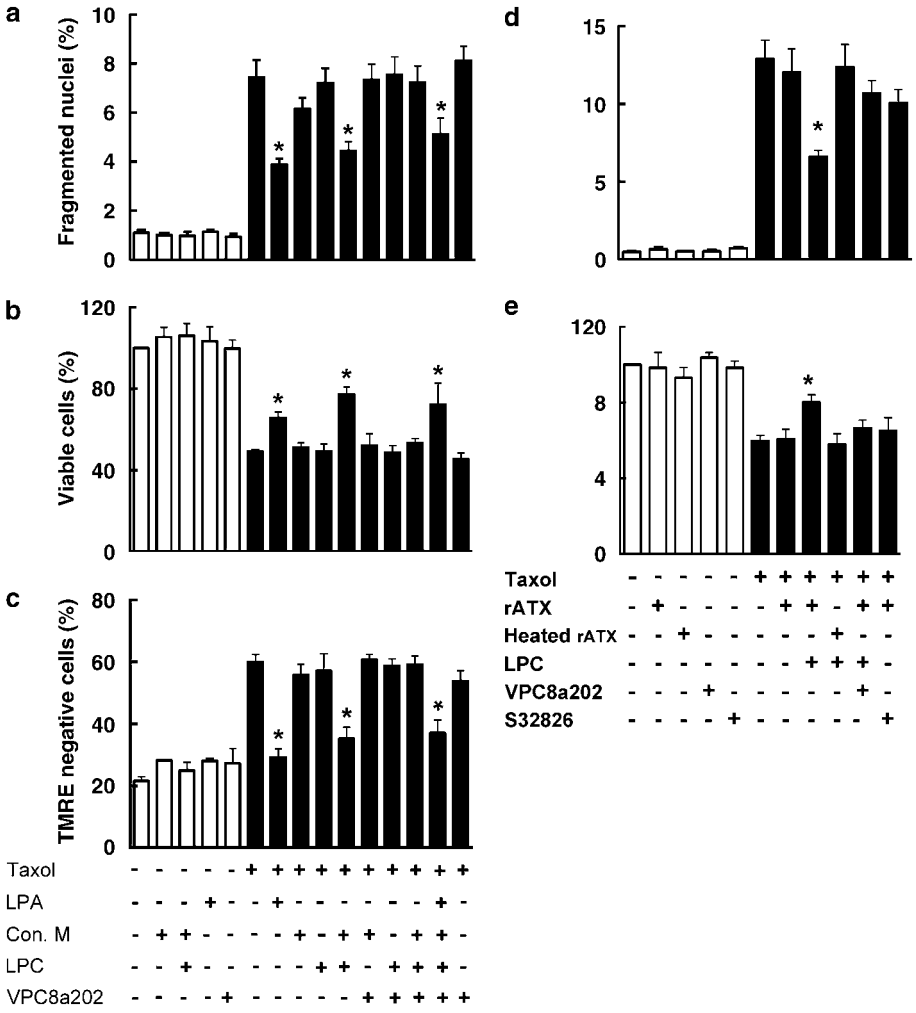

Figure 4 Autotaxin protects against Taxol-induced apoptosis in MCF-7 cells. Combinations of concentrated medium from MDA-MB-435 cells (medium/435) or recombinant autotoxin (ATX) (50 ng/ml), with lysophosphatidate (0.5 μM for 4,6-diamidino-2-phenylindole (DAPI) staining and 5 μM for tetramethlyrhodamine ethyl ester (TMRE) assay), lysophosphatidylcholine (200 μM) and the ATX inhibitors, VPC8a202 (1 μM) and S32826 (1 μM), were added with 50 nM (**a**, **b**, **d**, **e**) or 30 nM Taxol (**c**). (**a**, **b**) The percentage of fragmented nuclei and the relative number of viable cells on the dishes as determined by DAPI staining after a 24 h incubation is shown. (**c**) The percentage of TMRE-negative cells after a 48 h incubation is shown. (**d**, **e**) The percentage of fragmented nuclei and the relative number of viable cells on the dishes as determined by DAPI staining after a 24 h incubation with 50 ng/ml recombinant ATX (rATX), rATX heated for 10 min at 70 °C to inhibit ATX activity >96% and the ATX inhibitors, VPC8a202 (1 μM) and S32826 (1 μM), is shown. The results are shown as means ± s.e.m. of three experiments. $*P<0.05$.

Adding 5 μM LPA decreased the cells in G2/M to 28% and this represented reversal of the Taxol-induced effect of about 44% ($P<0.05$) (Figures 10c and d). Adding LY294002 blocked most of the LPA effect in reducing ($P<0.05$) the cells trapped in G2/M in the presence of Taxol (Figures 10d and h). As controls, we showed that 50 nM LY294002 or 5 μM LPA alone or in combination had no significant effect on the cells in G2/M phase (Figures 10b, e and f). These results demonstrated the dominant role of the PI3K pathway in LPA protection against Taxol-induced apoptosis.

Discussion

Effective chemotherapy depends on successful induction of apoptosis and defects in apoptotic signaling are a major cause of drug resistance (Melet *et al*., 2008). Chemotherapeutic resistance results in poor responses and reduced overall survival in patients with metastatic breast cancer (McGrogan *et al*., 2008).

We used doses of Taxol, LPA and LPC up to 50 nM, 20 μM and 200 μM, respectively, with MCF-7 cells. These Taxol concentrations are used for the treatment of breast cancer patients (Marchetti *et al*., 2002), and the LPA and LPC concentrations are compatible with those in the circulation and tumor microenvironment (Moolenaar *et al*., 2004; Yue *et al*., 2004). We showed that Taxol-induced killing is strongly antagonized by LPA on the basis of measurement of nuclear fragmentation, loss of mitochondrial potential and the recovery of viable cells. LPA (0.5 μM) partially blocked the Taxol-induced increase in the percentage of apoptotic nuclei, but we needed 5 μM LPA to antagonize the effect of

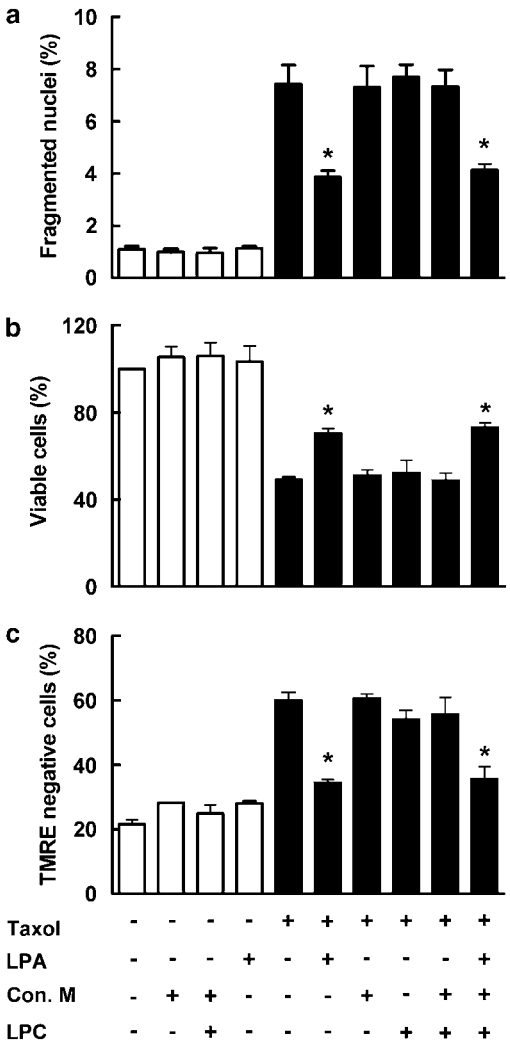

Figure 5 The effect of concentrated medium from MCF-7 cells on Taxol-induced apoptosis. Combinations of concentrated medium from MCF-7 cells (medium/MCF-7), together with lysophosphatidate (LPA) (0.5 μM), or lysophosphatidylcholine (200 μM) were added with 50 nM Taxol (**a**, **b**) or 30 nM Taxol (**c**). (**a**, **b**) The percentage of apoptotic cells and the relative number of viable cells on the dishes as determined by 4,6-diamidino-2-phenylindole staining after a 24 h incubation is shown. (**c**) The percentage of tetramethlyrhodamine ethyl ester-negative cells after a 48 h incubation where 5 μM LPA was used. The results are shown as means ± s.e.m. of three experiments. $*P<0.05$.

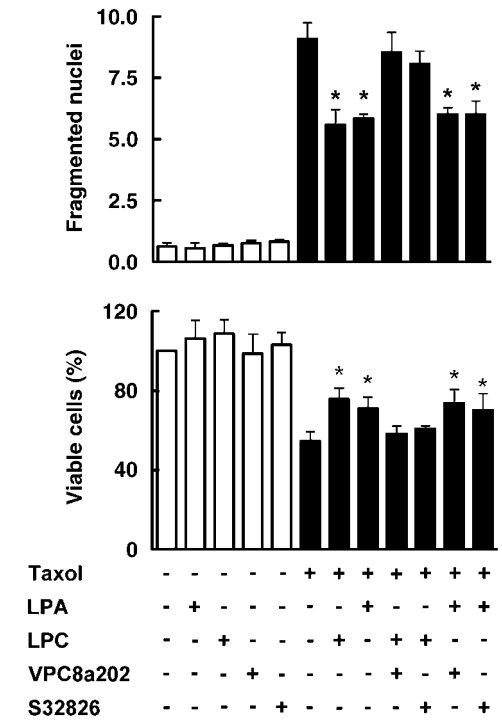

Figure 6 Autotaxin protects against Taxol-induced apoptosis in MDA-MB-435 cells. Lysophosphatidate (0.5 μM) or lysophosphatidylcholine (200 μM) and autotaxin inhibitors, VPC8a202 (1 μM) and S32826 (1 μM), were added with 50 nM Taxol. (**a**, **b**) The percentage of fragmented nuclei and the relative number of viable cells on the dishes as determined by 4,6-diamidino-2-phenylindole staining after a 24 h incubation, respectively, is shown. Results are shown as means ± s.e.m. of three experiments. $*P<0.05$.

Taxol in increasing the proportion TMRE-negative cells. The discrepancies suggest that cells that were protected at low LPA concentrations, where no differences in TMRE staining were observed, probably died by a mitochondria-independent and nonapoptotic (necrotic) mechanism. However, another major factor is that the DAPI and TMRE measurements determine only what happened to cells remaining on the dishes. We, therefore, do not have information concerning the mechanisms of cell death of more than 50% of cells that were not recovered. Consequently, it is significant that 0.5–10 μM LPA increased the number of cells that were recovered after Taxol treatment and that were then reflected in the percentage of apoptotic cells recorded in the DAPI and TMRE staining assays.

Accumulating evidence shows that LPA promotes survival of ovarian cancer cells (Frankel and Mills, 1996; Goetzl *et al*., 1999a), renal proximal tubular cells (Levine *et al*., 1997), lymphoblastoma T cells (Goetzl *et al*., 1999b), macrophages (Koh *et al*., 1998), neonatal Schwann cells (Weiner and Chun, 1999), fibroblast (Fang *et al*., 2000), mesangial cells (Inoue *et al*., 2001) and colon cancer cells (Rusovici *et al*., 2007) by preventing apoptosis. Different cell types express different LPA receptors, which have specific roles, and hence the effects of LPA signaling vary from cell to cell. In contrast to the survival role of LPA_1 in Schwann cells (Weiner and Chun, 1999; Contos *et al*., 2000), overexpression of LPA_1 in ovarian cancer cells induced apoptosis and anoikis (Furui *et al*., 1999), whereas LPA_2 appeared to mediate LPA-stimulated survival of ovarian cancer cells (Goetzl *et al*., 1999a). In T lymphoblasts, both LPA_1 and LPA_2 promoted LPA-induced survival (Goetzl *et al*., 1999a). LPA also prevents apoptosis in colon cancer cells through LPA_2 receptor (Rusovici *et al*., 2007).

LPA_2 is the predominant LPA receptor in MCF-7 cells (Chen *et al*., 2007). This is compatible with our finding that 1 μM VPC51299 (an $LPA_{1/3}$ receptor antagonist) failed to block the LPA protection against

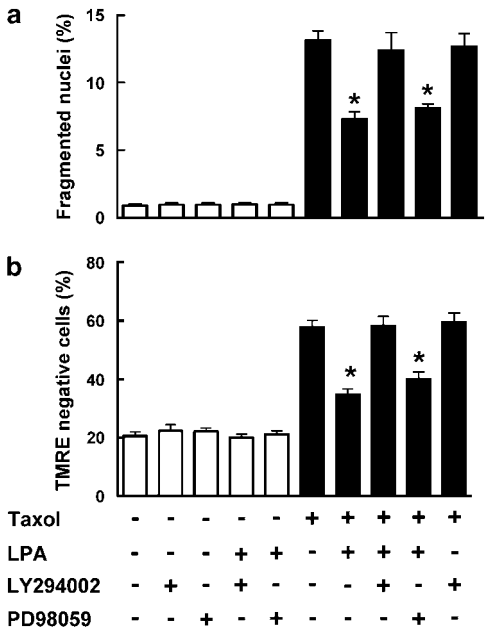

Figure 7 Phosphatidylinositol 3-kinase, but not extracellular signal-regulated kinase activation, is required for lysophosphatidate (LPA)-mediated protection against Taxol-induced apoptosis. (**a**) The effects of 50 μM LY294002 and 40 μM PD9805 on the percentage of apoptotic nuclei in MCF-7 cells treated for 24 h in the presence or absence of 50 nM Taxol and 0.5 μM LPA are shown. (**b**) The effects of 50 μM LY294002 and 40 μM PD9805 on percentage of tetramethlyrhodamine ethyl ester-negative cells after treatment in the presence or absence of 30 nM of Taxol with 5 μM LPA are shown. Results are shown as means ± s.e.m. of three experiments. $*P<0.05$.

Taxol-induced apoptosis in MCF-7 cells (results not shown). Unfortunately, no effective specific agonist for LPA_2 receptors has been developed.

Activation of PI3K-Akt protects primary lymphocytic leukemia cells, ovarian cancer cells and intestinal epithelial cells from apoptosis, whereas G_i-mediated activation of ERK is necessary for the survival of fibroblasts (Fang *et al*., 2000; Gauthier *et al*., 2001; Baudhuin *et al*., 2002; Dufour *et al*., 2004; Harnois *et al*., 2004; Hu *et al*., 2005). In this study, inhibition of PI3K blocked the protective effect of LPA on Taxol-induced apoptosis, whereas blocking ERK activation with PD98059 was without any effect.

Lysophosphatidylcholine is present in plasma and serum at >100 μM in a predominantly albumin-bound form (Croset *et al*., 2000) and it is also detected in media from tumor cells (Umezu-Goto *et al*., 2002). However, in our work, LPC alone did not antagonize Taxol-induced apoptosis unless concentrated medium from MDA-MB-435 cells or recombinant ATX was added. This protective effect was blocked by VPC8a202 and S32826, two ATX inhibitors (Cui *et al*., 2007; Ferry *et al*., 2008), or by heat inactivation of ATX activity. The MDA-MB-435 medium, compared with that produced by MCF-7 cells, contained abundant ATX. Our work establishes that LPC is inactive in protecting against Taxol-induced apoptosis unless it is converted to LPA by ATX. We also showed in our unpublished work that LPC only stimulates the migration of MDA-MB-231 breast cancer cells in the presence of active ATX. These conclusions are compatible with the view that the putative LPC receptors, G2A and GPR4, are proton-sensing receptors whose activity is negatively regulated by LPC (Tomura *et al*., 2005). Many reported biological effects of LPC are probably mediated through ATX and LPA production.

In vivo, ATX might also hydrolyze sphingosylphosphorylcholine to sphingosine 1-phosphate (Clair *et al*., 2003). LPA and sphingosine 1-phosphate show overlapping biological activities on cell survival by acting on distinct receptor families. However, the physiological significance of ATX in producing sphingosine 1-phosphate is not established.

Binding of Taxol to microtubules aberrantly engages the mitotic checkpoint, effecting sustained mitotic arrest (McGrogan *et al*., 2008). Ceramide levels regulate sustained mitotic arrest, apoptosis and mitotic slippage (Asakuma, 2003), and elevated ceramide concentrations are a known component of Taxol-mediated cell death (Charles *et al*., 2001; Sietsma *et al*., 2002; Swanton *et al*., 2007). Sustained ceramide elevation in the endoplasmic reticulum coordinately activates the stress responses and inactivates anti-apoptotic Akt, thus leading to apoptosis (Swanton *et al*., 2007). We showed that LPA attenuated the Taxol-induced increase in ceramides and subsequent apoptosis through PI3K/Akt activation.

In conclusion, our work demonstrates that the abundant extracellular lipid, LPC, protects MCF-7 breast cancer cells and MDA-MD-435 melanoma cells against Taxol-induced apoptosis, but only after its conversion to LPA by ATX. LPA itself showed strong antagonism against the apoptotic effects of Taxol. This work identifies that inhibition of ATX activity could improve the treatment of cancers by Taxol and possibly other chemotherapeutic agents in patients who express high ATX activity. It is, therefore, hoped that biologically stable ATX inhibitors will be developed to test this hypothesis *in vivo*.

Materials and methods

Materials

RPMI1640 medium, penicillin and streptomycin were obtained from GIBCO (Carlsbad, CA, USA). Trypsin-ethylenediaminetetraacetic acid, TMRE, goat anti-mouse IgG, ATX primers and superscript II reverse transcriptase were obtained from Invitrogen (Carlsbad, CA, USA). DAG kinase, PD98059 and dithiothreitol were obtained from EMD Chemicals Inc. (Gibbstown, NJ, USA). Fatty acid-free bovine serum albumin, paclitaxel (Taxol), activated charcoal (Norit), Hoechst33258, ATP, diethylenetriaminepentaacetic acid (DETAPEC), pertussis toxin, oleoyl-L-α-lysophosphatidic acid, sodium salt (LPA), oleoyl-L-α-LPC, ceramide and monoclonal anti-GAPDH were purchased from Sigma-Aldrich (Oakville, ON, Canada). VPC51299 and VPC8a202 were provided by Drs KR Lynch and TL Macdonald (University of Virginia, Charlottesville, VA, USA). LY294002 was obtained from Biomol Int. (Plymouth Meeting, PA, USA). S32826 was provided by Dr JA Boutin (Institut de Recherches Servier). [^{32}P]LPA was

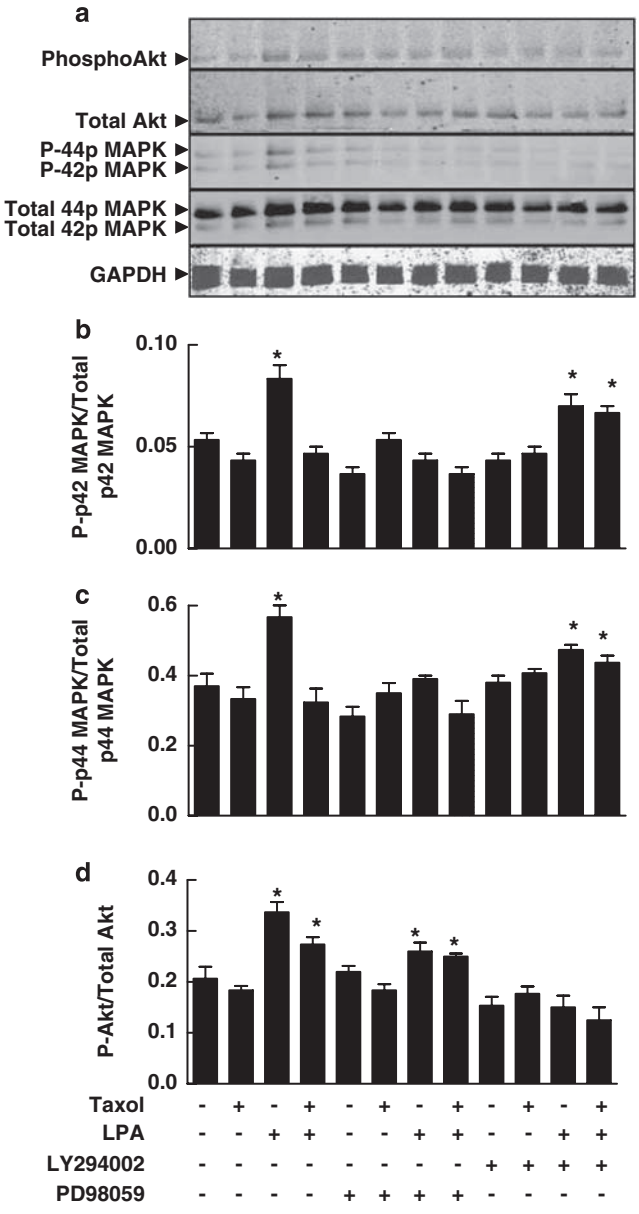

Figure 8 The effects of lysophosphatidate (LPA) on phosphatidylinositol 3-kinase (PI3K)/AKT and mitogen-activated protein kinase (MAPK) pathways. MCF-7 cells were incubated for 12 h with Taxol (30 nM) and LPA (5 μM) in the presence of 50 μM LY294002 (PI3K inhibitor) and 40 μM PD98059 (MAPK/extracellular signal-regulated kinase kinase inhibitor). Results in (**a**) show the western blot analyses for phospho- and total Akt, phospho- and total ERK (p42 and p44 MAPK) and glyceraldehyde phosphate dehydrogenase (GAPDH), which was used as a loading control. The results are representative of three independent experiments and they were quantified by densitometric analysis using a Licor Imaging System. (**b**) The densitometric ratio of phospho-p42MAPK/total p42MAPK is shown; (**c**) phospho-p44MAPK/total p44MAPK ratio is shown and in (**d**), phospho-Akt/total Akt is shown. The results are shown as means ± s.e.m. of three independent experiments. *Indicates the difference ($P<0.05$) from the nontreated cells.

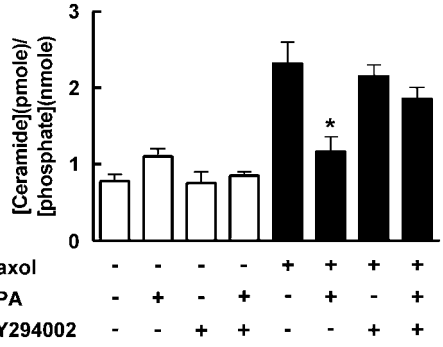

Figure 9 The role of Taxol and lysophosphatidate (LPA) in controlling ceramide concentrations. Ceramide mass was determined in MCF-7 cells after treating with 50 nM Taxol in the presence or absence of 0.5 μM of LPA or 50 μM LY294002 for 24 h. The mass of ceramide (pmol) was normalized to the concentration of phospholipid phosphate (nM) in each individual lipid extract. The results are expressed as means ± s.e.m. of eight individual dishes for each treatment. *$P<0.05$.

synthesized as before (Jasinska *et al*., 1999). Rabbit polyclonal antibody against ATX and recombinant ATX were gifts from Dr T Clair, through the Intramural Research Program of NIH, National Cancer Institute, Center for Cancer Research (Bethesda, MD, USA). Goat anti-rabbit IgG was obtained from Rockland (Gilbertsville, PA, USA). Polyclonal anti-Akt, phospho-Akt (S473) and monoclonal phospho-p44/42 MAP kinase were obtained from Cell Signaling Technology (Danvers, MA, USA). Polyclonal anti-MAP kinase (sc-93) was from Santa Cruz Biotechnology (Santa Cruz, CA, USA). FS-3 compound for the ATX assay was from Echelon Company (San Jose, CA, USA). FBS was from Medicorp Inc. (Montréal, PQ, Canada). RNAqueous kit, DNA-free kit and Syber Green buffer mix were obtained from Ambion (Austin, TX, USA).

Cell culture

The MCF-7 and MDA-MB-435 cells were obtained from the American Type Culture Collection. Cells were maintained in RPMI1640 medium with 10% FBS and 1% penicillin/streptomycin in a humidified atmosphere with 5% CO_2 at 37 °C.

Quantification of apoptotic nuclei using DAPI stain

MCF-7 cells (2×10^4 cells/well) were grown in 96-well plates. Cells (about 70% confluent) were washed with phosphate-buffered saline and treated in serum-free media for 24 h. Cells were then fixed in 4% paraformaldehyde for 20 min and permeabilized in 0.1% Triton X-100 for 15 min. Fixed cells were stained with 1 μg/ml Hoechst33258 for 15 min after evaporation of the fixing solution. Nuclear morphology of the cells was observed by fluorescence microscopy. Triplicate samples were prepared for each treatment and at least 300 cells were counted in random fields for each sample and apoptotic nuclei were identified (Sakashita *et al*., 2007).

Measurement of LPA breakdown

Six-well plates were seeded with 2×10^5 cells and these were grown to 70% confluence. The half-life of LPA was determined after adding 2 ml of medium containing ^{32}P-labeled LPA (100,000 d.p.m.) with 1 or 20 μM nonradioactive LPA and measuring $^{32}P_i$- and ^{32}P-labeled LPA during 24 h (Pilquil *et al*., 2006). The half-life of LPA was about 10 h and this was independent of the LPA concentration (results not shown).

Mitochondrial membrane potential (TMRE) assay

Breakdown of the mitochondrial membrane potential ($\Delta\Psi m$) was determined using TMRE staining. MCF-7 cells (2×10^5)

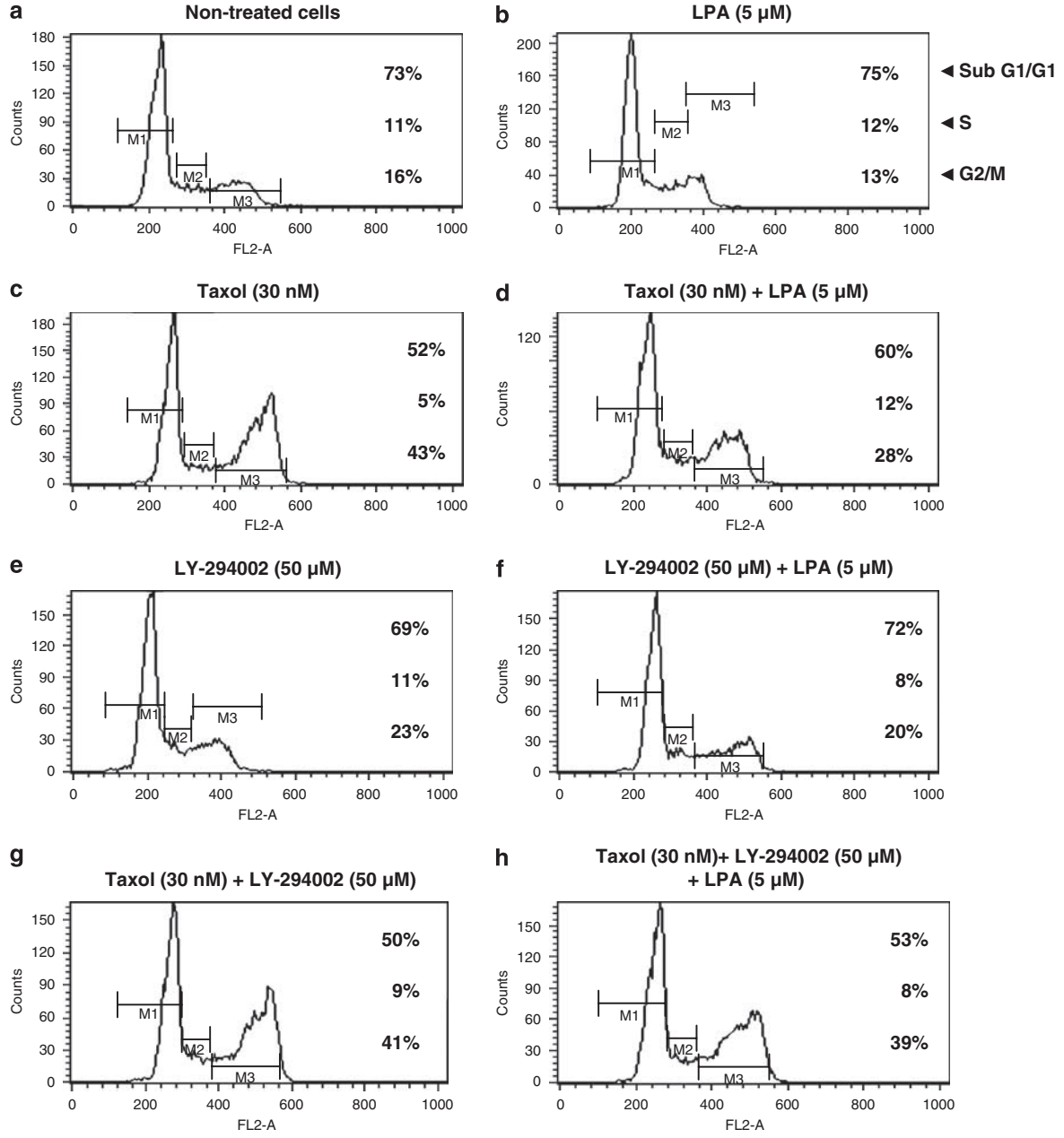

Figure 10 Effects of lysophosphatidate (LPA) and Taxol on cell cycle progression of MCF-7 breast cancer cells. MCF-7 cells were incubated for 48 h with 30 nM Taxol and 5 μM LPA. Then the cells were collected and stained with propidium iodide (PI) before analysis by fluorescence-activated cell sorting. DNA histograms were measured using CellQuest software and the percentage of G0/G1, S and G2/M cells were calculated. Results are representative of two independent experiments. The action of LPA in partially reversing the Taxol-induced G2/M arrest was also confirmed in a single experiment with a 24 h incubation.

were grown to confluence in six-well plates over 48 h in RPMI1640 medium with 10% FBS. The medium was changed to RPMI1640 medium with 10% of charcoal-treated FBS. This removed >95% of the LPA as assessed after adding ^{32}P-labeled LPA to the FBS (results not shown). Cells were incubated for an additional 48 h with LPA-depleted FBS with Taxol, or LPA as indicated. LPA concentrations were maintained by adding half of the original concentration of LPA every 10 h on the basis of the calculated half-life of LPA. Cells were then tripsinized, collected in 96 V-bottomed plate and exposed to TMRE (500 nM) for 30 min at 37 °C. Excess dye was removed with phosphate-buffered saline containing 0.1% fatty acid-free BSA and cell-associated fluorescence was measured with a Calibur Flow Cytometer (Becton Dickinson, San José, CA, USA) using Cell Quest software (Ramjaun *et al*., 2007).

ATX expression

mRNA expression Total RNA was extracted using the RNAqueous kit, according the manufacture's instruction. DNA-free kit was also applied to remove contaminating DNA from RNA preparation. Total RNA was treated with

superscript II reverse transcriptase. Real-time RT-PCR was performed with 25 µl of master mix containing 2 × Syber Green buffer mix and forward and reverse primers (Invitrogen). The internal control was the constitutively expressed housekeeping human glyceraldehyde 3-phosphate dehydrogenase (GAPDH). Primers for human ATX were as follows: sense, 5′-ACAACGAGGAGAGCTGCAAT-3′; antisense, 5′-AGAAGTCCAGGCTGGTGAGA-3; and for human GAPDH were as follows: sense, 5′-ACAGTCAGCCGCATC TTCTT-3′; antisense, 5′-GACAAGCTTCCCGTTCTCAG-3′. Samples were assayed in triplicate on the 7500 Real Time PCR System (Applied Biosystems).

Western blot analysis Serum-free medium from MD-MB-435 cells was concentrated to 200 µl per 10^6 cells by centrifugation using a Centricon Millipore's Ultracel YM cellulose membrane (Millipore Corporation, Bedford, TX, USA) and analysed using 10% SDS–polyacrylamide gel electrophoresis. Nitrocellulose membranes were treated with Odyssey blocking buffer for 24 h and incubated with 1:5000 dilution of ATX antibody for 60 min followed by four washes with phosphate-buffered saline + 0.1% Tween-20. Blots were incubated in 1:10 000 dilution of goat anti-rabbit IgG for 45 min. After washing four times, ATX was visualized at 800 nm with the Odyssey Infrared Scanner.

ATX activity assay ATX activity was assayed in 96-well plates using 1 µM FS-3 as a substrate. Fluorescence was read at 15 min intervals by a Synergy2 system (BioTek, Winooski, VT, USA) with excitation and emission wavelengths of 485 and 538 nm, respectively.

Ceramide mass assay
Cells (1×10^6) were plated in 10 cm culture dishes and grown to confluence in RPMI1640 medium with 10% FBS. After 48 h, the medium was changed to RPMI1640 medium with 10% of charcoal-treated FBS, and cells were incubated for 48 h with the indicated concentrations of Taxol, LPA and LY294002. After washing with phosphate-buffered saline, cell lysates were collected in methanol and the lipids were extracted (Martin *et al*., 1997). Ceramide concentrations were measured by conversion to ceramide 1-phosphate, using the diacylglycerol kinase and [γ-^{32}P]ATP and by comparison to standards of ceramide. Results were normalized to the phospholipid concentration of the extract (Martin *et al*., 1997).

Statistical analysis and determination of the interaction of Taxol with LPA on apoptosis
The interaction was evaluated by the isobologram technique (CalcuSyn software, Biosoft, Cambridge, UK). The experimental iso-effect points were the concentrations (relative to IC_{50} concentrations) of the two agents that when combined kill 50% of the cells. A quantitative index of these interactions was provided by the isobologram equation combination index $= (a/A) + (b/B)$, where A and B represent the Taxol and LPA concentrations that alone produce a fixed level of inhibition (IC_{50}), a and b represent the concentrations required for the same effect when they were combined. CI values of <1 indicate synergy; 1 represents addition and >1 indicate antagonism.

Statistical analysis was performed by analysis of variance with a Kruskal–Wallis *post hoc* test.

Abbreviations

ATX, autotaxin; DAPI, 4,6-diamidino-2-phenylindole; FBS, fetal bovine serum; LPA, lysophosphatidate; LPC, lysophosphatidylcholine; MAPK, mitogen-activated protein kinase; PI3K, phosphatidylinositol 3-kinase; TMRE, tetramethlyrhodamine ethyl ester.

Acknowledgements

We thank Mr M Czernick and Mr J Dewald for excellent technical support in the fluorescence-activated cell sorting analysis and preparing labeled LPA, respectively. We thank Dr M Sawyer for help with the isobologram analysis, Dr E Posse de Chaves for advice on DAPI staining and Drs F Bamforth and GS Cembrowski for their support. We thank Dr T Clair for providing recombinant ATX and the ATX antibody. Drs KR Lynch and TL Macdonald donated the VPC8a202 and VPC51299 and Dr JA Boutin gave us S32826. DNB is a Medical Scientist of the Alberta Heritage Foundation for Medical Research. ISG is a recipient of a Recruitment Award from the Alberta Cancer Board/Alberta Cancer Foundation. NS is a recipient of scholarships from Iranian Ministry of Health and the Bell McLeod Educational Fund, University of Alberta. The work was supported by the Canadian Institutes of Health Research (MOP 81137).

References

Aoki J, Taira A, Takanezawa Y, Kishi Y, Hama K, Kishimoto T *et al*. (2002). Serum lysophosphatidic acid is produced through diverse phospholipase pathways. *J Biol Chem* **277**: 48737–48744.

Asakuma J, Sumitomo M, Asano T, Asano T, Hayakawa M (2003). Selective Akt inactivation and tumor necrosis actor-related apoptosis-inducing ligand sensitization of renal cancer cells by low concentrations of paclitaxel. *Cancer Res* **63**: 1365–1370.

Baudhuin LM, Cristina KL, Lu J, Xu Y. (2002). Akt activation induced by lysophosphatidic acid and sphingosine-1-phosphate requires both mitogen-activated protein kinase kinase and p38 mitogen-activated protein kinase and is cell-line specific. *Mol Pharmacol* **62**: 660–671.

Bergstralh DT, Ting JP. (2006). Microtubule stabilizing agents: their molecular signaling consequences and the potential for enhancement by drug combination. *Cancer Treat Rev* **32**: 166–179.

Brindley DN. (1993). Hepatic secretion of lysphosphatidylcholine: a novel transport system for polyunsaturated fatty acids and choline. *J Nutr Biochem* **4**: 442–449.

Brindley DN. (2004). Lipid phosphate phosphatases and related proteins: signaling functions in development, cell division, and cancer. *J Cell Biochem* **92**: 900–912.

Chappell J, Leitner JW, Solomon S, Golovchenko I, Goalstone ML, Draznin B. (2001). Effect of insulin on cell cycle progression in MCF-7 breast cancer cells. Direct and potentiating influence. *J Biol Chem* **276**: 38023–38028.

Charles AG, Han TY, Liu YY, Hansen N, Giuliano AE, Cabot MC. (2001). Taxol-induced ceramide generation and apoptosis in human breast cancer cells. *Cancer Chemother Pharmacol* **47**: 444–450.

Chen M, Towers LN, O'Connor KL. (2007). LPA2 (EDG4) mediates Rho-dependent chemotaxis with lower efficacy than LPA1 (EDG2) in breast carcinoma cells. *Am J Physiol Cell Physiol* **292**: C1927–C1933.

Clair T, Aoki J, Koh E, Bandle RW, Nam SW, Ptaszynska MM *et al*. (2003). Autotaxin hydrolyzes sphingosylphosphorylcholine to produce the regulator of migration, sphingosine-1-phosphate. *Cancer Res* **63**: 5446–5453.

Contos JJ, Fukushima N, Weiner JA, Kaushal D, Chun J. (2000). Requirement for the lpA1 lysophosphatidic acid receptor gene in normal suckling behavior. *Proc Natl Acad Sci USA* **97**: 13384–13389.

Croset M, Brossard N, Polette A, Lagarde M. (2000). Characterization of plasma unsaturated lysophosphatidylcholines in human and rat. *Biochem J* **345**(Part 1): 61–67.

Cui P, Tomsig JL, McCalmont WF, Lee S, Becker CJ, Lynch KR *et al*. (2007). Synthesis and biological evaluation of phosphonate derivatives as autotaxin (ATX) inhibitors. *Bioorg Med Chem Lett* **17**: 1634–1640.

Demidenko ZN, Kalurupalle S, Hanko C, Lim CU, Broude E, Blagosklonny MV. (2008). Mechanism of G1-like arrest by low concentrations of paclitaxel: next cell cycle p53-dependent arrest with sub G1 DNA content mediated by prolonged mitosis. *Oncogene* **27**: 4402–4410.

Dennis J, Nogaroli L, Fuss B. (2005). Phosphodiesterase-Ialpha/autotaxin (PD-Ialpha/ATX): a multifunctional protein involved in central nervous system development and disease. *J Neurosci Res* **82**: 737–742.

Dufour G, Demers MJ, Gagne D, Dydensborg AB, Teller IC, Bouchard V *et al*. (2004). Human intestinal epithelial cell survival and anoikis. Differentiation state-distinct regulation and roles of protein kinase B/Akt isoforms. *J Biol Chem* **279**: 44113–44122.

Fang X, Schummer M, Mao M, Yu S, Tabassam FH, Swaby R *et al*. (2002). Lysophosphatidic acid is a bioactive mediator in ovarian cancer. *Biochim Biophys Acta* **1582**: 257–264.

Fang X, Yu S, LaPushin R, Lu Y, Furui T, Penn LZ *et al*. (2000). Lysophosphatidic acid prevents apoptosis in fibroblasts via G(i)-protein-mediated activation of mitogen-activated protein kinase. *Biochem J* **352**(Part 1): 135–143.

Ferry G, Moulharat N, Pradere JP, Desos P, Try A, Genton A *et al*. (2008). S32826: a nanomolar inhibitor of autotaxin. Discovery, synthesis and applications as a pharmacological tool. *J Pharmacol Exp Ther* **327**: 809–819.

Fox MA, Alexander JK, Afshari FS, Colello RJ, Fuss B. (2004). Phosphodiesterase-I alpha/autotaxin controls cytoskeletal organization and FAK phosphorylation during myelination. *Mol Cell Neurosci* **27**: 140–150.

Frankel A, Mills GB. (1996). Peptide and lipid growth factors decrease *cis*-diamminedichloroplatinum-induced cell death in human ovarian cancer cells. *Clin Cancer Res* **2**: 1307–1313.

Furui T, LaPushin R, Mao M, Khan H, Watt SR, Watt MA *et al*. (1999). Overexpression of edg-2/vzg-1 induces apoptosis and anoikis in ovarian cancer cells in a lysophosphatidic acid- independent manner. *Clin Cancer Res* **5**: 4308–4318.

Gauthier R, Harnois C, Drolet JF, Reed JC, Vezina A, Vachon PH. (2001). Human intestinal epithelial cell survival: differentiation state-specific control mechanisms. *Am J Physiol Cell Physiol* **280**: C1540–C1554.

Goetzl EJ, Dolezalova H, Kong Y, Hu YL, Jaffe RB, Kalli KR *et al*. (1999a). Distinctive expression and functions of the type 4 endothelial differentiation gene-encoded G protein-coupled receptor for lysophosphatidic acid in ovarian cancer. *Cancer Res* **59**: 5370–5375.

Goetzl EJ, Kong Y, Mei B. (1999b). Lysophosphatidic acid and sphingosine 1-phosphate protection of T cells from apoptosis in association with suppression of Bax. *J Immunol* **162**: 2049–2056.

Hama K, Aoki J, Fukaya M, Kishi Y, Sakai T, Suzuki R *et al*. (2004). Lysophosphatidic acid and autotaxin stimulate cell motility of neoplastic and non-neoplastic cells through LPA1. *J Biol Chem* **279**: 17634–17639.

Harnois C, Demers MJ, Bouchard V, Vallee K, Gagne D, Fujita N *et al*. (2004). Human intestinal epithelial crypt cell survival and death: complex modulations of Bcl-2 homologs by Fak, PI3-K/Akt-1, MEK/Erk, and p38 signaling pathways. *J Cell Physiol* **198**: 209–222.

Hu X, Haney N, Kropp D, Kabore AF, Johnston JB, Gibson SB. (2005). Lysophosphatidic acid (LPA) protects primary chronic lymphocytic leukemia cells from apoptosis through LPA receptor activation of the anti-apoptotic protein AKT/PKB. *J Biol Chem* **280**: 9498–9508.

Inoue CN, Nagano I, Ichinohasama R, Asato N, Kondo Y, Iinuma K. (2001). Bimodal effects of platelet-derived growth factor on rat mesangial cell proliferation and death, and the role of lysophosphatidic acid in cell survival. *Clin Sci (Lond)* **101**: 11–19.

Jasinska R, Zhang QX, Pilquil C, Singh I, Xu J, Dewald J *et al*. (1999). Lipid phosphate phosphohydrolase-1 degrades exogenous glycerolipid and sphingolipid phosphate esters. *Biochem J* **340**(Part 3): 677–686.

Jemal A, Siegel R, Ward E, Murray T, Xu J, Smigal C *et al*. (2006). Cancer statistics, 2006. *CA Cancer J Clin* **56**: 106–130.

Kabarowski JH, Zhu K, Le LQ, Witte ON, Xu Y. (2001). Lysophosphatidylcholine as a ligand for the immunoregulatory receptor G2A. *Science* **293**: 702–705.

Kim KS, Ren J, Jiang Y, Ebrahem Q, Tipps R, Cristina K *et al*. (2005). GPR4 plays a critical role in endothelial cell function and mediates the effects of sphingosylphosphorylcholine. *FASEB J* **19**: 819–821.

Koh JS, Lieberthal W, Heydrick S, Levine JS. (1998). Lysophosphatidic acid is a major serum noncytokine survival factor for murine macrophages which acts via the phosphatidylinositol 3-kinase signaling pathway. *J Clin Invest* **102**: 716–727.

Krajewski S, Krajewska M, Turner BC, Pratt C, Howard B, Zapata JM *et al*. (1999). Prognostic significance of apoptosis regulators in breast cancer. *Endocr Relat Cancer* **6**: 29–40.

Lee CW, Rivera R, Gardell S, Dubin AE, Chun J. (2006). GPR92 as a new G12/13- and Gq-coupled lysophosphatidic acid receptor that increases cAMP, LPA5. *J Biol Chem* **281**: 23589–23597.

Levine JS, Koh JS, Triaca V, Lieberthal W. (1997). Lysophosphatidic acid: a novel growth and survival factor for renal proximal tubular cells. *Am J Physiol* **273**: F575–F585.

Lin P, Ye RD. (2003). The lysophospholipid receptor G2A activates a specific combination of G proteins and promotes apoptosis. *J Biol Chem* **278**: 14379–14386.

Marchetti P, Urien S, Cappellini GA, Ronzino G, Ficorella C. (2002). Weekly administration of paclitaxel: theoretical and clinical basis. *Crit Rev Oncol Hematol* **44**(Suppl): S3–S13.

Martin A, Duffy PA, Liossis C, Gomez-Munoz A, O'Brien L, Stone JC *et al*. (1997). Increased concentrations of phosphatidate, diacylglycerol and ceramide in ras- and tyrosine kinase (fps)-transformed fibroblasts. *Oncogene* **14**: 1571–1580.

McGrogan BT, Gilmartin B, Carney DN, McCann A. (2008). Taxanes, microtubules and chemoresistant breast cancer. *Biochim Biophys Acta* **1785**: 96–132.

Melet A, Song K, Bucur O, Jagani Z, Grassian AR, Khosravi-Far R. (2008). Apoptotic pathways in tumor progression and therapy. *Adv Exp Med Biol* **615**: 47–79.

Mills GB, Moolenaar WH. (2003). The emerging role of lysophosphatidic acid in cancer. *Nat Rev Cancer* **3**: 582–591.

Moolenaar WH, van Meeteren LA, Giepmans BN. (2004). The ins and outs of lysophosphatidic acid signaling. *Bioessays* **26**: 870–881.

Murph MM, Hurst-Kennedy J, Newton V, Brindley DN, Radhakrishna H. (2007). Lysophosphatidic acid decreases the nuclear localization and cellular abundance of the p53 tumor suppressor in A549 lung carcinoma cells. *Mol Cancer Res* **5**: 1201–1211.

Nam SW, Clair T, Campo CK, Lee HY, Liotta LA, Stracke ML. (2000). Autotaxin (ATX), a potent tumor motogen, augments invasive and metastatic potential of ras-transformed cells. *Oncogene* **19**: 241–247.

Nam SW, Clair T, Kim YS, McMarlin A, Schiffmann E, Liotta LA *et al*. (2001). Autotaxin (NPP-2), a metastasis-enhancing motogen, is an angiogenic factor. *Cancer Res* **61**: 6938–6944.

Pasternack SM, von Kugelgen I, Aboud KA, Lee YA, Ruschendorf F, Voss K *et al*. (2008). G protein-coupled receptor P2Y5 and its ligand LPA are involved in maintenance of human hair growth. *Nat Genet* **40**: 329–334.

Pilquil C, Dewald J, Cherney A, Gorshkova I, Tigyi G, English D *et al*. (2006). Lipid phosphate phosphatase-1 regulates lysophosphatidate-induced fibroblast migration by controlling phospholipase D2-dependent phosphatidate generation. *J Biol Chem* **281**: 38418–38429.

Radeff-Huang J, Seasholtz TM, Matteo RG, Brown JH. (2004). G protein mediated signaling pathways in lysophospholipid induced cell proliferation and survival. *J Cell Biochem* **92**: 949–966.

Radu CG, Yang LV, Riedinger M, Au M, Witte ON. (2004). T cell chemotaxis to lysophosphatidylcholine through the G2A receptor. *Proc Natl Acad Sci USA* **101**: 245–250.

Ramjaun AR, Tomlinson S, Eddaoudi A, Downward J. (2007). Upregulation of two BH3-only proteins, Bmf and Bim, during TGF beta-induced apoptosis. *Oncogene* **26**: 970–981.

Rikitake Y, Hirata K, Yamashita T, Iwai K, Kobayashi S, Itoh H *et al*. (2002). Expression of G2A, a receptor for lysophosphatidylcholine, by macrophages in murine, rabbit, and human atherosclerotic plaques. *Arterioscler Thromb Vasc Biol* **22**: 2049–2053.

Rusovici R, Ghaleb A, Shim H, Yang VW, Yun CC. (2007). Lysophosphatidic acid prevents apoptosis of Caco-2 colon cancer cells via activation of mitogen-activated protein kinase and phosphorylation of Bad. *Biochim Biophys Acta* **1770**: 1194–1203.

Sakashita F, Osada S, Takemura M, Imai H, Tomita H, Nonaka K *et al*. (2007). The effect of p53 gene expression on the inhibition of cell proliferation by paclitaxel. *Cancer Chemother Pharmacol* **62**: 379–385.

Saunders DE, Lawrence WD, Christensen C, Wappler NL, Ruan H, Deppe G. (1997). Paclitaxel-induced apoptosis in MCF-7 breast-cancer cells. *Int J Cancer* **70**: 214–220.

Sietsma H, Dijkhuis AJ, Kamps W, Kok JW. (2002). Sphingolipids in neuroblastoma: their role in drug resistance mechanisms. *Neurochem Res* **27**: 665–674.

Snyder JP, Nettles JH, Cornett B, Downing KH, Nogales E. (2001). The binding conformation of Taxol in beta-tubulin: a model based on electron crystallographic density. *Proc Natl Acad Sci USA* **98**: 5312–5316.

So J, Wang FQ, Navari J, Schreher J, Fishman DA. (2005). LPA-induced epithelial ovarian cancer (EOC) in vitro invasion and migration are mediated by VEGF receptor-2 (VEGF- R2). *Gynecol Oncol* **97**: 870–878.

Spankuch B, Kurunci-Csacsko E, Kaufmann M, Strebhardt K. (2007). Rational combinations of siRNAs targeting Plk1 with breast cancer drugs. *Oncogene* **26**: 5793–5807.

Stracke ML, Krutzsch HC, Unsworth EJ, Arestad A, Cioce V, Schiffmann E *et al*. (1992). Identification, purification, and partial sequence analysis of autotaxin, a novel motility-stimulating protein. *J Biol Chem* **267**: 2524–2529.

Sun B, Nishihira J, Suzuki M, Fukushima N, Ishibashi T, Kondo M *et al*. (2003). Induction of macrophage migration inhibitory factor by lysophosphatidic acid: relevance to tumor growth and angiogenesis. *Int J Mol Med* **12**: 633–641.

Swanton C, Marani M, Pardo O, Warne PH, Kelly G, Sahai E *et al*. (2007). Regulators of mitotic arrest and ceramide metabolism are determinants of sensitivity to paclitaxel and other chemotherapeutic drugs. *Cancer Cell* **11**: 498–512.

Tigyi G, Parrill AL. (2003). Molecular mechanisms of lysophosphatidic acid action. *Prog Lipid Res* **42**: 498–526.

Tomura H, Mogi C, Sato K, Okajima F. (2005). Proton-sensing and lysolipid-sensitive G- protein-coupled receptors: a novel type of multi-functional receptors. *Cell Signal* **17**: 1466–1476.

Umezu-Goto M, Kishi Y, Taira A, Hama K, Dohmae N, Takio K *et al*. (2002). Autotaxin has lysophospholipase D activity leading to tumor cell growth and motility by lysophosphatidic acid production. *J Cell Biol* **158**: 227–233.

Weiner JA, Chun J. (1999). Schwann cell survival mediated by the signaling phospholipid lysophosphatidic acid. *Proc Natl Acad Sci USA* **96**: 5233–5238.

Xu Y, Shen Z, Wiper DW, Wu M, Morton RE, Elson P *et al*. (1998). Lysophosphatidic acid as a potential biomarker for ovarian and other gynecologic cancers. *Jama* **280**: 719–723.

Yang SY, Lee J, Park CG, Kim S, Hong S, Chung HC *et al*. (2002). Expression of autotaxin (NPP-2) is closely linked to invasiveness of breast cancer cells. *Clin Exp Metastasis* **19**: 603–608.

Ye X, Ishii I, Kingsbury MA, Chun J. (2002). Lysophosphatidic acid as a novel cell survival/apoptotic factor. *Biochim Biophys Acta* **1585**: 108–113.

Yue J, Yokoyama K, Balazs L, Baker DL, Smalley D, Pilquil C *et al*. (2004). Mice with transgenic overexpression of lipid phosphate phosphatase-1 display multiple organotypic deficits without alteration in circulating lysophosphatidate level. *Cell Signal* **16**: 385–399.

Zhu K, Baudhuin LM, Hong G, Williams FS, Cristina KL, Kabarowski JH *et al*. (2001). Sphingosylphosphorylcholine and lysophosphatidylcholine are ligands for the G protein- coupled receptor GPR4. *J Biol Chem* **276**: 41325–41335.

MOLECULAR CARCINOGENESIS 48:801–809 (2009)

Inhibition of Autotaxin Production or Activity Blocks Lysophosphatidylcholine-Induced Migration of Human Breast Cancer and Melanoma Cells

Cristoforo G. Gaetano,[1] Nasser Samadi,[2] Jose L. Tomsig,[3] Timothy L. Macdonald,[4] Kevin R. Lynch,[3] and David N. Brindley[1]*

[1]*Department of Biochemistry, Signal Transduction Research Group, University of Alberta, Edmonton, Alberta, Canada*
[2]*Laboratory Medicine and Pathology, Signal Transduction Research Group, University of Alberta, Edmonton, Alberta, Canada*
[3]*Department of Pharmacology, University of Virginia, Charlottesville, Virginia*
[4]*Department of Chemistry, University of Virginia, Charlottesville, Virginia*

Increased expression of autotaxin in tumors including glioblastoma, breast, renal, ovarian, lung, and thyroid cancers is associated with increased tumor aggressiveness. Autotaxin promotes metastasis as well as cell growth, survival, and migration of cancer cells. These actions could depend on the noncatalytic effects of autotaxin on cell adhesion, or the catalytic activity of autotaxin, which converts lysophosphatidylcholine into lysophosphatidate in the extracellular fluid surrounding the tumor. Both lysophosphatidylcholine (LPC) and lysophosphatidate have been reported to stimulate migration through their respective G-protein coupled receptors. The present study determines the roles of autotaxin, LPC, and lysophosphatidate in controlling the migration of two cancer cell lines: MDA-MB-231 breast cancer cells, which produce little autotaxin and MDA-MB-435 melanoma cells that secrete significant levels of autotaxin. LPC alone was unable to stimulate the migration of either cell type unless autotaxin was present. Knocking down autotaxin secretion, or inhibiting its catalytic activity, blocked cell migration by preventing lysophosphatidate production and the subsequent activation of $LPA_{1/3}$ receptors. We conclude that inhibiting autotaxin production or activity could provide a beneficial adjuvant to chemotherapy for preventing tumor growth and metastasis in patients with high autotaxin expression in their tumors.

Key words: chemotherapy; lysophosphatidate; lysophosphatidylcholine; metastasis

INTRODUCTION

The ability of cancer cells to migrate and invade surrounding tissues is the main determinant of whether metastases will develop. Most aggressive cancers will metastasize and this results in a poorer prognosis for patients requiring treatment. The ability to prevent the formation of metastases after surgical intervention or chemotherapy would provide a powerful tool in decreasing the morbidity and mortality associated with cancer.

Autotaxin (ATX) is a secreted glycoprotein whose level of expression within tumors correlates strongly with their aggressiveness and invasiveness [1]. ATX was first identified in human melanoma A2058 cells [2] and it has also been detected in several other tumor cell lines [3–6]. ATX expression in breast and other cancers is strongly associated with tumor cell survival, growth, migration, invasion, and metastasis [1,7–11]. However, the mechanisms by which ATX modifies cell signaling within the tumor to stimulate angiogenesis, cancer cell migration and metastasis are still not fully understood. A noncatalytic effect of ATX was shown to occur in oligodendrocytes where ATX acts on adhesion through integrin-dependent focal adhesion assembly [12,13]. ATX may thus regulate cell to extracellular matrix interactions that could be linked to cancer aggressiveness. Another mechanism of ATX action is through the conversion of extracellular lysophosphatidylcholine (LPC) to lysophosphatidate (LPA) [14,15], which could change the balance of cell activation by LPC versus LPA.

LPC is an abundant extracellular lipid that is found at up to 200 μM in the circulation [16]. It is produced by the liver, which secretes mainly

Abbreviations: ATX, autotaxin; LPC, lysophosphatidylcholine; LPA, lysophosphatidate; GPR4, G protein-coupled receptor-4; GAPDH, glyceraldehyde phosphate dehydrogenase; FBS, fetal bovine serum; siCTRL, siControl.

*Correspondence to: Department of Biochemistry (Signal Transduction Research Group), University of Alberta, Edmonton, Alberta, Canada T6G 2S2.

Received 18 November 2008; Revised 23 December 2008; Accepted 3 January 2009

DOI 10.1002/mc.20524

Published online 9 February 2009 in Wiley InterScience (www.interscience.wiley.com)

polyunsaturated LPC [16]. Alternatively, mainly saturated LPC is produced by lecithin/cholesterol acyltransferase, which circulates in high-density lipoproteins [17]. It has been proposed that LPC stimulates cell signaling and cell migration through acting as an extracellular ligand for G2A (G_2 accumulation) and G protein-coupled receptor-4 (GPR4) receptors [18–23]. Alternatively, LPC can signal after its conversion to LPA by ATX [7,14].

LPA is a potent signaling molecule that stimulates cell proliferation, neurite retraction, chemotaxis, and wound healing [24,25]. These effects are mediated by at least six G-protein coupled receptors on the cell surface: LPA_1/EDG2, LPA_2/EDG4, LPA_3/EDG7, LPA_4/GPR23/p2y9, LPA_5/GRP92, and LPA_6/p2y5 [26–28]. The expression of these LPA receptors is cell-specific, and each can elicit different responses upon LPA binding. Initial evidence that LPA can be involved in carcinogenesis came from the identification of its role as an activating factor in ovarian cancer. LPA is present in high concentrations in the ascites fluid of ovarian tumors and it stimulates cell proliferation and metastasis [29,30]. These actions are mediated mainly through LPA_1 and LPA_3 receptors [11,31–33]. LPA stimulates angiogenesis by elevating levels of vascular endothelial growth factor [8]. LPA also increases the synthesis of macrophage migration inhibitory factor, a tumor promoter, in a colon cancer line [34] and it decreases the expression of the tumor suppressor, p53, in lung cancer cells [35].

Two main pathways have been identified for LPA production of extracellular LPA [36]. During inflammation, secretory PLA_2 is produced, which generates LPA from phosphatidate on exposed membranes [37]. The second, and more significant source of extracellular LPA, is through the action of ATX on extracellular LPC [14].

In the present work, we examined the effects of LPC and LPA on the migration of MDA-MB-231 breast cancer cells, which produce very little ATX, and MDA-MB-435 melanoma cells [38], which secrete abundant ATX. We found that MDA-MB-231 cells migrate in response to LPC only if ATX is present. Also, knocking down ATX expression in MDA-MB-435 cells, or inhibiting the catalytic action of ATX, blocked cell migration in the presence of LPC, but not LPA. We propose that inhibiting the production, or activity of ATX could decrease new tumor growth and metastasis following surgical excision of a tumor given that LPC is abundant in the environment of malignant tumors and it can readily be converted to LPA by tumor-derived ATX.

MATERIALS AND METHODS

Materials

Mouse anti-glyceraldehyde 3-phospate dehydrogenase (GAPDH) was from Sigma–Aldrich (Oakville, ON, Canada). Rabbit anti-ATX and recombinant ATX were gifts from Dr. T. Clair (National Cancer Institute, Bethesda, MA). Secondary antibodies were: AlexaFluor© 680 goat anti-mouse IgG, A-21057 was from Invitrogen Life Technologies (Carlsbad, CA); IRDye 800 goat anti-rabbit IgG (Rockland Immunochemicals, Philadelphia, PA). VPC32183 was purchased from Avanti Polar Lipids (Alabaster, AL). Oleoyl-L-α-lysophosphatidic acid, sodium salt (LPA), oleoyl-L-α-LPC, fatty acid-free bovine serum albumin, activated charcoal (Norit®), Hoechst 33258, horseradish peroxidase, choline oxidase, 4-aminoantipyrine, N-ethyl-N-(2-hydroxy-3-sulfopropyl)-m-toluidine and fibronectin were purchased from Sigma–Aldrich (Oakville, ON, Canada and St. Louis, MO). Fetal bovine serum (FBS) was from Medicorp, Inc. (Montréal, PQ, Canada). The ATX inhibitors, VPC8a202 and S32826 were synthesized as described previously [39,40]. Transwells® (polycarbonate, 13 mm D, 12 μm pore size) were obtained from Corning (Corning, NY). On the day before the migration assays they were coated with 120 μL of 0.15 mg/mL fibronectin and allowed to dry.

Cell Culture

MDA-MB-435 and MDA-MB-231 cells were obtained from the American Type Culture Collection. The cells were cultured in RPMI 1640 medium (GIBCO, Burlington, ON, Canada) supplemented with 10% FBS and an antibiotic/antimycotic cocktail (penicillin, streptomycin, amphotericin B) (Invitrogen Life Technologies) at 5% CO_2, 95% humidity and 37°C.

Collection and Concentration of Conditioned Media

Equal numbers of cells were plated onto 10 cm dishes and they were grown until 90% confluence. Dishes were washed and then 10 mL of RPMI 1640 containing 0.1% BSA (≥96% fatty acid free) was added. After 24 h cells were washed and 10 mL of RPMI 1640 was added. The dishes were incubated for a further 24 h, the conditioned media was collected and cells on each dish were counted. Collected conditioned media were then centrifuged at $1{,}500 \times g$ for 10 min to remove whole cells and debris and they was then stored at −20°C. Conditioned media were concentrated approximately 20- to 30-fold using Centricon® YM-10 centrifugal filter devices (Millipore, Billerica, MA). Filters were prerinsed with 2 mL of water to remove glycerine and samples were centrifuged at 5,000*g* for 120 min, or until the desired final volume was obtained. Filters were then inverted and centrifuged at 1,500*g* for 2 min to collect concentrated media. The final volume was determined by weighing.

mRNA Expression

Total RNA was extracted from cell lysates using the RNAqueous kit (Ambion, Streetsville, ON,

Canada) according the manufacturer's instruction. Extracted RNA was treated with DNAase (DNA-free kit, Ambion). RNA reverse transcription reaction was performed with Superscript II reverse transcriptase (Invitrogen Life Technologies) in the presence of random primers according to the manufacturer's instructions. A control reaction without reverse transcriptase was performed in parallel to detect genomic DNA contamination. cDNA was calculated assuming 100% conversion from RNA. Real time-RT-PCR was performed by mixing 25 μL of master mix containing 2 × SYBR Green buffer mix and forward and reverse primers (Invitrogen Life Technologies) to a 3.5 μL of sample of cDNA in 96 well plates. A 316 bp fragment of the constitutively expressed housekeeping human GAPDH was used to normalize the expression of ATX mRNA. Primers for human ATX were: sense, 5′-ACAACGAGGAGAGCTGCAAT-3′, and anti-sense, 5′-AGAAGTCCAGGCTGGTGAGA-3′. Primers for human GAPDH were: sense, 5′-ACAGTCAGCCGCATCTTCTT-3′ and antisense, 5′-GACAAGCTTCCCGTTCTCAG-3′. Samples of cDNA were assayed in triplicates on the 7500 Real Time PCR System (Applied Biosystems, Streetsville, ON, Canada). The transcript number of human GAPDH was quantified, and each sample was normalized on the basis of GAPDH mRNA content.

Boyden Chamber Assay for Migration

Two million cells were seeded in a 25 cm^2 flask with growth medium for at least 48 h. Starvation medium (RPMI 1640 containing 0.1% BSA, ≥96% fatty acid free) was added for the last 18 h before the migration experiment. Cells were washed twice with HBS, trypsinized, and collected in starvation media and then 1 mL of 0.1% trypsin inhibitor solution in HBS was added. Cells were centrifuged down, media were removed by aspiration, and cells were resuspended in starvation media and counted. Cells (300 000) were seeded into each of the fibronectin coated Transwell® filters and incubated for 45 min for attachment. Filters were then transferred into bottom chambers that contained 1.5 mL of starvation medium with 0.2% charcoal-treated FBS (FBS-C) and various agonists. This charcoal treatment removed >95% of the LPA as assessed after spiking the FBS with ^{32}P-labeled LPA. This means that the concentration of LPA added in the diluted serum should have been <1 nM. Chambers were incubated at 37°C and cells were allowed to migrate through the pores in the filter for 3 or 6 h. The basal level of migration was measured with 0.2% FBS-C in the bottom chamber and 5% FBS was used as a positive control for stimulated migration. After migration, cells were then fixed in 5% formaldehyde for 1 h, or overnight. Filters were then rinsed in water and placed in 1 μg/mL Hoechst 33258 stain for 2 h. Then the upper surface of the filters was cleaned with a moist cotton swab to remove cells that had not migrated. Filters were washed again and placed in PBS. Four to six random fields were photographed under a Leica DM IRB fluorescence microscope at 40× magnification without knowing the treatment and the average numbers of cells per field was calculated.

Western Blot Analysis

Concentrated conditioned media were analyzed by SDS–PAGE according to Laemmli [41]. Proteins were transferred at 450 mA for 5 h onto nitrocellulose membranes (Trans-Blot® Transfer Medium, Bio-Rad, Mississauga, ON, Canada) in transfer buffer (192 mM glycine, 24 mM Tris base, pH 8.5 and 20% (v/v) ethanol). Membranes were blocked in 50% PBS and 50% Odyssey™ blocking buffer (Li-Cor Biosciences, Lincoln, NE) for a minimum of 1.5 h. All antibodies were diluted in 50:50 PBS/Odyssey™ blocking buffer with 0.1% (v/v) Tween-20. Membranes were incubated with anti-ATX (rabbit, 1:10 000) for 1 h. Membranes were then washed four times with PBS containing 0.1% Tween-20 and incubated in IRDye 800 goat anti-rabbit IgG (Rockland Immunochemicals, 1:10 000) for 1 h and washed three times in wash buffer and once in PBS alone. Membranes were scanned using the Odyssey™ Imager (Li-Cor).

Autotaxin Activity Assay

The assay of ATX activity in cells was based on the method described by Ferguson et al. [42] using a fluorogenic phospholipid ATX substrate, FS-3 (Echelon Biosciences, Salt Lake City, UT). FS-3 was diluted to 3.1 μM in a solution containing: 140 mM NaCl, 5 mM KCl, 1 mM $CaCl_2$, 1 mM $MgCl_2$, 50 mM Tris–HCl, pH 8.0, and 1 mg/mL BSA. The solution was heated at 60°C for 10 min to destroy any enzymatic activity in the BSA and then cooled to 37°C before use. Forty microliters of FS-3 solution was added to 10 μL of cell lysate, or concentrated conditioned media in a black-wall, clear-bottom 96 well Costar® half-area plate. Measurements were then taken at appropriate intervals using a Fluoroskan Ascent fluorometer (Thermo Lab Systems, Gormley, ON, Canada) at an excitation wavelength of 485 nm and an emission wavelength of 527 nm.

For the kinetic studies, human recombinant ATX was subcloned into the mammalian expression vector cDNA3.1/V5His-TOPO (Invitrogen Life Technologies) and expressed as a C-terminus V5- and 6xHis-tagged protein in HEK-293 cells using PolyFect® (Qiagen, Germantown, MD) as a transfection reagent. ATX was purified from the culture medium using a nickel-Sepharose resin (Qiagen) according to manufacturer's instructions and the buffer was changed to PBS using 30 kDa cutoff Centricon tubes (Millipore). ATX DNA was generated from an EST I.M.A.G.E. clone 5174518 using the following forward and reverse primers 5′-CGC GCT AGC ATG GCA AGG AGG AGC TCG TTC-3′; 5′-AAT CTC GCT

CTC ATA TGT ATG CAG-3′ to amplify the ATX ORF. ATX activity was measured essentially as described by Umezu-Goto et al. [7] by determining the release of choline after incubation at 37°C for 18 h in 100 μL of a buffer consisting of 100 mM Tris–HCl, pH 9.0, 500 mM NaCl, 5 mM $MgCl_2$, 30 μM $CoCl_2$, 0.05% Triton X-100, 0.5 μM VPC8a202 and various concentrations of oleoyl-LPC (Avanti Polar Lipids). Choline was detected colorimetrically at 555 nm after adding 100 μL of 50 mM Tris–HCl, pH 8.0, 5 mM $MgCl_2$, 50 U/mL horseradish peroxidase, 18 U/mL choline oxidase, 5 mM 4-aminoantipyrine, and 3 mM N-ethyl-N-(2-hydroxy-3-sulfopropyl)-m-toluidine.

Knockdown of Autotaxin Expression Using siRNA

Knockdown of ATX was achieved using SMARTpool® siRNAs (Dharmacon, Inc., Lafayette, CO). About 800 000 cells were plated on 10 cm dishes with 15 mL of antibiotic-free RPMI 1640 containing 10% FBS. Cells were grown for 2 d until about 50% confluency. Before transfection, the medium was replaced with 7 mL of fresh antibiotic-free media. Ten microliters of stock siRNA (50 μM) was diluted in 1.5 mL of Opti-MEM Reduced Serum Medium (Invitrogen Life Technologies). In a separate tube, 30 μL of Lipofectamine 2000 (Invitrogen Life Technologies) was mixed with 1.5 mL Opti-MEM and incubated at room temperature for 15 min. The siRNA and the Lipofectamine solutions were then combined and incubated for another 15 min at room temperature. Each dish of cells received 3 mL of the siRNA-Lipofectamine 2000 complex that was added drop-wise while swirling the dish. The final concentrations of Lipofectamine 2000 and siRNA were 1.4 μg/mL and 50 nM respectively. Cells were then incubated for 24 h at 37°C and the medium was collected as described above. Cells on each dish were trypsinized and counted so that equivalent amounts of concentrated media could be used in the migration assays.

Statistics

Results are presented as means ± SEM from at least three independent experiments, unless otherwise indicated. Statistical differences were calculated using GraphPad 4 software (Prism) by ANOVA with a Newman–Keuls post-hoc test and paired *t*-tests.

RESULTS

Differential Effects of Lysophosphatidylcholine and Lysophosphatidate on the Migration of MDA-MB-231 Breast Cancer Cells and MDA-MB-435 Melanoma Cells

We first compared the migration of MDA-MB-231 breast cancer cells and MDA-MB-435 cells, which are now known to be derived from M14 melanoma cells [38]. MDA-MB-231 and MDA-MB-435 showed a similar migratory response to LPA over 6 h, with maximum migration occurring with about 0.5 μM LPA. This LPA concentration elicited a migratory response similar to that obtained with 5% charcoal treated-FBS (Fig. 1A). MDA-MB-231 cells showed no significant stimulation of migration over the 6 h incubation with any LPC concentration employed (Fig. 1B). By contrast, MDA-MB-435 cells showed a stimulation of migration in response to LPC concentrations of ≥5 μM in the bottom chamber.

ATX Activity Is Required for Lysophosphatidylcholine-Induced Cell Migration

The results in Figure 1 could be explained in two ways. First, the MDA-MB-231 cells may not express putative receptors that respond to LPC, whereas MDA-MB-435 cells express these receptors. Second,

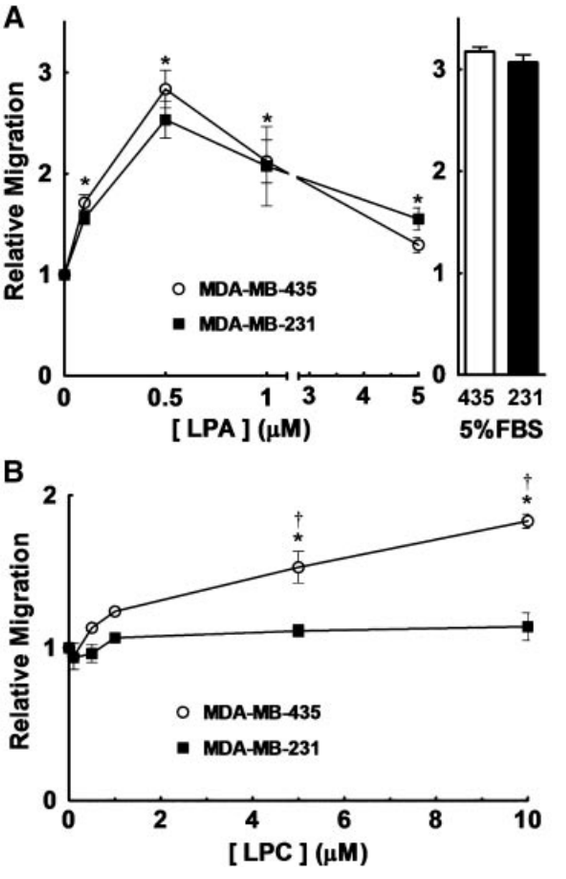

Figure 1. Effects of lysophosphatidate and lysophosphatidylcholine on the migration of MDA-MB-435 and MDA-MB-231 cells. Panel A shows the migration of MDA-MB-435 (○), and MDA-MB-231 (■) cells after a 3 h incubation with different concentrations of LPA. Migration in response to 5% charcoal-stripped FBS was used as a positive control. Panel B shows migration when the cells were incubated for 6 h with different concentrations of LPC. Results are expressed relative to the number of cells migrating with only basal media (RPMI 1640 with 0.1% BSA and 0.2% FBS-C), which was given a value of 1. Typically, basal migration consisted of approximately 75 cells per field for a 3 h incubation and 120 cells per field for a 6 h incubation. Results are means ± SEM from at least three independent experiments. Statistically significant differences between basal migration and agonist-stimulated migration are indicated by $*P < 0.01$ and between cell lines are indicated by $^{\dagger}P < 0.01$.

and more likely, MDA-MB-435 cells could express ATX that produces LPA from LPC, which stimulates cell migration, whereas MDA-MB-231 cells do not express ATX. To test the latter hypothesis, we measured ATX expression in both cells lines. The MDA-MB-435 cells expressed significantly more ($P < 0.05$) ATX mRNA than the MDA-MB-231 cells as shown by real-time RT-PCR analysis (Fig. 2A). Furthermore, concentrated medium from MDA-MB-231 cells showed very low ATX activity compared to MDA-MB-435 medium (Fig. 2B). Western Blot analysis of medium from MDA-MB-435 cells (Fig. 2C) showed marked expression of ATX, which migrated with the recombinant ATX standard at about 100 kDa as expected [7]. MDA-MB-435 cells can, therefore, be used as a convenient source of ATX for future experiments described below. By contrast, ATX was barely detectable in equivalent amounts of medium from MDA-MB-231 cells.

We could not detect any significant ATX activity or protein expression in the lysates from MDA-MB-435 and MDA-MB-231 cells (results not shown), which implies that ATX is mainly a secreted protein as shown previously [14].

Concentrated Medium From MDA-MB-435 Cells Stimulates Cell Migration in the Presence of Lysophosphatidylcholine Because of its Autotaxin Activity

To determine why MDA-MB-435 and MDA-MB-231 cells respond differently to LPC, we measured the effects of adding concentrated media from these cells to the bottom well of the migration chamber. MDA-MB-231 cells show no significant migration in the presence of LPC and their own concentrated medium. By contrast, a migratory response similar to that obtained with 5% charcoal-treated FBS, or 0.5 μM LPA was obtained when concentrated medium from MDA-MB-435 and LPC were added to the bottom chamber. This latter effect was completely abolished by the addition of 1 μM VPC8a202, an ATX inhibitor [39], to the wells (Fig. 3A).

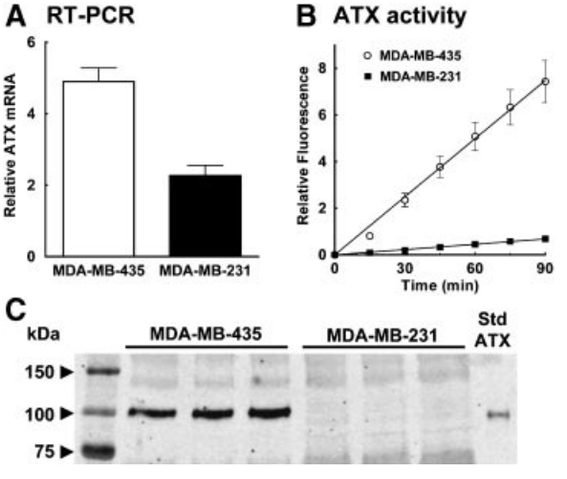

Figure 2. MDA-MB-435 cells secrete significant amounts of active ATX into the extracellular medium compared to MDA-MB-231 cells. Panel A shows the relative mRNA levels of ATX compared to GAPDH in MDA-MB-435 and MDA-MB-231 cells. Results are means ± SEM from at least three independent experiments. Panel B shows the results from the fluorescence assay for ATX activity of concentrated conditioned media collected from MDA-MB-435 (○), or MDA-MB-231 (■) cells. Results are means ± SEM from at least three independent experiments. Panel C shows the Western blot analysis for ATX of concentrated media collected from three separate dishes of MDA-MB-435 or MDA-MB-231 cells. Recombinant ATX from Dr. T. Clair was used as a standard (StdATX).

A similar experiment was performed with MDA-MB-435 cells. Addition of concentrated medium from MDA-MB-231 cells had no significant effect on the migration of MDA-MB-435 cell in the presence, or absence of LPC (Fig. 3B). By contrast, a significant stimulation of migration was observed when concentrated medium from MDA-MB-435 cells was added to the bottom chamber with LPC. This response was completely blocked by the addition of 1 μM of the ATX inhibitor, VPC8a202. We also used 1 μM S32826 ([4-(tetradecanoylamino)-benzyl]-phosphonic acid), another ATX inhibitor [40], and found that it also completely blocked LPC-induced migration of MDA-MB-435 cells (Fig. 3C). As controls for the experiments in Figure 3B and C, we used LPA to stimulate migration through its G-protein coupled receptors. VPC8a202 and S32826 did not significantly affect this LPA-induced stimulation of migration for either cell line (Fig. 3B and C). This demonstrates that neither inhibitor affects migration per se and that the inhibition of migration depends on blocking the conversion of LPC to LPA.

To provide further evidence to support the conclusion that the stimulatory effect of LPC on the migration of MDA-MB-435 and MDA-MB-231 cells depends on the catalytic activity of ATX, we established that VPC8a202 and S32826 inhibited ATX activity under the conditions of the FS-3 fluorescence assay by about 93% and 90%, respectively. We also performed more detailed kinetic studies on the inhibition of ATX activity by VPC8a202 using the natural substrate, LPC. Our results show that VPC8a202 acts mainly as a competitive inhibitor of ATX and that it prevents the conversion of LPC to LPA as expected from a substrate analogue, with a K_i of about 390 nM (Fig. 4). Previous work showed that S32826 is also a nM inhibitor of ATX [40]. Concentrations of VPC8a202 and S32826 in the μM range are, therefore, effective at inhibiting ATX and this supports our interpretation that the observed migratory effects of LPC reflect the conversion of LPC to LPA by ATX.

To further validate the results with the ATX inhibitors on migration, we also knocked down ATX expression in MDA-MB-435 cells using siRNA. Conditioned media from siATX treated cells showed an 85% decrease in ATX activity compared to the siControl (siCTRL) treated cells (Fig. 5A).

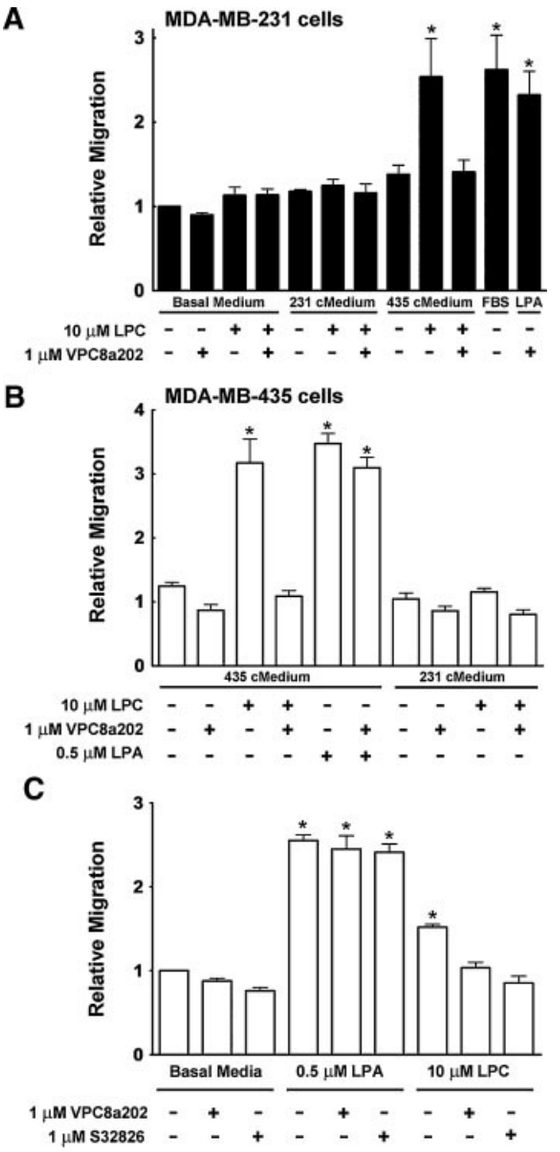

Figure 3. Stimulation of migration by lysophosphatidylcholine depends on autotaxin activity. Panel A shows the migration of MDA-MB-231 cells over 3 h in the presence of basal medium or concentrated medium prepared from either MDA-MB-231 cells (231 cMedium), or from MDA-MB-435 cells (435 cMedium). These experiments were performed in the presence or absence of 10 μM LPC, or 1 μM of the ATX inhibitor, VPC8a202. Migration of MDA-MB-231 cells with only basal media (RPMI 1640 with 0.1% BSA and 0.2% FBS) present was given a value of 1. Migrations in the presence of 5% FBS and 0.5 μM LPA plus VPC8a202 were used as controls. Panel B shows results from similar experiments using MDA-MB-435 cells over a 3 h period. Panel C shows the effects of the ATX inhibitors, VPC8a202 and S32826, on the migration of MDA-MB-435 cells over 3 h in the absence of concentrated medium. Results are means ± SEM from at least three independent experiments. Statistically significant differences are indicated by $*P < 0.01$.

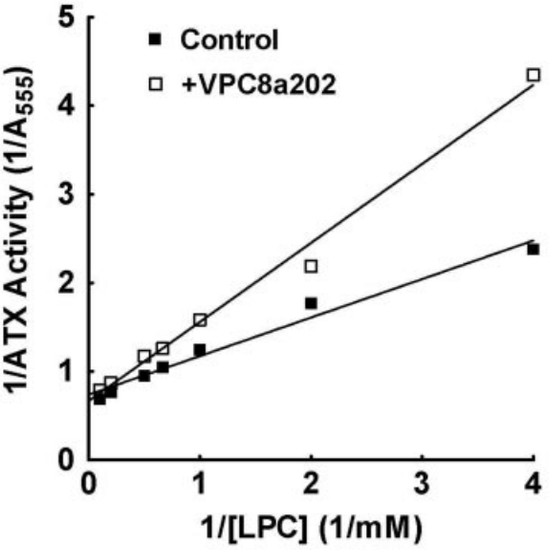

Figure 4. Kinetics of inhibition of ATX activity by VPC8a202. The initial rate of recombinant ATX activity was measured colorimetrically at different concentrations of LPC in presence and absence of 0.5 μM VPC8a202. Activity was expressed as the release of choline during 18 h and it is represented by the absorbance of the product at 555 nm (A555). Each point is the average of three measurements (SD values for the reaction rates were less than 5% of every measurement and are not depicted). Consumed substrate was less than 10% in every case thus ensuring an initial rate of reaction. Results were fitted to a straight line by linear regression. The apparent K_m for LPC was about 588 μM.

Furthermore, expression of the ATX protein in conditioned media from siATX treated cells was markedly reduced to levels that were undetectable by Western blotting (Fig. 5B).

There was no stimulation of the migration of MDA-MB-435 cells when we added only concentrated media from cells treated with siATX, or siCTRL. By contrast, addition of LPC to concentrated medium from cells treated with the siCTRL elicited a migratory response (Fig. 5C), but this stimulation was not observed when ATX formation was blocked with siATX.

We also tested the migration of MDA-MB-435 when exposed to LPC, or LPA directly, but using a 6 h incubation for the migration assay. The siCTRL and the siATX treated cells migrated to the same extent in the absence of agonist. Addition of 10 μM LPC stimulated the migration of siCTRL treated cells, but not siATX-treated cells. As a control, we showed that the siATX treated cells still showed a normal migration with 0.5 μM LPA. The results emphasize that the cells treated with siATX were not migration deficient. They we able to respond normally to LPA, but they were unable to migrate to LPC because of the ATX knockdown (Fig. 6).

These results establish that the LPC effect in stimulating cell migration is dependent on the catalytic activity of ATX and LPA production, which could then stimulate migration through LPA receptors. This is confirmed in Figure 7 where 1 μM VPC32183, an $LPA_{1/3}$ receptor antagonist [43], was added to the concentrated medium from MDA-MB-

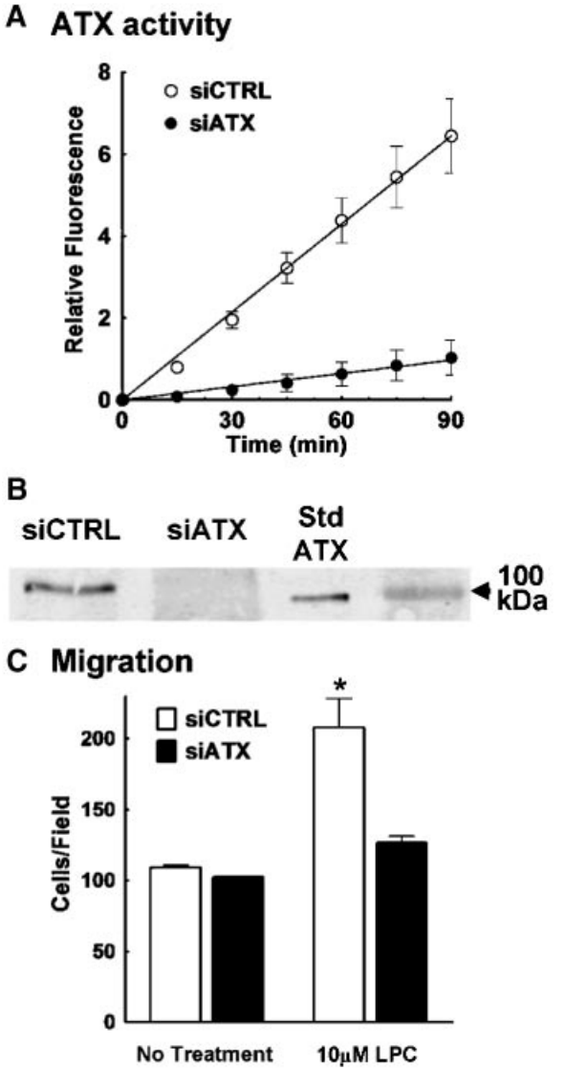

Figure 5. Knock-down of ATX with siRNA significantly decreases the migratory potential of concentrated medium from MDA-MB-435 cells. Concentrated medium was collected from three dishes of MDA-MB-435 cells treated with siRNA for ATX (siATX) and three dishes treated with control siRNA (siCTRL). Panel A shows a fluorescence assay representing ATX activity in siCTRL concentrated medium (○) and in siATX concentrated medium (●). Error bars indicate the SEM of three experimental values. Panel B shows the Western blot analysis of a representative sample of concentrated media that were probed for ATX. Recombinant ATX was used as a standard (StdATX). Panel C compares the migration of MDA-MB-435 cells over a 3 h incubation in the presence or absence of LPC and concentrated medium collected from MDA-MB-435 cells that were treated with siCTRL (white bars) or siATX (dark bars). Results are means ± SEM from three independent experiments. Statistically significant differences are indicated by $*P < 0.01$.

435 cells. VPC32183 inhibited LPC-induced migration in the presence of concentrated medium, demonstrating that the effect of LPC depends on its conversion to LPA. As a control, we also showed that VPC32183 inhibited migration when LPA was added

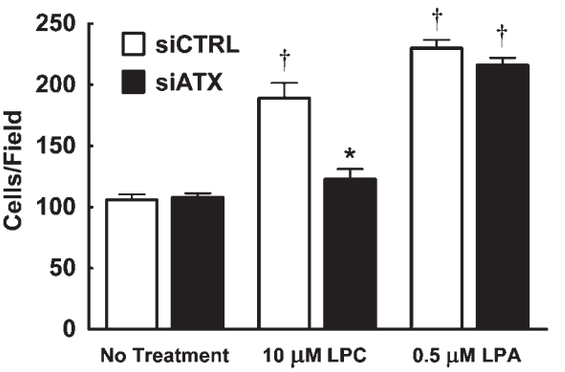

Figure 6. Knockdown of ATX with siRNA in MDA-MB-435 cells abolishes stimulation of migration by lysophosphatidylcholine. A 6 h incubation was used to measure the migration of MDA-MB-435 cells that were treated with siATX or siCTRL. Migration in basal media (RPMI 1640 with 0.1% BSA and 0.2% FBS-C) was compared to migration in the presence of 10 μM LPC, or 0.5 μM LPA. Results are means ± SEM from four independent experiments. Statistically significant differences between alternate siRNA treated cells are indicated by $*P < 0.01$ and between treatments compared to control are indicated by $^{\dagger}P < 0.01$.

directly. There was also a small inhibitory effect of VPC32183 when neither LPC nor LPA was added, which probably resulted from the presence of some secreted LPC or LPA in the concentrated medium from the MDA-MB-435 cells.

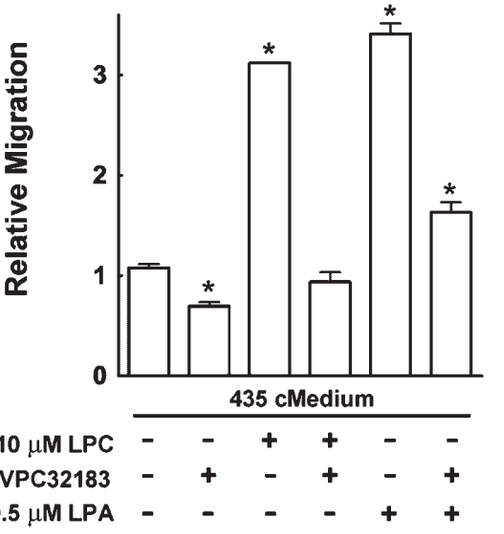

Figure 7. The LPA receptor antagonist, VPC32183, inhibits migration of MDA-MB-435 cells. A 3 h incubation was used to measure the migration of MDA-MB-435 cells in the presence of their own concentrated medium with either LPC or LPA, and in the presence or absence of the $LPA_{1/3}$ receptor antagonist, VPC32183. Migration in the presence of agonists/antagonists was compared to the number of cells migrating in basal media (RPMI 1640 with 0.1% BSA and 0.2% FBS-C), which is given a value of 1. Results are means ± SEM from at least three independent experiments. Statistically significant differences compared to the untreated control are indicated by $*P < 0.01$.

DISCUSSION

Increased ATX expression in tumors such as glioblastoma, lung, breast, renal, ovarian, and thyroid cancers is correlated with their aggressiveness [6–10,24]. In this article, we investigated the mechanisms for this local effect of ATX by studying the migration of MDA-MB-435 melanoma cells and MDA-MB-231 breast cancer cells. These cells are both able to migrate well in response to serum, or LPA. We found that MDA-MB-435 cells secrete abundant ATX, whereas ATX secretion from MDA-MB-231 was barely detectable. Significantly, MDA-MB-435 cells migrated in response to LPC, whereas MDA-MB-231 did not. We, therefore, hypothesized that LPC does not induce migration of these cells per se, but rather its effects depend on its conversion to LPA by ATX. Therefore, decreased expression or inhibition of ATX should diminish the LPC response.

We verified this hypothesis as follows: (a) addition of medium from MDA-MB-435, but not from MDA-MB-231 cells, enabled MDA-MB-231 cells to migrate in response to LPC; (b) this effect was abolished by the suppression of ATX expression using siRNA for ATX, (c) inhibition of ATX activity with two different ATX inhibitors, VPC8a202 and S32826, completely blocked the stimulatory effect of LPC on migration and (d) LPC-induced migration was inhibited by an $LPA_{1/3}$ receptor antagonist, VPC32183. These results establish that the major action of ATX on migration in MDA-MB-435 and MDA-MB-231 cells in this system is through the conversion of LPC to LPA. However, we cannot rule out that ATX could exert a noncatalytically action on migration in vivo through its C-terminal region, which can modify cell adhesion.

Although LPC has been widely described to stimulate cell activation and migration directly through its putative action on G2A and GPR4 receptors [18], much of this work is now in question. G2A and GPR4 are now considered to be proton-sensing receptors whose response is negatively regulated by LPC [44,45]. We found no evidence that the zwitterionic lipid, LPC, is able to stimulate migration. Rather its action depends on conversion to the acidic lipid, LPA, by ATX. This conclusion is also supported by two very recent publications. First, independent work shows that small molecule inhibitors of ATX block melanoma cell migration and invasion [46]. Secondly, we showed that ATX activity is required for LPC to protect MCF-7 breast cancer and MDA-MB-435 melanoma cells against Taxol-induced apoptosis [47].

LPC is present in blood and extracellular fluids at concentrations up to 200 μM. Secretion of ATX into the blood or the interstitial fluid surrounding a tumor can convert the relatively abundant LPC, which does not stimulate migration, into the potent bioactive modulator, LPA. This lipid provides a survival signal for cancer cells and it causes them to migrate and metastasize. This is consistent with the fact that high levels of ATX are often found in aggressive cancers. Our work demonstrates that inhibition of ATX expression, or blocking its catalytic activity, could provide very powerful tools to improve the efficacy of surgery and chemotherapy in the treatment of metastatic disease in patients where ATX expression is high. It is, therefore, hoped that our work will lead to the development of ATX inhibitors that can be used therapeutically as an adjuvant in the treatment of cancer.

ACKNOWLEDGMENTS

We thank Mr. J. Dewald for excellent technical assistance, and Dr. F. Bamforth and Dr. G.S. Cembrowski for their support of this study. We also thank Dr. T. Clair for providing recombinant ATX and the ATX antibody and Dr. J.A. Boutin (Institut de Recherches Servier) for supplying S32826. DNB is a recipient of a Medical Scientist Award from the Alberta Heritage Foundation for Medical Research. NS is a recipient of scholarships from Iranian Ministry of Health and the Bell McLeod Educational Fund from Department of Laboratory Medicine and Pathology, University of Alberta. This work was supported by grants to DNB from the Canadian Institute of Health Research (MOP 81137) and from NIH (R01 GM052722) to KRL. The provision of recombinant ATX and ATX antibody through Dr. T. Clair was made possible by the Intramural Research Program of the NIH, National Cancer Institute, Center for Cancer Research.

REFERENCES

1. Yang SY, Lee J, Park CG, et al. Expression of autotaxin (NPP-2) is closely linked to invasiveness of breast cancer cells. Clin Exp Metastasis 2002;19:603–608.
2. Stracke ML, Krutzsch HC, Unsworth EJ, et al. Identification, purification, and partial sequence analysis of autotaxin, a novel motility-stimulating protein. J Biol Chem 1992;267: 2524–2529.
3. Kishi Y, Okudaira S, Tanaka M, et al. Autotaxin is overexpressed in glioblastoma multiforme and contributes to cell motility of glioblastoma by converting lysophosphatidylcholine to lysophosphatidic acid. J Biol Chem 2006;281:17492–17500.
4. Euer N, Schwirzke M, Evtimova V, et al. Identification of genes associated with metastasis of mammary carcinoma in metastatic versus non-metastatic cell lines. Anticancer Res 2002;22:733–740.
5. Stassar MJ, Devitt G, Brosius M, et al. Identification of human renal cell carcinoma associated genes by suppression subtractive hybridization. Br J Cancer 2001;85:1372–1382.
6. Kehlen A, Englert N, Seifert A, et al. Expression, regulation and function of autotaxin in thyroid carcinomas. Int J Cancer 2004;109:833–838.
7. Umezu-Goto M, Kishi Y, Taira A, et al. Autotaxin has lysophospholipase D activity leading to tumor cell growth and motility by lysophosphatidic acid production. J Cell Biol 2002;158:227–233.
8. So J, Wang FQ, Navari J, Schreher J, Fishman DA. LPA-induced epithelial ovarian cancer (EOC) in vitro invasion and

migration are mediated by VEGF receptor-2 (VEGF-R2). Gynecol Oncol 2005;97:870–878.
9. Nam SW, Clair T, Campo CK, Lee HY, Liotta LA, Stracke ML. Autotaxin (ATX), a potent tumor motogen, augments invasive and metastatic potential of ras-transformed cells. Oncogene 2000;19:241–247.
10. Nam SW, Clair T, Kim YS, et al. Autotaxin (NPP-2), a metastasis-enhancing motogen, is an angiogenic factor. Cancer Res 2001;61:6938–6944.
11. Hama K, Aoki J, Fukaya M, et al. Lysophosphatidic acid and autotaxin stimulate cell motility of neoplastic and non-neoplastic cells through LPA1. J Biol Chem 2004;279: 17634–17639.
12. Fox MA, Alexander JK, Afshari FS, Colello RJ, Fuss B. Phosphodiesterase-I alpha/autotaxin controls cytoskeletal organization and FAK phosphorylation during myelination. Mol Cell Neurosci 2004;27:140–150.
13. Dennis J, Nogaroli L, Fuss B. Phosphodiesterase-Ialpha/autotaxin (PD-Ialpha/ATX): A multifunctional protein involved in central nervous system development and disease. J Neurosci Res 2005;82(6) 737–742.
14. Tokumura A, Majima E, Kariya Y, et al. Identification of human plasma lysophospholipase D, a lysophosphatidic acid-producing enzyme, as autotaxin, a multifunctional phosphodiesterase. J Biol Chem 2002;277:39436–39442.
15. Baker DL, Fujiwara Y, Pigg KR, et al. Carba analogs of cyclic phosphatidic acid are selective inhibitors of autotaxin and cancer cell invasion and metastasis. J Biol Chem 2006;281: 22786–22793.
16. Brindley DN. Hepatic secretion of lysphosphatidylcholine: A novel transport system for polyunsaturated fatty acids and choline. J Nutr Biochem 1993;4:442–449.
17. Aoki J, Taira A, Takanezawa Y, et al. Serum lysophosphatidic acid is produced through diverse phospholipase pathways. J Biol Chem 2002;77:48737–48744.
18. Radu CG, Yang LV, Riedinger M, Au M, Witte ON. T cell chemotaxis to lysophosphatidylcholine through the G2A receptor. Proc Natl Acad Sci USA 2004;101:245–250.
19. Kim KS, Ren J, Jiang Y, et al. GPR4 plays a critical role in endothelial cell function and mediates the effects of sphingosylphosphorylcholine. FASEB J 2005;9:819–821.
20. Zhu K, Baudhuin LM, Hong G, et al. Sphingosylphosphorylcholine and lysophosphatidylcholine are ligands for the G protein-coupled receptor GPR4. J Biol Chem 2001;76: 41325–41335.
21. Rikitake Y, Hirata K, Yamashita T, et al. Expression of G2A, a receptor for lysophosphatidylcholine, by macrophages in murine, rabbit, and human atherosclerotic plaques. Arterioscler Thromb Vasc Biol 2002;2:2049–2053.
22. Kabarowski JH, Zhu K, Le LQ, Witte ON, Xu Y. Lysophosphatidylcholine as a ligand for the immunoregulatory receptor G2A. Science 2001;93:702–705.
23. Lin P, Ye RD. The lysophospholipid receptor G2A activates a specific combination of G proteins and promotes apoptosis. J Biol Chem 2003;78:14379–14386.
24. Mills GB, Moolenaar WH. The emerging role of lysophosphatidic acid in cancer. Nat Rev Cancer 2003;3:582–591.
25. Brindley DN. Lipid phosphate phosphatases and related proteins: signaling functions in development, cell division, and cancer. J Cell Biochem 2004;92:900–912.
26. Lynch KR. Lysophospholipid receptor nomenclature. Biochim Biophys Acta 2002;1582:70–71.
27. Lee CW, Rivera R, Gardell S, Dubin AE, Chun J. GPR92 as a new G12/13- and Gq-coupled lysophosphatidic acid receptor that increases camp, LPA5. J Biol Chem 2006;281: 23589–23597.
28. Pasternack SM, von Kugelgen I, Aboud KA, et al. G protein-coupled receptor P2Y5 and its ligand LPA are involved in maintenance of human hair growth. Nat Genet 2008;40: 329–334.
29. Xu Y, Fang XJ, Casey G, Mills GB. Lysophospholipids activate ovarian and breast cancer cells. Biochem J 1995;309:933–940.
30. Xu Y, Gaudette DC, Boynton JD, et al. Characterization of an ovarian cancer activating factor in ascites from ovarian cancer patients. Clin Cancer Res 1995;1:1223–1232.
31. Van Leeuwen FN, Olivo C, Grivell S, Giepmans BN, Collard JG, Moolenaar WH. Rac activation by lysophosphatidic acid LPA1 receptors through the guanine nucleotide exchange factor Tiam1. J Biol Chem 2003;278:400–406.
32. Shida D, Kitayama J, Yamaguchi H, et al. Lysophosphatidic acid (LPA) enhances the metastatic potential of human colon carcinoma DLD1 cells through LPA1. Cancer Res 2003;63: 1706–1711.
33. Yamada T, Sato K, Komachi M, et al. Lysophosphatidic acid (LPA) in malignant ascites stimulates motility of human pancreatic cancer cells through LPA1. J Biol Chem 2004;279: 6595–6605.
34. Sun B, Nishihira J, Suzuki M, et al. Induction of macrophage migration inhibitory factor by lysophosphatidic acid: Relevance to tumor growth and angiogenesis. Int J Mol Med 2003;12:633–641.
35. Murph MM, Hurst-Kennedy J, Newton V, Brindley DN, Radhakrishna H. Lysophosphatidic acid decreases the nuclear localization and cellular abundance of the p53 tumor suppressor in A549 lung carcinoma cells. Mol Cancer Res 2007;5:1201–1211.
36. Xie Y, Meier KE. Lysophospholipase D and its role in LPA production. Cell Signal 2004;16:975–981.
37. Fourcade O, Simon MF, Viode C, et al. Secretory phospholipase A2 generates the novel lipid mediator lysophosphatidic acid in membrane microvesicles shed from activated cells. Cell 1995;80:919–927.
38. Rae JM, Creighton CJ, Meck JM, Haddad BR, Johnson MD. MDA-MB-435 cells are derived from M14 melanoma cells—A loss for breast cancer, but a boon for melanoma research. Breast Cancer Res Treat 2007;104:13–19.
39. Cui P, Tomsig JL, McCalmont WF, et al. Synthesis and biological evaluation of phosphonate derivatives as autotaxin (ATX) inhibitors. Bioorg Med Chem Lett 2007;17: 1634–1640.
40. Ferry G, Moulharat N, Pradère J-P, et al. S32826: A nonomolar inhibitor of autotaxin. Discovery, synthesis and applications as a pharmacological tool. J Pharmacol Expt Therap 2008; 327:809–819.
41. Laemmli UK. Cleavage of structural proteins during the assembly of the head of bacteriophage T4. Nature 1970;227: 680–685.
42. Ferguson CG, Bigman CS, Richardson RD, van Meeteren LA, Moolenaar WH, Prestwich GD. Fluorogenic phospholipid substrate to detect lysophospholipase D/autotaxin activity. Org Lett 2006;8:2023–2026.
43. Lee S, Lynch KR. Brown recluse spider (Loxosceles reclusa) venom phospholipase D (PLD) generates lysophosphatidic acid (LPA). Biochem J 2005;391:317–323.
44. Seuwen K, Ludwig MG, Wolf RM. Receptors for protons or lipid messengers or both? J Recept Signal Transduct Res 2006;26:599–610.
45. Murakami N, Yokomizo T, Okuno T, Shimizu T. G2A is a proton-sensing G-protein-coupled receptor antagonized by lysophosphatidylcholine. J Biol Chem 2004;279:42484–42491.
46. Saunders LP, Ouellette A, Bandle R, et al. Identification of small-molecule inhibitors of autotaxin that inhibit melanoma cell migration and invasion. Mol Cancer Ther 2008;7:3352–3362.
47. Samadi N, Gaetano C, Goping IS, Brindley DN. Autotaxin protects MCF-7 breast cancer and MDA-MB-435 melanoma cells against Taxol-induced apoptosis. Oncogene 2008; [Epub ahead of print].